HABILITATION A DIRIGER DES RECHERCHES

Présentée devant

L'Université Jean Monnet, Saint Etienne

Ablation laser femtoseconde pour le dépôt de couches minces

Par

Florence GARRELIE
Maître de Conférence

Soutenance prévue le 14 Novembre 2008 devant la commision d'examen :

Rapporteurs :

Christian GODET,	Directeur de Recherche CNRS, Laboratoire PALMS, Université Rennes 1
Jacques PERRIERE,	Directeur de Recherche CNRS, INSP Paris, Université Paris 7
Michael STUKE,	Senior Research Scientist, Max-Planck Institute, Goettingen (Allemagne)

Examinateurs :

Alain CATHERINOT,	Professeur, Laboratoire SPCTS, Université de Limoges
Eric AUDOUARD,	Professeur, Laboratoire Hubert Curien, Université Saint Etienne
Christophe DONNET,	Professeur, Membre IUF, Laboratoire Hubert Curien, Université Saint Etienne

Préambule

Ce manuscrit présente mon activité de recherche au cours des 9 annnées écoulées au sein du Laboratoire TSI (Traitement du Signal et Instrumentation (UMR CNRS 5516)) devenu depuis le 1er janvier 2007 le Laboratoire Hubert Curien. Au sein de ce laboratoire, l'activité de recherche dans laquelle je me suis impliquée a débuté à mon arrivée en 1999 pour apparaître maintenant comme un projet structurant du laboratoire.

Le manuscrit est divisé en trois parties. La première partie est consacrée à une présentation synthétique de l'ensemble de mes activités, tant en terme de production scientifique, de recherche et d'encadrement doctoral que d'enseignement. Je suis en effet enseignante-chercheur, partagée entre l'IUT de Saint Etienne (Département Mesures Physiques) et le Laboratoire Hubert Curien, l'activité d'enseignement occupant une part non négligeable de mon temps.

Le mémoire de recherche est présenté dans la seconde partie de ce manuscrit. J'y présenterai dans un premier temps, un résumé des principaux résultats obtenus au cours de ces années. Le détail des travaux pourra être trouvé dans les publications jointes. Dans la seconde partie de ce mémoire de recherche, j'exposerai les perspectives envisagées pour faire évoluer la thématique que nous développons.

Enfin, les publications les plus significatives sont jointes dans la troisième partie de ce manuscrit. Elles complètent le mémoire de recherche en terme de résultats et complètent également la liste de références bibliographiques.

SOMMAIRE

- ✓ F. GARRELIE et al, *Surface and Coatings Technology*, **163-164** (2003), 306.
- ✓ A.S. LOIR et al, *Surface and Coatings Technology* **188-189** *(2004), 728-734.*
- ✓ T. KATSUNO et al, *Applied Physics A* **81**, (3) (2005), 471-476.
- ✓ N. BENCHIKH et al*, Thin Solid Films* **482**(1-2), (2005) pp287-292.
- ✓ N. BENCHIKH et al, Thin solid films, **494** (1-2) (2006), 98-104.
- ✓ R. MAALOUF et al, Talanta **72** (2007), 310-314.
- ✓ A. SIKORA et al, à paraître dans Solid State Science 2008.
- ✓ A.S. LOIR et al, *Applied Surface Science*, **208-209** (2003),pp553-560.
- ✓ F. GARRELIE et al, Applied Physics A **90** (2008) 211-217
- ✓ M. GUILLERMIN et al, à paraître dans Applied Surface Science 2008.

Extended Abstract

This manuscript presents my activities since 9 years in the Laboratory TSI, which became the Laboratory Hubert Curien in 2007. It will be divided into 3 parts. In a first part, I will present an overall view of my career and my activities in terms of research, teaching, scientific production, and students supervision. Indeed, my position of teaching-researcher leads to non negligible time-counsuming training activities. In a second part, I will present my research report. I will resume the major results obtained in our laboratory and I will outline the foreseen prospects for our scientific activities. In the last part, the most significant publications will be reported.

I arrived on an assistant professor support in the Laboratory TSI in Saint Etienne in 1999, after a PhD thesis and a one-year ATER support in the Laboratory SPCTS in Limoges. Since 2003, I also benefit from a PEDR ("Prime d'Encadrement doctoral et de recherche", Bonus from thesis supervision and research).

Since 1999, I have made different courses, tutorial or practical work (about 200 h per year), related to materials science, physics, vacuum technology, but also electronic microscopies and physics and technology of plasma in junior college. I have developed new courses but also a lot of practical works in our technical institute. More recently, I also provide two courses for Master's students at the Faculty of Science and technology related to electronic microscopies (6 h, Master OIV) and plasma science (2 h, Master Erasmus Mundus Cimet), and a training for graduate school (2h). I have also ensured the responsability of the professional trainings of our institute during two years (2006-2008, about 90 students per year), and I am now in charge with Christophe Donnet of a bachelor's degree in our institute of technology.

Concerning my research activities, I have developped some works on Pulsed Laser Deposition by femtosecond and nanosecond lasers. This activity started in the Laboratory in 1999, with my arrival. We have worked on different support : Région Rhone-Alpes, CNRS Programme Matériaux, GIS Massif Central, two ANR support still in progress and two support from the University ("Bonus Qualité Recherche"). Different academic collaborations have been developped with for instance, SPCTS from University of Limoges, LMBTS - SMS from Ecole des Mines of Saint Etienne, LTDS from Ecole Centrale de Lyon, LSA from Université Claude Bernard Lyon I, Institut Neel from Grenoble or DIOM from University of Saint Etienne.

I have contributed to the supervision of 4 thesis with 3 under joint supervision.

I participated to the organisation of a french conference (UVX2004, Saint Etienne, 7-11 juin 2004) and a national workshop "Modélisation des procédés laser ultra-brefs" in Saint Etienne in 2005. I was also in the scientific committee of a thematic school organized by the GDR 2449 of CNRS.

Since 2007, I am the manager of the project "Laser Ablation for thin films deposition" in the Laboratory Hubert Curien .

My research report concern mainly the elaboration of thin films by femtosecond Pulsed laser deposition (PLD) and the characterization of the plasma plume. I

present an overview of the results obtained on pure Diamond-Like Carbon (DLC) thin films with the goal of depositing films with high hardness and low friction and wear coefficients, with good adhesive properties on various biomedical substrates, including stainless steel or polyethylene. We succeeded in depositing such films on the femoral head of hip joints. We also tried to compare the properties of DLC films elaborated by femtosecond and nanosecond PLD through the optical properties of the films and the properties of the laser-induced plasma plume.

We have also deposited nanoparticles by femtosecond PLD and included these nanoparticles in an amorphous matrix of DLC. By this way, we deposited metal-doped DLC films with tantalum or nickel due to their different chemical affinity with respect to carbon. The films have been characterized by various techniques including AFM (Atomic force microscopy) or SEM (scanning electronic microscopy), EFTEM (energy-filtered Transmission electronic microscopy), XRD (X-Ray diffraction) RBS (Rutherford Backscattering spectrometry), XPS (X-ray photoelectron spectroscopy) or Raman spectroscopy. Two different crystalline phases are obtained in the case of the tantalum-doped DLC film, with the surprising presence of a metastable β-Ta phase, which is correlated to the properties of the plasma plume. Tantalum carbide is also evidenced in a thin layer at the edge of the tantalum clusters.

Pure DLC and metal-doped DLC films have been investigated in the frame of electrodes for biosensors. We shown the possibility of using such materials with high sensitivity and low detection limits. The optimization through the incorporation of an other dopant (boron) is the main subject of an ANR project involving various industrial partners (Suez-environnement, Cemagref-Othu , ...).

We are now also investigating the possibility of using such boron-doped DLC films for thermal and nanocalorimetric sensors in an another ANR support framework. The DLC thermometers are integrated in suspended isolated structures and show already suitable properties, such as high TCR coefficient (Temperature Coefficient of Resistance).

During all my research activities, I also tried to investigate the plasma plume properties and provide some correlations with the films properties. In particular, the behavior of the carbon plasma induced by femtosecond laser ablation has been largely studied for the elaboration of pure DLC or tantalum-doped DLC films .

In the last part of my research report, I present the propects of our works through the temporal shaping of the laser beam. The outcome has potential interest for thin films elaboration or nanoparticles synthesis. Indeed, a possible way to achieve higher film quality and better control of the ablation process is to regulate the interaction process via spatio-temporal modification of the laser beam. We have developped an experimental tool allowing the possibility of tailoring the plasma plume by adaptive temporal shaping.. I present preliminary results on the use of an adaptive feedback optimization procedure that adjust the laser temporal form for modulating plasma optical properties. This work is focused on the enhancement of the ionic emission with respect to the neutral emission lines of the plasma induced by laser irradiation of an aluminum sample. Such an optimization leads to plasma plume properties rather different from conventional femtosecond pulses (such as double or long pulses) and to films with lower density of nanoparticles, which is promising for future works.

NOTICE

INDIVIDUELLE

Cette partie a pour objectif de présenter de manière synthétique mon activité d'enseignante-chercheur durant ces 9 années depuis mon arrivée au laboratoire TSI, devenu ensuite Laboratoire Hubert Curien.

Elle débute par un aperçu de mon parcours pour arriver jusqu'à Saint Etienne. Je présenterai ensuite l'intégralité de ma production scientifique, ainsi que mes activités en matière d'enseignement. J'exposerai ensuite la thématique scientifique sur laquelle je me suis impliquée ainsi que mes activités d'encadrement. J'ai fait le choix de présenter, dans cette première partie, une synthèse de mon activité scientifique, permettant d'avoir une vue d'ensemble de mes activités de recherche, détaillant les contrats ou projets dans lesquels je me suis investie.

CURRICULUM VITAE

37 ans
Vie maritale, 2 enfants

Formation / Titres universitaires

- Maîtrise de Physique E.E.R. (Energétique, Electronique et Rayonnement) et applications
Juin 1994 *mention Très Bien*

- D.E.A. Matériaux Céramiques et Traitements de Surface
Juillet 1995 *mention Très Bien*

- Thèse de doctorat
Soutenue le 25 Septembre 1998 *mention Très honorable et félicitations du jury*
Titre : "Simulation Monte Carlo de l'expansion d'un panache plasma créé par ablation laser - Comparaison avec l'expérience"
Spécialité : Matériaux Céramiques et Traitements de surface

Directeur de thèse : A. CATHERINOT, Laboratoire Sciences des Procédés Céramiques et de Traitement de surface, SPCTS UMR 6638 - Limoges
Membres du jury :

Président :	P. FAUCHAIS	Université de Limoges
Rapporteurs :	J. P. BŒUF	Université de Toulouse
	J.C. GAUTHIER	L.U.L.I. Ecole Polytechnique - Palaiseau
Examinateurs :	M. AUTRIC	I.R.P.H.E. - Marseille
	A. CATHERINOT	Université de Limoges
	C. CHAMPEAUX	Université de Limoges
	J. P. ROMAIN	E.N.S.M.A. - Poitiers
	M. STUKE	Institut Max-Planck - Goettingen (Allemagne)

Fonctions successives :

1995-1998 **Allocataire de recherche M.E.S.R**. – Laboratoire Sciences des Procédés Céramiques et de Traitement de surface, SPCTS UMR 6638 – Université de Limoges

1995-1998 **Monitrice d'enseignement supérieur** – Faculté des Sciences et Techniques - Université de Limoges

1998-1999 **Attaché Temporaire d'Enseignement et de Recherche** - Laboratoire Sciences des Procédés Céramiques et de Traitement de surface, SPCTS UMR 6638 - Université de Limoges

1999 **Maître de Conférence** – Laboratoire Traitement du Signal et Instrumentation (LTSI) puis Laboratoire Hubert Curien (LaHC), UMR CNRS 5516- Université Jean Monnet - Saint Etienne

2003 -2007 Attribution de la Prime d'Encadrement Doctoral et de Recherche

2007 –2011 Renouvellement de la Prime d'Encadrement Doctoral et de Recherche

LISTE DES TRAVAUX

PUBLICATIONS dans des revues à comité de lecture

Revues internationales :

[1] B. ANGLERAUD, C. GIRAULT, C. CHAMPEAUX, F. GARRELIE, C. GERMAIN, A. CATHERINOT, *Applied Surface Science* **96-98** (1996), 117-121.

[2] F. GARRELIE, J. AUBRETON, A. CATHERINOT, *Journal of Applied Physics* **83**(10) (1998), 5075-5082.

[3] B. ANGLERAUD, F. GARRELIE, F. TETARD, A. CATHERINOT, *Applied Surface Science* **138-139** (1999), 507.

[4] F. GARRELIE, A. CATHERINOT, *Applied Surface Science* **138-139** (1999), 97.

[5] F. GARRELIE, C. CHAMPEAUX, A. CATHERINOT, *International of Journal of Thermal Sciences* **38**(5) (1999), 452.

[6] F. GARRELIE, C. CHAMPEAUX, A. CATHERINOT, *Applied Physics A* **69** (1999), 45.

[7] F. GARRELIE, C. CHAMPEAUX, A. CATHERINOT, *Applied Physics A* **69** (1999), S55.

[8] F. GARRELIE, A.S. LOIR, F. GOUTALAND, R. LE HARZIC, B. ANGLERAUD, Y. OUERDANE, P. LAPORTE, *SPIE Proceedings* **4760** (2002), 301.

[9] P. LAPORTE, E. AUDOUARD, F. GARRELIE, *SPIE Proceedings* **4760** (2002), 347.

[10] F. GARRELIE, A.S. LOIR, C. DONNET, F. ROGEMOND, R. LE HARZIC, M. BELIN, E. AUDOUARD, P. LAPORTE, *Surface and Coatings Technology*, **163-164** (2003), 306.

[11] A.S. LOIR, F. GARRELIE, J.L. SUBTIL, F. GOUTALAND, M. BELIN, R. LE HARZIC C. DONNET, Y. OUERDANE, F. ROGEMOND, P. LAPORTE, *Applied Surface Science*, **208-209** (2003),pp553-560.

[12] A.-S. LOIR, F. GARRELIE, C. DONNET, M. BELIN, B. FOREST, F. ROGEMOND, P. LAPORTE, *Thin Solid Films* **453-454** , (2004), pp531-536.

[13] A.S. LOIR, F. GARRELIE, C. DONNET, F. ROGEMOND, J.L. SUBTIL , B. FOREST, M. BELIN, P. LAPORTE, *Surface and Coatings Technology* **188-189** *(2004), 728-734.*

[14] A.-S. LOIR, F. GARRELIE, C. DONNET, J.-L. SUBTIL, M. BELIN, B. FOREST, F. ROGEMOND, P. LAPORTE, *Applied Surface Science* **247**, 225-231 (2005).

[15] N. BENCHIKH, F. GARRELIE, C. DONNET, B. BOUCHET-FABRE, K. WOLSKI, F. ROGEMOND, A.S LOIR, J.L. SUBTIL *Thin Solid Films* **482**(1-2), (2005) pp287-292.

[16] T. KATSUNO, C. GODET, J.C. ORLIANGES, A.-S. LOIR, F. GARRELIE, AND A. CATHERINOT, *Applied Physics A* **81**, (3) (2005), 471-476.

[17] R. MAALOUF, N. JAFFREZIC-RENAULT, O. VITTORI, M. SIGAUD, Y. SAIKALI, H. CHEBIB, A.-S. LOIR, F. GARRELIE, C. DONNET, T. TAKENO, T. TAKAGI, *Journal of Advanced Science*, **18** (2006), p 31-36.

[18] N. BENCHIKH, F. GARRELIE, K. WOLSKI, C. DONNET, R.Y. FILLIT, F. ROGEMOND, J.L. SUBTIL, Thin solid films, **494** (1-2) (2006), 98-104.

[19] R. MAALOUF, A. SOLDATKIN, O. VITTORI, Y. SAIKALI, H. CHEBIB, A.S. LOIR, F. GARRELIE, C. DONNET, N. JAFFREZIC-RENAULT, Materials Science and Engineering: C **26** (2-3), (2006), pp564-567.

[20] N. BENCHIKH, F. GARRELIE, C. DONNET, K. WOLSKI, R.Y. FILLIT, F. ROGEMOND, J.L. SUBTIL, J.N. ROUZAUD, J.Y. LAVAL, Surface and Coatings Technology **200** (22-23), (2006), pp 6272-6278

[21] T. KATSUNO, C. GODET, A.-S. LOIR, F. GARRELIE, Journal of Non-Crystalline Solids, **352**(9-20) (2006), pp 1421-1424.

[22] R. MAALOUF, H. CHEBIB, Y. SAIKALI, O. VITTORI, M. SIGAUD, F. GARRELIE, C. DONNET AND N. JAFFREZIC-RENAULT, Talanta **72** (2007), 310-314.

[23] M. GUILLERMIN, F. GARRELIE, N. SANNER, E. AUDOUARD, H. SODER, Applied Surface Science **253** (2007), 8075-8079

[24] F. GARRELIE, N. BENCHIKH, C. DONNET, R.Y. FILLIT, J.N. ROUZAUD, J.Y. LAVAL, V. PAILLERET, Applied Physics A **90** (2008) 211-217

[25] A. SIKORA, A. BERKESSE, O. BOURGEOIS, J.-L. GARDEN, C. GUERRET-PIECOURT, A.-S. LOIR, F. GARRELIE, C. DONNET, à paraître dans Applied Physics A 2008.

[26] A. SIKORA, A. BERKESSE, O. BOURGEOIS, J.-L. GARDEN, C. GUERRET-PIECOURT, J.N. ROUZAUD, A.-S. LOIR, F. GARRELIE, C. DONNET, à paraître dans Solid State Science 2008, doi : 10.1016/j.solidstatesciences.2008.07.013.

[27] M. GUILLERMIN, C. LIEBIG, F. GARRELIE, R. STOAIN, A.-S. LOIR, E. AUDOUARD, à paraître dans Applied Surface Science 2008, doi:10.1016/j.apsusc.2008.07.207

Revues nationales :

[28] F. GARRELIE, C. GIRAULT, B. ANGLERAUD, C. CHAMPEAUX, A. CATHERINOT, *Annales de Physique*, supplément au n°1/2, vol 22 (1997), C1_123-C1_124.

[29] F. GARRELIE, C. GIRAULT, C. CHAMPEAUX, A. CATHERINOT, *Annales de Physique*, supplément au n°1/2, vol 22 (1997), C1_125-C1_126.

[30] F. GARRELIE, A. CATHERINOT, *Journal de Physique IV* 9 (1999), Pr5_135-Pr5_138.

[31] F. GARRELIE, C. JONIN, A. CATHERINOT, C. CHAMPEAUX, E. BAUBEAU, E. AUDOUARD, P. LAPORTE, *Journal de Physique IV* 11 (2001), Pr7_95.

[32] A.-S. LOIR, F. GARRELIE, C. DONNET, F. GOUTALAND, M. BELIN, J.L. SUBTIL, R. LE HARZIC, F. ROGEMOND, Y. OUERDANE, , P. LAPORTE, *Journal de Physique IV, 108,* (2003).

[33] A.S. LOIR, F. GARRELIE, C. DONNET, J.L. SUBTIL, M. BELIN, B. FOREST, F. ROGEMOND, P. LAPORTE, *Journal de Physique IV*, **127**, 193-197 (2005).

CONFERENCES INVITEES

[34] F. GARRELIE, A. CATHERINOT, Colloque U.V.X. 98, Collonges La Rouge, 6-9 Octobre 1998.

[35] F. GARRELIE, Intersurface, "Congrès international des traitements et revêtements de surface high tech", Saint Etienne, 29&30 janvier 2002

[36] P. LAPORTE, E. AUDOUARD, F. GARRELIE, HPLA'2002, High Power Laser Ablation, Taos (New Mexico), 21-26 avril 2002.

[37] F. GARRELIE, "Elaboration de couches minces par ablation laser femtoseconde", ECOLE "Couches minces de carbone amorphe et nanostructuré (synthèse, caractérisations, applications)", Château du Goutelas (Marcoux, Loire), 2-8 juin 2004.

[38] F. GARRELIE, C. DONNET, "New trends in femtosecond Pulsed Laser Deposition and femtosecond produced plasma diagnostics", HPLA'2006, High Power Laser Ablation, Taos (New Mexico), 8-12 Mai 2006.

[39] F. GARRELIE**, "**Nanostructured materials elaborated by femtosecond pulsed laser deposition"**,** LASERION® 2007, "Microfabrication, nanostructured materials and biotechnology", July 1-6, 2007, Schloss Ringberg/Tegernsee (Allemagne)

[40] F. GARRELIE, C. DONNET, A.-S. LOIR, A. SIKORA, "Couches minces de Diamond-Like Carbon : élaboration et propriétés d'usage", GFEC 2008, Journées scientifiques du Groupe Français d'Etude des Carbones, Chambon sur Lac, France, 31 Mars -3 Avril 2008

BREVET

[41] F. FOURNEL, J. MEZIERE, A. BAVARD, F. PIGEON, F. GARRELIE
«Procédé de nanostructuration de la surface d'un substrat», Brevet européen FRA 0652981 (11 juillet 2007).

COMMUNICATIONS EN CONGRES INTERNATIONAL avec comité de lecture

[42] B. ANGLERAUD, C. GIRAULT, C. CHAMPEAUX, F. GARRELIE, A. CATHERINOT, , e-MRS 1995 Spring Meeting, Strasbourg (France), 22-26 Mai 1995.

[43] F. GARRELIE, J. AUBRETON, C. CHAMPEAUX, A. CATHERINOT, S.P.I.E. Proceedings n° 3404, ALT'97, Advanced Laser Technologies, Limoges, 8-12 Septembre 1997, 351-358.

[44] B. ANGLERAUD, F. GARRELIE, F. TETARD, A. CATHERINOT, , e-MRS 1998 Spring Meeting, Strasbourg (France), 16-19 Juin 1998.

[45] F. GARRELIE, A. CATHERINOT, , e-MRS 1998 Spring Meeting, Strasbourg (France), 16-19 Juin 1998

[46] F. GARRELIE, C. CHAMPEAUX, A. CATHERINOT, *COLA'99, 5th International Conference on Laser Ablation*, Göttingen (Allemagne), 19-23 juillet 1999.

[47] F. GARRELIE, C. JONIN, E. BAUBEAU, E. AUDOUARD, P. LAPORTE, A. CATHERINOT, C. CHAMPEAUX, *CLEO 2000, Conference on Laser and Electro-Optics*, San Francisco, 7-12 Mai 2000.

[48] F. GARRELIE, A.S. LOIR, C. DONNET, F. ROGEMOND, R. LE HARZIC, M. BELIN, E. AUDOUARD, P. LAPORTE, International Conference on Metallurgical coatings and thin films, ICMCTF'2002, San Diego (USA), 22-26 avril 2002.

[49] F. GARRELIE, A.S. LOIR, F. GOUTALAND, R. LE HARZIC, B. ANGLERAUD, Y. OUERDANE, P. LAPORTE, HPLA'2002, High Power Laser Ablation, Taos (New Mexico, USA), 21-26 avril 2002.

[50] A.-S. LOIR, F. GARRELIE, F. GOUTALAND, M. BELIN, R. LE HARZIC, C. DONNET, Y. OUERDANE, F. ROGEMOND AND P. LAPORTE, e-MRS 2002 Spring Meeting, Strasbourg (France), 18-21 Juin 2002.

[51] A.-S. LOIR, F. GARRELIE, C. DONNET, M. BELIN, B. FOREST, F. ROGEMOND AND P. LAPORTE, e-MRS 2003 Spring Meeting, Strasbourg (France), 10-13 Juin 2003.

[52] A.S. LOIR, F. GARRELIE, C. DONNET, F. ROGEMOND, B. FOREST, M. BELIN, P. LAPORTE, International Conference on Metallurgical Coatings and Thin Films, ICMCTF 2003, San Diego, 28 Avril –2Mai 2003.

[53] A.-S. LOIR, F. GARRELIE, C. DONNET, M. BELIN, B. FOREST, F. ROGEMOND, P. LAPORTE, e-MRS 2004 Spring Meeting , Strasbourg (France), 24 – 28 Mai 2004.

[54] N. BENCHIKH, F. GARRELIE, K. WOLSKI, C. DONNET, B. BOUCHET-FABRE , F. ROGEMOND, A.S LOIR, J.L. SUBTIL, e-MRS 2004 Spring Meeting , Strasbourg (France), 24 – 28 Mai 2004.

[55] A.S. LOIR, F. GARRELIE, C. DONNET, F. ROGEMOND, J.L. SUBTIL , B. FOREST, M. BELIN, P. LAPORTE, International Conference on Metallurgical Coatings and Thin Films, ICMCTF 2004, San Diego, 19–23 Avril 2004.

[56] N. BENCHIKH, F. GARRELIE, K. WOLSKI, C. DONNET, R.Y. FILLIT, F. ROGEMOND, J.L. SUBTIL, *International Conference on Metallurgical Coatings and Thin Films*, San Diego (USA) 2 – 6 Mai 2005.

[57] J. FONTAINE, M. BELIN, N. BENCHIKH, F. GARRELIE, C. DONNET, *International Conference on Metallurgical Coatings and Thin Films*, San Diego (USA) 2 – 6 Mai 2005.

[58] N. BENCHIKH, F. GARRELIE, C. DONNET, K. WOLSKI, R.Y. FILLIT, F. ROGEMOND, J.L. SUBTIL, J.N. ROUZAUD, J.Y. LAVAL, e-MRS 2005 Spring Meeting, Strasbourg (France), 31 Mai – 3 Juin 2005.

[59] F. GARRELIE, J.L. SUBTIL, N. BENCHIKH, C. DONNET, A.S. LOIR, C. PAREIGE, E. AUDOUARD, e-MRS 2005 Spring Meeting, Strasbourg (France), 31 Mai – 3 Juin 2005.

[60] C. GODET, T. KATSUNO, F. GARRELIE, A.S. LOIR, *21st International Conference on Amorphous and Nanocrystalline Semiconductors* (ICANS21), Lisbon (Portugal) 5 – 9 Septembre 2005.

[61] F. GARRELIE, N. BENCHIKH, C. DONNET, E. AUDOUARD, 8th International Conference on Laser Ablation, COLA 05, Banff (Canada), 11-16 Septembre 2005.

[62] R. MAALOUF, N. JAFFREZIC-RENAULT, O. VITTORI, M. SIGAUD, Y. SAIKALI, H. CHEBIB, A.-S. LOIR, F. GARRELIE, C. DONNET, T. TAKENO, T. TAKAGI, International Joint Conference of JFSIMS and SMEBA 2005 (Japan-France Seminar on Intelligent Materials and Structures and International Symposium on Smart Materials for Engineering and Biomedical Application), Tokyo et Hakone (Japon), 29-31 Octobre 2005.

[63] N. BENCHIKH, A. ZEINERT, Y.GAGOU, C. DONNET, F. GARRELIE, K. ZELLAMA, A. PAILLERET, F. ROGEMOND, *International Conference on Metallurgical Coatings and Thin Films*, San Diego (USA) 1 – 5 Mai 2006.

[64] N. BENCHIKH, F GARRELIE, C. DONNET, K. WOLSKI, F. ROGEMOND, HPLA'2006, *High Power Laser Ablation*, Taos (New Mexico), 8-12 Mai 2006.

[65] M. GUILLERMIN, A. TISHCHENKO, J.-P. COLOMBIER, F. GARRELIE, E. AUDOUARD. *Plasmonics*, Singapore Décembre 2006.

[66] J. FONTAINE, F. GARRELIE, C. DONNET, C. PAREIGE, M. BELIN, F. ROGEMOND, *International Conference on Metallurgical Coatings and Thin Films*, San Diego (USA) 23-27 Avril 2007.

[67] A. SIKORA, A. BERKESSE, O. BOURGEOIS, J.-L. GARDEN, C. GUERRET-PIECOURT, A.S. LOIR, F. GARRELIE, C. DONNET, *Conférence ITFPC 2007* (Innovations on Thin Films Processing and Characterisation), Nancy, 20-23 Novembre 2007.

[68] A. SIKORA, A. BERKESSE, O. BOURGEOIS, JEAN-LUC GARDEN, C. GUERRET-PIECOURT, A.S. LOIR, F. GARRELIE, C. DONNET, *International Conference on Metallurgical Coatings and Thin Films*, San Diego (USA) 28Avril-2Mai 2008.

[69] A. SIKORA, A. BERKESSE, O. BOURGEOIS, J.-L. GARDEN, C. GUERRET-PIECOURT, J.-N. ROUZAUD, A.-S. LOIR, F. GARRELIE, C. DONNET, e-MRS 2008 Spring Meeting, Strasbourg (France), 26-30 Mai 2008.

[70] M. GUILLERMIN, C. LIEBIG, F. GARRELIE, R. STOAIN, A.-S. LOIR, E. AUDOUARD, e-MRS 2008 Spring Meeting, Strasbourg (France), 26-30 Mai 2008.

ACTIVITES D'ENSEIGNEMENT

J'ai été nommée en 1999 sur un poste de maître de conférences à l'Université Jean Monnet de Saint Etienne en Section CNU 28 (Milieux denses et matériaux). Depuis ma nomination sur ce poste à temps plein, j'ai assuré différents enseignements au département Mesures Physiques de l'IUT de Saint Etienne, que ce soit en 1ère ou 2ème année de DUT ou en Licence Professionnelle Techvimat (Technologie du Vide et Traitement sous Vide des Matériaux) :

- Travaux Pratiques de Physique en 1ère année,
- Cours, Travaux dirigés et Travaux Pratiques en matériaux en 1ère et 2ème année,
- Cours et Travaux dirigés en techniques du vide en 2ème année,
- Cours et Travaux dirigés en matériaux en Licence Professionnelle Techvimat,
- Cours Microscopie électronique en Licence Professionnelle Techvimat,
- Cours et travaux dirigés en plasmas (Physique et caractérisation des plasmas, procédés plasmas) en Licence Professionnelle Techvimat.

J'assure également depuis l'année 2007, 2 heures de formation à l'Ecole Doctorale de Saint Etienne dans le Module " Surfaces : fonctionnalités et usages pour la technologie". J'y effectue une présentation des plasmas et leurs applications aux traitements de surface.

Depuis la rentrée 2008, j'assure également, à la Faculté des Sciences et Techniques de Saint Etienne, 6 heures de cours sur les microscopies électroniques en Master 2 OIV ("Optique, Image, Vision") et 2H de cours sur les procédés plasmas en Master 2 Erasmus Mundus CIMET ("Color in Informatics and MEdia Technology").

Jusqu'à la rentrée 2008, la répartition globale de ces enseignements s'équilibrait assez bien entre les cours, les Travaux Dirigés et les Travaux Pratiques.

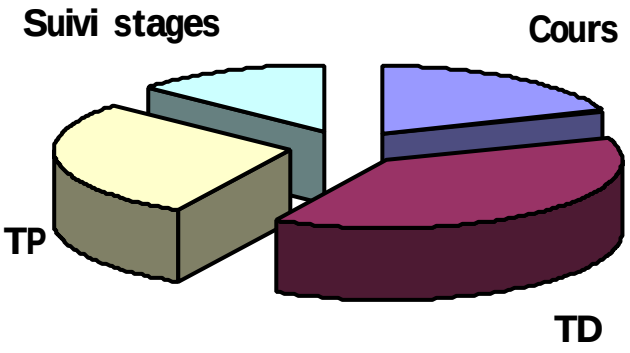

Dès la première année de mon recrutement, on m'a demandé de m'investir dans **l'enseignement des matériaux** au sein du département Mesures Physiques, l'enseignement des matériaux étant peu important par rapport au volume prévu. J'ai donc du mettre en place un nouveau cours et des travaux dirigés pour l'enseignement des matériaux en 2ème année de DUT Mesures Physiques : Structure des matériaux, défauts dans les solides, propriétés mécaniques des matériaux, caractérisation des matériaux.

Parallèlement à ces enseignements, dès mon arrivée au département Mesures Physiques, j'ai assuré la **responsabilité des Travaux Pratiques de Physique** (Mécanique, Thermodynamique, Optique) en 1ère année de DUT. Ces TP représentaient un volume important d'heures (8 à 10 séances de TP par semaine, avec 30 semaines de TP par an). J'ai coordonné le fonctionnement de ces TP pendant 7 ans, en assurant l'organisation des Travaux Pratiques, la liaison entre tous les intervenants et en modifiant et créant un grand nombre de manipulations.

Depuis l'année 2005, j'assure les enseignements de Techniques du vide au département Mesures Physiques (2ème année de DUT). J'ai mis en place un cours et des Travaux dirigés sur les thèmes suivants : Introduction aux techniques du vide, Propriétés des gaz aux basses pressions : Théorie cinétique des gaz, Techniques du vide (Ecoulement des gaz dans une canalisation, Types d'écoulements, Conductance) , Pompes à vide, Mise en œuvre des moyens de pompage, Mesure des basses pressions. J'ai également mis en place une manipulation sur les techniques du vide pour les Travaux Pratiques d'Acquisition du Signal en 2ème année : temps de pompage, application du vide à la génération de plasma, mise en évidence du point triple de l'eau.

Suite à l'arrivée de nouveaux collègues et compte tenu de la modification de la maquette pédagogique, avec une forte augmentation du volume horaire consacré aux matériaux, j'effectue depuis quelques années, la majeure partie de mon service statutaire dans l'enseignement des matériaux.

J'ai été amenée au cours de l'année 2005-2006 à mettre en place quelques manipulations en TP matériaux 1ère année : Structure de la matière (logiciel Cristal), Mesures de viscosité par chute de bille et rhéomètre, Mesures de propriétés mécaniques par essai de traction et microdureté.

Au cours des dernières années, j'ai été amenée à concevoir et mettre en place de nombreuses manipulations en TP matériaux 2ème année : Microscope électronique à balayage (2 manipulations), Microanalyse par sonde EDX (avec achat de la sonde EDX), Structure de la matière (Logiciel Carine), Caractérisation des propriétés mécaniques par essai de traction, Microdureté Vickers, Elaboration de couches minces par pulvérisation cathodique magnétron, Mesures de viscosité par rhéomètre (avec achat du matériel), Contrôle non destructif par ressuage, Analyse thermique par DSC (avec achat du

matériel, et mise en place de 2 manipulations portant sur le diagramme de phase Pb-Sn et l'analyse de polymères), …
J'ai assuré la **responsabilité et la coordination de ces Travaux Pratiques Matériaux** depuis ma nomination en 1999 jusqu'en juillet 2008.

Je participe également à l'enseignement en **Licence Professionnelle Techvimat** à l'IUT de Saint Etienne. J'y assure en particulier les enseignements de Physique des plasmas (cours/TD 15h) et de microscopie électronique et je participe au suivi des alternants dans leurs entreprises. J'ai également mis en place une manipulation sur la caractérisation *in situ* de plasmas de dépôt PVD (pulvérisation cathodique magnétron) par analyse des gaz résiduels et spectroscopie optique d'émission.

Au cours des années universitaires 2006-2007 et 2007-2008, j'ai été **responsable des stages** au sein du département Mesures Physiques, pour l'ensemble des étudiants de 2ème année de DUT (environ 90 étudiants). Cette activité comprend la coordination des offres de stage (environ 80 offres par an), le suivi et le contact avec les entreprises, le suivi de la recherche de stage des étudiants, l'organisation des stages et de soutenances de fin d'année. Cette activité est relativement couteuse en temps de part les nombreux échanges avec les entreprises et les étudiants.

Depuis la rentrée 2008, je suis **co-responsable de la Licence Professionnelle par alternance Techvimat**, avec pour mission, la relation avec les entreprises et le suivi des candidats à l'alternance.

ACTIVITES DE RECHERCHE

L'équipe Laser et Applications, au sein du Laboratoire TSI, dans laquelle j'ai effectué mes activités de recherche a débuté en 1999, année de mon arrivée au Laboratoire, deux nouvelles thématiques de recherche concernant les applications des laser à impulsions ultra-brèves (femtosecondes) : l'application au micro-usinage de tout type de matériaux et la réalisation de couches minces par ablation laser femtoseconde (Pulsed Laser Deposition, PLD), thématique dans laquelle je me suis investie.

Suite au démarrage de l'activité de dépôt de couches par ablation laser femtoseconde sur Saint Etienne, mes premiers travaux ont concerné la réalisation des premières expériences de diagnostic de plasma créé par ablation laser femtoseconde et de réalisation de couches carbone DLC. Des travaux ont également été effectués dans le cadre d'un contrat avec la société Hydrodynamique Et Frottement (Andrézieux Bouthéon, Loire). L'ensemble de ces travaux a été effectué en collaboration avec l'équipe du Professeur Alain Catherinot du Laboratoire SPCTS de Limoges (UMR CNRS 6638), qui a mis à disposition une enceinte de dépôt.

J'ai ensuite conçu et installé une enceinte de dépôt qui a été opérationnelle en septembre 2000. Une thèse sur la réalisation de couches minces de carbone amorphe a d'ailleurs débuté sur cette installation en octobre 2000. Cette thèse, préparée par Anne-Sophie LOIR, concernait le dépôt de couches minces de Diamond-Like Carbon par ablation laser femtoseconde pour application aux biomatériaux. Elle s'effectuait dans le cadre d'un *programme thématique prioritaire de la Région Rhône-Alpes* (2000-2002). Les partenaires du projet étaient le Laboratoire de Tribologie et Dynamique des Systèmes de l'Ecole Centrale de Lyon, le Laboratoire de mécanique des biomatériaux et traitement de surface (LMBTS) de l'Ecole Nationale Supérieure des Mines de Saint Etienne et l'industriel HEF (Hydromécanique et Frottement, Andrézieux Bouthéon, 42). Le projet visait la mise en œuvre de la technique d'ablation laser femtoseconde pour le dépôt de couches minces de carbone. Les objectifs étaient d'abord de maîtriser la technique d'élaboration de couches minces par ablation laser femtoseconde, puis de déterminer les propriétés de ces couches et leur aptitude à répondre aux exigences d'applications biomédicales (revêtement de prothèse de hanche).

A l'issue de ce programme de recherche sur les couches de DLC, deux perspectives se sont offertes :

* Un projet de recherche d'une durée de trois ans (2002-2005), dont j'étais responsable, a été développé dans le cadre du Groupement d'Intérêt Scientifique (GIS) du *programme Matériaux du Massif Central* (P2MC – Matériaux innovants). Ce projet intitulé "Dépôt de couches minces de carbone amorphe par ablation laser" regroupait trois laboratoires (TSI – Saint Etienne, SPCTS – Limoges, Centre SMS – Ecole Nationale Supérieure des Mines de Saint Etienne). L'objectif était d'une part, d'optimiser l'adhérence de ces couches dures, en particulier sur substrat métallique, et

d'autre part, d'établir une comparaison entre l'ablation laser femtoseconde et l'ablation laser nanoseconde en montrant le niveau d'aptitude à l'industrialisation du procédé.

* Un projet intitulé "Couches minces composites nanostructurées, à base carbone, déposées par ablation laser", dont le coordinateur était Christophe Donnet, s'est effectué en relation avec le Laboratoire de Tribologie et Dynamique des Systèmes de l'Ecole Centrale de Lyon et le Laboratoire Sciences des Procédés Céramiques et de Traitement de Surface de l'Université de Limoges dans le cadre des appels d'offres Matériaux du CNRS. Le but de ce projet de recherche interdisciplinaire était de synthétiser par ablation laser nanoseconde et femtoseconde des couches minces dures de composite silicium-carbone, azote-carbone et métal-carbone nanostructurées, d'étudier leurs propriétés physiques (composition, micro- et nanostructure, propriétés mécaniques) et de mettre en évidence les mécanismes d'usure par frottement.
Le travail de thèse de doctorat de Nadia BENCHIKH s'est inscrit dans le cadre de ce projet.

Suite à un regroupement du laboratoire TSI avec le Laboratoire Eurise, et dans le cadre de la nouvelle organisation du laboratoire, devenant le Laboratoire Hubert Curien au 1er janvier 2007, les différentes activités ont été regroupées au sein de deux départements scientifiques, eux-mêmes divisés en deux thématiques. Des projets scientifiques structurants du Laboratoire ont été identifiés au sein de ces différentes thématiques. L'activité "Dépôt de couches minces par ablation laser" a été identifiée comme un projet structurant au sein du Laboratoire, et j'ai été sollicitée pour être la responsable de ce projet. Ce projet relève de la thématique "Interaction laser-matière" au sein du département "Optique & Photonique". L'objectif de ce projet est de mettre en œuvre la technique d'ablation laser (nanoseconde et femtoseconde) pour le dépôt de couches minces, en particulier de matériaux nanostructurées et à leur microstructuration.
Les premiers travaux publiés en la matière ont démontré une originalité très attractive liée à l'emploi du laser femtoseconde : la possibilité, dans certaines conditions, d'élaborer des couches nanostructurées, ce qui n'est pas le cas en général avec un laser nanoseconde. Les processus d'ablation en mode femtoseconde sont à l'origine de la présence, dans le plasma d'ablation, d'espèces précurseurs de ces nanostructures, qui constituent la couche lors de sa croissance. Cette capacité vient à point nommé dans un contexte de recherches internationales sur les couches minces qui s'orientent actuellement de manière durable sur l'élaboration et la caractérisation de couches minces nanostructurées, en raison des combinaisons de propriétés tout à fait remarquables que ces couches peuvent présenter.

Trois thématiques sont identifiés au sein de ce projet :

① L'élaboration de couches minces nanostructurées
② La nanostructuration de matériaux par laser ultra-brefs
③ L'élaboration de couches nanostructurées dopées ou alliées

Parallèlement à ces travaux d'élaboration de couches minces dopées ou non, et afin de corréler les propriétés des couches minces avec le procédé d'ablation laser, nous menons des caractérisations du plasma créé par ablation laser femtoseconde, par imagerie résolue en temps et par spectroscopie optique d'émission.

Les programmes de recherche dans le cadre de ce projet ont fait l'objet de collaborations académiques, avec un soutien financier de l'Université Jean Monnet (BQR 2006 et 2008), de la région Rhône-Alpes (programme CIBLE 2006), et de l'ANR (Projet ANR Blanc "SENSOCARB" et Projet ANR PRECODD "INTEGREAU"). Deux thèses ont débuté sur ce projet, en 2005 (Matthieu Guillermin, ADR MENSR, "*Contrôle du panache plasma pour l'optimisation du traitement des matériaux et étude des mécanismes d'ablation laser femtoseconde*") et 2006 (Aurélien Sikora, ADR Région Rhône-Alpes, "*Elaboration de couches nanostructurées dopées ou alliées pour applications aux capteurs et microcapteurs à base de carbone de synthèse, pour mesures thermiques, chimiques, biologiques et tribologiques*").
De nombreuses collaborations ont été mises en place sur les différents axes de ce projet : Laboratoire de Tribologie et Dynamique des Systèmes (LTDS UMR 5513, Ecole Centrale de Lyon), Laboratoire des Sciences Analytiques (LSA UMR 5180, Université Claude Bernard Lyon 1), Institut Louis Néel (Centre de Recherche sur les Très Basses Températures CRTBT, UPR 5001, CNRS Grenoble), Laboratoire DIOM (Unviversité Jean Monnet), CEA LETI, Cottbus JointLab (Allemagne).

① *Elaboration de couches minces nanostructurées :*

Le procédé PLD femtoseconde est mis en œuvre pour la synthèse de matériaux pour application magnéto-optique (Collaboration avec le Laboratoire DIOM, Projet BQR 2006 de l'Université Jean Monnet). Ces travaux précurseurs donnent une bonne indication sur la possibilité d'obtention de couches minces avec une qualité cristallographique suffisante afin de s'affranchir du recuit post- élaboration nécessaire lors de l'utilisation de tout autre procédé de synthèse. Les premiers résultats sont prometteurs et indiquent des propriétés magnétiques intéressantes pour ces couches minces élaborées, sans recuit, par PLD femtoseconde. Un projet CIBLE a été déposé en 2007 et 2008 auprès de la Région Rhône-Alpes, mais non financé.

Des travaux avaient également été initiés dans le cadre d'une collaboration avec l'Institut des Nanosciences de Paris et le Groupe de Recherche sur l'Energétique des Milieux Ionisés de l'Université d'Orléans afin d'amorcer une étude sur la problématique "*Films "nanocristallins" synthétisés et organisés par ablation laser avec contrôle de leur surface spécifique*". Ces travaux devaient entrer dans le cadre d'un projet ANR PNANO soumis en 2006 mais non financé.

② Nanostructuration de matériaux par laser ultra-brefs*:*

Cette activité concerne plus spécifiquement l'interaction laser ultra-bref – matière avec notamment pour objectif la nanostructuration des matériaux. Une allocation doctorale de recherche MENSR a été attribuée à Matthieu Guillermin sur ce sujet à la rentrée 2005. Une partie des travaux de cette thèse concerne l'étude de la formation de ripples par laser femtoseconde. Une collaboration a également été initiée en 2008 avec Juergen REIF de l'université de Cottbus (Projet BQR 2008 de l'Université Jean Monnet) et une thèse est prévue en cotutelle à la rentrée 2008.

L'autre partie du travail de thèse de Matthieu Guillermin concerne toujours l'interaction laser – matière mais pour l'optimisation de la qualité des couches obtenues par PLD. Pour cela, nous envisageons l'utilisation d'une mise en forme temporelle ("shapping") de l'impulsion laser afin de chosir les chemins thermodynamiques subis par

le matériau et ainsi créer des espèces en phase gazeuse avec des propriétés requises. Cette étude a permis la conception et l'installation d'une mise en forme temporelle de l'impulsion laser femtoseconde et une optimisation de la forme temporelle du faisceau laser à partir des caractéristiques du plasma. Ces développements toujours en cours seront détaillés dans la seconde partie du mémoire de recherche.

Une étude est également en cours en collaboration avec le CEA LETI de Grenoble afin d'obtenir une nanostructuration périodique de la surface d'un substrat avec des périodes typiquement de l'ordre de quelques dizaines de nanomètres (Brevet).

③ *Elaboration de couches nanostructurées dopées ou alliées* :

Cette activité s'inscrit dans le cadre du programme CIBLE obtenu en 2006 auprès de la région Rhône-Alpes dont le coordinateur est Christophe Donnet (Professeur). Ce projet s'est effectué en collaboration avec le Laboratoire de Tribologie et Dynamique des Systèmes (LTDS UMR 5513, Ecole Centrale de Lyon), le Laboratoire des Sciences Analytiques (LSA UMR 5180, Université Claude Bernard Lyon 1), et l'Institut Louis Néel (ex- Centre de Recherche sur les Très Basses Températures CRTBT, UPR 5001, CNRS Grenoble). Ce projet faisait suite à des travaux préliminaires effectués en collaboration avec le Laboratoire des Sciences Analytiques de Lyon (N. Jaffrezic), sur l'étude de couches DLC pour capteurs électrochimiques et enzymatiques. Il s'agissait d'explorer et d'élargir significativement les propriétés fonctionnelles de deux formes génériques « modèles » de carbone, les couches minces Diamond-Like Carbon (DLC) dopé ou allié synthétisées par PLD femtoseconde et nanoseconde, et les couches de diamant dopé, par des caractérisations structurales et une investigation des propriétés électriques, thermiques et tribologiques. Ces connaissances acquises devront être ensuite appliquées à la réalisation des capteurs spécifiques en validant les approches choisies par des tests de fonctionnement en situation réelle. Un financement de thèse a été obtenu auprès de la région Rhône-Alpes en octobre 2006 pour Aurélien Sikora.

A l'issue de ce programme de recherche, deux projets ANR sont en cours depuis 2007:

- un projet ANR Blanc "SENSOCARB", dont le Laboratoire coordinateur est le Laboratoire Hubert Curien (Responsable scientifique : Christophe Donnet). Ce projet s'effectue en collaboration avec le Laboratoire de Tribologie et Dynamique des Systèmes (LTDS UMR 5513, Ecole Centrale de Lyon) et l'Institut Louis Néel (ex-Centre de Recherche sur les Très Basses Températures CRTBT, UPR 5001, CNRS Grenoble). L'objectif de ce projet est de proposer l'utilisation de couches minces de DLC élaborées par PLD femtoseconde et nanoseconde pour les capteurs thermiques, nano-calorimétriques et tribologiques.

- un projet ANR PRECODD "INTEGREAU", dont le Laboratoire coordinateur est le Laboratoire des Sciences Analytiques (Responsable scientifique : Nicole Jaffrezic). Ce projet va s'effectuer en collaboration avec de nombreux industriels (SUEZ-ENVIRONNEMENT, CEMAGREF-OTHU, SCA Solaize, Société ELTA). L'objectif est de développer des capteurs chimiques à base de carbone pour fabriquer des microélectrodes pour des chaînes analytiques portables sur site, dans le but d'effectuer de la détection de polluants.

ACTIVITES D'ENCADREMENT

ACTIVITES D'ENCADREMENT DOCTORAL :
PARTICIPATION A LA CO-DIRECTION OU L'ENCADREMENT DE THESES:

* Anne-Sophie LOIR : Co-direction de thèse (dérogation Conseil Scientifique de l'Université)

Directeur : Pr François ROGEMOND

Titre : " Elaboration de couches minces de carbone par ablation laser femtoseconde pour application aux biomatériaux implantables"

Date début : 1 Octobre 2000

Soutenue le : 13 Février 2004

Financement : P*rogramme thématique prioritaire de la Région Rhone-Alpes* (2000-2002).

Partenaires du projet : Laboratoire de Tribologie et Dynamique des Systèmes de l'Ecole Centrale de Lyon, Laboratoire de Mécanique des Biomatériaux et Traitement de Surface (BMTS) de l'Ecole Nationale Supérieure des Mines de Saint Etienne et l'industriel HEF (Hydromécanique et Frottement, Andrézieux Bouthéon, 42).

* Nadia SBAI BENCHIKH : *Participation à l'encadrement (50 %)*

Directeur : Pr Christophe DONNET, *co-directeur* : Kristoph WOLSKI (ENSMSE)

Titre : " Couches minces nanostructurées de carbone dopées ou alliées : Elaboration par ablation laser femtoseconde et caractérisations"

Date début : 1 Octobre 2002

S*outenue le* : 10 Novembre 2005

Financement : Bourse MENRT

Partenaires du projet : Centre SMS de l'Ecole Nationale Supérieure des Mines de Saint Etienne (ENSMSE), LPMC de l'Université d'Amiens, Ecole Nationale Supérieure de Paris, Ecole Supérieure de Physique Chimie de Paris, Laboratoire de Tribologie et Dynamique des Systèmes de l'Ecole Centrale de Lyon.

* Matthieu GUILLERMIN : Co-direction de thèse (dérogation Conseil Scientifique de l'Université)

Directeur : Pr Eric AUDOUARD

Titre : " Contrôle du panache plasma pour l'optimisation du traitement des matériaux et étude des mécanismes d'ablation laser femtoseconde "

Date début : 1 Octobre 2005

S*outenance prévue* : Mars 2009

Financement : Bourse MENRT

Partenaires du projet : ILT (Institute für LaserTechnische, Aachen (Allemagne)

* Aurélien SIKORA : Co-direction de thèse (dérogation Conseil Scientifique de l'Université)

Directeur : Pr Christophe DONNET

Titre : " Elaboration et caractérisation de couches de Diamond Like Carbon dopées ou alliés pour éléments actifs de capteurs thermiques et (nano)calorimétriques "

Date début : 1 Octobre 2006

Soutenance prévue : Septembre 2009

Financement : P*rogramme CIBLE de la Région Rhone-Alpes* (2006-2009).

Partenaires du projet : Laboratoire de Tribologie et Dynamique des Systèmes (LTDS UMR 5513, Ecole Centrale de Lyon), Laboratoire des Sciences Analytiques (LSA UMR 5180, Université Claude Bernard Lyon 1), Institut Louis Néel (Centre de Recherche sur les Très Basses Températures CRTBT, UPR 5001, CNRS Grenoble)

* Mourad BOUNHALLI : *Participation à l'encadrement (50 %)*

Directeur : Pr Florent PIGEON, *co-directeur* : Juergen REIF (Cottbus JointLab, Allemagne)

Titre : " Etude des mécanismes de formation des ripples en régime femtoseconde"

Date début : 1 Octobre 2008

Soutenance prévue : 2011

Financement : Bourse MENRT

Partenaire du projet : Université technologique de Cottbus

ACTIVITES D'ENCADREMENT : MASTER ET TECHNICIENS

*** Razika MANSOURI** Diplôme : **Master 1 OIV Saint Etienne**
Titre: Elaboration par ablation laser femtoseconde, de DLC dopé au soufre pour des applications tribologiques
Date début : 01/03 /2006 Date fin : 30/06/2006 % encadrements :50 %
Noms et % des co-directeurs : Christophe DONNET – 50 %

* **Jonathan ARSENAULT-ROY** Diplôme : **DUT (Quebec – Canada)**
Titre: Installation et mise en place d'un spectromètre pour analyse de plasma
Date début : 24/05/2005 Date fin : 29/07/2005 % encadrements :100 %

*** Mario LANDRY** Diplôme : **DUT (Quebec – Canada)**
Titre: Dépôt de couches minces par ablation laser ; Mise en place du pilotage par ordinateur d'un système multi-cibles pour application aux dépôts multi-couches.
Date début : 01/05/2002 Date fin : 31/07/2002 % encadrements :100 %

IMPLICATION COLLECTIVE RESPONSABILITES ADMINISTRATIVES

Participation à l'organisation de conférences :

Dans le cadre du GDR CNRS 2449 ("Carbone amorphe et nanostructuré en couches minces", Responsable Christian Godet), une école thématique "Couches minces de carbone amorphe ou nanostructuré : synthèse, caractérisation, applications" a été organisée du 2 au 8 juin 2004. J'étais membre du Conseil scientifique de cette école.

J'ai été membre du comité d'organisation de la conférence UVX 2004 (7ème Colloque sur les Sources Cohérentes et Incohérentes UV, VUV et X : Applications et développements récents, 7-11 juin 2004, Saint Etienne).

J'ai été co-organisatrice, avec Eric Audouard, des journées "Modélisation des procédés laser ultra-brefs", les 21 et 22 Mars 2005 à Saint Etienne, dans le cadre du réseau Femto et dans le cadre de la Formation Permanente du CNRS.

Implication collective :

- Représentante du laboratoire TSI au GDR CNRS 2449 ("Carbone amorphe et nanostructuré en couches minces", Responsable Christian Godet)
- Membre titulaire de la Commission de spécialistes (Sections CNU 28/30) et membre titulaire de la Commission de spécialistes (Section CNU 31) de l'Université Jean Monnet.
- Membre titulaire élue du Conseil du Laboratoire TSI du 1er janvier 2003 au 31 décembre 2006.
- Membre titulaire élue du Conseil d'administration de l'IUT depuis Novembre 2002.
- Activité de "reviewing" pour les journaux *Applied Physics A*, *Applied Surface Science*, *Journal of Thermal Spray Technology* et *Journal of Laser Micro/NanoEnginnering*.

Responsabilités administratives :

- Responsable des stages au sein du département Mesures Physiques de l'IUT de Saint Etienne au cours des années 2006-2007 et 2007-2008.

- Co-responsable de la licence professionnelle Techvimat (Technologie du Vide et Traitement sous Vide des Matériaux) à compter de la rentrée 2008

- Coordination du Projet "Ablation Laser pour le dépôt de couches minces" au sein du Laboratoire Hubert Curien depuis le 1er janvier 2007.

MEMOIRE DE RECHERCHE

Ce mémoire fait état de mon activité de recherche depuis mon affectation sur un poste titulaire d'enseignant-chercheur. Il se divise en deux parties : une première partie relative à mes travaux de recherche depuis septembre 1999 jusqu'à maintenant et une seconde partie relative aux développements futurs et perspectives qui peuvent s'offrir à l'utilisation des lasers femtosecondes pour le dépôt de couches minces. Il y sera notamment question de l'avenir de la thématique développée au cours de ces 9 années de recherche.

1ère Partie

L'ablation laser femtoseconde pour le dépôt de couches minces

Cette première partie de mon mémoire dresse un bilan de mes travaux effectués au cours de ces 9 années au Laboratoire Hubert Curien. Les études retenues montrent l'intérêt de l'utilisation d'un laser femtoseconde pour synthétiser des couches minces ou des nanoparticules. J'essaierai de mettre en avant les intérêts des développements que nous avons effectués au Laboratoire Hubert Curien, en comparant évidemment avec les développements liés à la PLD utilisant les lasers nanoseconde. Cette communauté scientifique "PLD nanoseconde", très large et parallèle à la communauté "PLD femtoseconde", a marqué mes premiers pas dans le monde de la recherche : je continue à suivre avec grand plaisir et intérêt tous ses développements. Il est en effet primordial, je pense, de ne pas chercher à utiliser un laser femtoseconde dans le seul but d'utiliser un laser femtoseconde, pour le coté "novateur" du travail, mais bien pour se démarquer des possibilités du laser nanoseconde. Cette démarche a constitué, je l'espère, le fil conducteur de mon travail de recherche.

A l'intérieur de cette première partie, les principaux résultats sont exposés. L'ensemble des résultats relatifs à chaque étude sont détaillés dans les publications citées et jointes dans la troisième partie de ce manuscrit. Les références autres que les notres sont indexées en bas de page et ne sont pas exhaustives. Cette liste de référence complète la nombreuse liste présente dans les publications reproduites en fin de ce rapport.

1. L'ablation laser

L'objet de ce paragraphe n'est pas de faire une présentation exhaustive des travaux présentés dans la littérature en ablation laser mais bien plutôt de situer mon travail dans ce domaine.

L'ablation laser consiste à irradier un matériau par un laser, le plus souvent impulsionnel. Il s'en suit sur le matériau des modifications de nature très variables. Le domaine qui nous intéresse ici est celui où on a ablation de matière sous forme d'un plasma, plasma qui peut être ensuite collecté pour former une couche mince (**Figure 1**).

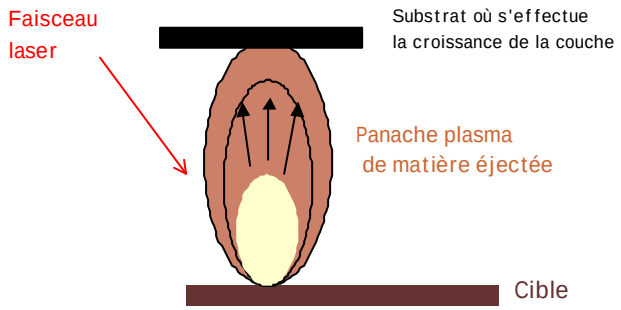

Figure 1 : principe du dépôt de couches minces par ablation laser.

De nombreux travaux ont été consacrés à l'utilisation d'un laser pour synthétiser des couches minces[1]. Toutes sortes de types de films et d'applications ont été explorés, la technique ayant acquis ses lettres de noblesse avec les couches oxydes supraconductrices dans les années 1990.

Ma formation d'origine (thèse et ATER au Laboratoire SPCTS) m'avait conduit à utiliser des laser excimères de durée d'impulsion nanoseconde. Dès mon arrivée au Laboratoire TSI, j'ai utilisé des lasers de durée d'impulsion femtoseconde, pour lesquels la technologie et les procédures expérimentales sont très différentes. Depuis quelques années, nous disposons également d'un laser excimère que j'ai mis en place, nous permettant ainsi d'effectuer une comparaison détaillée des processus mis en jeu.

[1] D.B. Chrisey and G.K. Hubler. « Pulsed laser deposition of thin films ». John Wiley & Sons, Inc., 1994. 613 pages. ISBN 0-471-59218-8.

Dans le cadre de mes activités de recherche, je me suis investie dans la synthèse et la caractérisation de couches minces : couches minces de Diamond-Like Carbon (DLC) (Thèse Anne-Sophie LOIR), couches minces de DLC dopées par des métaux (Thèse Nadia BENCHIKH) ou dopées par du bore (Thèse Aurélien SIKORA), couches minces d'oxydes magnétique (YIG), synthèse de nanoparticules...

Je me suis également impliquée dans la caractérisation du plasma formé lors de l'interaction laser – matière (Thèses Anne-Sophie LOIR et Matthieu GUILLERMIN). Mes premiers pas dans la recherche ont relevé de cette thématique, puisque mon travail de thèse concernait la simulation du plasma créé par ablation laser nanoseconde. Ce type de caractérisation apparaît néanmoins primordial si nous voulons franchir un saut technologique dans l'utilisation des lasers pour le dépôt de couches minces, comme nous le verrons dans la dernière partie de ce mémoire.

Enfin, je m'implique également dans l'interaction laser – matière. Cette étape est en effet primordiale dans le procédé de dépôt, et mes travaux actuels tendent à renforcer cette activité au travers de la thèse de Matthieu GUILLERMIN sur la mise en forme temporelle d'impulsions laser femtosecondes. Cette thématique d'interaction laser – matière va également être développée dans la cadre d'une thèse en cotutelle avec l'Université technologique de Cottbus qui va débuter en octobre 2008 (Thèse Mourad BOUNHALLI) sur la compréhension de la formation des ripples par laser femtoseconde (nanostructures périodiques induites par l'irradiation).

2. Synthèse de couches minces de Diamond-Like Carbon

De nombreux travaux ont été effectués depuis plus de dix ans sur l'élaboration de couches minces de Diamond-Like Carbon (DLC) par ablation laser. L'appellation DLC regroupe en fait, une large variété de matériaux, hydrogénés ou non, présentant des taux très variables de carbone hybridé sp^3, comme reporté sur le diagramme ternaire présenté par Robertson[2] (**Figure 2**). Les DLC possèdent ainsi une grande diversité de compositions chimiques, donnant lieu à des propriétés différentes, se rapprochant plus ou moins de celles du diamant.

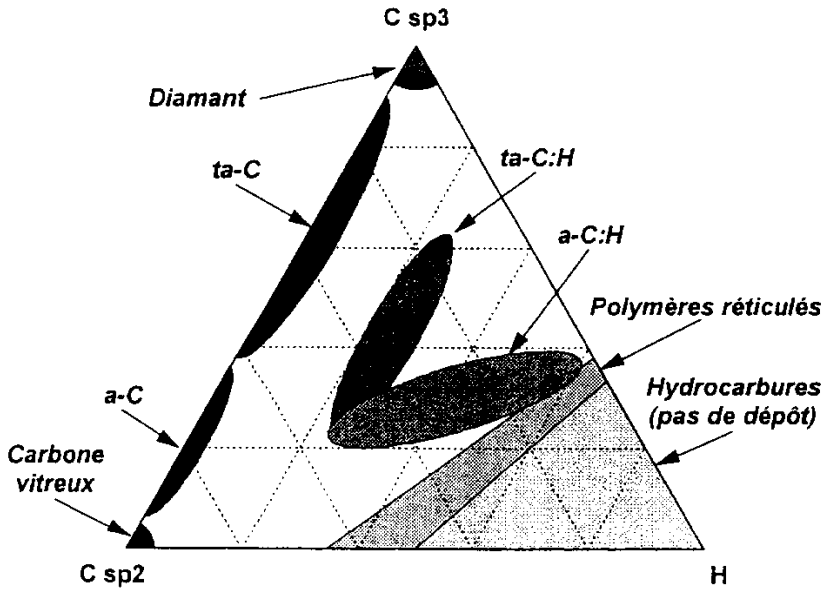

Figure 2 : Diagramme ternaire proposé par Robertson

Les lasers utilisés pour la synthèse de DLC sont des lasers impulsionnels, le plus souvant excimères ou YAG éventuellement triplé ou quadruplé[3,4,5]. Les couches, élaborées à température ambiante, présentent en général un fort taux d'hybridation

[2] J. Robertson, "Diamond-like amorphous carbon", *Materials Science and Engineering Reports,* 37(4-6) (2002) 129-281.
[3] A.A.Voevodin and M.S. Donley, Surf. Coat. Technol. **82** (1996), 199-213.
[4] M. Bonelli, A.P. Fioravanti, A. Miotello and P.M. Ossi, , Europhys. Lett. **50** (4) (2000), 501-506.
[5] J. C. Orlianges, C. Champeaux, A. Catherinot, Th. Merle, B. Angleraud *Thin Solid Films*, *453-454*, *(2004) 285-290.*

sp^3, une dureté élevée (40- 80 GPa) mais des contraintes résiduelles élevées. Par ailleurs, on note l'existence de particules de taille micométrique, altérant la qualité de l'état de surface. Plusieurs voies ont été explorées pour limiter le nombre et la taille de ces particules, dont l'utilisation de lasers de courte longueur d'onde, la défocalisation du laser, l'emploi de shutter mécanique, l'ablation par double faisceau laser croisés ou encore l'utilisation de cibles de carbone amorphe[1,5,6].

Au fur et à mesure des développements de lasers de plus courte durée d'impulsion, des essais ont été effectués pour synthétiser un matériau carboné de bonne qualité, avec pour objectifs principaux de réduire la densité de particules de taille micronique et d'augmenter le taux d'hybridation sp^3. Les premiers développements en terme de synthèse de couches minces par ablation laser femtoseconde ont concerné l'élaboration de matériaux "métastables" pour lesquels on pouvait espèrer que le caractère fortement énergétique de l'interaction laser-matière conduirait à la structure recherchée. Ainsi, des travaux ont été initiés sur l'élaboration de couches minces de Diamond-Like Carbon par ablation laser femtoseconde[7,8].

2.1. Couches minces de DLC pour application biomédicale

Nos travaux sont inscrits dans cette logique, avec la mise au point d'une installation permettant le dépôt de DLC par ablation laser femtoseconde (**Figure 3**). Les objectifs étaient d'abord de maîtriser la technique d'élaboration de couches minces par ablation laser femtoseconde, de déterminer les propriétés de couches minces de DLC, d'examiner leur application potentielle au domaine biomédical et leur aptitude à répondre aux exigences de l'application prothèse. En quelques mots, l'objectif était clairement d'obtenir des couches minces de DLC, adhérente sur acier inox sans sous-couche d'accrochage, et présentant des caractéristiques mécaniques et tribologiques

[6] J.C. Orlianges, Thèse de l'Université de Limoges, 2003.

[7] F. Qian, V. Craciun, R.K. Singh, S.D. Dutta and P.P. Pronko, J. Appl. Phys. 86 (4) (1999), 2281-2280.

[8] P.S. Banks, L. Dinh, B.C. Stuart, M.D. Feit, A.M. Komashko, A.M. Rubenchik, M.D. Perry and W. McLean, Appl. Phys. A 69 [Suppl.] (1999), S347-S353.

compatibles avec un revétement de prothèse de hanche, à savoir une grande dureté et des coefficients de frottement et d'usure les plus faibles possibles.

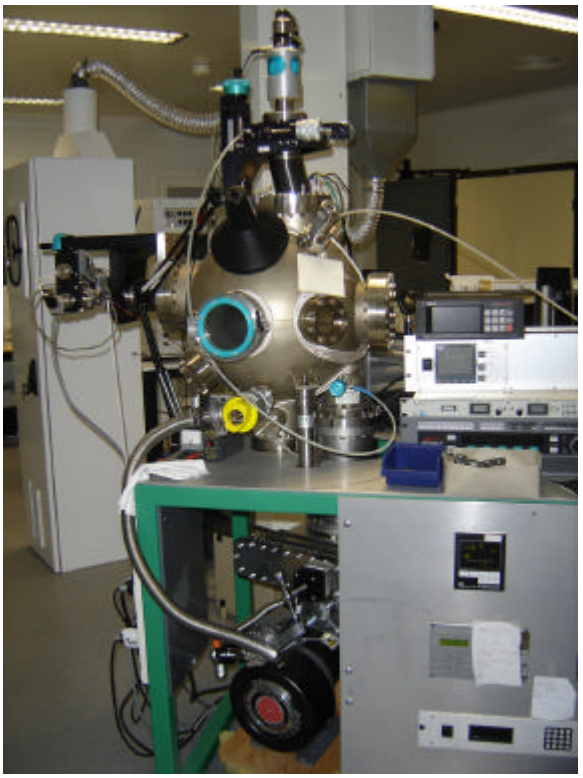

Figure 3 : Dispositif expérimental mis en place au Laboratoire Hubert Curien

Dans un premier temps, des couches minces ont été élaborées puis caractérisées en fonction des différents paramètres du procédé, le principal étant la fluence laser. Ces travaux ont fait l'objet de la thèse d'Anne-Sophie LOIR. Ces premiers travaux sont détaillés dans la publication [10] (F. GARRELIE et al, *Surface and Coatings Technology*, **163-164** (2003), 306.). Nous ne rappellerons ici que les résultats majeurs.

L'état de surface de ces couches minces de DLC est un paramètre critique pour le revêtement de prothèse de hanche dans la mesure où le rugosité doit répondre à une norme[9], à savoir être inférieure à 0,05 µm. L'utilisation d'un laser femtoseconde a

[9] Norme internationale ISO 7206-2:1996(F), « Implants chirurgicaux–Prothèses partielles et totales de l'articulation de la hanche– Partie 2 : Surfaces articulaires constituées de matériaux métalliques, céramiques et plastiques ».

revêtu ici tout son intérêt dans la mesure où les résultats escomptés pour l'utilisation d'un laser femtoseconde étaient une réduction voire disparition des particules de taille sub-micronique ("escarbilles") présentes lors du procédé de dépôt PLD. Les résultats obtenus ont confirmé ces attentes, dans la mesure où des " escarbilles" sont bien présentes mais en nombre et taille limités par rapport aux dépôts obtenus en PLD nanoseconde. Des effets thermiques étaient suggérés comme pouvant être à l'origine de la présence de ces escarbilles : l'utilisation d'un laser femtoseconde, diminuant sensiblement les effets thermiques au sein du matériau irradié semble donc réduire significativement cet inconvénient du process PLD nanoseconde. La rugosité des dépôts ainsi réalisés est de l'ordre du nanomètre, tout à fait compatible avec l'application visée.

Les contraintes résiduelles ont été estimées par la méthode de la flèche, à partir de la courbure du substrat avant et après dépôt, en utilisant la formule de Stoney. Une augmentation de la fluence laser, dans la gamme 1 à 5 J/cm², conduit à une augmentation des contraintes de –0,8 à –2,8 GPa. Ces valeurs, relativement faibles pour des couches minces de DLC déposées par PLD, peuvent être expliquées par un flux de particules plus faible en PLD femtoseconde qu'en PLD nanoseconde, et une probable relaxation des contraintes due au bombardement de la couche en croissance par les ions énergétiques du plasma créé par le laser femtoseconde[10].

La qualité structurale des couches de DLC notamment en terme de taux d'hybridation sp^3 a été estimée par XPS, Raman et XANES. A partir du spectre XANES (**Figure 4**), et en utilisant une méthode de déconvolution conventionelle[11], nous pouvons déduire un taux d'hybridation sp^3 voisin de 70 %.

Un des principaux avantages des couches minces de DLC est la combinaison entre les propriétés mécaniques remarquables (grande dureté) et un comportement

[10] J. Perrière, E. Millon, W. Seiler, C. Boulmer-Leborgne, V. Craciun, O. Albert, J.C. Loulergue and J. Etchepare, J. Appl. Phys. 91 (2) (2002), p 690-696.
[11] D.L. Pappas, K.L. Saenger, J.Bruley, W. Krakow, J.J. Cuomo, T. Gu and R.W. Collins, J. Appl. Phys **71** (11) (1992), 5675-5684.

tribologique intéressant (faibles coefficient de frottement et d'usure). Nos couches ont également été caractérisées d'un point de vue mécanique et tribologique. Les valeurs de dureté et de module d'élasticité obtenues par nanoindentation sont reportées dans le **Tableau 1**.

Ces valeurs de dureté restent modestes pour un DLC non hydrogéné, élaboré par PLD. En effet, certaines couches élaborées par PLD nanoseconde peuvent atteindre des valeurs de dureté de 70 GPa. Cependant, la dureté évolue fortement en fonction du taux d'hybridation sp^3 entre 70 et 90 % sp^3 et nos valeurs semblent correspondrent au taux d'hybridation sp^3 déduit des mesures XANES, comme reporté dans la **Figure 5**.

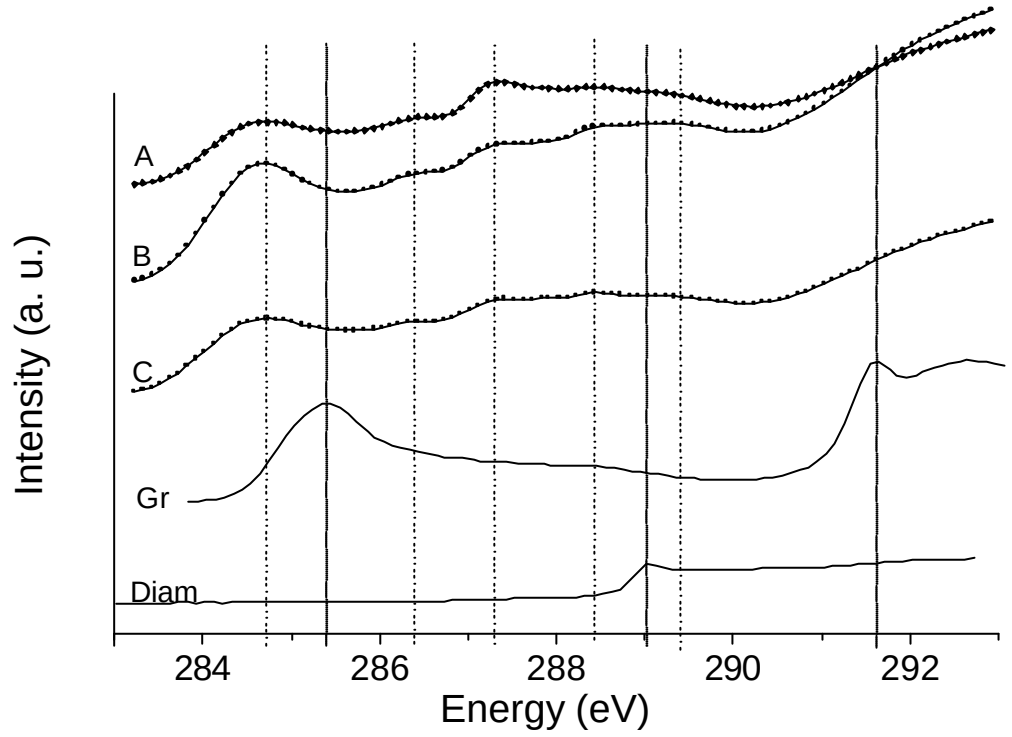

Figure 4 : Spectre XANES du seuil K du Carbone 1s des films de DLC déposés à une fluence laser de 1,4 ; 2,8 et 5,2 J/cm² et spectres de référence du graphite (Gr) et du diamant déposé par CVD (Diam)

Fluence laser ($J.cm^{-2}$)	1,4	2,8	5,2
Nanodureté (GPa)	$20,0 \pm 2,3$	$25,0 \pm 2,5$	$18,0 \pm 1,3$
Module d'Young (GPa)	240 ± 29	260 ± 10	210 ± 13

Tableau 1 : Valeurs de dureté et de Module d'Young des films réalisés dans des conditions de fluences laser différentes.

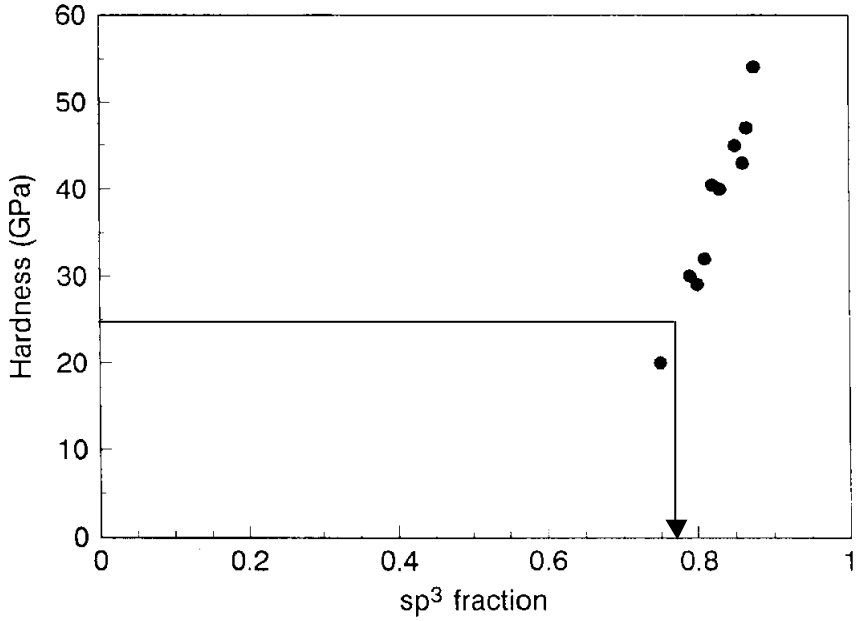

Figure 5 : Evolution de la dureté des couches minces de DLC non hydrogéné en fonction du taux de liaisons sp^3 (à partir de [12])

Afin d'étudier les propriétés anti-frottement et anti-usure des films déposés par ablation laser femtoseconde, des essais tribologiques ont été réalisés au LTDS de l'Ecole Centrale de Lyon. Quelle que soit la fluence laser, les coefficients de frottement moyens obtenus (μ) sont de l'ordre de 0,1 sans variation significative sur l'ensemble des cycles. Pour toute la gamme de fluence laser analysée (1-5 J/cm^2), les coefficients d'usure se situent dans la gamme 10^{-8} $mm^3.N^{-1}.m^{-1}$ (pour une pression de 0,5 GPa). La fluence laser n'affecte donc pas le coefficient d'usure du matériau déposé. Il faut noter

[12] Shi Xu, D. Flynn, B.K. Tay, S. Prawer, K.W. Nugent, S.R.P. Silva, Y. Lifshitz and W.I. Milne, Philo. Mag. B **76** (3) (1997), 351-361.

que le volume d'usure est extrêmement faible. Pour donner un ordre de grandeur de l'usure associée, une telle usure correspond à 0,5 nm pour 1000 cycles (soit 25 nm pour 50 000 cycles). Un revêtement est considéré comme un bon lubrifiant solide pour un coefficient de frottement $\mu < 0,3$ et un coefficient d'usure $K < 10^{-6}$ $mm^3.N^{-1}.m^{-1}$. Nous pouvons donc classer les couches de DLC élaborées par PLD femtoseconde parmi les matériaux à haute résistance à l'usure ce qui a constitué un résultat significatif concernant l'application prothèse de hanche, finalité de ce travail.
Notons également que les conditions de test sur les DLC déposés étaient dix fois plus sévères que dans les conditions naturelles (pression exercée par le corps humain sur une prothèse de hanche estimée à 50 MPa).

Les potentialités de ces couches minces de DLC pour le revêtement de prothèses de hanche étaient clairement établies à partir de dépôts standarts sur substrats en silicium. Notre objectif a ensuite été de déposer ce même type de matériau sur substrat biocompatible (acier inox 316L), sur surface de "grande taille" non plane, avec une bonne adhérence.

Ces travaux sont détaillés dans l'article [13] (A.-S. Loir et al., *Surface and Coatings Technology* 188-189 (2004), 728-734

Un point clé de cette étude a concerné la possibilité de déposer ces couches minces de DLC sur substrat acier inox poli miroir sans sous-couche d'accrochage, afin de s'affranchir de problèmes d'usure et de bio-compatibilité de cette sous-couche. Nous avons mis en place un système de décapage *in situ* du substrat par plasma d'argon avant dépôt de la couche de DLC. Une photographie du plasma est reportée sur la **Figure 6**. Ces conditions de décapage n'altèrent pas la rugosité du substrat et sont donc compatibles avec l'application visée. L'adhérence des dépôts a quant à elle été grandement améliorée, comme reporté sur la **Figure 7**. Les valeurs d'adhérence obtenues sont supérieures ou égales à 45 MPa, dans la mesure où les tests d'ahérence

(collage de plot puis essai de traction selon la norme[13]) ont conduit à une rupture cohésive au niveau de la colle et non du dépôt.

Figure 6 : Photographie optique du plasma d'argon crée lors du décapage ionique in situ d'une tête sphérique de prothèse de hanche

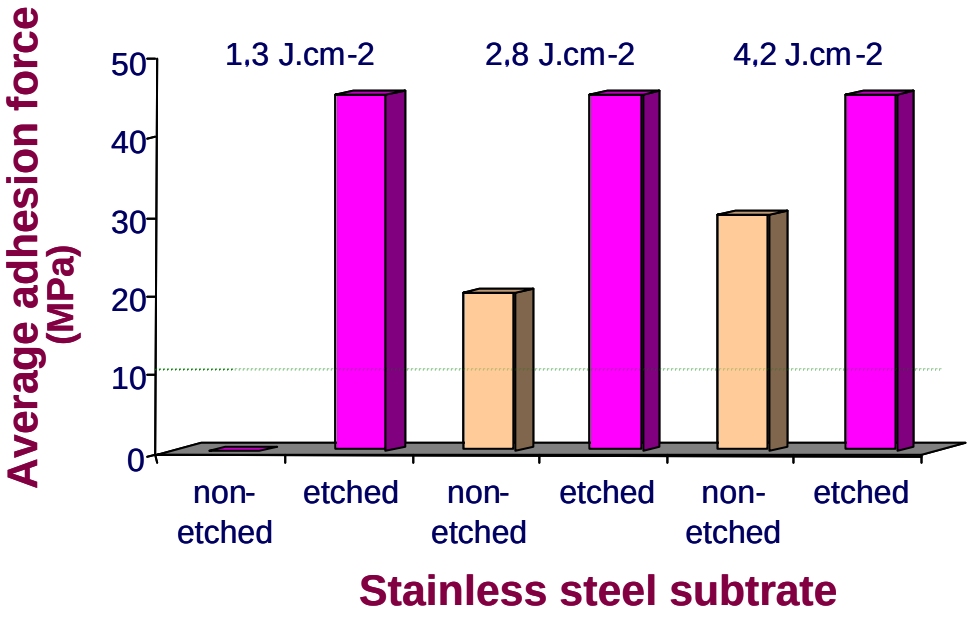

Figure 7 : *Adhérence des films de DLC élaborés sur des substrats acier inox non décapés ou décapés durant 5 minutes préalablement au dépôt*

[13] Norme française AFNOR NF S 94-072, Novembre 1998, Matériaux pour implants chirurgicaux « Détermination de l'adhérence en traction des revêtements phosphocalciques pour applications biomédicales ». ISSN 0335-3931.

Compte tenu de la taille d'une prothèse de hanche (diamètre 22,2 mm) et du caractère très directionnel du procédé de dépôt par PLD, nous avons mis en place un système permettant le dépôt sur grande dimension, par dépôt hors-axe et rotation de la pièce à revêtir.

Nous avons finalement pu déposer sur pièce réelle, à savoir une tête de prothèse de hanche, une couche mince de DLC d'épaisseur environ 150 nm, homogène en épaisseur, adhérente sans sous-couche d'accrochage (**Figure 8**).

a) tête sphérique vierge b) tête sphérique revêtue d'un film de DLC après un décapage ionique *in situ*

Figure 8 : Tête sphérique de prothèse de hanche (diamètre = 22,2 mm) avant et après dépôt d'un film de DLC.

L'utilisation du procédé PLD pour synthétiser des couches minces de DLC permet également de réaliser les dépôts sur des matériaux thermiquement sensibles (polymères), compte du dépôt à température ambiante et de l'élévation de température négligeable au cours du dépôt. Nous avons ainsi déposer une couche mince de DLC sur du poléthylène à haut poids moléculaire (UHMWPE), qui sert de matériau constituant pour la cupule de prothèse de hanche.

2.2. Comparaison PLD femtoseconde / PLD nanoseconde

De part mon cursus en recherche (travaux en ablation laser nanoseconde pendant la thèse et l'ATER au SPCTS à Limoges), je veille d'un regard interéssé sur les travaux faits en PLD nanoseconde, y compris bien sûr pour le dépôt de DLC. Compte tenu par ailleurs de la complexité et du coût d'un laser femtoseconde, qui est beaucoup moins "presse-bouton" qu'un laser nanoseconde, et afin d'apporter des éléments de compréhension sur les phénomènes mis en jeu, il est intéressant de comparer la qualité des couches élaborées par ces deux procédés.

De nombreux travaux ont été consacrés à la comparaison entre les couches minces élaborées par PLD nanoseconde et femtoseconde[10,14]. Lors de l'utilisation d'un laser femtoseconde, la qualité cristalline apparaît le plus souvent de moins bonne qualité, avec une plus grande mosaïcité, des grains de taille plus faible, même si une température de substrat plus faible suffit parfois à cristalliser la couche[15]. On note également une quantité de défauts plus importante, sans doute corrélée aux plus faibles valeurs de contraintes résiduelles mesurées avec les couches élaborées par PLD femtoseconde.

En collaboration avec Christian Godet (LPICM, Palaiseau), nous avons comparé, en terme de propriétés optiques, les couches minces de DLC élaborées par PLD femtoseconde au Laboratoire Hubert Curien à Saint Etienne et par PLD nanoseconde au SPCTS à Limoges. Ces travaux sont détaillés dans l'article [16] (T. KATSUNO et al., *Applied Physics A* **81**, (3) (2005), 471-476).

L'objectif était de caractériser les propriétés optiques de ces couches par ellipsométrie spectroscopique et de corréler ces propriétés avec les caractéristiques de l'interaction laser – matière et donc les caractéristiques du plasma d'ablation.

Pour cela, une modélisation de la structure du film en différentes sous-couches d'épaisseur et de nature variables a été mise en place pour interpréter les résultats d'ellipsométrie spectroscopique. Le modèle le plus satisfaisant consiste en une couche

[14] Z. Zhang, P.A. VanRompay, J.A. Nees, R. Clarke, X. Pan and P.P. Pronko, Appl. Surf. Sci. 154-155 (2000), p 165-171.
[15] M. Jelinek, A. Klini, C. Grivas, J. Lancok, V. Studnicka, J. Chval, A. Mackova, C. Fotakis, Appl. Surf. Sci. 197-198 (2002), p 416-420

épaisse (bulk), surmontée d'une fine couche (top layer) majoritairement sp^2. La rugosité de surface est négligeable (quelques nanomètres), ce qui confirme bien les résultats obtenus sur les couches minces de DLC pour application biomédicale. Une corrélation entre les valeurs d'indice de refraction (mesuré à 2 eV) et le gap optique est reportée sur la **Figure 9**. Les valeurs obtenues pour le corps de la couche (bulk) ainsi que pour la couche de surface (top layer) y sont reportées.

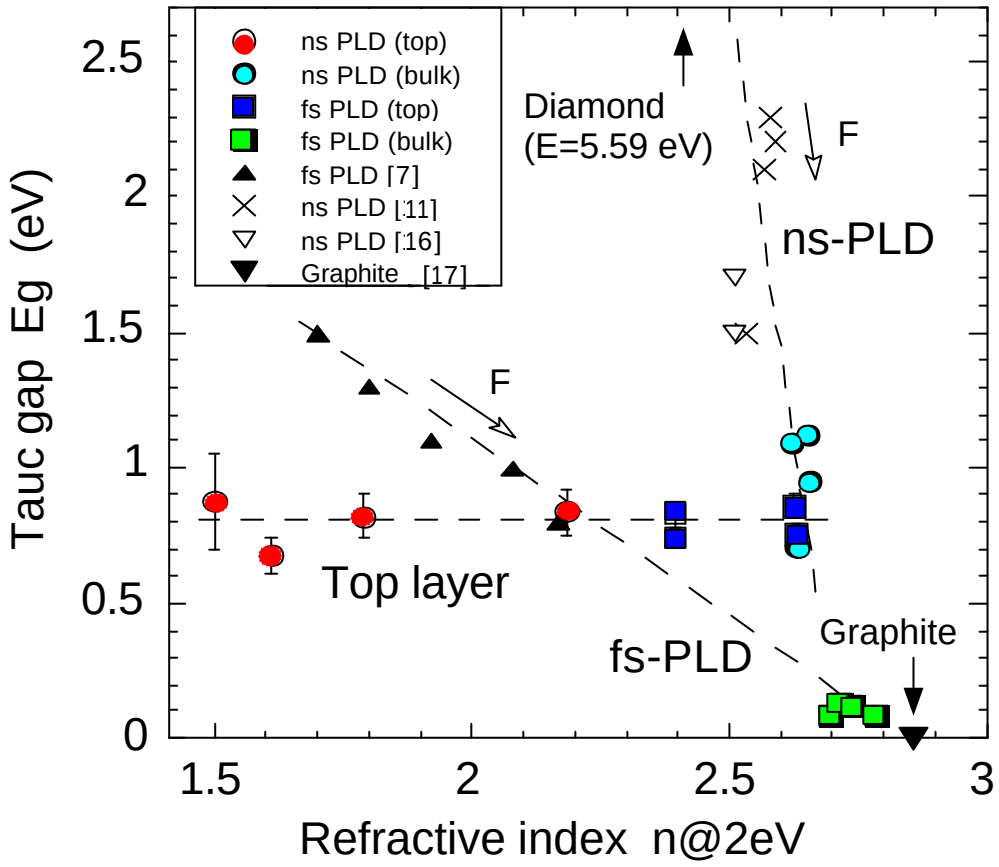

Figure 9 : Comparaison de l'indice de refraction et du gap optique (Tauc Gap) pour des couches de DLC déposées par PLD fs et ns. D'autres résultats en PLD ns[11,16,17] et PLD fs[7] sont présentés.

Les valeurs de gap optique du bulk de chacune des couches nanoseconde et femtoseconde sont très différentes et peuvent être corrélées aux transitions π - π^*. Il

[16] H.C. Ong, R.P.H. Chang: Phys. Rev. B **55**, 13213 (1997).

[17] A. Borghesi, G. Guizzetti: in "Handbook of optical constants of solid II" (E.D. Palik ed.) Academic Press Inc. (1991) 449.

semble donc que la PLD nanoseconde conduise à des couches plus riches en carbone hydridé sp^3. Les valeurs d'indice de réfraction sont très similaires, mais en raison d'un indice légèrement plus élevé dans le cas des films obtenus par PLD femtoseconde, la densité est légèrement plus élevée que celle des films obtenus par PLD nanoseconde. On note également que le gap optique de la couche majoritairement sp^2 en surface est indépendant du procédé de dépôt. La couche sp^2 de surface apparaît cependant plus dense et plus épaisse dans le cas de la couche obtenue par PLD femtoseconde.

Ces résultats confirment la croissance de couches denses (indice de réfraction proche de 2.7) et peuvent être interprétés à partir du modèle de sub-plantation proposé par Robertson[2] qui décrit qualitativement la formation des liaisons sp^3 dans la couche en fonction de l'énergie des espèces du plasma de dépôt. En effet, en dessous de l'énergie optimale (environ 100 eV[18,19]), le taux de sp^3 dans la couche croît avec l'énergie des espèces en raison d'une pénétration plus importante des espèces, permettant ainsi de densifier la couche en croissance. Au delà de cette valeur optimale, le taux de sp^3 diminue par des phénomènes de relaxation $sp^3 \rightarrow sp^2$.

Les résultats obtenus par ellipsométrie spectroscopique peuvent également être corrélés avec les énergies des espèces du plasma. A partir de mesures de temps de vol par spectroscopie optique d'émission, nous pouvons accéder aux distributions en énergie des espèces. La **Figure 10** présente les fonctions de répartition d'énergie cinétique des espèces obtenues en PLD nanoseconde et femtoseconde. Ce type d'analyse ne permet pas d'accéder aux espèces très énergétiques présentes dans le front du plasma, comme nous le verrons par la suite dans la partie caractérisation du plasma de ce mémoire.

Nous pouvons déduire de ces mesures que la proportion d'espèces faiblement énergétiques est plus faible en PLD nanoseconde, conduisant ainsi à une couche sp^2 de surface moins épaisse, comme observé par les caractérisations optiques des couches. Dans le cas de l'utilisation d'un laser de durée d'impulsion nanoseconde, il y a en effet absorption d'une partie de l'énergie du laser par le plasma, s'en suivant une

[18] 'P.J. Fallon, V.S. Veerasamy, C.A. Davis, J. Robertson, G.A.J. Amaratunga, W.I. Mime, J. Koskinern, Phys. Rev. B 48 (1993), 4777.

[19] V.I. Merkulov, D.H. Lowndes, G. E. Jellison, Jr., A. A. Puretzky, and D. B. Geohegan, Appl. Phys. Lett. 73 (1998) 2591.

redistribution de l'énergie par des processus collisionnels et donc une thermalisation du plasma. La proportion d'espèces ayant une énergie élevée étant plus importante en PLD nanoseconde, cela contribue à implanter plus en profondeur les espèces lors de la croissance et favorise donc une augmentation du taux de liaisons sp^3, par des mécanismes de subplantation.

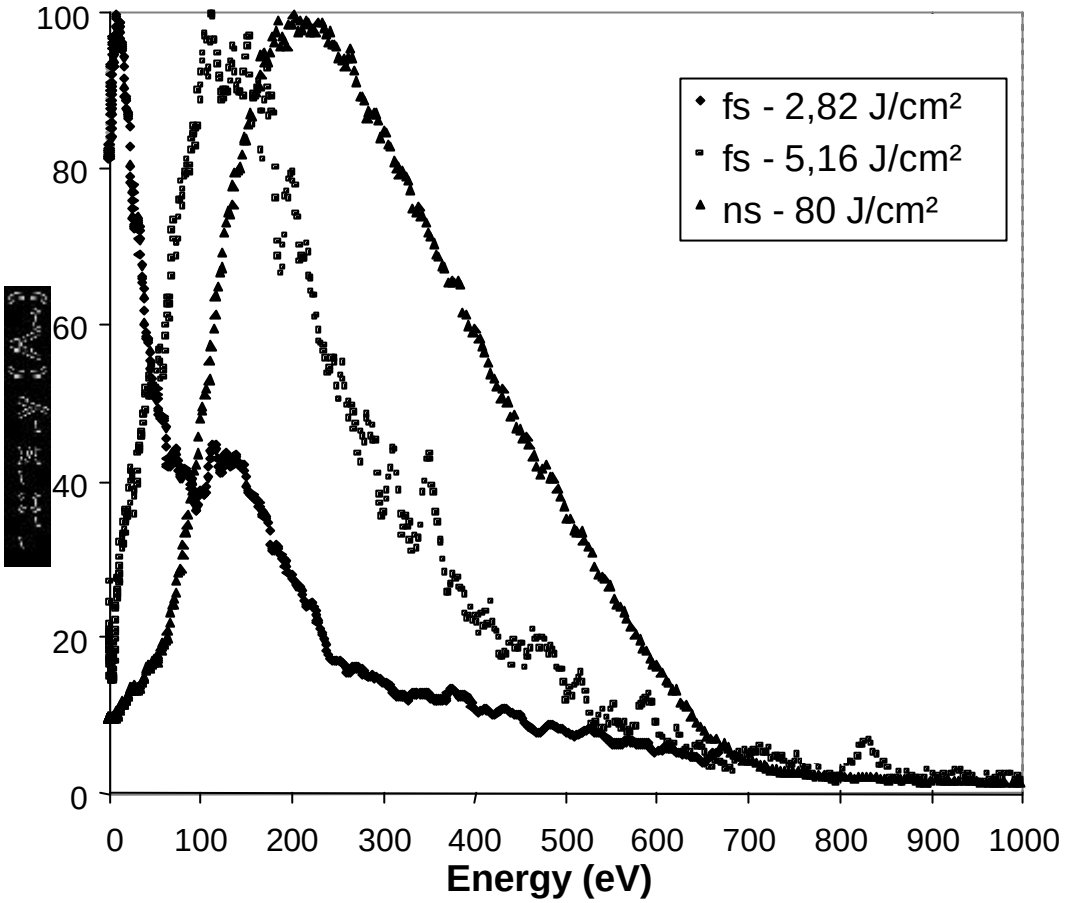

Figure 10 : Distribution d'énergie cinétique des espèces émettrices du plasma d'ablation, déduites par mesures de temps de vol

Des caractérisations structurales plus approfondies peuvent être menées afin de comparer les couches minces de DLC élaborées par PLD femtoseonde et nanoseconde. En particulier, la spectroscopie Raman multi longueur d'onde peut être utilisée pour quantifier le taux d'hybridation sp^3 mais également la nature de la phase sp^2 en terme de structures (chaines graphitiques, cycles plus ou moins désordonnés...). Nous disposons

au Laboratoire de tous les équipements pour déposer des couches minces par ablation laser femtoseconde (laser Titane:Sapphire) et nanoseconde (laser excimère KrF), ainsi que de l'équipement de spectroscopie Raman multi longueur d'onde (Visible et U.V.). L'élaboration de couches par PLD nanoseconde ainsi que les caractérisations Raman sont en cours dans le cadre de la thèse d'Aurélien SIKORA et vont être publiées prochainement.

3. Synthèse de nanoparticules.

L'ablation laser femtoseconde est très rapidement apparue comme une technique intéressante pour le dépôt de nanoparticules, en une seule étape. La plupart des matériaux conduisent en effet à la synthèse de couches minces présentant une forte proportion de nanoparticules.

L'origine de la présence de ces nanoparticules constitue un sujet de recherche à part entière et de nombreux groupes se sont penchés sur ce problème à la fois d'un point de vue expérimental en précisant les conditions de formation de ces nanoparticules[20,21] et d'un point de vue théorique par la compréhension des mécanismes de formation[22,23,24,25].

Lors de l'irradiation d'un matériau par un laser femtoseconde, les espèces éjectées peuvent se trouver, en des proportions variables, sous des formes différentes : atomes, ions, nanoparticules, particules de taille micronique, comme reporté sur la **Figure 11**, issue de travaux de S. Amoruso[26].

Ces résultats expérimentaux montrent bien la présence d'ions très rapides, comme nous les avons observés par imagerie rapide (résultats dans le paragraphe 5, Etude du plasma). Ils montrent également la présence de nanoparticules ayant des énergies plus faibles que les espèces atomiques et ioniques. Il est possible de mettre en évidence ces nanoparticules directement dans le plasma, comme nous le verrons également dans le paragraphe relatif à l'étude du plasma.

---

[20] G. Ausanio, S. Amoruso, A.C. Barone, R. Bruzzese, V. Iannotti, L. Lanotte, M. Vitiello, Appl. Surf. Sci. 252 (2006), 4678.

[21] R. Benzerga, Thèse de doctorat, Université d'Orléans, 2005.

[22] L. V. Zhigilei, *Appl. Phys. A* 76 (2003), 339-350.

[23] S. Amoruso, R. Bruzzese, X. Wang, N.N. Nedialkov, P.A. Atanasov, Nanotechnology 18 (2007), 145612

[24] T. Itina, K. Gouriet, L.V. Zhigilei, S. Noel, J. hermann, M. Sentis, Appl. Surf. Sci. 253 (19) (2007), 7656-7661.

[25] J. P. Colombier, P. Combis, R. Stoian, and E. Audouard, Phys. Rev. B **75**, (2007) 104105.

[26] S. Amoruso, G. Ausanio, R. Bruzzese, L. Gragnaniello,L. Lanotte, M. Vitiello, X. Wang, Applied Surface Science 252 (2006) 4863–4870.

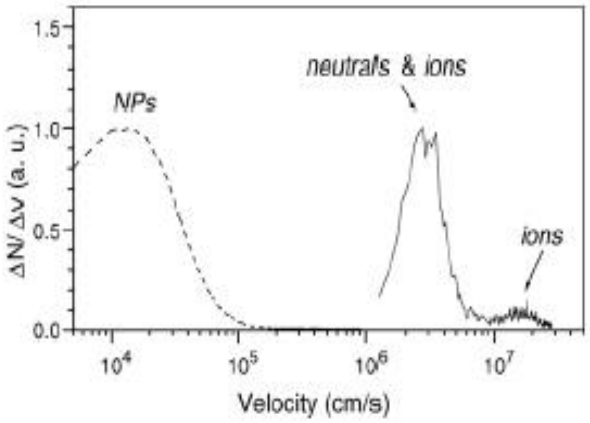

Figure 11 : Distribution de vitesses des espèces éjectées obtenue par imagerie résolue en temps d'un plasma de silicium produit par une impulsion 0.9 ps/1055 nm pulse, à une fluence laser de 0.75 J/cm2. D'après Ref [26].

Deux mécanismes peuvent être proposés pour expliquer la présence de ces nanoparticules : une formation par nucléation à partir de la phase gazeuse ou une éjection directe de la cible irradiée. D'après la communauté scientifique, il apparait clairement maintenant que ces nanoparticules proviennent d'un état thermodynamique particulier, propre au régime femtoseconde générant la formation de couches de liquide à la surface et à l'intérieur de la cible. Il est usuel de représenter les trajectoires thermodynamiques suivies par le matériau dans un diagramme température-densité[27] ou pression-densité, comme reporté sur la **Figure 12,** issue des travaux de J.P. Colombier et al[25].

Suite au chauffage électronique pendant l'impulsion laser femtoseconde, la pression électronique augmente ce qui conduit à une transition verticale ((a) sur la Figure 12). La fin de l'impulsion correspond au maximum de pression électronique et donc au pic de compression. La diminution de la pression est ensuite due d'une part à une augmentation du volume local et d'autre part à un refroidissement par relaxation électron-phonon ((b) sur la Figure 12). Deux types de trajectoires sont ensuite observées : celles, non conventionelles, passant au-dessus de la courbe binodale, ((d) sur la Figure 12), qui induisent donc une expansion sans transition liquide-gaz et conduisent à la fragmentation ou la décomposition spinodale. Le deuxième type de comportement correspond à des zones plus profondes de la cible, (trajectoires (c) puis (e) sur la Figure 12) pour lesquelles les courbes passent au travers de la zone de fusion : le liquide

[27] D. Perez, L.K. Béland, D. Deryng, L.J. Lewis, M. Meunier, Phys. Rev B 77 (2008), 014108

persiste alors à haute densité malgré une diminution de pression. La nucléation homogène est alors supposée contrôler le phénomène d'ablation.

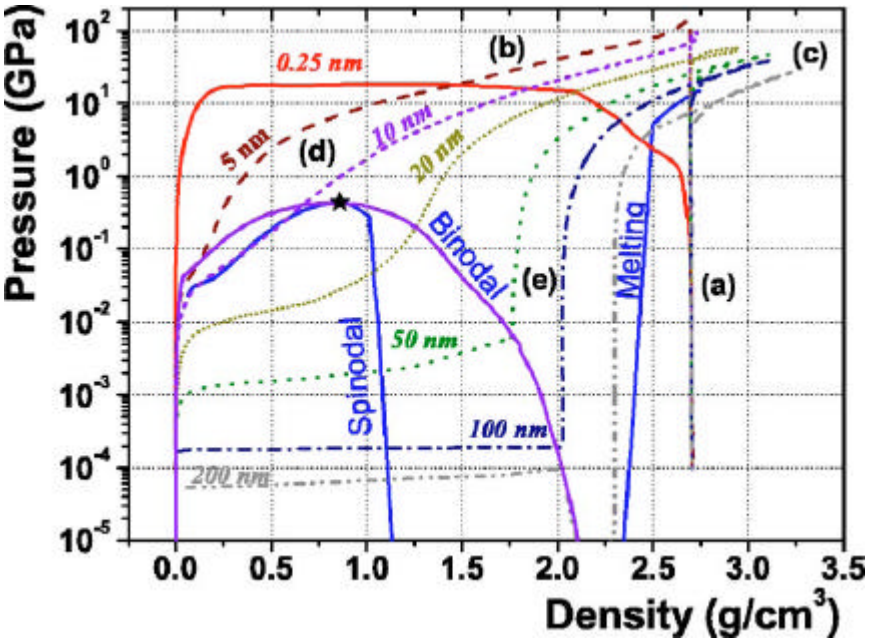

Figure 12 : Diagramme de phase pression-densité pour l'aluminium exposé à un faisceau laser femtoseconde (5 J/cm²). Les trajectoires thermodynamiques de différentes couches du matériau sont reportées pour différentes profondeurs dans la cible. D'après Ref [25].

Nous avons, au Laboratoire Hubert Curien, synthétisé des couches minces de métaux purs : tantale, nickel, aluminium .... Nous avons également effectué quelques dépôts d'oxydes de titane pour intier un projet ANR PNANO non financé en 2006.
A titre d'exemple, des images obtenues par MEB-FEG de nanoparticules d'aluminium ou de tantale sont reportées sur la **Figure 13**.

Une analyse par diffraction de rayons X en incidence rasante a révélé des tailles de cristallites du même ordre de grandeur que la taille moyenne morphologique déduite de mesures MEB. Par ailleurs, le paramètre de maille déduit de ces diffractogrammes XRD est plus faible que le paramètre de maille du matériau massif, en raison vraisemblablement de contraintes résiduelles. Une étude systématique en fonction de la pression résiduelle a révélé une augmentation de la taille des nanoparticules en fonction de la pression résiduelle au cours du dépôt.

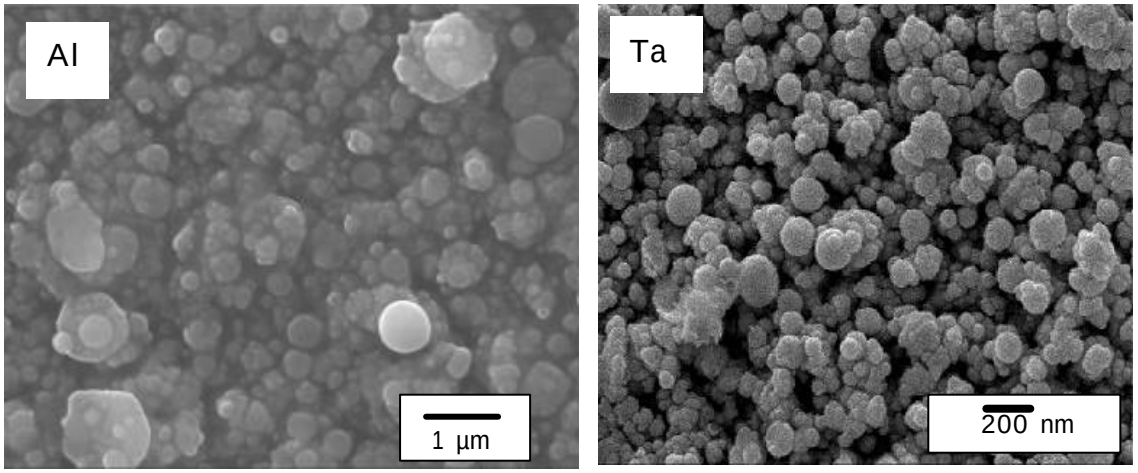

Figure 13 : Images MEB-FEG de nanoparticules d'aluminium et de tantale synthétisées par ablation laser femtoseconde.

Cependant, aucun paramètre "simple" de l'interaction (fluence laser, pression résiduelle..) ne permet de contrôler la taille de ces nanoparticules. Comme nous le verrons dans la dernière partie de ce mémoire, nous envisageons de mettre en place une mise en forme temporelle de l'impulsion laser pour agir directement sur les mécanismes de formation de ces nanoparticules.

A l'issue des travaux sur le dépôt de couches minces de DLC pur et de métaux purs, nous avons envisagé de déposer des couches minces de DLC dopées par des nanoparticules de métal, comme résumé dans la paragraphe suivant.

4. Synthèse de couches minces de DLC dopées

Les couches DLC sont étudiées depuis une quinzaine d'années pour leurs propriétés mécaniques et leur résistance à l'usure[28]. De nombreuses applications "grand public" leur ont conféré leurs "lettres de noblesse" dans des secteurs d'activités comme la motorisation automobile (revêtements DLC indispensables dans les injecteurs diesel HDi), dans les technologies de stockage de l'information (couche lubrifiante sur têtes de lecture d'ordinateurs), dans de nombreuses applications strictement mécaniques (composants à bas frottement dans les mécanismes hydrauliques, revêtements anti-usure dans les machines pour l'industrie textile) ou biomécaniques (revêtements de prothèses de hanche ou de genou).

Robertson[2] dresse un état de l'art récent démontrant qu'un second palier d'innovations est désormais accessible avec les DLC, en contrôlant leur proportion Csp^2/Csp^3, ou en introduisant au cours de procédé de synthèse des hétéroatomes en proportion contrôlée. Cette approche, de type "chimie combinatoire", permet d'explorer le large spectre de propriétés électriques et thermiques de ces films minces.

Depuis plusieurs années, de nombreuses équipes s'intéressent en effet au dopage de couches minces de DLC par différents éléments[2] : silicium, azote, fluor, bore, phospore, métaux de transitions,... L'objectif est de concevoir des matériaux multifonctionnels, avec une modification de l'énergie de surface et de la réactivité, un contrôle de la sensibilité tribologique à l'environnement ou encore un contrôle de la conductivité électrique lors du dopage par des métaux.

Le dopage de couches minces de DLC par des éléments métalliques a connu depuis quelques années un intérêt croissant, y compris en utilisant des procédés de dépôt tels que l'ablation laser nanoseconde[6,29]. Le dopage conduit à différentes compositions chimiques et nanostructures. Les caractéristiques physico-chimiques et structurales des ta-C dopés ou alliés mettent en évidence des modes de liaison et d'incorporation

[28] A. Erdemir, C. Donnet, Modern Tribology Handbook, Vol. 2, B. Bhushan (ed.) CRC Press (2000) 871-908.

[29] Q. Wei, R.J. Narayan, J. Narayan, J. Sankar and A.K. Sharma, Materials Science and Engineering B, 53 (3) (1998) 262-266.

spécifiques au procédé de dépôt, ainsi que des nanostructures particulières. La dispersion de particules métalliques de taille nanométrique dans une matrice diélectrique conduit alors à des materiaux aux propriétes singulières.

Au laboratoire Hubert Curien, nous nous sommes intéréssés au dopage de couches minces de DLC par deux métaux, le tantale et le nickel, puis par le bore, pour des applications diverses, tribologiques, électrochimiques puis également thermiques et nanocalorimétriques en ce qui concerne le dopage par le bore.

4.1. Synthèse de couches minces de DLC dopées par des métaux.

(a) Caractérisation

Les couches minces de DLC dopées par du Nickel (a-C:Ni) ou du tantale (a-C:Ta) ont été déposées par ablation laser femtoseconde avec différents taux de dopage en nickel ou tantale. Le tantale et le nickel ont été choisis en fonction de leur affinité très dférente avec le carbone. Différentes analyses ont été mises en place sur ces couches : analyse élémentaire quantitative (RBS) et qualitative (XPS), analyse structurale (GIXRD, TEM, Raman, FTIR) et morphologique (SEM/FEG, AFM) afin de corréler la nanostructure de ces matériaux au procédé d'elaboration.

Ce travail a fait l'objet de la thèse de Nadia BENCHIKH et les résultats dont la courte synthèse est présentée à la suite sont détaillés dans les articles [15] et [18] (N. Benchikh et al., *Thin Solid Films* 482 (2005) 287-292 et N. Benchikh et al., *Thin Solid Films* 494 (2006) 98-104).

La microstructure des couches a été examinée par Microscopie électronique en Transmission filtrèe en énergie (TEM-EELS) en collaboration avec le LTDS de l'Ecole Centrale de Lyon. Les résultats obtenus dans le cas du dopage au nickel sont reportés sur la **Figure 14**. Nous observons des nanoparticules de nickel, avec une forte dispersion en taille, comme observé lors du dépôt de nickel pur. Ces nanoparticules sont enfermées dans une matrice de carbone amorphe.

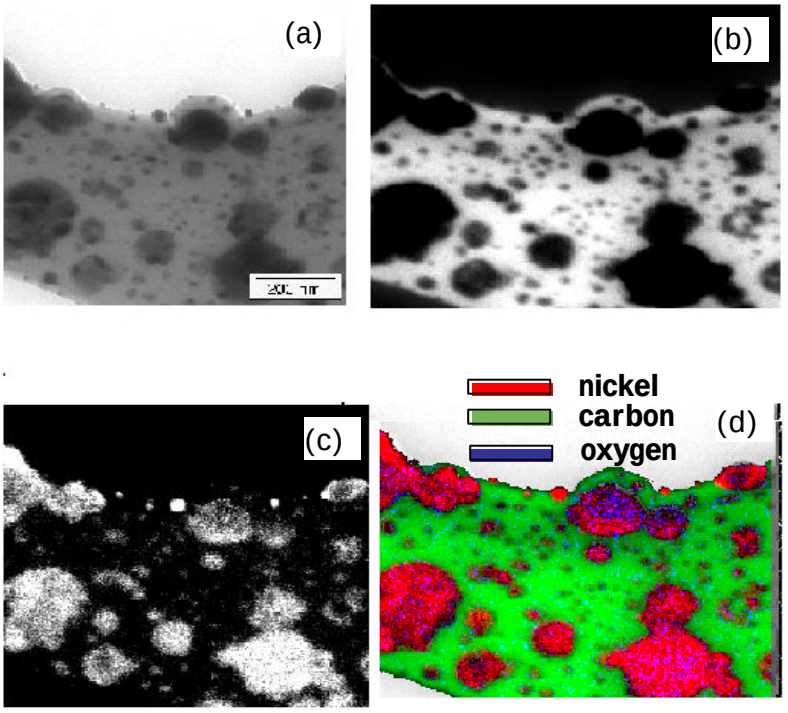

Figure 14 : Images TEM filtrées en énergie du film a-C :Ni 15% at.
(a) sans perte d'énergie (zéro-loss), au seuil (b) du carbone, (c) du nickel et (d) image assemblée à partir des images seuils. Le carbone, l'oxygène et le nickel sont identifiés par les surfaces claires sur les images respectivement (b) et (c)

Des caractérisations structurales ont été effectuées sur ces différentes couches par diffraction de rayons X en incidence rasante, comme reporté sur la **Figure 15**.
Une seule contribution apparaît sur le diffractogramme du film a-C:Ni 15% qui correspond à la phase stable cubique faces centrèes du nickel, phase identique à celle de la cible utilisée pour effectuer le dépôt. La taille des cristallites (déduite de la largeur à mi-hauteur des pics, par la formule de Scherrer) est de l'ordre de 80 nm pour la phase CFC du nickel.

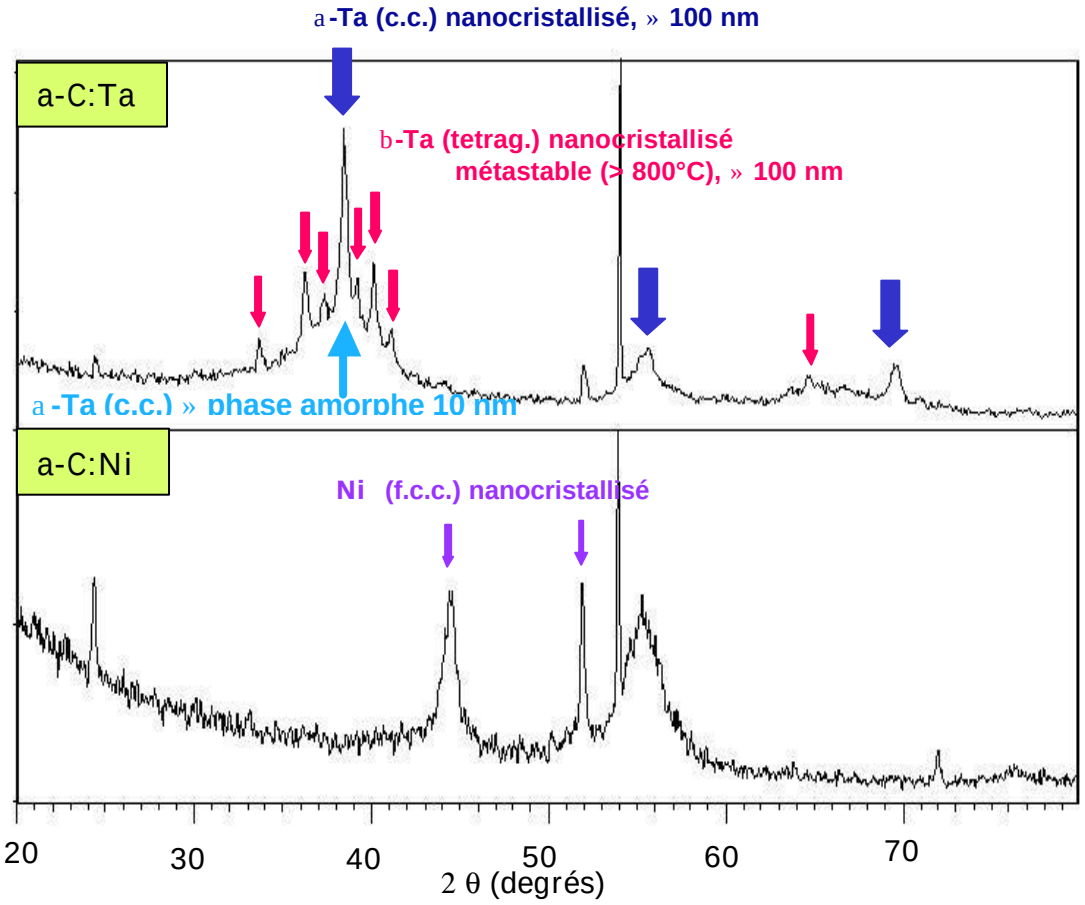

Figure 15 : Diffractogrammes (XRD) de films a-C:Ta 15 % et a-C:Ni 15 %.

En ce qui concerne la couche mince de DLC dopée au tantale (a-C:Ta 15%), différentes phases peuvent être mises en évidence :

- Une phase de tantale cubique centrèe (αTa) qui est une phase stable dans les conditions normales de température et de pression et qui est identique à celle présente dans la cible metallique de tantale utilisée pour effectuer le dépôt. La taille des cristallites de cette phase est de 100 nm environ.

- Une phase métastable de tantale quadratique (βTa) qui a deja été observée à des températures supérieures à 800°C [30].

- Une troisième contribution correspondant probablement à la présence d'une phase amorphe, compte tenu de la "bosse" très large centrèe sur le pic de la phase stable αTa.

[30] P.T. Moseley, C.J. Seabrook, Acta Crystallogr B29 (1973), 1170.

Nous avons tenté d'interpréter la présence de cette phase partciulière (β Ta) à partir de caractérisations du plasma créé lors de l'ablation laser femtoseconde du tantale. Ces résultats sont présentés dans le paragraphe relatif à l'étude du plasma.

La caractérisation structurale par GIXRD a été complétée par une analyse en microscopie électronique à très haute résolution (HRTEM). Les résultats obtenus par analyse des franges de réseau montrent une bonne adéquation avec les analyses par GIXRD, mettant en évidence la présence des deux phases αTa et βTa. En outre, il semble que le carbure de tantale puisse être mis en évidence par HRTEM.
Cette ambiguité a été levée par analyse par spectroscopie de photoélectrons issus de l'irradiation X (XPS) de l'interface métal-carbone. Il apparaît clairement que le nickel reste sous forme métallique dans le film a-C:Ni tandis que la présence de liaisons TaC a pu être mise en évidence dans le cas des films a-C:Ta. L'analyse par XPS n'étant qu'une analyse de surface (quelques nanomètres sondés) et compte tenu du signal détecté, il semble qu'une couche de carbure de tantale de quelques nanomètres puisse se former pendant le dépôt. Ceci est confirmé par analyse HRTEM avec mesure locale de la composition (EDS). Nous avons tenté de corréler ces observations avec les caractérisations du plasma, comme présenté dans le dernier paragraphe de ce chapitre.

(b) Couches minces pour capteurs électrochimiques

Le carbone est un matériau de choix pour l'élaboration de capteurs ampérométriques. La réalisation de couches fonctionnelles de DLC ou de diamant, à propriétés optimisées, est en outre parfaitement intégrable dans les technologies planaires de la microélectronique. Cet élément est déjà utilisé à l'état massif ou de revêtement (fibres, vitreux) pour la réalisation de nombreux systèmes actifs (capteurs, électrodes) en raison de ses propriétés physiques (conductivité dépendant de l'hybridation du carbone et de la microstructure) et chimiques (inertie) remarquables. Le spectre de propriétés des formes carbonées actuellement utilisées limite cependant les domaines d'utilisation des capteurs, notamment en conditions extrême d'usage (milieu, température) tout comme leur intégration dans des microsystèmes. En

collaboration avec Nicole Jaffrezic (Laboratoire des Sciences Analytiques, Lyon), nous avons envisagé d'utiliser les couches de DLC et DLC dopé élaborées par PLD femtoseconde comme élément actif de capteur ampérométrique. Les résultats sont détaillés dans la publication [22] (R. Maalouf et al., *Talanta* 72 (2007), 310).

Les couches minces de DLC élaborées par PLD femtoseconde peuvent être utilisées comme biocapteur ampérométrique de glucose oxidase, même si la sensibilité est inférieure aux électrodes en carbone vitreux. Deux voies ont été envisagées pour abaisser la limite de détection :

- l'utilisation de couches de DLC dopé au nickel (a-C:Ni5%) afin d'augmenter la conductivité électrique, ce qui a permis d'atteindre une limite de détection de 30 µM

- l'utilisation d'une pression résiduelle d'argon lors du dépôt afin de freiner les particules du plasma lors de leur expansion, et augmenter ainsi la proportion d'hybridation sp^2 au sein des couches de DLC pur, ce qui a conduit à une limite de détection de 20 µM.

La sensibilité de ces biocapteurs est également améliorée par l'utilisation de ces deux types de couches minces, même si la stabilité dans le temps reste encore un problème majeur.

Dans le cadre d'un projet ANR, des travaux sont en cours sur des couches minces de DLC dopé au bore. En effet, de nombreux travaux sont consacrés à l'utilisation de bdd (Boron doped Diamond) en tant qu'élément actif de capteur[31]. L'application envisagée dans ce cas est la détection de polluants (métaux lourds).

[31] C. Provent, W. Haenni, E. Santoli and P. Rychen, Electrochim. Acta, 49 (2004) 3737.

4.2. Synthèse de couches minces de DLC dopées au bore.

Le bore est apparu depuis quelques années comme un élément très intéressant pour doper le diamant ou les couches minces de DLC[32]. Les applications envisagées sont bien évidemment des applications électriques et thermiques mais également des applications électrochimiques avec l'utilisation croissante du bdd (boron Doped Diamond)[31], ou encore des applications utilisant l'émission à effet de champ[33]. Le diamant polycristallin dopé au Bore réalisé sur Silicium par MPCVD trouve par exemple actuellement des applications technologiques diversifiées qui touchent tout à la fois les composants électroniques passifs et actifs et les électrodes pour l'électrochimie.

Nous nous intéressons au Laboratoire Hubert Curien au dopage de couches de DLC par le bore. Trois applications ont été identifiées :

- éléments actifs de capteurs thermiques : membranes suspendues réalisées par des techniques de microfabrication pour l'étude thermodynamique par nanocalorimétrie de petits objets, en particulier sur la gamme de température 4K – 300K,
- détecteur d'usure en temps réel en vue de quantifier l'usure par une mesure de conductivité électrique,
- éléments actifs de capteurs électrochimiques pour les mesures de concentration de polluants (métaux lourds, molécules organiques) dans les eaux et les effluents.

Ces travaux, encore en cours de réalisation, entrent dans la cadre de la thèse d'Aurélien SIKORA.

Les premiers travaux d'élaboration par PLD femtoseconde et de caractérisation de couches minces de DLC dopé au bore ont permis de mettre en évidence l'intérêt de

[32] A.Deneuville, Thin-Film diamond I, Semiconductors and Semimetals, Vol.76, Christoph E.Nebel et Jürgen Ristein, Ed., Elsevier Academic Press, Amsterdam (2003)

[33] Y. Suda, Y. Suganuma, Y. Sakai, K. Suzuki, J. Tsujino and N. Homma, App. Surf. Sci., 197-198 (2002) 603-606.

ces couches en terme de capteurs de température. Ces travaux sont présentés dans la publication [26] (A. Sikora et al., *Solid State Science*, à paraître 2008).

La caractérisation électrique permet de mettre en évidence un comportement de conduction par saut (modèle de type VRH, variable range hopping) suivant la loi de Mott.

L'incorporation de bore conduit à une variation de la résisitivité des films en fonction du taux de dopage, comme reporté sur le **Tableau 2** synthétisant les caractéristiques électriques de ces films. Une décroissance notable de la résistivité est engendrée par l'introduction de bore. Il faut noter que les valeurs de résistivité obtenues pour les couches a-C:B déposées par PLD femtoseconde sont relativement faibles par rapport aux résultats présentés dans la littérature[34,35], se situant plutot aux environ de 100 Ω.cm.

Il serait bien entendu très intéressant de comparer ces caractéristiques électriques avec celles obtenues pour des couches déposées par PLD nanoseconde, qui devraient présenter un dopage de type atomique plutôt qu'un dopage sous forme de nanoparticules de bore. Ces études sont en cours de réalisation.

	Taux de dopage	R_{77K} (MΩ)	R_{300K} (MΩ)	ρ_{300K} (Ω.cm)	α_{300K} (K^{-1})
DLC	0 %	X	1250	100	0.02
a-C:B	2 %	6.64	26.67	2.13	0.01
a-C:B	4 %	6.79	12.93	1.3	0.004
a-C:B	8 %	5.32	57.74	4.61	0.012
NbN		0.009	0.308	0.025	0.01

Tableau 2 : Résumé des caractéristiques électriques des films de DLC pur et dopés au bore. α est le coefficient de température à 300 K. Les valeurs de NbN sont également reportées[36].

Les couches minces obtenues peuvent être également examinées en terme de variation de la résistivité électrique en fonction de la température (coefficient α), qui traduit la sensibilité du thermomètre. Les résultats obtenus sur les couches minces de

[34] X. Tian, M. Rusop, Y. Hayashi, T. Soga, T. Jimbo, and M. Umeno, Jap. J. Appl. Phys., 41 (2002) L970

[35] B. Kleinsorge, A. Ilie, M. Chhowalla, W. Fukarek, W.I. Milne and J. Robertson, Diamond Relat. Mater., 7 (1998) 472.

[36] O. Bourgeois, E. Andre, C. Macovei, and J. Chaussy, Rev. Sci. Instrum., 77 (2006) 126108.

DLC pur et dopé par du bore montrent, sur la plage 50-300K un comportement tout à fait intéressant par rapport au nitrure de niobium (NbN) ou les films amorphes Nb-Si, qui apparaissent actuellement comme les films références en matière de thermomètre résistif sous forme de couche mince.

A titre d'exemple, la **Figure 16** présente le coefficient de température α de ces couches minces de DLC et de a-C:B en fonction de la température sur la gamme 50-300 K.

En terme de propriétés tribologiques de ces couches minces de DLC dopées au bore, des caractérisations tribologiques couplées à des mesures de résistance au cours du frottement ont été mises en oeuvre au Laboratoire de tribologie et dynamique des systèmes (LTDS) de l'Ecole Centrale de Lyon et montrent une augmentation du coefficient de frottement avec l'introduction du bore et une instabilité de ce coefficient au cours du frottement, contrairement à une couche de DLC pur présentant un frottement faible et stable.

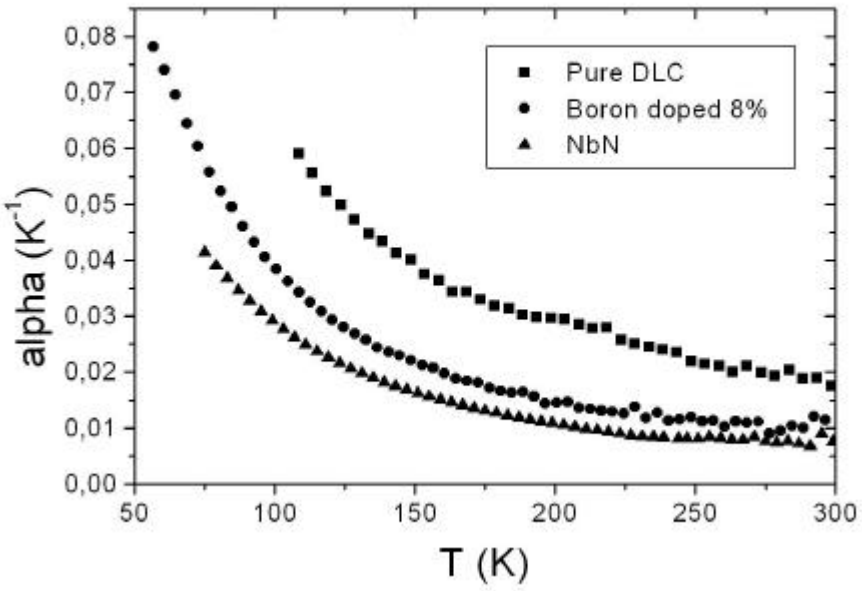

Figure 16 : Coefficient de temperature (Temperature coefficient of the resistance TCR) pour une couche mince de DLC pur et une couche mince de DLC dopé au bore a-C:B8%. Les valeurs du nitrure de niobium sont également reportées.

5. *Analyse du plasma.*

L'utilisation des lasers pour le dépôt de couches minces nécessite un contrôle du plasma, vecteur des espèces de la cible jusqu'au substrat. Ce contrôle permet non seulement une maitrîse du procédé mais également une compréhension des mécanismes mis en jeu lors de la croissance de la couche mince.

Mes premiers pas dans le monde de la recherche ont concerné l'étude du plasma, par le développement d'un code de simulation du plasma créé par ablation laser nanoseconde. Ces travaux ont été développés dans le cadre de ma thèse puis d'un poste ATER au Laboratoire Science des Procédés Céramiques et de Traitements de Surface (SPCTS).

Au cours de l'ensemble de mes activités de recherche, outre mes travaux théoriques sur la description de l'expansion du panache plasma, j'ai utilisé différents outils expérimentaux pour caractériser le plasma créé par ablation laser (nanoseconde ou femtoseconde) : l'imagerie résolue en temps et la spectroscopie optique d'émission résolue et temps et spatialement. La difficulté de ce type de caractérisation est double : d'une part, les laser utilisés étant impulsionnels, il faut synchroniser l'acquisition avec le pulse laser, d'autre part, les signaux à détecter, de faible intensité, nécessitent l'utilisation de dispositifs intensifiés. Néanmoins, il est possible d'accéder à la nature des espèces émettrices dans le plasma, et à leur énergie. Le contrôle de ces deux paramètres est bien entendu primordial pour la croissance de couches minces de qualité.

Dans ce paragraphe, je vais donc résumer les travaux effectués en matière de caractérisation du plasma, en lien avec l'élaboration de couches minces.

Les premiers travaux de diagnostic du plasma de carbone ont fait l'objet de conférences orales aux congrès CLEO2000 [47] et HPLA2002 [49]. Les études suivantes sont détaillées dans les publications [11] (A.S. Loir et al., *Applied Surface Science* 208-209 (2003), 553) et [24] (F. Garrelie et al, *Applied Physics A* 90 (2008),

211), respectivement dédiées au plasma de carbone et au plasma créé lors du dépôt de couches minces de DLC dopé.

La **Figure 17** présente des images résolues en temps du plasma créé par ablation laser femtoseconde d'une cible de carbone. Une analyse quantitative de ces images permet d'accéder à l'énergie cinétique des particules (**Figure 18**).

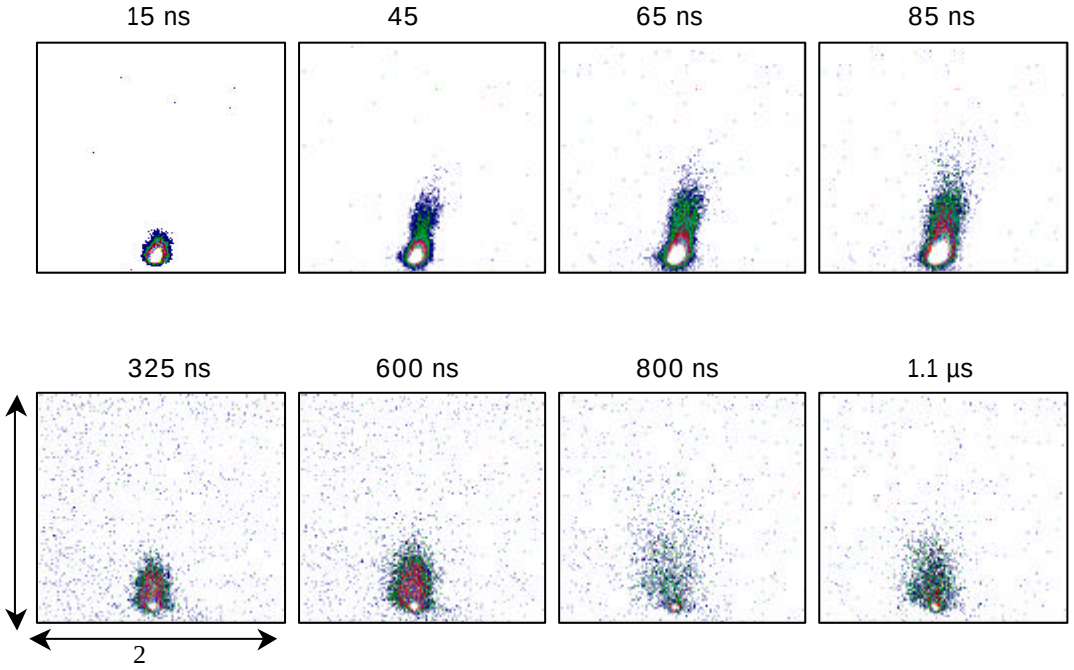

Figure 17 : Images du plasma créé par ablation laser femtoseconde d'une cible de carbone à différents délais après le pulse laser et à une fluence laser de 2 J/cm².

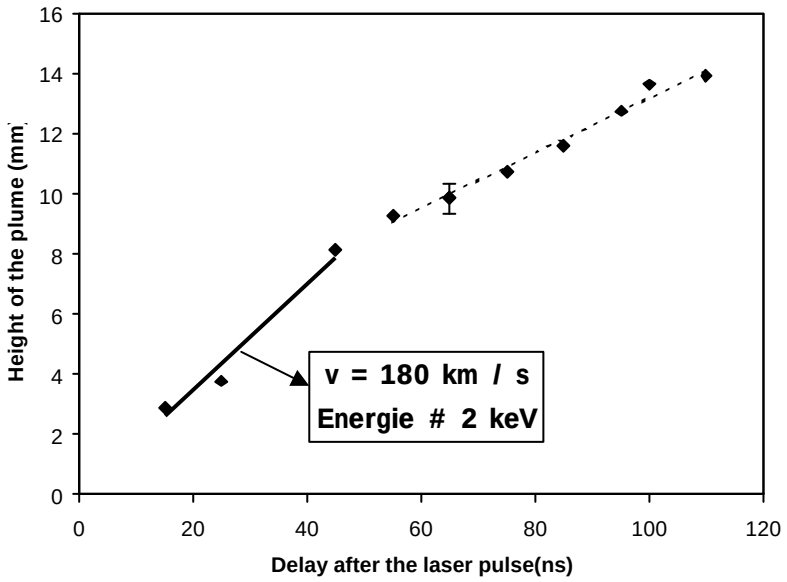

Figure 18 : Analyse quantitative des images résolues en temps du plasma créé par ablation laser femtoseconde d'une cible de carbone à une fluence laser de 2 J/cm².

Ces résultats mettent bien en évidence les deux composantes du plasma, à savoir des espèces très rapides (énergie voisine de 2 keV) et des espèces d'énergie proche de 100 eV. Ces espèces rapides sont donc très probablement responsables d'une relaxation des contraintes au sein de la couche, permettant ainsi au procédé PLD de limiter les valeurs de contraintes au sein de couches de DLC.

Cependant, contrairement aux premiers travaux laissant espèrer des couches de DLC exemptes de microparticules[8] altérant la surface, nous observons l'éjection dans le plasma de ces particules de taille micrométrique (**Figure 19**). Ces observations sont confirmées par l'observation des couches par microscopie optique ou microscopie électronique.

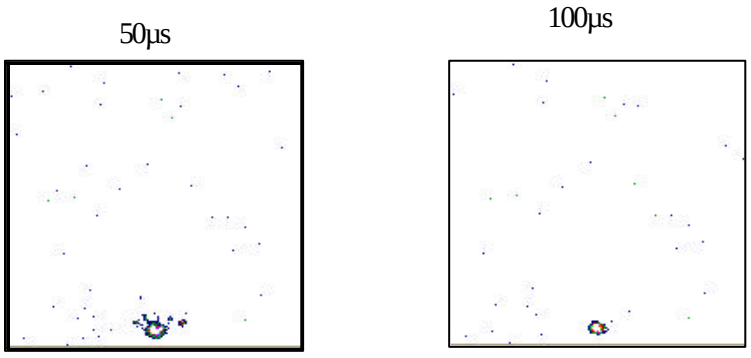

Figure 19 : Images du plasma créé par ablation laser femtoseconde d'une cible de carbone à différents délais après le pulse laser et à une fluence laser de 2 J/cm²

Afin de complèter cette caractérisation, et compte tenu de l'émission préférentielle des ions carbones dans le domaine U.V., nous avons effectué une résolution spectrale de nos images par l'utilisation de deux objectifs d'acquisition, un transmettant uniquement dans le visible et l'autre transmettant également dans l'U.V. Les résultats sont présentés sur la **Figure 20**. Deux fluences laser ont été examinées avec les deux objectifs d'acquisition d'images. Un comportement différent est observé en fonction de la fluence laser, que ce soit en terme de forme du plasma, ou en terme de nature des espèces émettrices. En effet, une fluence laser plus faible conduit à une expansion plus monodimensionnelle, comme cela a pu être mis en évidence en PLD nanoseconde ou par les calculs théoriques d'expansion du plasma que j'ai développés

pendant mon travail de thèse[37]. En effet, les gradients de pression initiaux dans le plasma semblent être à l'origine de ce changement de comportement dans l'expansion. Ces observations peuvent être corrélées avec les propriétés des couches de DLC, pour lesquelles, nous notons, à faible fluence laser, une vitesse de dépôt plus importante et des contraintes résiduelles plus faibles.

En ce qui concerne la structure du plasma, et compte tenu de l'absence de raies d'émission ionique dans le domaine visible, nous pouvons conclure que les espèces les plus rapides du plasma sont ionisées et que plus la fluence laser est élevée, plus le taux d'ionisation est élevé.

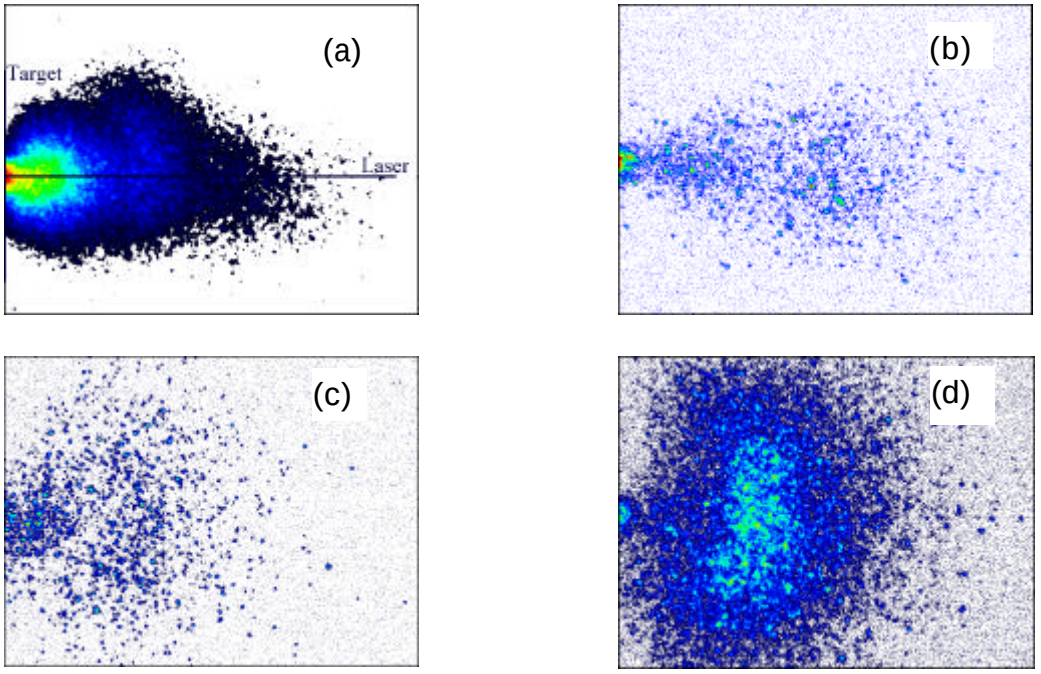

Figure 20 : Images du plasma créé par ablation laser femtoseconde d'une cible de carbone, pour une fluence laser de 2,82 J/cm² (a et b) et 5,16 J/cm² (c et d) et pour une émission dans le domaine visisble (a et c) et UV-Visible (b et d). Taille de chaque image : 5.6 × 4.2 cm.

Le plasma créé par ablation femtoseconde de cibles métalliques a également été caractérisé par imagerie résolue en temps et par spectroscopie optique d'émission. L'objectif était de corréler les observations avec les caractéristiques des couches de DLC dopées par les métaux a-C:Ta et a-C:Ni. Les nanoparticules ont pu être mises en évidence dans le plasma grâce au spectre d'émission de rayonnement de corps noir

[37] F. Garrelie, Thèse de doctorat, Université de Limoges, 1998.

(**Figure 21**). Une estimation de la température des nanoparticules peut être déduite à partir de la longueur d'onde du maximum d'émission[38] qui conduit à une valeur de l'ordre de 4000 K. Cette température est plus élevée que celle requise pour la formation de tantale en phase β (800 °C). Il est donc tout à fait probable que les nanoparticules aient subi une transformation allotropique au cours de leur séjour dans le plasma.

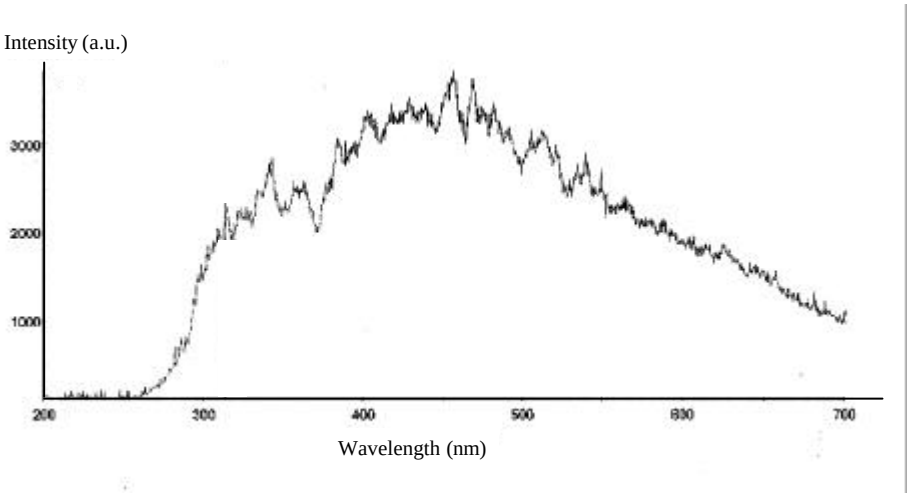

Figure 21 : Spectre d'émission du plasma de tantale créé par ablation laser femtoseconde, enregistré à un délai de 1 µs après le tir laser.

L'analyse détaillée des couches a-C:Ta par HRTEM et XPS a également révélé la présence d'une couche de TaC à la périphérie des nanoparticules de tantale. La formation de cette fine couche de tantale requiert évidemment une bonne affinité chimique du tantale avec le carbone mais également une énergie élevée des espèces carbonées arrivant sur le film de tantale en croissance. L'énergie cinétique moyenne des ions a été estimée à 250 eV. La profondeur de pénétration d'ions carbone frappant une surface de tantale à une énergie de 250 eV a été estimée en utilisant un logiciel de simulation (code TRIM) à 2 nm. Cette valeur est tout à fait comparable à celle déduite de mesures HRTEM ou encore de la profondeur sondée par XPS.

[38] D. Grojo, J. Hermann, A. Perronne, J. Appl. Phys 97 (2005), 063306

6. Bilan

Au travers de ces quelques études menées au Laboratoire Hubert Curien, il me semble important de souligner le caractère interdisciplinaire des travaux que nous avons pu mener, qui ne se limitent pas aux matériaux ou encore à l'optique appliquée des lasers.

Les révêtements que nous avons cherchés à optimiser présentent le plus souvent un côté applicatif. Pourtant, dans le but d'une compréhension aboutie des phénomènes mis en jeu, je me suis systématiquement efforçée d'adopter une méthodologie s'appuyant sur une caractérisation du plasma.

Ces travaux au caractère fortement interdisciplinaire m'ont permis d'approfondir mes connaissances dans des domaines proches de ceux abordés pendant mon doctorat (interaction laser-matière, plasma d'ablation) mais aussi d'aborder des domaines très différents, comme les lasers femtoseconde, l'élaboration de couches minces, la tribologie, ou encore le vaste domaine des propriétés électriques et optiques des matériaux.

Il apparaît néanmoins, au regard de la littérature et des travaux que nous avons pu mener, que le procédé de dépôt par ablation laser femtoseconde, même s'il autorise l'élaboration de films minces aux propriétés remarquables, atteint ses limitations en terme de maîtrise du process, en particulier pour la synthèse de nanoparticules, qui pourrait constituer un des avantages les plus précieux de ce procédé. Il apparaît donc primordial à ce stade de durée de vie de ce process PLD femtoseconde d'envisager un saut technologique important, ne se limitant plus aux seules explorations de paramètres tels que la fluence laser ou la pression de dépôt. C'est ce qui a motivé mon orientation vers les travaux de mise en forme temporelle de l'impulsion laser que je vais présenter succinctement dans le seconde partie de ce mémoire.

2ème Partie

Perspectives :

Mise en forme temporelle du laser femtoseconde pour la synthèse de couches minces

Cette deuxième partie de mon mémoire a pour objectif de mieux comprendre dans quelle mesure une mise en forme temporelle de l'impulsion laser autoriserait un contrôle du procédé de dépôt par PLD femtoseconde. Cette étude est relativement novatrice dans la mesure où peu de travaux s'intéressent au dépôt de couches minces avec des pulses laser modifiés temporellement. Cette thématique est donc plutôt empruntée à des applications telles que la femtochimie, comme nous le verrons dans un premier paragraphe. Je présenterai ensuite les premiers travaux encourageants dans cette voie.

1. Contexte de la mise en forme temporelle d'impulsions lasers femtosecondes

L'apparition de sources laser femtoseconde a vu se développer une intense activité sur les process pouvant en découler, tels que le micro-usinage, la photoinscription de guides d'onde ou encore le dépôt de couches minces. L'irradiation d'un matériau par un laser femtoseconde a en effet la possibilité de porter le matériau dans des états fortement hors équilibre et induire ainsi des transformations rapides du matériau irradié, conduisant à la formation de phases métastables. Ainsi, l'ablation laser femtoseconde peut conduire la matière ablatée par des chemins thermodynamiques particuliers, proches du point critique[39], autorisant ainsi la formation de nanoparticules. La température et la densité initiales de la vapeur créée définissent pour une bonne part, la cinétique de condensation résultante.

Cependant, le contrôle de la formation des nanoparticules par PLD femtoseconde reste encore limité, sans aucune maîtrise claire des paramètres expérimentaux autorisant un contrôle de la taille ou de la nature en terme par exemple de structure cristalline de ces nanoparticules[40]. Il en va de même pour la maîtrise de la qualité des couches minces. Afin d'accroitre donc l'intérêt de ce process, il apparait nécessaire d'envisager un moyen de contrôle autre que ceux actuellement développés, qui se limitent à la fluence laser, aux conditions d'irradiation, à la pression résiduelle ou encore à l'utilisation d'un deuxième faisceau laser, présentant un délai par rapport au faisceau d'ablation.

Le développement des sources laser femtoseconde a été suivi de développements sur la mise en forme temporelle des impulsions laser. En effet, il est possible de modifier la forme temporelle de l'impulsion, s'en suivant évidemment une modification des conditions d'interaction et donc des produits d'ablation. Cette voie apparait prometteuse pour franchir un saut technologique important afin de mieux maîtriser le procédé.

---

[39] J. P. Colombier, P. Combis, A. Rosenfeld, I. V. Hertel, E. Audouard, and R. Stoian, Phys. Rev. B, 74 (2006) 224106.

[40] S. Amoruso, G. Ausanio, A.C. Barone, R. Bruzzese, C. Campana, X. Wang, Appl. Surf. Sci. 254 (2007), 1012-1016.

Peu d'études ont été consacrées à l'utilisation de la mise en forme d'impulsions laser femtoseconde pour le dépôt de couches minces, principalement avec des doubles pulse pour le dépôt de DLC[41] ou de SiC[42].

Cependant, comme la connaissance de l'interaction entre un laser et le matériau dans le régime femtoseconde n'est pas accessible, la relation entre une forme temporelle particulière du laser et les effets induits n'est pas aisement prédictible. Dans ce cas, les procédures d'optimisation adaptative apparaissent comme le moyen le plus prometteur pour conduire la matière dans un état particulier[43].

Ces techniques de mise en forme temporelle adaptative ont été largement mises en place dans le domaine de la femtochimie[44] via un pilotage en temps réel du faisceau laser. Dans le contexte de l'ablation laser, ce type de technique a déjà montré son efficacité pour le contrôle de l'éjection d'ions[43,45] ou pour la synthèse de nanoparticules de taille choisie[46]. Des applications en spectroscopie ou caractérisation de faiceau laser ont également été envisagées[47,48]. Le dépôt de couches minces ou la LIBS (Laser Induced Breakdown Spectroscopy) apparaissent alors également comme des applications potentielles.

Ces techniques adaptatives nécessitent un moyen de diagnostic du procédé qui sert ensuite de boucle de rétro-action sur les conditions d'interaction. Diverses techniques peuvent être utilisées : spectrométrie de masse à temps de vol pour caractériser les ions éjectés, décharge Corona pour déterminer la taille des nanoparticules.

---

[41] N. Jegenyes, Z. Toth, B. Hopp, J. Klebniczki, Z. Bor, and C. Fotakis, Appl. Surf. Sci., 252 (2006) 4667

[42] C. Ristoscu, G. Socol, C. Ghica, I.N. Mihailescu, D. Gray, A. Klini, A. Manousaki, D. Anglos, and C. Fotakis, Appl. Surf. Sci., 252 (2006) 4857.

[43] R. Stoian, A. Mermillod-Blondin, N.M. Bulgakova, A. Rosenfeld, I.V. Hertel, M. Spyridaki, E. Koudoumas, P. Tzanetakis, and C. Fotakis, Appl. Phys. Lett., 87 (2005) 124105.

[44] R.S. Judson, and H. Rabitz, Phys. Rev. Lett., 68 (10) (1992) 1500.

[45] H. Dachraoui, and W. Husinsky, Phys. Rev. Lett., 97 (2006) 107601

[46] R. Hergenröder, M. Miclea, and V. Hommes, Nanotechnology, 17 (2006) 4065.

[47] R. Ackermann, E. Salmon, N. Lascoux, J. Kasparian, P. Rohwetter, K. Stelmaszczyk, S. Li, A. Lindinger, L. Wöste, P. Béjot, L. Bonacina, and J-P. Wolf, Appl. Phys. Lett., 89 (2006) 171117

[48] V.V. Lozovoy, B. Xu, Y. Coello, and M. Dantus, Optics Express, 16 (2) (2008) 592.

Nous avons fait le choix de mettre en place une mise en forme temporelle du faisceau laser femtoseconde sur la base de la caractérisation du plasma par spectroscopie optique d'émission. En effet, dans les conditions de réalisation de couches minces (fluence laser assez éloignée du seuil d'ablation), il existe une corrélation forte entre les caractéristiques des espèces ablatées et les propriétés des films obtenus. La spectroscopie optique d'émission est un moyen de diagnostic, amplement utilisé et permettant d'accéder à une large palette de grandeurs : nature des espèces (atomes, ions, ..), énergie des espèces, taux d'ionisation....

2. Contrôle du plasma par mise en forme temporelle adaptative d'impulsions lasers femtosecondes

Ces travaux préliminaires font l'objet de la thèse de Matthieu GUILLERMIN. Ils sont détaillés dans la publication [27] (M. GUILLERMIN et al., *Applied Surface Science,* à paraître 2008).

Un dispositif spécifique a été conçu et mis en place (**Figure 22**). Il s'agit de caractériser le plasma d'ablation par spectroscopie optique d'émission et d'insérer les résultats issus de cette caractérisation dans une boucle de rétro-action, agissant alors sur la forme temporelle de l'impulsion. Cette mise en forme est effectuée via un SLM (Spatial Light Modulator), qui permet un retard relatif des composantes spectrales du faisceau laser, pilotant ainsi la forme temporelle de l'impulsion. La boucle d'optimisation est basée sur un algorithme génétique, développé en dehors de ce travail[43].

Les premiers travaux ont été consacrés à l'étude de l'ablation de l'aluminium, avec le souhait d'augmenter la proportion d'ions dans le plasma, tout en diminuant l'émission des espèces neutres. Les résultats sont présentés sur les **Figure 23** et **Figure 24**, représentant respectivement les raies atomiques (AlI) et ionique (AlII) et les formes temporelles des impulsions courte (SP) et optimisée (OP).

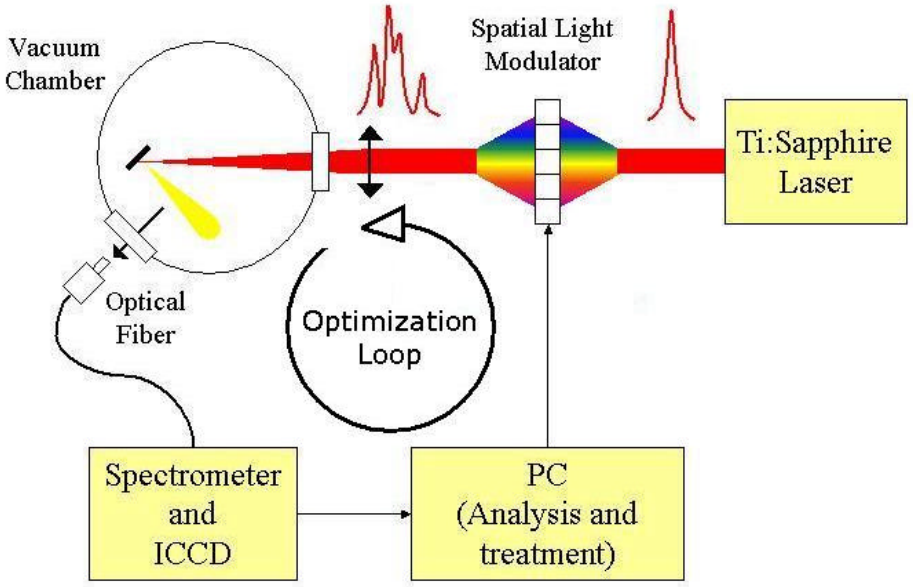

Figure 22 : Dispositif expérimental mis en place pour la mise en forme temporelle adaptative de l'impulsion laser à partir de la caractérisation du plasma par spectroscopie optique d'émission.

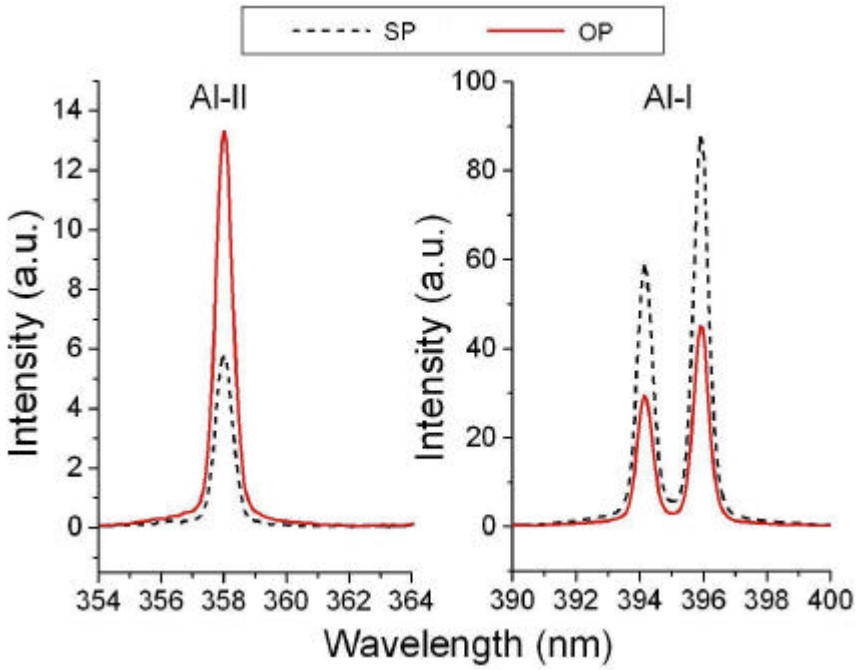

Figure 23 : Raies ionique et atomique de l'aluminium obtenues avec l'impulsion laser femtoseconde (SP) et l'impulsion laser optimisée (OP)

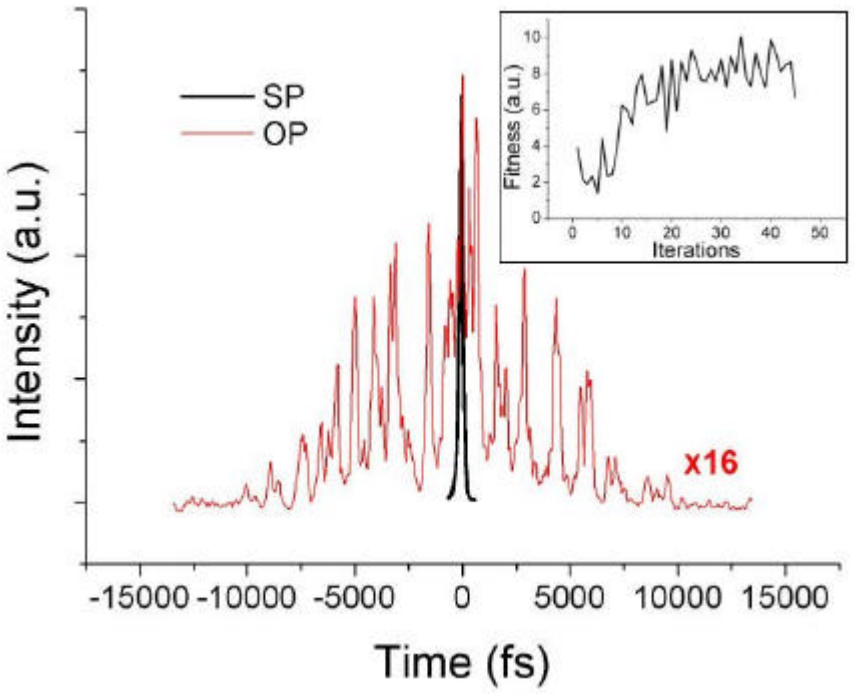

Figure 24 : Forme temporelle de l'impulsion laser femtoseconde (SP) et optimisée (OP).

Ce dispositif permet donc de multiplier le signal issu d'une raie d'émission ionique par un facteur supérieur à 3 tout en abaissant le signal issu des atomes d'aluminium. Ces résultats peuvent être comparés avec des impulsions de forme plus classique, du type double pulse ou pulse élargi, extraits de la forme temporelle optimisée et montrent l'intérêt d'une optimisation adaptative puisque les résultats permettent d'aller au delà de ce qui peut être obtenu avec ces impulsions classiques. En effet, un pulse élargi (τ = 6 ps) conduit à une augmentation du signal ionique tandis qu'un double pulse (Δt = 10 ps) conduit à une diminution du signal atomique, sans doute dû à des effets d'écrantage. La forme optimisée déduite de ce type d'expérimentation apparait donc comme un bon compromis entre ces deux types de formes temporelles.

Il est donc tout à fait envisageable que la morphologie ou la structure cristalline des couches soit modifiées. Des premières analyses mettent en effet en évidence une proportion nettement plus faible de nanoparticules dans le cas où l'impulsion laser de forme temporelle optimisée est utilisée (**Figure 25**).

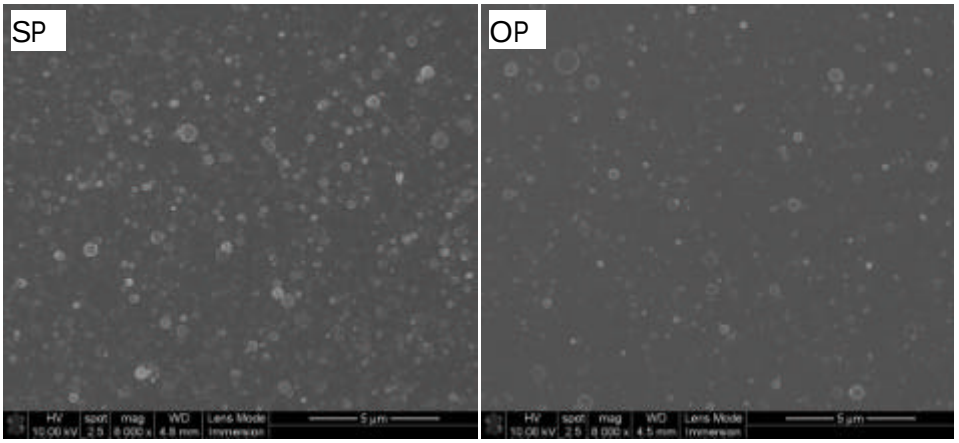

Figure 25 : images MEB de dépôts d'aluminium obtenus avec une impulsion femtoseconde (SP) et une impulsion femtoseconde optimisée (OP)

Ces premiers travaux mettent bien en évidence les potentialités de cette technique, même si, bien sûr, ces premiers résultats obtenus dans le cas d'un matériau extrêmement simple doivent être complétés et étendus. Il faudra appliquer ce dispositif au contrôle de la nature et de l'énergie cinétique des particules du plasma.

La suite de ce travail envisage donc de mieux comprendre les effets d'une mise en forme temporelle de l'impulsion laser femtoseconde sur les propriétés des produits d'ablation et donc des couches minces élaborées. Cela passera nécessairement par une confrontation avec des travaux théoriques (en collaboration avec J.P. Colombier et R. Stoian) de modélisation de l'interaction laser – matière afin de maîtriser et surtout influencer les trajectoires thermodynamiques suivies par le matériau irradié (du type de la Figure 12, page 47). Une modification de la répartition entre les effets mécaniques et les effets thermiques conduisant à l'ablation du matériau permettrait alors de modifier le temps de piégeage des couches de liquide formées dans la cible irradiée. Un des objectifs majeurs reste en effet le contrôle de la taille des nanoparticules suite à des schémas d'interaction pilotés directement par la forme temporelle de l'impulsion laser.

En outre, cette étude devra être appliquée au dépôt de couches minces et de fait, ne devra évidemment donc pas se limiter à des matériaux simples. Nous envisageons de l'étendre à des matériaux composés, pour lesquels un contrôle de la stoechiométrie et

de la cristallinité serait primordial, comme par exemple ZnO, pour lequel de nombreux travaux ont été effectués aussi bien en PLD nanoseconde que femtoseconde.

Compte tenu des travaux que nous avons nous-même conduits sur la synthèse de DLC par PLD femtoseconde, il n'est pas exclu d'utiliser ce type de dispositif pour tenter de piloter l'énergie cinétique des espèces ablatées, comme cela a déjà été obtenu sur du silicium[43]. Cela permettrait alors peut être d'augmenter le taux de sp^3 dans la couche (pour se rapprocher de celui obtenu en PLD nanoseconde) tout en maintenant à la fois un taux de contraintes résiduelles et une proportion de particules de taille micronique faibles.

Un aspect qui nous semble également primordial serait la possibilité de contrôler la stoéchiométrie des produits d'ablation, avec une application évidente à des techniques de caractérisation comme la LIBS pour laquelle une ablation congruente fait toujours défaut obligeant le recours aux impulsions courtes et aux impulsions de type double pulse.

L'essentiel du travail reste donc à faire en termes d'exploitation du dispositif pour la synthèse de couches minces, la synthèse de nanoparticules ou encore l'application à des techniques telles que la LIBS femtoseconde.

Publications

significatives

- F. GARRELIE, A.S. LOIR, C. DONNET, F. ROGEMOND, R. LE HARZIC, M. BELIN, E. AUDOUARD, P. LAPORTE, *Surface and Coatings Technology*, **163-164** (2003), 306.
- A.S. LOIR, F. GARRELIE, C. DONNET, F. ROGEMOND, J.L. SUBTIL , B. FOREST, M. BELIN, P. LAPORTE, *Surface and Coatings Technology* **188-189** *(2004), 728-734.*
- T. KATSUNO, C. GODET, J.C. ORLIANGES, A.-S. LOIR, F. GARRELIE, AND A. CATHERINOT, *Applied Physics A* **81**, (3) (2005), 471-476.
- N. BENCHIKH, F. GARRELIE, C. DONNET, B. BOUCHET-FABRE, K. WOLSKI, F. ROGEMOND, A.S LOIR, J.L. SUBTIL *Thin Solid Films* **482**(1-2), (2005) pp287-292.
- N. BENCHIKH, F. GARRELIE, K. WOLSKI, C. DONNET, R.Y. FILLIT, F. ROGEMOND, J.L. SUBTIL, Thin solid films, **494** (1-2) (2006), 98-104.
- R. MAALOUF, H. CHEBIB, Y. SAIKALI, O. VITTORI, M. SIGAUD, F. GARRELIE, C. DONNET AND N. JAFFREZIC-RENAULT, Talanta **72** (2007), 310-314.
- A. SIKORA, A. BERKESSE, O. BOURGEOIS, J.-L. GARDEN, C. GUERRET-PIECOURT, J.N. ROUZAUD, A.-S. LOIR, F. GARRELIE, C. DONNET, à paraître dans Solid State Science 2008.
- A.S. LOIR, F. GARRELIE, J.L. SUBTIL, F. GOUTALAND, M. BELIN, R. LE HARZIC C. DONNET, Y. OUERDANE, F. ROGEMOND, P. LAPORTE, *Applied Surface Science*, **208-209** (2003),pp553-560.
- F. GARRELIE, N. BENCHIKH, C. DONNET, R.Y. FILLIT, J.N. ROUZAUD, J.Y. LAVAL, V. PAILLERET, Applied Physics A **90** (2008) 211-217
- M. GUILLERMIN, C. LIEBIG, F. GARRELIE, R. STOAIN, A.-S. LOIR, E. AUDOUARD, à paraître dans Applied Surface Science 2008.

ELSEVIER

Surface and Coatings Technology 163–164 (2003) 306–312

SURFACE & COATINGS TECHNOLOGY

www.elsevier.com/locate/surfcoat

Femtosecond pulsed laser deposition of diamond-like carbon thin films for tribological applications

F. Garrelie[a], A.S. Loir[a], C. Donnet[a,b,*], F. Rogemond[a], R. Le Harzic[a], M. Belin[b], E. Audouard[a], P. Laporte[a]

[a]*Laboratoire Traitement du Signal et Instrumentation, UMR 5516, Université J. Monnet, 23 rue du Dr P. Michelon, 42023 Saint-Etienne Cedex 2, France*

[b]*Laboratoire de Tribologie et Dynamique des Systèmes, UMR 5513, Ecole Centrale de Lyon, 36 avenue Guy de Collongue, 69134 Ecully Cedex, France*

Abstract

Pulsed laser ablation is a well-known technique used for thin film deposition of hard and wear resistant diamond-like carbon (DLC) films. Most of the previous studies were carried out by using pulse duration in the nanosecond range. Compared to conventional nanosecond laser ablation, femtosecond laser allows the production of high energy (up to a few keV) ions in the plasma, which may strongly affect the structure and properties of the deposited films. The present study was achieved by ablating graphite targets with femtosecond (10^{-15} s range) laser pulses. DLC films were deposited under vacuum onto (1 0 0) p-type silicon substrates at room temperature. The laser pulse energy was 1.5 mJ at a repetition rate of 1 kHz. The fluence (or energy density) range was between 1 and 6 J/cm^2. The nature and mechanical properties of the films are characterized by X-ray absorption near-edge spectroscopy and nanoindentation techniques. The tribological behavior of the films are also investigated in a pin-on-plate configuration. Correlations between the structure of the films and some of their properties are highlighted, depending on the deposition conditions. Discussion is focused on the comparison between present results obtained using the femtosecond mode, with previously published results related to DLC films deposited using the nanosecond mode.

Keywords: Diamond-like carbon; Pulsed laser deposition; X-ray absorption near-edge spectroscopy; Friction

1. Introduction

Pulsed laser deposition (PLD), known for well over two decades, has gained prominence on the deposition of a wide variety of thin film materials. In particular, the synthesis of diamond-like carbon (DLC) films still has a large share of PLD research and development studies [1,2]. The interest in deposition of DLC by PLD stems from the fact that unhydrogenated DLC films with high purity can be obtained with a predominance of sp^3 hybridization at low deposition temperature. Control over coating deposition and properties is achieved by selecting target materials, laser wavelength and output energy, pulse frequency, background pressure, eventually additional substrate heating, biasing, and ionization assistance [3]. Most of the studies were performed by using pulse laser duration in the nanosecond range, as described in a selection of recent papers [4–12] where correlations between the deposition process, the nature of the film and some of their physical properties are discussed.

However, correlations with mechanical properties and tribological behaviors are less systematically proposed, as pointed out early by Voevodin and Donley [3]. A minimum laser power density on the target surface seems to be required to deposit coatings with design properties for wear protection. This level is approximately 10^{11} W/cm^2 for YAG lasers with wavelength $\lambda = 1.06$ μm, while for excimer lasers with $\lambda = 193$ or 248 nm, this level is approximately 10^8 W/cm^2. The combination of these conditions with a vacuum range below 10^{-5} Pa during deposition is required to obtain a plume containing ions and excited atoms with energy up to a few hundred eV. Deposition rates are controlled with the laser pulse frequency, which is typically varied

*Corresponding author. Tel.: +33-4-77-46-11-20; fax: +33-4-77-48-51-20.

E-mail address: christophe.donnet@univ-st-etienne.fr (C. Donnet).

0257-8972/03/$ - see front matter © 2002 Elsevier Science B.V. All rights reserved.
PII: S0257-8972(02)00481-4

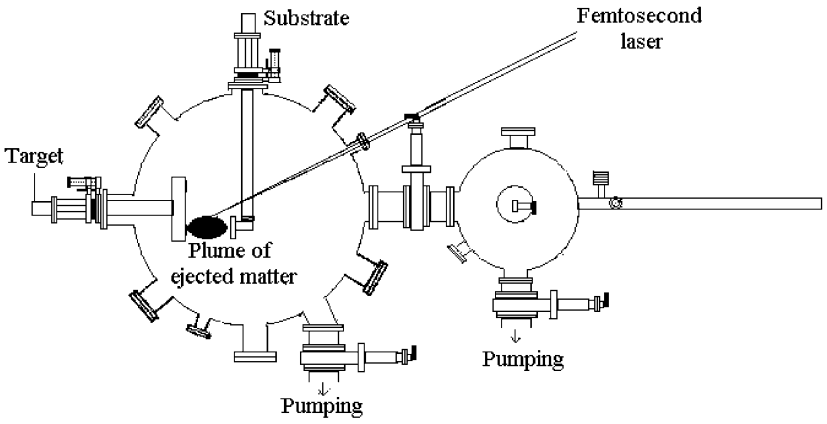

Fig. 1. Schematic of the deposition device.

between 1 and 100 Hz. By optimizing these parameters, hardness values between 20 and 70 GPa, and friction coefficients in the 0.1 range up to 10^5 cycles for contact pressures less than 0.8 GPa (depending on the contacting materials and relative humidity) have been published. At higher contact pressures, film failures after 10^2–10^3 cycles have been recorded, with strong evidence of insufficient adhesion of the films to the substrates. Increasing the qualities of the films, including adhesion, for severe tribological applications is critical. Two approaches can be developed to improve adhesion: one is to deposit supporting interlayers, and another is to modify the substrate during deposition. The second approach can be achieved in PLD by increasing the energy of the deposited carbon species to levels sufficient to implant them into the substrate and form an interfacial transition layer. This can be realized by the introduction of additional energy in ablated plumes by different biasing methods [3]. This can be also theoretically achieved by using ultra-short pulses (femtosecond) allowing higher power density ($>10^{11}$ W/cm^2) and kinetic energies of deposited carbon species (keV range), compared to conventional nanosecond pulses.

Recently, several research groups have developed pico- and femto-second PLD for the deposition of DLC films [13–19]. These studies are mainly focused on the characterization of the kinetic energies of the ions of the plasma produced from the femtosecond pulses and on the film structure [13,15]. In particular, it has been shown that the plasma plume may contain ions with energy up to a few keV. The present work presents the first steps related to the optimization of DLC films produced by femtosecond PLD, with highlights on the correlation between the process parameters (mainly the laser fluence, 1–6 J/cm^2 range), the nature of the films (investigated by X-ray absorption near-edge spectroscopy, XANES) and some of their mechanical and tribological properties.

2. Experimental

The schematic diagram of the growth system is shown in Fig. 1. DLC films were deposited using a mode-locked Ti: sapphire laser. The femtosecond laser (Concerto, BMI/TCL) working at 800 nm, with an output energy per pulse of 1.5 mJ and a pulse duration of 150 fs at a repetition rate of 1 kHz, is focused with an incidence angle of 45° onto a high purity graphite target (99.997%) to a spot of approximately 200 μm in diameter. The target is continuously rotated during the deposition process. Experiments take place in a high vacuum chamber (residual pressure below 10^{-5} Pa). The (1 0 0) p-type silicon substrate (approximate area of 15×15 mm^2) is located in front of the target at a distance of approximately 4 cm and the deposition is performed at ambient temperature.

Table 1
Experimental conditions for femtosecond PLD of DLC films

Laser source	Ti: sapphire 800 nm
Pulse width (FWHM)	150 fs
Pulse energy	1.5 mJ
Repetition rate	1 kHz
Deposition time	5 min
Fluence range (energy density)	1.0–6.0 J/cm^2
Laser intensity (power density)	6.7×10^{12} to 4×10^{13} W/cm^2
Substrate	Si with SiO_2 natural top surface layers
Substrate temperature	Room temperature (no heating but intrinsic heating during deposit may occur)

Table 2
Characteristics and properties of the selected films

Sample	Fluence (J/cm^2)	Thickness (nm)	Deposition rate (nm/min)	sp^3 content (%)	Hardness (GPa)	Young's modulus (GPa)	Residual stress (GPa)
A	1.35	300	50	71	20 ± 2.3	240 ± 29	-0.81
B	2.82	150	30	73	25 ± 2.5	260 ± 10	-1.85
C	5.18	95	20	70	18 ± 1.3	210 ± 13	-2.83

The deposition conditions for DLC films are summarized in Table 1. Before the deposition, the silicon substrates were ultrasonically cleaned for 3 min in acetone and ethanol bath prior to entering the vacuum chamber. During the deposition processes, three different laser fluences were achieved by varying the focusing of the laser spot. All other parameters are kept constant, in order to examine the influence of the kinetic energy of the plume species on the properties of the films. The laser fluence, which is strongly correlated to the plume expansion dynamics [13,15] and may be ascribed as the main parameter process, should strongly influence the adhesion and the structure of the films, as already pointed out.

After deposition, the film thickness was measured by a Dektak profilometer using a masked area on the samples. These measurements also provide film roughness estimations. By measuring the radius of curvature of the film before and after deposition, it was also possible to calculate the internal stress, as described in Ref. [20]. The carbon hybridizations of the films were investigated by XANES performed at the Canadian synchrotron radiation facility on the SGM beamline. The data was collected in the total electron yield mode by directly monitoring the sample current and was normalized to the simultaneously recorded signal from a nickel mesh. Additional normalization was performed by recording the signal from a HF etched Si (1 0 0) wafer in the regions under study, to eliminate the absorption due to the contamination in the beamline optics. The resolution is better than 0.2 eV at the C–K-edge. The mechanical properties of the films were determined from load–displacements curves obtained using a Nano Indenter® XP apparatus. The system has load and displacement resolution of 0.3 μN and 0.8 nm, respectively. A three-sided pyramid Berkovich indenter was used in all the experiments. The hardness was calculated, as the applied force required to induce plastic penetration divided by the projected area of contact between the indenter and the specimen. Young's modulus E was determined from the slope of the unloading force–displacement curve. The tribological behavior of the films has been studied at room temperature using a reciprocating pin-on-flat configuration in ambient air (25–30% relative humidity). The evolution of the friction coefficient was recorded using AISI52100 steel balls 6.00-mm diameter sized for normal applied loads ranging between 0.5 and 2 N, consistent with maximum Hertzian contact pressures ranging between 0.5 and 1.3 GPa. The sliding speed was 6 mm/s over a 3.0 mm-long wear track. In order to estimate the wear resistance, several cross-sectional profiles were taken across the wear track on the films after 50 000 cycles.

3. Results and discussion

3.1. Thickness, deposition rate, roughness

DLC films were deposited on silicon substrates during 5 min using three different laser fluences (or energy density). The fluence values for DLC films and the properties of these films are summarized in Table 2. As expected, the thickness of the films depends on laser fluence. By increasing fluence, one equilibrates the gradients in the plasma in the two directions of expansion of the plasma plume, leading to a broadening of the thickness distribution [21]. Indeed, at the highest fluences, the spot size is reduced (since the energy per pulse in constant) and the plume expands in two directions (parallel and perpendicular to the surface). On the contrary, at the lowest fluences, the spot size is higher, thus leading to a preferential expansion perpendicular to the surface. Consequently, the use of low fluences (sample A) leads to thicker films than those obtained with higher fluences (sample C).

The film topography is altered by micron-sized particles. The splashing of these micron-sized particles is observed in the plasma plume at wide time intervals after the laser pulse [18]. However, the average size and the number of these micron-sized particles is lower than when using nanosecond laser. As already observed with nanosecond PLD, femtosecond laser produced large chunks with number increasing with increasing laser fluence [22].

3.2. Carbon hybridization

The potential for the use of XANES as an unambiguous method for determining carbon film quality was

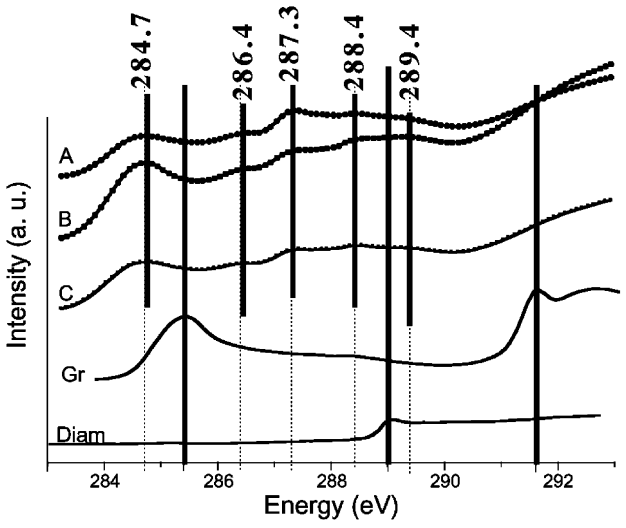

Fig. 2. C(1s) K-edge XANES spectra of the DLC films deposited with a laser fluence of (A) 1.35 J/cm^2 (9.00×10^{12} W/cm^2); (B) 2.82 J/cm^2 (1.89×10^{13} W/cm^2) and (C) 5.18 J/cm^2 (3.45×10^{13} W/cm^2). Reference spectra for graphite (Gr) and diamond (Diam).

shown by Capehart et al. [23] and recent investigations of XANES compared to other techniques such as electron energy loss spectroscopy (EELS) or Raman spectroscopy (RAMAN) were proposed for DLC, CN and BCN films [24,27]. XANES does not suffer the long range order sensitivity that other techniques such as RAMAN exhibit. EELS delivers the same information as XANES, but with a significant lower energy resolution and generally higher beam induced degradations during analysis. The XANES spectra corresponding to the transitions at the C–K-edge are depicted in Fig. 2, as a function of the laser fluence. The spectra of graphite and synthetic diamond recorded in the same experimental conditions are also plotted in the same figure. We carefully investigated the fine structure of the carbon K-edge, which appears as a mixture of different features. The spectra exhibit five distinct contributions, respectively, at 284.7, 286.4, 287.3, 288.4 and 289.4 eV, whatever the laser fluence. The peak at 284.7 eV can be attributed to the $1s\rightarrow\pi^*$ transition, even if it appears slightly below the peak corresponding to this transition in graphite. Such a shift compared to the graphitic reference has already been observed by others [27]. The two consecutive peaks at higher photon energies can be also attributed to $1s\rightarrow\pi^*$ transitions, described as some excitonic resonance for films containing hydrogen [24] or other elements such as B or N [25,26]. However, these elements should not be present in our films and this point remains unclear. The rather complex feature which was observed may thus be attributed to a mixture of different forms of molecular structure in the femtosecond PLD films, without further accurate interpretation available yet. The two last peaks are very close (<0.4 eV) of the $1s\rightarrow\sigma^*$ peak of synthetic diamond, whose absorption edge appears at 289.0 eV. A precise comparison between the three DLC indicates that the respective contribution of each peak depends very little on the laser fluence. An estimation of the $sp^3/(sp^2+sp^3)$ ratio may be deduced from the spectra, according to the method proposed by Pappas et al. [28]. Results are depicted in Table 2. The films have a predominant sp^3 hybridization (70–73%) and the slight differences in the hybridization from one film to the other are not significant from our point of view, even if the highest sp^3 content is observed for the intermediate fluence corresponding to the film exhibiting the highest hardness and Young's modulus.

3.3. Stress

Whatever the laser fluence, films exhibit compressive stress, which progressively increase from -0.81 GPa for the lowest fluence, to -2.83 GPa for the highest one, with an intermediate value (-1.85 GPa) for the intermediate fluence. Successful preparation of DLC films have long suffered from high compressive stress, as high as -10 GPa [1], regardless of the film growth technique used. High values of carbon species energy arriving at the substrate surface are known to contribute to high internal stress and adhesive failure of the coating may occur when the internal stress exceeds a critical value. Consequently, the rather moderate stress obtained with the present set of DLC films is rather surprising, considering that, from our knowledge, no stress measurements have been previously performed on DLC deposited by femtosecond PLD. For a short comparison between femtosecond PLD and nanosecond PLD, the laser–target interaction as well as the plume characteristics can be roughly discussed in both processes. Nanosecond PLD leads to lower values of carbon species energy in the plasma. However, due to the higher energy contained per laser pulse, the particle flow is higher than in femtosecond PLD. The unexpected values of stress of films obtained by femtosecond PLD may be ascribed to this feature. This result, if confirmed by further experiments, should be a noticeable advantage of femtosecond PLD compared to nanosecond PLD.

3.4. Mechanical properties

The nanohardness (H) and Young's modulus (E) as a function of indentation depth were measured for the three laser fluences and results are summarized in Table 2, with standard deviation corresponding to five different measurements per sample. Both mechanical properties

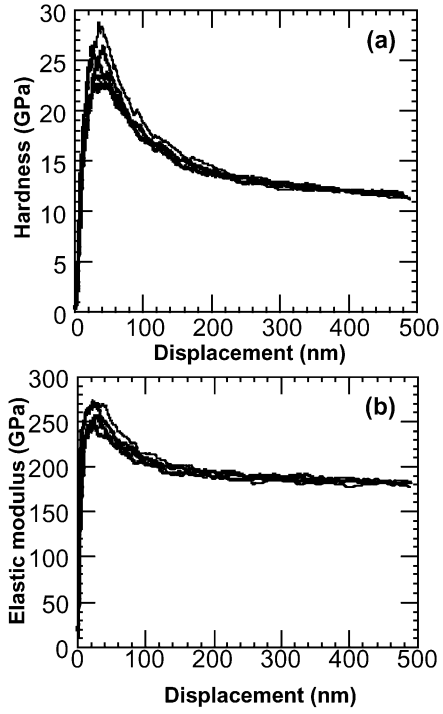

Fig. 3. (a) Hardness and (b) elastic modulus variations, measured by nanoindentation, as a function of the indentation depth, related to the DLC film deposited with a laser fluence of 2.82 J/cm^2 (1.89×10^{13} W/cm^2).

reach a maximum for the intermediate fluence (2.82 J/cm^2), with a hardness and Young's modulus of 25 and 260 GPa, respectively, (Fig. 3). Lower values of hardness and Young's modulus were observed both at a lower and a higher fluence. By comparing to nanoindentation results obtained with nanosecond PLD DLC films, the femtosecond DLC films exhibit rather moderate mechanical properties. Indeed, it has already been shown that both hardness and Young's modulus increase with fluence, reaching values as high as 55 and 500 GPa, respectively, for fluences higher than 17 J/cm^2 [29]. Present results indicate that a significant increase of the laser intensity, due to the ultra-short duration of the laser pulse in femtosecond mode, does not lead to an additional increase of the mechanical properties, in spite of rather high sp^3 contents deduced from XANES. But the present results seem to be in agreement with previous works related to the dependence between hardness and sp^3 content related to ta-C films: Shi et al. [30] observed a strong increase of the hardness from 20 up to 60 GPa, when the sp^3 content increases from 70 to 90%. Nevertheless, these moderate values of nanohardness and Young's modulus are correlated to moderate values of internal compressive stress and finally, an enhancement of the adhesive properties of the films is expected, compared to nanosecond PLD films. This seems to be a promising behavior of ta-C deposited from femtosecond PLD.

3.5. Tribology

The film deposited at the medium fluence (B, 2.82 J/cm^2) exhibits an average friction coefficient which remains stable in the 0.1 range, without any significant fluctuation versus the number of sliding cycles. The friction results are in the same range whatever the contact pressure during the friction experiment. Such a behavior is typical of most of the published results related to unhydrogenated DLC films tested in ambient air [31]. Fig. 4 shows the wear track of the silicon plane coated with the DLC deposited at 2.82 J/cm^2, after the first 1000 cycles of friction performed at the highest contact pressure (1.3 GPa). The track width is approximately 90 mm, consistent with the theoretical Hertzian diameter of contact at the highest load (2 N). The wear resistance of this film was measured by performing a test over 50 000 cycles at a contact pressure of 0.5 GPa in ambient air. The wear coefficient is 1.6×10^{-8} mm^3/(N m), which corresponds to a wear of 0.5 nm per 1000 cycles. The films deposited at other fluences have not been tested yet. Considering that the objective of the present study is to explore the potentialities of femtosecond PLD for the deposition of DLC tribological films, these preliminary friction and wear results are encouraging to go further in the optimization of the deposition process.

4. Conclusion

Structural, mechanical and tribological properties of these films are studied, in relation to the laser fluence, and compared with those obtained in nanosecond regime. Whatever the fluence, the character of the carbon bonds deduced from the XANES analysis is predominantly sp^3 ($\sim$70%), although the values of the nanohardness and Young's modulus are rather moderate (compared to nanosecond PLD). On the other hand, the compressive stresses which increase with the laser fluence have unexpected low values, which could constitute an important advantage of the femtosecond PLD method, compared to the conventional ones. These preliminary results show that the femtosecond laser is a good candidate for the elaboration of DLC films for tribological applications. Complementary characterizations as well as elaboration of other materials are under way.

Acknowledgments

The present study has been achieved with the financial support of the Région Rhône-Alpes and the Conseil

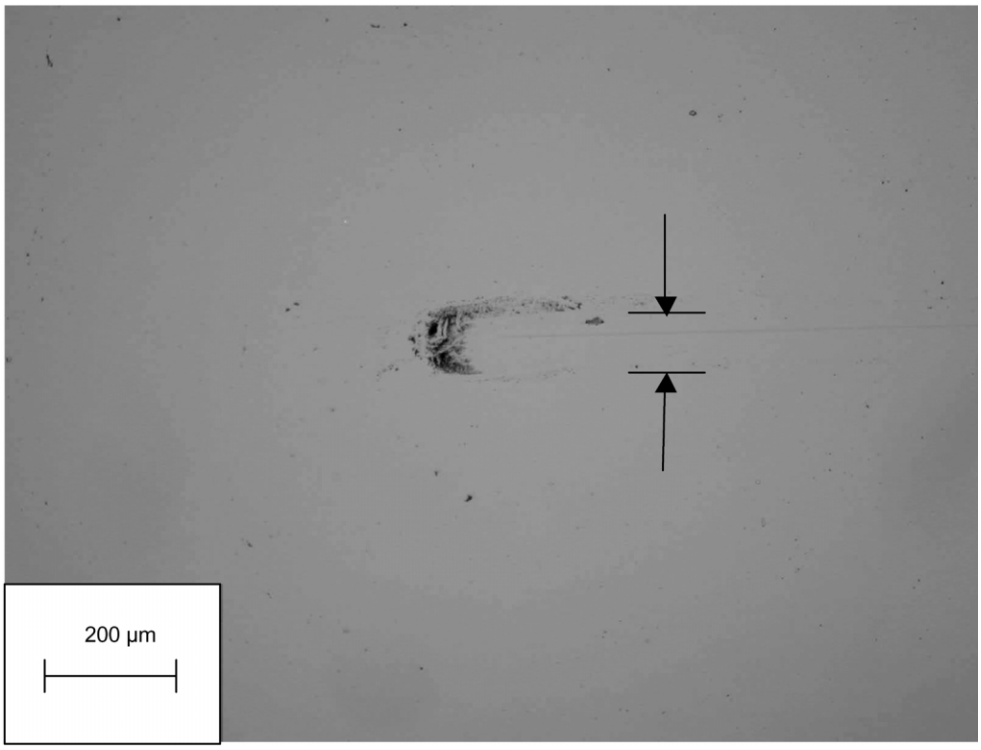

Fig. 4. Optical micrograph of the wear track related to the DLC film deposited with a laser fluence of 2.82 J/cm^2 (1.89×10^{13} W/cm^2), after 1000 cycles in ambient air.

Général de la Loire (France), the European Community (1997–1999 FEDER program). The authors acknowledge S. Pavan and Dr J.L. Loubet for nanoindentation experiments, and Dr M. Kasrai for XANES experiments.

References

[1] A.A. Voevodin, M.S. Donley, J.S. Zabinski, Surface and Coatings Technology 92 (1997) 42.
[2] D.B. Chrisey, C.K. Hubler (Eds.), Pulsed Laser Deposition of Thin Films, Naval Research Laboratory, Washington, DC, 1994.
[3] A.A. Voevodin, M.S. Donley, Surface and Coatings Technology 82 (1996) 199.
[4] V.I. Merkulov, D.H. Lowndes, G.E. Jellison Jr., A.A. Puretzky, D.B. Geohegan, Applied Physics Letters 73 (18) (1992) 2591.
[5] M. Tabbal, P. Merel, M. Chaker, et al., Journal of Applied Physics 85 (7) (1999) 3860.
[6] K.J. Koivusaari, J. Levoska, S. Leppavuori, Journal of Applied Physics 85 (5) (1999) 2915.
[7] S. Rey, F. Antony, B. Prevot, et al., Applied Physics A: Materials Science and Processing 71 (2000) 433.
[8] M. Bonelli, A.P. Fioravanti, A. Miotello, P.M. Ossi, Europhysics Letters 50 (4) (2000) 501.
[9] K.S. Shim, S.M. Kim, S. Hyuck Bae, S. Yeol Lee, H.S. Jung, H.H. Park, Applied Surface Science 154/155 (2000) 482.
[10] A.K. Sharma, R.J. Narayan, J. Narayan, K. Jagannadham, Materials Science and Engineering B77 (2000) 139.
[11] N. Matsuyama, K. Yukimura, T. Maruyama, Journal of Applied Physics 89 (3) (2001) 1938.
[12] Q. Wei, J. Sankar, J. Narayan, Surface and Coatings Technology 146/147 (2001) 250.
[13] F. Qian, V. Craciun, R.K. Singh, S.D. Dutta, P.P. Pronko, Journal of Applied Physics 86 (4) (1999) 2281.
[14] A.V. Rode, B. Luther-Davies, E.G. Gamaly, Journal of Applied Physics 85 (8) (1999) 4222.
[15] P.S. Banks, L. Dinh, B.C. Stuart, et al., Applied Physics A69 (1999) S347.
[16] M. Okoshi, S. Higuchi, M. Hanabusa, Applied Surface Science 154/155 (2000) 376.
[17] D.S. Yao, J.R. Liu, L.G. Wang, C.X. Yu, R.J. Zhan, Chinese Physics Letters 17 (7) (2000) 540.
[18] F. Garrelie, C. Jonin, E. Baubeau, et al., CLEO CFK5, May 7–12 (2000) 615.
[19] M.D. Shirk, P.A. Molian, Carbon 39 (2001) 1183.
[20] V. Stambouli, O. Burat, D. Bouchier, G. Gautherin, Surface and Coatings Technology 43/44 (1990) 137.
[21] J.C.S. Kools, T.S. Baller, S.T. de Zwart, J. Dieleman, Journal of Applied Physics 71 (9) (1992) 4547.
[22] B. Angleraud, F. Garrelie, F. Tetard, A. Catherinot, Applied Surface Science 138/139 (1999) 507.
[23] T.W. Capehart, T.A. Perry, C.B. Beetz, et al., Applied Physics Letters 55 (1989) 957.
[24] F.L. Coffman, R. Cao, P.A. Pianetta, S. Kapoor, M. Kelly, L.J. Terminello, Applied Physics Letters 69 (4) (1996) 568.
[25] R. Gago, I. Jimenez, T. Sajavaara, E. Rauhala, J.M. Albella, Diamond and Related Materials 10 (2001) 1165.
[26] J.C. Sanchez-Lopez, C. Donnet, F. Lefèbvre, C. Fernandez-Ramos, A. Fernandez, Journal of Applied Physics 90 (2) (2001) 675.
[27] S. Bhattacharyya, M. Lübbe, P.R. Bressler, D.R.T. Zahn, F. Richter, Diamond and Related Materials 11 (2002) 8.

[28] D.L. Pappas, K.L. Saenger, J. Bruley, W. Krakow, J.J. Cuomo, Journal of Applied Physics 71 (11) (1992) 5675.
[29] A.A. Voevodin, S.J.P. Laube, S.D. Wlack, J.S. Solomon, M.S. Donley, J.S. Zabinski, Journal of Applied Physics 78 (6) (1995) 4123.
[30] X. Shi, D. Flynn, B.K. Tay, et al., Philosophical Magazine B 76 (1997) 351.
[31] A. Erdemir, C. Donnet, in: B. Bhushan (Ed.), Modern Tribology Handbook, vol. 2, CRC Press LLC, Boca Raton, 2000, p. 871, Chapter 24.

Available online at www.sciencedirect.com

SCIENCE DIRECT

Surface & Coatings Technology 188–189 (2004) 728–734

SURFACE & COATINGS TECHNOLOGY

www.elsevier.com/locate/surfcoat

Towards the deposition of tetrahedral diamond-like carbon films on hip joints by femtosecond pulsed laser ablation

A.S. Loir[a], F. Garrelie[a], C. Donnet[a,b,*], F. Rogemond[a], J.L. Subtil[a], B. Forest[c], M. Belin[b], P. Laporte[a]

[a]*Université Jean Monnet, Laboratoire Traitement du Signal et Instrumentation UMR 5516, Bâtiment F, 10 rue Barrouin, 42000 Saint-Etienne, France*
[b]*Ecole Centrale de Lyon, Laboratoire de Tribologie et Dynamique des Systèmes UMR 5513, 36 avenue Guy de Collongue, 69 134 Ecully, France*
[c]*Ecole Nationale Supérieure des Mines, Centre Science des Matériaux et des Structures, 158 cours Fauriel, 42023 Saint-Etienne Cedex, France*

Available online 1 September 2004

Abstract

Compared to conventional nanosecond laser ablation, femtosecond pulsed laser deposition (PLD) allows the production of higher energy ions (up to a few keV) in the plasma plume, which strongly affect the structure and properties of the deposited films. In this work, tetrahedral diamond-like carbon (ta-C) films have been deposited by femtosecond PLD on various substrates, including 316L stainless steel, in order to extend the wear resistance of materials used for hip joint replacement. The deposition process has been optimized to obtain smooth and wear-resistant carbon films by ablating a graphite target in ultra-high vacuum conditions at room temperature, with a laser fluence (energy density) ranging from 1 to 6 J cm^{-2}. In situ sputter cleaning of the substrates in an argon atmosphere prior to carbon deposition has been widely investigated: tensile tests show that the adhesion of the films on stainless steel substrates is remarkably enhanced by removing the contamination and oxidized top-coats. The films exhibit high wear resistance (in the 10^{-8} to 10^{-9} mm^3 N^{-1} m^{-1} range) with moderate hardness (in the 20–30 GPa range), which may be favorable for the accommodation motion between contacting surfaces in a hip joint. The ability of these films to satisfy the biomedical requirements is discussed and the possibility to deposit homogeneous ta-C films on a 22.2-mm diameter hemispherical surface is examined. Finally, homogeneous films have been deposited on a 316L stainless steel femoral head, whose wear behavior will be quantified using a walking simulator during several millions of cycles (corresponding to the human activity during several years).

Keywords: DLC; Femtosecond pulsed laser deposition; Adhesion; Hip joint

1. Introduction

Various medical devices, including hip and knee joints, coronary stents, heart valves, intraocular lenses, are implanted in the human body to fulfill biological and mechanical functions. The implants should prevent infections and uncontrolled cell growth, maintain their integrity inside the body, withstand dynamical mechanical contact pressures and avoid formation of debris over a desired long-term biological interaction with the surrounding biological tissue. As pointed out by Tiainen [1], total hip replacement is one of the most challenging type of human implants from the material science's point of view. The highly corrosive environment and the low tolerance of the body to some dissolution products strongly restrict the materials available for implants. For hip prosthesis, the femoral head is made of metallic alloys (stainless steel, CoCr or some Ti-based alloys) or ceramics (Al_2O_3 or ZrO_2). The acetabular cup (socket) is usually made of ultra-high molecular weight polyethylene (UHMWPE). In spite of improvements in the optimization of prosthesis (design, material composition, surface roughness, etc.), the lifetime of a hip implant is limited. With time, the wear, corrosion or biological reactions with the tissue leading to

* Corresponding author. Tel.: +33 4 77 91 58 01; fax: +33 4 77 91 57 81.
E-mail address: Christophe.Donnet@univ-st-etienne.fr (C. Donnet).

0257-8972/$ - see front matter © 2004 Elsevier B.V. All rights reserved.
doi:10.1016/j.surfcoat.2004.07.046

the implant degradation, increase so that after 10 years, about 10% of the implants have to be renewed and practical lifetime can be as low as 5–15 years.

Coating the implants with protective functional films may reduce or alleviate the problems described above and extend the lifetime of the implants. To achieve such surface improvements, a promising approach consists in choosing an existing biocompatible generic coating and exploring the way to optimize its deposition onto conventional biomaterials. Due to its bio-and haemocompatible nature, diamond-like carbon (DLC) films have known considerable developments for orthopedic and other implant applications. DLC is a metastable amorphous form of carbon with high wear resistance, low friction, chemical inertness and high-corrosion resistance [2]. Recent reviews [1,3,4] have pointed out the considerable work performed from the 1990s to improve the properties of DLC films in biological applications.

However, due to the diversity of DLC film structures and compositions, together with the versatility of deposition conditions, there is no agreement for specific DLC compositions dedicated to biological applications. Moreover, the adhesion of a DLC film strongly depends on the substrate (composition, surface preparation). In most of applications, underlayers are required to enhance the adhesion of the DLC on the substrate and thus to extend its wear life [5]. These underlayers are generally carbon-based gradient films containing alloying elements, such as Ti, Si or Cr. However, the presence of some of these elements may be forbidden in the human body due to reactions with the biological tissues.

The present study is focused on the ability of a rather emerging deposition process, femtosecond pulsed laser deposition (PLD), to the synthesis of unhydrogenated tetragonal amorphous DLC (ta-C) exhibiting both high adhesion without underlayers and high wear resistance compatible with the hip joint application. PLD has proved to be an effective technique for the deposition of a wide variety of thin film materials, extending from DLC to oxides or nanostructured materials [6–8]. The interest in the deposition of DLC by PLD stems from the fact that unhydrogenated DLC films with high purity can be obtained with a predominance of sp^3 hybridization (diamond) at low deposition temperature (room temperature range). The advantages of femtosecond pulsed laser deposition compared to nanosecond one (higher power density values, very smooth surface films, etc.) have been detailed by some of us [9–11] and others [12]. The present paper is based on previous works dedicated to the DLC characterization [9–11,13] which will be shortly summarized. The optimization of adherence on biocompatible substrates, together with deposition on larger areas than the conventional cm^2 range usually investigated in basic coating studies, will be highlighted. At least, the deposition onto the hemispherical surface of a hip prosthesis has been performed and its test on a walking simulator during several millions cycles is in progress.

2. Experimental

Diamond-like carbon films have been deposited under vacuum conditions at room temperature onto (100) p-type silicon and 316L stainless steel, using a mode-locked Ti/sapphire laser. The experimental arrangement has been presented previously [9,10]. The femtosecond laser (Concerto, BMI/TCL) gives pulses of 150 fs with an output energy per pulse of 1.5 mJ at 800 nm, at a repetition rate of 1 kHz. The laser beam is focused with an incidence angle of 45° onto a high purity rotating graphite target (purity 99.997%). Laser fluences, in the range 1 to 6 J cm^{-2}, are obtained by keeping the laser beam energy constant on the target surface and by changing the illuminated area size. The adhesion of the deposited film onto biocompatible stainless steel substrates has been enhanced by sputter cleaning the substrates in an argon atmosphere prior to deposition. The experimental set-up of the plasma-sputtering configuration is depicted in Fig. 1. A pulsed direct current power supply (Advanced Energy) can provide up to 5 kW over the 325 to 650 V DC range with a maximum current of 15.5 A, depending on the output regulation selected. An inverter section converts DC to high-frequency voltage by alternating the current through switching transistors. This supply is employed as a current source of 0.25 A with a reverse time of 2 μs and a pulsation frequency of 120 kHz. The mean power is about 165 W with a high-frequency voltage of 657 V. Etching at an argon pressure of 1.5 Pa has been carried out during 5 min prior to deposition.

After deposition, film thickness and roughness have been estimated by profilometer measurements and atomic force microscopy. Other characterizations have been performed and are detailed in previous papers [9–11,13]. They include X-ray Absorption Near Edge Spectroscopy (XANES), Raman spectroscopy, nanoindentation and tribological tests.

The adhesion properties of the DLC films on 316L stainless steel substrates have been investigated by tensile tests. The adhesion measurement procedure carried out is detailed in paper [13]. Let us recall that it is based on the specifications of the French NF S 94-072, November 1998, standard that applies for adhesion measurements of Ca, P-based coatings in biomedical applications by means of a tensile test. Two cylindrical posts, diameter 15 mm, are used. The planar surface of an AISI 316L cylindrical post is polished to R_a=20 nm and then covered with a DLC coating. The planar surface of another AISI 316L cylindrical post is sand-blasted with aluminum oxide particles (60 μm diameter) and then stuck to the first post with glue (Eponal 317, Elf Atochem Corporation). Sticking is performed during 48 h before the tensile test, with a compressive force of 100 N between the two posts during the first 24 h. Tensile tests are performed at 3 mm/min. Tensile stress at breaking down is used as the measurement of adhesion. Three tests have been carried out for each deposition condition. The breaking position is recorded, giving information on the adhesion mechanism: breaking at the DLC coating/316L steel inter-

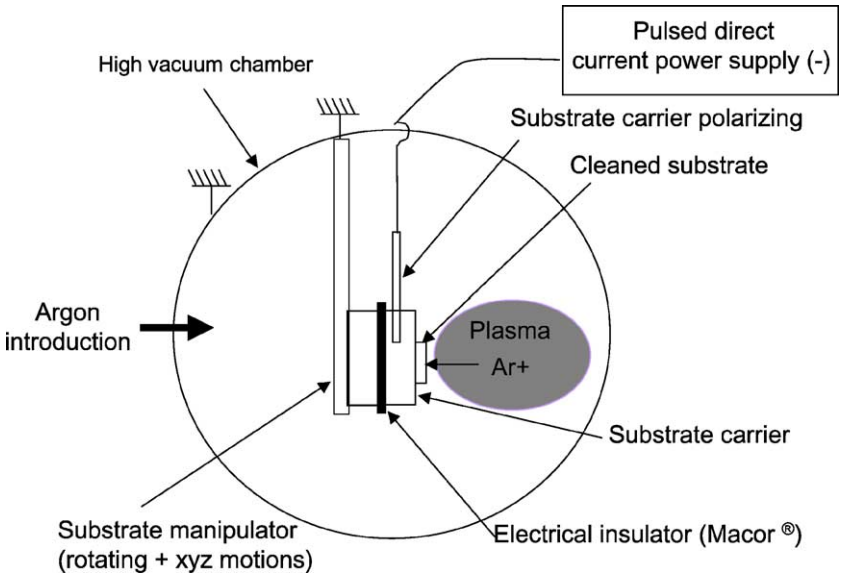

Fig. 1. Schematic view of the device of the sputter cleaning of 316L substrates.

face gives a pertinent adhesion limit of the coating. Breaking inside the glue or within other interfaces does not allow to quantify the adhesion between DLC coating and the 316L steel, but may give an quantitative indication below which the DLC is adherent on the steel substrate.

The deposition on a 316L stainless steel femoral head of a hip joint (diameter of 22.2 mm) has been performed with a designed sample holder set up in the vacuum chamber (Fig. 2). Due to the hemispherical surface, this device combines both tilting of 45° and rotation of the femoral head to

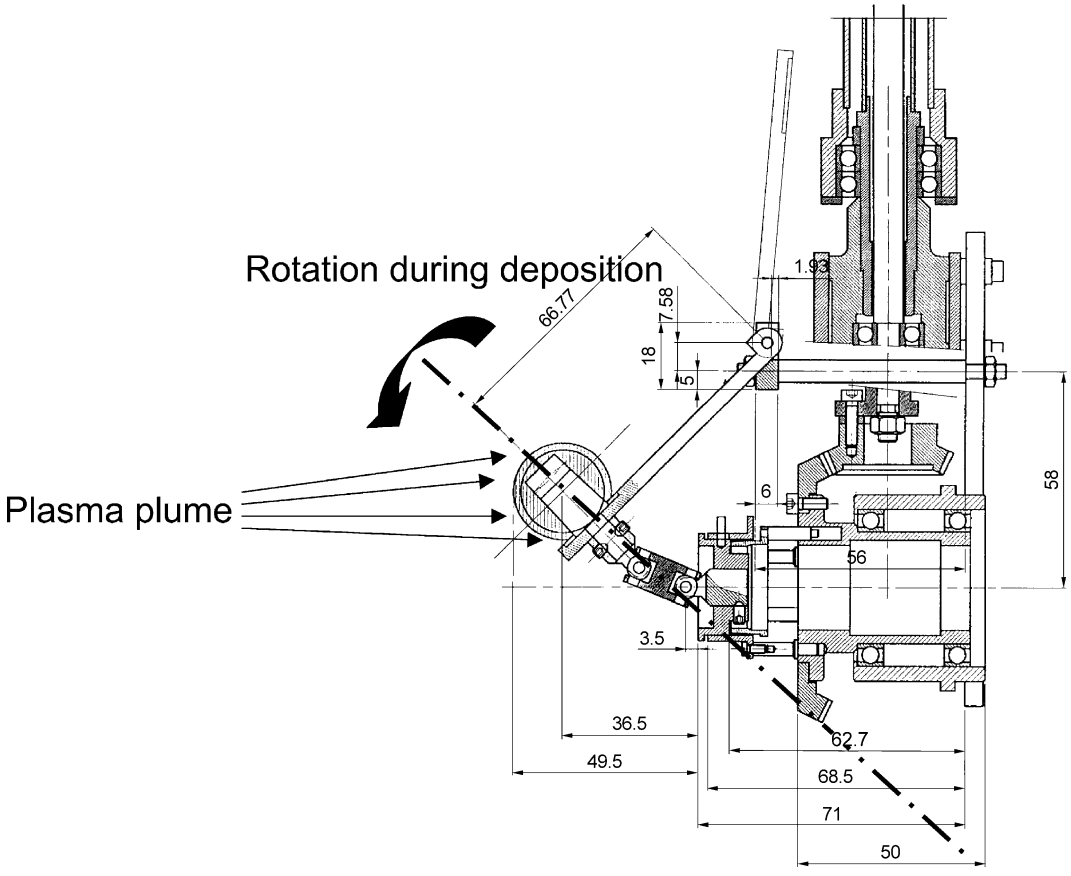

Fig. 2. Experimental device put in the vacuum chamber for the deposition on a 22.2-mm femoral head. The apparatus combines rotation and 45° tilting of the hemispherical surface.

achieve homogeneous off-axis deposition. It can be polarized for sputter cleaning of the 316L stainless steel head prior to carbon deposition. For a given laser fluence, a comparable DLC thickness has been deposited onto the usual cm^2 surface and the largest areas by adjusting the deposition duration to achieve homogenous DLC deposition on the largest surfaces [13].

3. Results and discussion

3.1. Film composition and structure

Table 1 summarizes some of the characteristics and mechanical properties of the films investigated, depending on the laser fluence within the range available with the deposition system at hands. Since most of these results have been already published [9–11], we propose a summary of these characteristics and properties, compared to other DLC films. The deposition rate depends on the laser fluence. Indeed, by increasing the fluence, one equilibrates the gradients in the plasma in the two directions of the expansion of the plasma plume, leading to a broadening of the thickness distribution [11]. Consequently, the deposition rate is lower at the highest fluence, as depicted in Table 1. Considering a deposition of 5 min at each fluence, the DLC thickness is 275, 135 and 90 nm respectively at 1.3, 2.8 and 5.2 J cm^{-2}. An estimation of the $sp^3/(sp^2+sp^3)$ ratio has been deduced from XANES experiments [10], according to the method proposed by Pappas et al. [14]. Whatever the fluence, the films present a predominant sp^3 hybridization of about 70%. From these estimations, the investigated films are rather tetragonal unhydrogenated amorphous DLC, labeled ta-C in the classification proposed by Robertson [2], as depicted in Fig. 3. Moreover, films deposited using the three laser fluences exhibit compressive stresses which progressively increase from −0.81 GPa for the lowest fluence value, to −2.83 GPa for the highest one. These compressive stresses are rather low for ta-C films and the use of femtosecond laser pulses has been correlated to these moderate values compared to nanosecond pulsed laser deposition, as already discussed in [10]. Such low values of compressive stresses may be an advantage to extend the wear life of the film in severe tribological conditions. Hardness (H) and Young's modulus (E), deduced from nanoindentation experiments [10], do not strongly depend on the laser fluence. Maximum values of H=25 GPa and E=260 GPa have been observed for the intermediate fluence. The order of magnitude of the hardness is consistent with a sp^3 percentage of 70%, in agreement with the already published dependence between hardness and sp^3 content related to ta-C films, as summarized by Shi et al. [15]. Visible Raman spectroscopy has been used to characterize the structure of the deposited materials [9]. Two features at about 1340 and 1500 cm^{-1}, known as the D and G bands respectively and related to sp^2 graphitic bonding in disordered carbon [2], have been observed, as with other DLC films deposited by nanosecond PLD [16,17]. A sharper peak located at 1140 cm^{-1} has been also observed and should tentatively be assigned to a vibrational mode of the nanocrystalline diamond phase [9,18,19]. Even if no quantification of the carbon hybridization can be deduced from visible Raman spectroscopy, these results are consistent with the coexistence of both sp^2 and sp^3 carbon hybridizations observed by XANES investigations.

3.2. Adhesion enhancement

In biomedical applications such as joint prosthesis, coating adhesion is paramount. Whatever the deposition process, DLC films on 316L stainless steel substrates generally show weak adhesion [20–23]. In order to improve this property, in situ sputter cleaning of the substrates has been carried out before DLC deposition. The cleaning process consists in removing the contaminated and oxidized surface layers by the argon plasma phase prior the DLC deposition, in the conditions described in Section 2. The thickness of the etched layer and the substrate roughness after etching, R_a, have been measured by profilometry; they were found to be respectively 0.01 μm and 20 nm. The substrate roughness is thus not significantly modified by etching. The adhesion of DLC films have been measured by tensile tests and the effect of etching has been quantified (Table 2). On non-etched substrates (L1, L3 and L5 batches), DLC films exhibit poor adhesion. The film deposited at a fluence of 1.3 J cm^{-2} shows no adhesion at all and at higher fluences, respectively 2.8 and 4.2 J cm^{-2}, adhesion is about 20 and 30 MPa only. When etching is performed (L2, L4 and L6

Table 1
Characteristics, mechanical properties and wear resistance (pin-on-flat, 50,000 cycles with a contact pressure of 500 MPa) of the ta-C films deposited by femtosecond pulsed laser deposition [9–11]

Sample	Fluence (J/cm^2)	Deposition rate (nm mn^{-1})	sp^3 content (%)	Residual stress (GPa)	Hardness (GPa)	Young's modulus (GPa)	Wear coefficient mm^3 $(Nm)^{-1}$
A	1.3	55	71	−0.81	20	240	$5.4\ 10^{-9}$
B	2.8	27	73	−1.85	25	260	$1.3\ 10^{-8}$
C	5.2	18	70	−2.83	18	210	$1.4\ 10^{-9}$*

* The wear rate of $1.4\ 10^{-9}$ mm^3 $(Nm)^{-1}$ has been obtained with a DLC film deposited at a fluence of 4.2 J cm^{-2}.

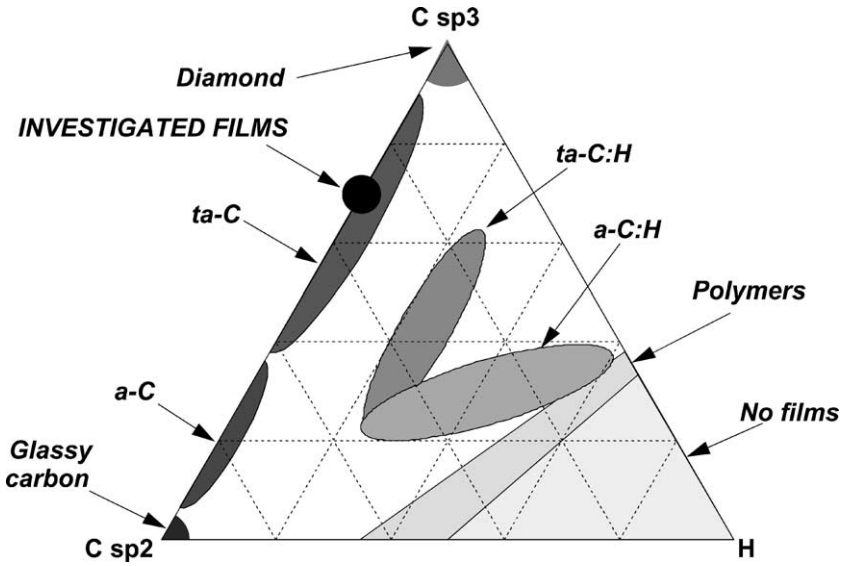

Fig. 3. Ternary representation of the four main categories of DLC films (from Robertson [2]). The films investigated in the present study are ta-C coatings with a $sp^3/(sp^3+sp^2)$ of about 0.7, as deduced from XANES experiments [9].

batches), adhesion is dramatically enhanced: whatever the fluence, cohesive ruptures in glue instead of adhesive ruptures between the DLC film and the substrate are observed, thus adhesion values of DLC films are estimated to be higher than 45 MPa. These results are in agreement with those published by Morshed et al. [20,24] showing that sputter cleaning prior deposition significantly enhances the film adhesion. These results support further development of such a deposition procedure to go further in the use of these DLC films in orthopaedic applications.

3.3. Tribological behavior

The tribological behavior of the films has been investigated in a first step by using the pin-on-flat configuration, to study the wear resistance of the films deposited onto the 316L steel substrates after ion bombardment, as described in the previous part. The pin-on-flat testing conditions are rather severe in terms of contact pressure (500 MPa) and media (dry friction), compared to the conditions related to a natural hip joint contact (less than 50 MPa, lubricated media). However, the duration of our tests is significantly lower compared to tests usually performed on a walking simulator (several millions of cycles, representing the human activity during many years). The objective of these pin-on-flat tests is thus to compare the tribological performances of our films with the tribological behavior of typical DLC films, as widely published in the literature [5].

Whatever the laser fluence, the films deposited by femtosecond PLD exhibit an average friction coefficient in the 0.1–0.2 range, without any significant fluctuation during the tests. Over a period of 50000 cycles, the wear is rather low for DLC films, with wear coefficients in the 10^{-8} to 10^{-9} range, as depicted in Table 1. This corresponds to an average wear of less than 1 nm per sliding cycle for the lowest wear coefficient. Both friction and wear are not significantly influenced by the laser fluence within the investigated range. Compared to already published data on the tribology of DLC films [5], femtosecond PLD, with in situ plasma cleaning of the steel substrate prior deposition, is a promising way to achieve the synthesis of wear-resistant DLC films without deposition of intermediate layers usually necessary to enhance adhesion between the steel substrate and the carbonaceous coating. Even if the comparison between various deposition processes is not easy, femtosecond PLD is characterized by a plasma plume containing higher energy species (up to a few hundred of eV) compared to nanosecond PLD [11,12,25]. These characteristics may be responsible for moderate stress values (due to some stress relaxation during the film growth) and enhanced adhesion

Table 2
Adhesion of DLC thin films deposited onto stainless steel substrates without (batches L1, L3 and L5) and with ion etching prior the DLC deposition (batches L2, L4 and L6)

Batch	Fluence (J cm^{-2})	Thickness (nm)	Average adhesion force (MPa)	Standard deviation (MPa)	Mechanism of rupture
L1	1.3	150	–	–	no adhesion of the DLC film
L2	1.3	150	>44.3	1.3	cohesive (glue)
L3	2.8	110	29.9	6.5	adhesive (DLC film/substrate)
L4	2.8	110	>47.5	1.9	cohesive (glue)
L5	4.2	110	18.9	1.6	adhesive (DLC film/substrate)
L6	4.2	90	>48.9	1.9	cohesive (glue)

With etching, the cohesive rupture is localized inside the glue between the DLC film and the cylindrical post used for the test.

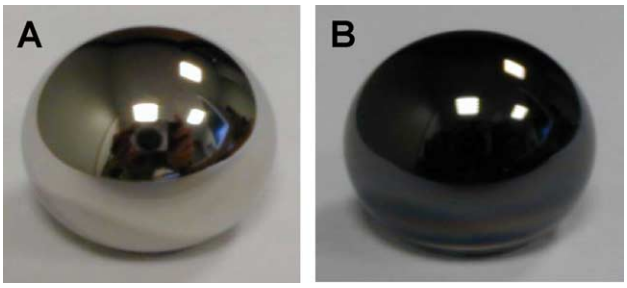

Fig. 4. Uncoated (A) and DLC-coated (B) femoral head in AISI 316L stainless steel.

on in situ etched metallic surfaces, both favorable to a higher wear resistance.

3.4. Deposition on a femoral head

In previous works [13], we examined the possibility to deposit homogeneous DLC films on larger surfaces than the conventional cm^2 area of deposition used for most of PLD devices. This has been achieved on 30 mm diameter silicon surfaces. From this optimization, homogeneous DLC films can be deposited onto a 22.2-mm diameter hemispherical surface of a 316L stainless femoral head using the experimental setup described above. The femoral head is sputter cleaned in an argon atmosphere prior to carbon deposition by using the procedure detailed previously. Then DLC has been deposited during 30 min at a laser fluence of 2.8 J cm^{-2}. This time of deposition has been optimized in [13] to achieve the same order of magnitude of film thickness (about 150 nm) than on conventional cm^2 surfaces, taking into account the rotation of the femoral head during deposition, with a tilt of 45° in respect to the direction of plasma expansion (Fig. 2). The uncoated and DLC coated femoral head are depicted in Fig. 4. The wear behavior of the DLC coated head will be tested in a Ringer solution during several months on a hip joint simulator, against a UHMWPE cup. Careful qualitative and quantitative investigations of the wear processes will be carried out at different steps of the tests. Moreover, the behavior of the DLC film when exposed to the gamma radiations for sterilization will be also investigated.

4. Conclusion

The deposition of DLC thin films on larger areas than the conventional cm^2 range (usually studied in basic coating characterization) has been investigated by femtosecond pulsed laser deposition on various substrates, including AISI 316L steel used in hip joint prostheses. Films are predominantly sp^3 hybridized and exhibit rather low compressive stress compared to most of DLC films deposited by other techniques. Biomedical applications such as hip prosthesis reveal adhesion of the coating as a critical parameter. Sputter cleaning of stainless steel substrates prior to deposition has been performed. Adhesion force of the coatings is improved by almost 100% on AISI 316L steel substrates. Low wear coefficients in the 10^{-8} to 10^{-9} range have been recorded in severe conditions (0.5 GPa of contact pressure, dry lubrication). These results show that DLC thin films deposited by femtosecond PLD are good candidates as protective coatings for articular joints. The deposition onto the hemispherical surface of a hip prosthesis has been performed and tests on a hip joint simulator during several millions of cycles are in progress.

Acknowledgements

The present study was supported by the Région Rhône-Alpes, the Conseil Général de la Loire (France) and the European Community (1997–1999 FEDER program). The authors acknowledge C. Boachon for tensile test experiments and P. Masschelein for profilometry experiments.

References

[1] V.-M. Tiainen, Diamond Relat. Mater. 10 (2001) 153.
[2] T.J. Robertson, Mater. Sci. Eng., R. 37 (4–6) (2002) 129.
[3] A. Grill, Diamond Relat. Mater. 12 (2003) 166.
[4] R. Hauert, Diamond Relat. Mater. 12 (2003) 583.
[5] A. Erdemir, C. Donnet, in: B. Bhushan (Ed.), Modern Tribology Handbook, vol. 2, CRC Press, Boca Raton, 2000, p. 871.
[6] A.A. Voevodin, M.S. Donley, Surf. Coat. Technol. 82 (1996) 199.
[7] D.B. Chrisey, C.K. Hubler (Eds.), Pulsed Laser Deposition of Thin Films, Naval Research Laboratory, Washington, DC, 1994.
[8] J. Bulí, M. Jelínek, V. Vorlícek, J. Zemek, V. Peina, Thin Solid Films 292 (1997) 318.
[9] F. Garrelie, A.-S. Loir, F. Goutaland, C. Donnet, R. Le Harzic, B. Angleraud, Y. Ouerdane, P. Laporte, Proc.-SPIE 4760 (2002) 301.
[10] F. Garrelie, A.S. Loir, C. Donnet, F. Rogemond, R. Le Harzic, M. Belin, E. Audouard, P. Laporte, Surf. Coat. Technol. 163–164 (2003) 306.
[11] A.-S. Loir, F. Garrelie, J.-L. Subtil, F. Goutaland, M. Belin, R. Le Harzic, C. Donnet, Y. Ouerdane, F. Rogemond, P. Laporte, Appl. Surf. Sci. 208–209 (2003) 553.
[12] J. Perrière, E. Millon, W. Seiler, C. Boulmer-Leborgne, V. Craciun, O. Albert, J.C. Loulergue, J. Etchepare, J. Appl. Phys. 91 (2) (2002) 690.
[13] A.S. Loir, F. Garrelie, C. Donnet, M. Belin, B. Forest, F. Rogemond, P. Laporte, Thin Solid Films 453–454 (2004) 531.
[14] D.L. Pappas, K.L. Saenger, J. Bruley, W. Krakow, J.J. Cuomo, J. Appl. Phys. 71 (11) (1992) 5675.
[15] X. Shi, D. Flynn, B.K. Tay, S. Prawer, K.W. Nugent, S.R.P. Silva, Y. Lifshitz, W.I. Milne, Philos. Mag., B 76 (1997) 351.
[16] N. Matsuyama, K. Ykimura, T. Maruyama, J. Appl. Phys. 89 (3) (2001) 1938.
[17] Q. Wei, J. Sankar, J. Narayan, Surf. Coat. Technol. 146–147 (2001) 250.
[18] J. Schwan, S. Ulrich, H. Roth, H. Ehrhardt, S.R.P. Silva, J. Robertson, R. Samlenski, R. Brenn, J. Appl. Phys. 79 (3) (1996) 1416.
[19] T. Sharda, T. Soga, T. Jimbo, M. Umeno, Diamond Relat. Mater. 10 (2001) 1592.

[20] M.M. Morshed, B.P. McNamara, D.C. Cameron, M.S.J. Hashmi, Surf. Coat. Technol. 163–164 (2003) 541.
[21] Y.Y. Tsui, D.G. Redman, Surf. Coat. Technol. 126 (2000) 96.
[22] B. Podgornik, J. Vizintin, Diamond Relat. Mater. 10 (2001) 2232.
[23] Q.R. Hou, J. Gao, Appl. Phys., A 68 (1999) 343.
[24] M.M. Morshed, D.C. Cameron, B.P. McNamara, M.S.J. Hashmi, Surf. Coat. Technol. 174–175 (2003) 579.
[25] F. Qian, V. Cracium, R.K. Singh, S.D. Dutta, P.P. Pronko, J. Appl. Phys. 86 (1999) 2281.

Appl. Phys. A 81, 471–476 (2005)
DOI: 10.1007/s00339-005-3257-6

Applied Physics A
Materials Science & Processing

T. KATSUNO[1]
C. GODET[1]
J.C. ORLIANGES[2]
A.S. LOIR[3]
F. GARRELIE[3]
A. CATHERINOT[2,✉]

Optical properties of high-density amorphous carbon films grown by nanosecond and femtosecond pulsed laser ablation

[1] Laboratoire de Physique des Interfaces et des Couches Minces, UMR 7647 CNRS – Ecole Polytechnique, 91128 Palaiseau-Cedex, France
[2] SPCTS, UMR 6638 CNRS, 123 av. A. Thomas, 87060 Limoges Cedex, France
[3] Laboratoire Traitement du Signal et Instrumentation, UMR 5516 CNRS, Université Jean Monnet, 10 Rue Barrouin, Bâtiment F, 42000 Saint-Etienne, France

Received: 8 March 2005/Accepted: 14 March 2005
Published online: 24 May 2005 •

ABSTRACT High-density tetrahedral amorphous carbon (ta-C) films have been prepared by nanosecond (17 ns) and femtosecond (150 fs) pulsed laser deposition (PLD) using fluences and repetition rates compatible with fast and homogeneous growth over large areas. Their optical properties were measured by spectroscopic ellipsometry from 1.0 to 4.7 eV and analyzed using a multi-layer Tauc-Lorentz model. In spite of very different ablation mechanisms, both PLD techniques produce high density bulk layers as revealed by a refractive index (n at 2 eV) of 2.7 ± 0.1 for both fs-PLD and ns-PLD. Films are covered by a few nm-thick sp^2-rich top layer which is denser and thicker in femtosecond PLD as compared to nanosecond PLD. The respective roles of low and high energies in the kinetic energy distribution of the incident carbon species are discussed in terms of densification and $sp^3 \mapsto sp^2$ configurational relaxation predicted by the subplantation growth model. The significantly higher optical gap found in the ns-PLD films is attributed to the larger contribution of energetic species with kinetic energies $E_c \geq 200$ eV, as revealed by time-of-flight optical studies.

PACS 81.40.Tv; 81.05.Uw; 81.15.Fg

1 Introduction

Amorphous carbon materials show unique physical and chemical properties related to a complex structure due to the different types of hybridization of carbon atoms, which consist of tetrahedral sp^3, trigonal sp^2, and linear sp^1. The ratio of sp^3/sp^2 carbon atoms is one of the most important factors in understanding the properties of carbon based films. Optical properties are extremely sensitive to changes in the sp^3/sp^2 fraction [1] and can be used to detect lateral or in-depth growth inhomogeneities, and potential substrate effects on the growth mechanisms.

Tetrahedral amorphous carbon (ta-C) with high sp^3 content is an interesting material for electrical and mechanical applications because of its high optical energy band gap, high resistivity, and high hardness, along with high Young modulus and a low friction coefficient. Carbon films with a higher sp^3 content are usually obtained with high energy atomic or ionic carbon species, such as ta-C prepared by pulsed laser deposition (PLD) and by filtered cathodic vacuum arc (FCVA) as compared to films grown using sputtering, electron cyclotron resonance (ECR), and chemical vapor decomposition of hydrocarbons (CVD) [2–4].

However, at room temperature, with the thermodynamically stable form of carbon being graphite, the deposition of sp^3-rich films requires specific deposition mechanisms which allow the "freezing" of a metastable nanostructure. Laser ablation of a highly ordered pyrolytic graphite (HOPG) or glassy carbon target is one of the simplest deposition methods to produce metastable and homogeneous carbon-based materials. Due to recent progress in laser technology, PLD techniques using high power laser intensity and different pulse durations (from femtosecond to microsecond) have been developed and used for the synthesis of a wide variety of materials [5]. Due to the ablation mechanisms being different [6] for femtosecond and nanosecond pulses, a detailed comparison of nanostructure in both types of carbon films grown over large dimensions has not yet been performed.

In this paper, we studied the optical properties of ta-C films prepared by nanosecond (ns) and femtosecond (fs) PLD on different kinds of substrates in order to investigate the different film structures as deduced from their optical parameters. Spectroscopic ellipsometry (SE) is a non-destructive analysis which allows the detection of lateral inhomogeneities and optical contrast between bulk and interfaces. Using an analytical parameterization of the dielectric function, some parameters such as refractive index n, extinction coefficient k, and optical gap energy E_{opt} can be obtained. These optical properties being related to transitions between π bonding valence band and π^* anti-bonding conduction band (and at higher energies, between σ bonding valence band and σ^* anti-bonding conduction band), changes in density of states, and film nanostructure can be determined from the SE measurements.

2 Experimental details

The deposition conditions for both types of PLD carbon films were selected in order to obtain micro-particle free carbon films deposited homogeneously over large area (~ 25 cm^2) substrates located at about 5 cm from the target and maintained at room-temperature.

✉ Fax: +33-5-5545-7211, E-mail: catherinot@unilim.fr

The ns-PLD samples were obtained in a vacuum chamber with base pressure $< 10^{-7}$ Torr, using 248 nm PLD from a glassy carbon target. The KrF excimer laser (Lambda Physik; EMG 150 MSC) was operated at a repetition rate of 10 Hz with 17 ns pulse duration and 150∼250 mJ energy per pulse. The fs-PLD samples were prepared in a vacuum chamber with base pressure $< 10^{-7}$ Torr, by PLD of a graphite target, using a 800 nm mode-locked Ti:sapphire laser (Concerto BMI/TCL) with 150 fs pulse duration and 1.5 mJ energy per pulse at a repetition rate of 1 kHz (Table 1). Both preparation methods are described in detail elsewhere [7, 8].

It has been established that femtosecond laser pulses have a significantly lower ablation and plasma breakdown threshold fluences compared to nanosecond pulses on different materials [9]. By changing the focusing of laser spot, laser fluences of ns-PLD and fs-PLD were adjusted to 80 J/cm^2 and 2.8–5.2 J/cm^2, respectively. These conditions allow the deposition of thick films (up to 300 nm) on oxidized crystalline silicon (c-Si) and Corning glass substrates without delamination, and, in the case of fs-PLD samples, good tribological coatings on stainless steel for biomedical implant applications [10].

The ex situ optical measurements were carried out with a phase-modulated spectroscopic ellipsometer (Jobin Yvon UVISEL) in the photon energy range from 1.0 to 4.7 eV with a step of 0.02 eV. The incidence angle of the light source was 70.00° and the diameter of the monochromatic light on the sample was under 2×2 mm^2. The values Is and Ic provided by the signal processing system are related to the Fresnel coefficients r_s and r_p for s- and p-polarized plane waves, respectively:

$$I\mathrm{s} = 2\mathrm{Im}\{r_s r_p^*/(r_s r_s^* + r_p r_p^*)\} \quad (1)$$
$$I\mathrm{c} = 2\mathrm{Re}\{r_s r_p^*/(r_s r_s^* + r_p r_p^*)\}$$

where r_s^* and r_p^* indicate the complex conjugates of r_s and r_p, respectively. The ellipsometric spectra are analyzed using the Tauc–Lorentz (TL) model derived by Jellison and Modine [11]. The imaginary part of the dielectric function ε_2 is given by:

$$\varepsilon_2 = (1/E) A E_0 C (E - E\mathrm{g})^2 / \left\{ \left(E^2 - E_0^2\right)^2 + C^2 E^2 \right\} \quad (2)$$
$$\text{if } E > E\mathrm{g}$$
$$\varepsilon_2 = 0 \quad \text{if } E \leq E\mathrm{g}$$

where Eg is the energy band gap, E_0 is the peak transition energy, C is the broadening term, and A is related to the transition probability. The real part of the dielectric function ε_1 is calculated by the Kramers–Kronig dispersion relation from ε_2. The refractive index n and extinction coefficient k were determined from $\varepsilon_1 = n^2 - k^2$ and $\varepsilon_2 = 2nk$.

The Tauc model (built in the Tauc–Lorentz parametrization) is often used to describe the optical band gap in disordered semiconducting materials such as amorphous carbon and amorphous silicon. The Tauc gap Eg is given by $(\alpha E)^{1/2} = B(E - E\mathrm{g})$, where $\alpha = 4\pi k/\lambda$ is the absorption coefficient, λ is the photon wavelength, E is the photon energy, and B is a constant [12]. The value of n at a photon energy of 2 eV (in a photon range where graphite and diamond have nearly the same value) has been selected to get information related to the film density.

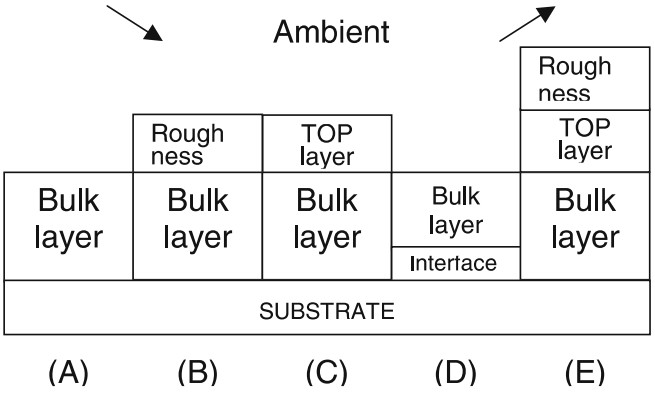

FIGURE 1 Optical models used in the analysis of PLD carbon films. The best χ^2 values are : 4.6 (A), 2.5 (B), 1.6 (C), 3.5 (D), 1.5 (E) for ns-PLD (sample n2), and 0.24 (A), 0.060 (B), 0.027 (C), 0.053 (D), 0.027 (E) for fs-PLD (sample f1)

The most simple optical model assumes a homogeneous film with atomically abrupt interfaces (ambient/film/substrate) as shown in Fig. 1(A), but real films may show some chemical intermixing with the substrate material or have a surface roughness. Ta-C films obtained by PLD may also have an sp^2-rich surface or, in the case of films grown at very high fluence, embedded sp^2 microscopic particles. Therefore we also used additional models: ambient/film (top layer)/film (bulk layer)/substrate without (model C) or with (model E) roughness layer, or ambient/bulk/interface/substrate (model D). Top (respectively interface) layer and bulk layer are independent materials with different dielectric functions to be determined in order to detect different optical properties at the surface (respectively the film/substrate interface). Oxide-free c-Si substrates were used for fs-PLD, while thermally oxidized c-Si substrates (with a 2.3 μm-thick SiO_2 layer included in the modeling) were used for ns-PLD. The fitted parameters are obtained from DeltaPsi2 software (Jobin–Yvon). The quality of the fit is given by low values of the χ^2 parameter, which is the sum of squares of the differences between experimental and simulated (I_C, I_S) values.

3 Experimental results

A comparison of preparation conditions and film thicknesses of ta-C films prepared by the ns-PLD and fs-PLD techniques is presented in Table 1. The film thicknesses are averaged values deduced from optical measurements. Spatially resolved measurements from profilometric measurements are in good agreement. Using model A, we checked the lateral homogeneity of fs-PLD carbon films deposited on 25 cm^2 c-Si substrates, with a reproducibility of ±2% for the refractive index (n at 2 eV) and a decrease of 14% of the film thickness towards the edges.

The experimental (Is, Ic) data of ta-C samples (n1 and n4) prepared by ns-PLD on different substrates are shown in Fig. 2. Many oscillations appear within the whole photon range for the ta-C sample (n4) grown on oxidized c-Si substrate due to interferences within the thick SiO_2 (with modeled thickness of 2307 ± 2 nm). For both substrates, the broad

	Sample name	Laser fluence (J/cm^2)	Repetition rate (Hz)	Deposition time (min)	Substrate	χ^2	Film thickness (top) (nm)	Film thickness (bulk) (nm)
ns-PLD (17 ns)	n1	80	10	10	glass	0.041	0.4 ± 0.1	71 ± 0.4
	n2			18	c-Si+2.3	1.6	1 ± 0.1	132 ± 0.4
	n3			23	μm SiO_2	2.9	1.5 ± 0.2	165 ± 0.8
	n4			39		2.5	1.3 ± 0.2	279 ± 1.1
fs-PLD (150 fs)	f1	2.9	1000	30	c-Si	0.027	4 ± 0.2	104 ± 0.4
	f2				glass	0.031	6 ± 0.2	121 ± 0.4
	f3	5.2			c-Si	0.025	10 ± 0.4	145 ± 0.4
	f4				glass	0.037	7 ± 0.2	134 ± 0.6

TABLE 1 Preparation conditions and film thickness for ta-C films prepared by ns and fs PLD techniques

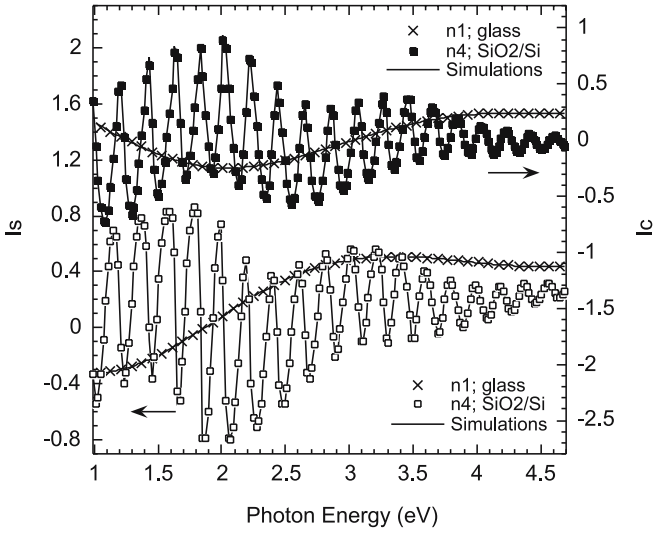

FIGURE 2 Experimental Is (*bottom curves*) and Ic (*top curves*) data and Tauc–Lorentz model, as a function of photon energy, for ns-PLD carbon films grown on glass substrate (n1, *crosses*) and SiO_2/Si substrate (n4, *squares*)

modulation pattern corresponds to interferences within the thin carbon films, which are damped in the UV due to ta-C absorption.

At first, we illustrate the comparison of the different models (Fig. 1) using an ns-PLD carbon sample (n2) grown on oxidized c-Si substrate. For the most simple three-medium model (A), the χ^2 value is 4.6. If a roughness layer (defined as a mixture of the same bulk ta-C layer (50%) and void (50%)) is added (model B), the χ^2 value shows some improvement, with a roughness layer thickness of 1.2 nm. For model (C) consisting of two independent ta-C layers, χ^2 is decreased significantly (by a factor of three) as compared with model (A). In model (D), incorporation of a film/substrate interface different from the bulk is not satisfactory. In model (E), the incorporation of an additional rough layer (with thickness of 1.1 nm) does not improve the result as compared to model (C), which indicates that the surface of ns-PLD carbon films is smooth. The excellent agreement of experimental (Is, Ic) data and TL dispersion best fit (using model C) of ta-C samples (n1 and n4) on glass and Si/SiO_2 substrates is illustrated in Fig. 2.

Second, the same models were applied to a fs-PLD carbon sample (f1) grown on c-Si substrate. If a 2.0 nm thick rough layer (using a mixture of the bulk ta-C (50%) and void (50%)) is added, the χ^2 value improves significantly as compared with model (A). For model (C) incorporating a top layer, the χ^2 value improves by one decade as compared to model (A), while the χ^2 values for models (D) and (E) do not give further improvement as compared to model (C). The thickness of the roughness layer is 1.5 nm in model (E), which again indicates a smooth surface. As will be shown below, the (αd) values (product of absorption coefficient and film thickness) being larger for fs-PLD films, SE measurements may be less sensitive to the film/substrate interface.

Although some roughness exists in both ns-PLD and fs-PLD films, we conclude from our optical investigation, that roughness and substrate intermixing layers are almost negligible in our films. Hence, model (C) consisting of top layer and bulk layer is in fact a good approximation to the true film structure. The χ^2 values calculated from model (C) for all samples are given in Table 1. The larger χ^2 of samples (n2–n4) as compared with other samples of comparable thickness results from the high amplitude interferences inside the SiO_2 layer which modulate the carbon film optical response. The top layer thickness is smaller for the ns-PLD carbon films (1–2 nm) as compared to the fs-PLD carbon films (4–10 nm). The fitted bulk layer $n(E)$ and $k(E)$ spectra for ta-C samples prepared by ns-PLD on glass and Si/SiO_2 are shown in Fig. 3. The good agreement between n and k spectra with different film thickness (from 132 to 279 nm) shows that the ta-C

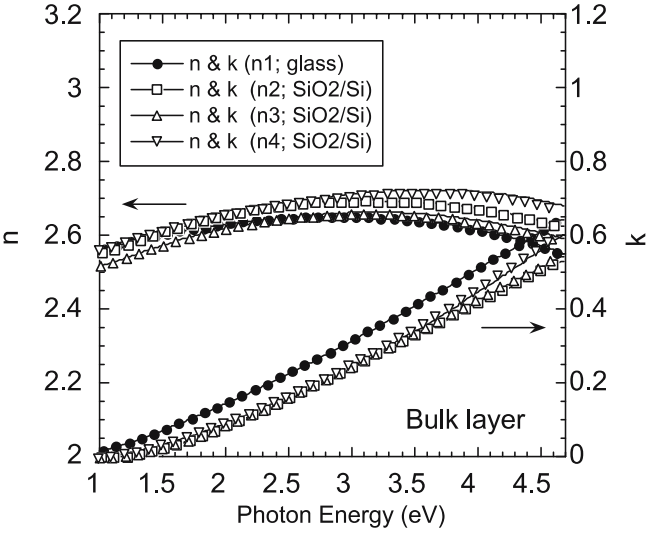

FIGURE 3 Film thickness dependence of $n(E)$ and $k(E)$ spectra (derived from model C) for the bulk of ta-C films obtained by ns-PLD on glass and oxidized c-Si substrates

films grow homogeneously on oxidized c-Si substrates, while a slightly higher absorption is detected for the film grown on glass.

Figure 4 shows $n(E)$ and $k(E)$ spectra of fs-PLD carbon samples grown with variable laser fluence on different substrates. For c-Si substrates, the refractive index of carbon films slightly increases with increasing fluence, but the dependence is even smaller for ta-C on glass. For both substrates, $k(E)$ spectra increase with increasing laser fluence, while the values for ta-C on c-Si are slightly higher than those of ta-C on glass at the same laser fluence. Hence, on c-Si substrates, fs-PLD carbon films with a higher absorption coefficient α are obtained using a high laser fluence.

4 Discussion

For our carbon films grown by ns-PLD and fs-PLD, the roughness and substrate intermixing layers are found to be almost negligible and an optical model made of a top layer and a bulk layer is a good approximation to the real film structure. The large area homogeneity and the constant deposition mechanism up to thickness values of 300 nm have been shown. However, the total film thicknesses obtained by SE correspond to very different amounts of matter ablated from the target, typically 1.2×10^{-2} nm/pulse is deposited in the ns-PLD regime as compared to 7×10^{-5} nm/pulse in the fs-PLD regime.

Different ablation mechanisms may be responsible for different structures because the network bonding can be affected by carbon species implantation and by relaxation effects. SE measurements reveal strong differences in the sp^2 phase organization of bulk carbon films, with a larger optical gap Eg (attributed to $\pi - \pi^*$ transitions) found in ns-PLD films ($0.43 \sim 1.12$ eV for ns-PLD) as compared with fs-PLD films ($0.08 \sim 0.13$ eV). A different shape of $\pi - \pi^*$ transitions is also observed with $k(E)$ reaching a maximum at 4.5 eV in fs-PLD samples, while the latter is located above 4.7 eV for ns-PLD carbon films. However, the density of fs-PLD films ($n = 2.7 \sim 2.8$ at 2 eV) is slightly larger than that of ns-PLD ($n = 2.6 \sim 2.7$ at 2 eV).

In addition, one may consider the possible electrical charging of insulating substrates which would decrease the kinetic energy of the charged ionic carbon species from the plume impinging on the film, or thermal effects which may result from the different thermal conductivity of glass and oxidized c-Si substrates. This work shows that no significant influence of the substrate nature could be detected so that these potential effects can be neglected in our study.

In the particular conditions suitable for large area deposition, as used in this study (Table 1), optical gap values indicate that the ns-PLD technique seems to be more appropriate to create sp^3-rich bulk carbon matrix than the fs-PLD one. However, the surface sp^3 content in our ns-PLD (resp. fs-PLD) carbon films has been estimated at 60% (resp. 70%–73%) from X-ray photoelectron spectroscopy (resp. X-ray absorption near edge spectroscopy) measurements [7, 8].

High Eg values are expected for large sp^3 content, but the relation may not be true in highly constrained a-C materials because Eg could depend both on the relative amount of sp^3/sp^2 and on their distribution in the film structure. In particular, it has been shown that distortions of C=C bonds induced by high local stress may lead to a significant decrease of the $\pi - \pi^*$ optical transition energy [13]. High values of the typical residual compressive stress of comparable magnitudes have been estimated as 2.0 ± 0.2 GPa [14] (resp. 1.8 GPa and 2.8 GPa) for ns-PLD (resp. fs-PLD at laser fluences of 2.9 and 5.2 J/cm^2) carbon films [8].

In order to gain a better understanding of the deposition mechanisms, a correlation between refractive index (n at 2 eV) and Tauc gap (Eg) for our ta-C films is shown in Fig. 5, in-

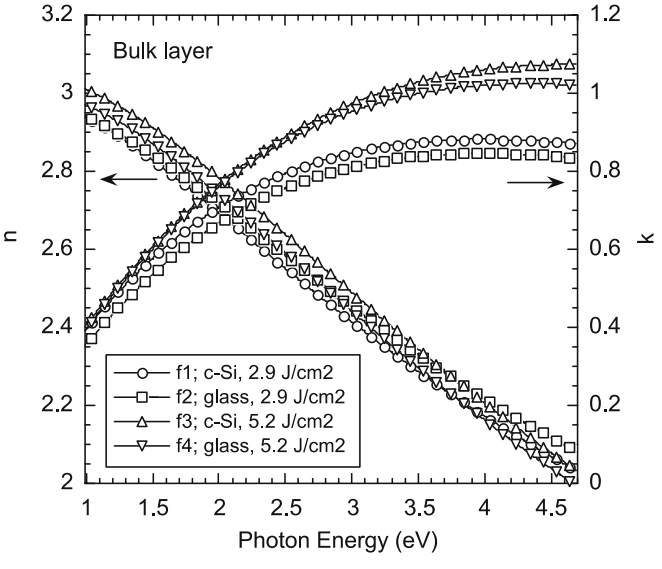

FIGURE 4 Fluence dependence of $n(E)$ and $k(E)$ spectra for the bulk of ta-C films grown on different substrates by fs-PLD

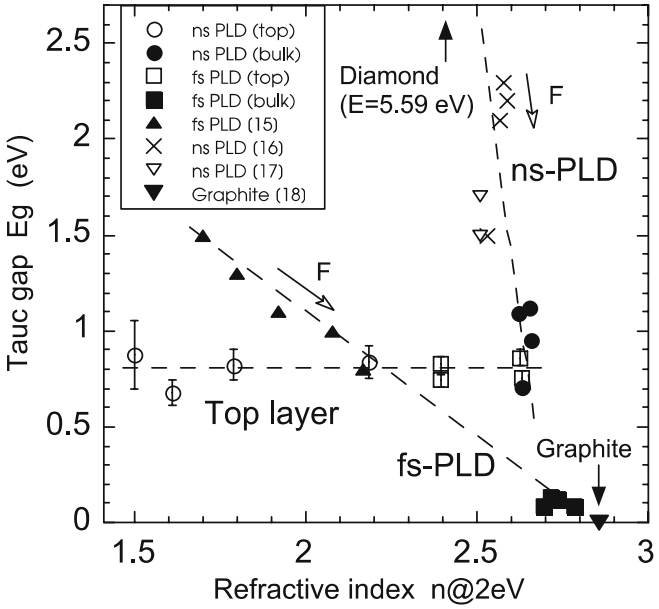

FIGURE 5 Comparison of refractive index (n at 2 eV) and Tauc gap (Eg) for carbon films prepared by ns-PLD (*solid circles*: this study; *crosses*: [16] and *open triangles*: [17]) and by fs-PLD (*solid squares*: this study; *solid triangles*: [15]). The top layer characteristics of ns and fs-PLD carbon are shown by *open circles* and *open squares*, respectively. The *lines* are guides to the eyes

cluding both bulk layer and top layer of ns-PLD and fs-PLD samples. A similar tendency is obtained from the correlation between refractive index and optical gap energy E_{04} (obtained at an absorption coefficient of $10^4\ cm^{-1}$). As far as the bulk layer optical characteristics are concerned, although the optical gaps of ns-PLD and fs-PLD carbon films are rather different, their n values are very similar. Interestingly, the gap of the top layer is almost independent of the ablation process (Fig. 5, horizontal line) while a significantly larger top layer density is obtained with the fs-PLD ($n \geq 2.3$) as compared to ns-PLD ($n \leq 2.3$) carbon deposition.

For comparison, some results obtained by other groups [15–17] are also shown in Fig. 5, along with guiding lines indicating the main tendencies as a function of fluence. All samples were prepared without hydrogen during deposition and consist of carbon atoms with different bonding configurations. Basically, as the laser fluence increases, Eg values of fs-PLD samples gradually decrease with increasing n values [15], while those of ns-PLD samples [16, 17] sharply decrease with little change in n values. Interestingly, the ordinary (in-plane electric field) refractive index of graphite (2.86 at 2 eV [18]) with a zero bandgap and index $n = 2.4133$ (at 2.066 eV) of diamond with an absorption edge at 5.59 eV [19]) appear to be aligned with the extrapolated ns-PLD guiding line.

In the laser ablation process, the atoms and ions average kinetic energy increases with increasing laser fluence [3] and is an important factor to produce the sp^3 phase. A subplantation model has been proposed in order to describe the maximum in the sp^3 content observed as a function of ion energy Ec for FCVA deposited ta-C films [2, 20]. Below the optimal Ec value, the fraction of metastable sp^3 C atoms increases for increasing ion energy due to the increasing ion penetration probability, while above the optimal Ec value, the sp^3 content decreases by the effect of $sp^3 \mapsto sp^2$ relaxation with increasing ion energy. For increasing laser fluence in ns-PLD, more carbon species penetrate into the film and increase the localized pressure necessary for the creation of a high percentage of fourfold coordinated C bonds. For fluences higher than optimum, as is the case for the present investigation, the Tauc gap of the films with high density decreases by the effect of $sp^3 \mapsto sp^2$ relaxation induced by highly energetic species. As a consequence of the same relaxation effect, in the plot showing fs-PLD carbon films from [15], Eg decreases with increasing index n.

For fs-PLD (full triangles in Fig. 5 [15]) as the laser fluence increases from 30 to 600 J/cm^2 (10 Hz repetition rate) the guiding line (Eg vs. n) extrapolates towards the values found for our fs-PLD samples, which were prepared at much lower fluences of $2.9 \sim 5.2$ J/cm^2 (1 kHz rate). This apparent contradiction may indicate that the presence of an ns background on the fs pulse of the Ti:Sapphire laser could play a crucial role. One must also be careful about the distribution of sp^3 sites in amorphous DLC, as sp^2 sites must be spatially correlated to produce a band gap. The observed tendency can be correlated to defects states induced by the energetic ions of the plasma plume. Moreover, as the contrast of the laser pulse (defined by the ratio of the femtosecond pulse to the nanosecond background) decreases, this energetic ion component of the plume continues to decrease to finally disappear [21]. Then, the pulse contrast (not known for [15]), appears to be a predominant parameter, as well as the laser fluence.

The different tendencies found for fs-PLD and ns-PLD could also be tentatively interpreted by the distribution of carbon kinetic energies rather than its average value. The beginning of the interaction produces very fast electrons which drag very fast ions at the plume front while the core of the plume is mainly composed of excited atoms and energetic ions. Contrary to PLD in the fs regime, in ns-PLD the laser pulse duration is sufficient to induce a breakdown and to strongly interact with the plume of ejected material, leading to a relatively hot plasma medium where collisional processes will tend to homogenize the kinetic energy distribution. Consequently, rather different kinetic energy distributions are expected in ns and fs regimes. This is confirmed by the results presented in Fig. 6, respectively for 80 J/cm^2 and 2.8–5.2 J/cm^2 [22]. These results, deduced from optical time of flight measurements, clearly indicate that the proportion of low kinetic energy emitting species is much smaller in ns-PLD as compared to fs-PLD.

By arbitrarily separating the energy distribution of emitted species into three groups, (i) low energy range; Ec < 50 eV,

Kinetic energy	Ec < 50 eV	50 eV < Ec < 250 eV	Ec > 250 eV
fs-PLD 2.8 J/cm^2	30%–40%	50%	20%–10%
fs-PLD 5.2 J/cm^2	10%–15%	60%	30%–25%
ns-PLD 80 J/cm^2	2%	42%	56%

TABLE 2 Ratios of ejected particles as function of their kinetic energies Ec in fs-PLD and ns-PLD

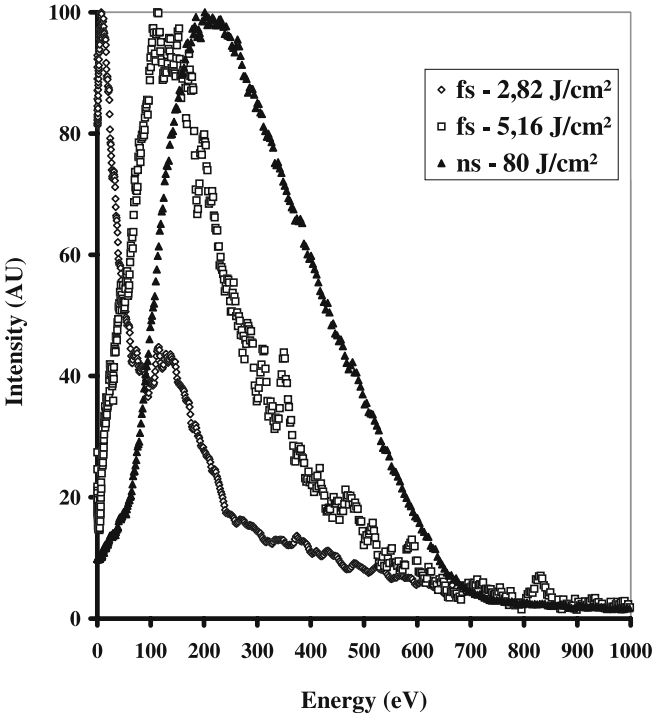

FIGURE 6 Kinetic energy distributions of emitting species in the ablation plume deduced from optical time of flight measurements (ICCD camera), integrated on the UV-visible emission spectrum, in fs (2.8–5.2 J/cm^2) and ns (80 J/cm^2) interaction regimes

(ii) middle energy range, 50–250 eV and (iii) high energy range, $Ec \geq 250$ eV, the respective fractions measured in fs-PLD and ns-PLD (Table 2) reveal that ns-PLD presents a very small ratio of (i) as compared to fs-PLD. The large ratio of (i) in fs-PLD contributes to the sticking of low energy species on the top layer surface while the carbon species with middle and high energies are implanted at a few nanometers below the film surface (subplantation mechanism).

In ns-PLD, in agreement with our optical measurements, the density of low kinetic energy species is much smaller as compared to fs-PLD, therefore giving a thinner top layer in carbon films, possibly related to the $sp^3 \mapsto sp^2$ configurational relaxation. Keeping in mind that the amount of matter ablated from the target per laser pulse is about 200 times larger in ns-PLD as compared to fs-PLD, we can expect that the supra-thermal species (> 250 eV) in the fs-PLD process could be efficient in the densification of this top layer, which is found to be nearly as dense as the bulk, as well as in the creation of defects [23], while the high flux of particles (iii) in the case of ns-PLD can lead to sputtering of the film surface and creation of vacancies in the top layer.

5 Conclusion

Spectroscopic ellipsometry has been used to investigate the optical properties related to growth and structure in ta-C films prepared by ns-PLD and fs-PLD. For both ablation techniques, tetrahedral amorphous carbon films grow homogeneously as a high density bulk layer (as revealed by a refractive index of 2.7 ± 0.1) covered by a thin sp^2-rich top layer without roughness.

The significantly higher optical gap found in the ns-PLD carbon films is attributed to the larger contribution of energetic species with kinetic energies $Ec \geq 200$ eV, as revealed by time-of-flight optical studies.

The gap of the top layer is almost independent of the laser pulse width, while its density and thickness are larger in fs-PLD carbon. The top layer being produced by sticking of low energy carbon species or by ion-induced $sp^3 \mapsto sp^2$ relaxation. It is thus important to compare quantitatively (e.g. using time-resolved optical emission spectroscopy) the respective density distributions of impinging carbon species, at low and high kinetic energies. The large density and thickness of the top layer in the fs-PLD carbon films may have important consequences on their tribological properties, which are currently investigated and tested as biomedical coatings.

ACKNOWLEDGEMENTS One of the authors (T.K.) is grateful to Ecole Polytechnique (Direction des Relations Extérieures) for a post-doctoral grant during this work.

REFERENCES

1 M. Chhowalla, J. Robertson, C.W. Chen, S.R.P. Silva, C.A. Davis, G.A.J. Amaratunga, W.I. Milne: J. Appl. Phys. **81**, 139 (1997)
2 J. Robertson: Mater. Sci. Eng. R **37**, 129 (2002)
3 A.A. Voevodin, M.S. Donley: Surf. Coat. Technol. **82**, 199 (1996)
4 C. Godet, N.M.J. Conway, J.E. Bourée, K. Bouamra, A. Grosman, C. Ortega: J. Appl. Phys. **91**, 4154 (2002)
5 A.A. Voevodin, J.S. Zabinski: In: *Amorphous Carbon: State of the Art* (S.R.P. Silva, J. Robertson, W.I. Milne, G.A. Amaratunga, Eds.) (World Scientific, Singapore 1998) p. 237
6 M.D. Shirk, P.A. Molian: Carbon **39**, 1183 (2001)
7 J.C. Orlianges, C. Champeaux, A. Catherinot, T. Merle, B. Angleraud: Thin Solid Films **453–454**, 285 (2004)
8 F. Garrélie, A.-S. Loir, C. Donnet, F. Rogemond, R. LeHarzic, M. Belin, E. Audouard, P. Laporte: Surf. Coat. Tech. **163–164**, 306 (2003)
9 Z. Zhang, P.A. VanRompay, J.A. Nees, P.P. Pronko: J. Appl. Phys. **92**, 2867 (2002)
10 A.S. Loir, F. Garrélie, C. Donnet, M. Belin, B. Forest, F. Rogemond, P. Laporte: Thin Solid Films **453–454**, 531 (2004)
11 G.E. Jellison, Jr., F. Modine: Appl. Phys. Lett. **69**, 371 (1996); **69**, 2137 (1996)
12 J. Tauc: *Amorphous and Liquid Semiconductors* (J. Tauc, Ed.) (Plenum, London 1974) p. 159
13 J. Robertson: Diam. Relat. Mater. **4**, 297 (1995)
14 J.C. Orlianges, A. Pothier, D. Mercier, P. Blondy, C. Champeaux, A. Catherinot, M.I. de Barros, S. Pavant: Thin Solid Films (2005), in press
15 F. Qian, V. Craciun, R.K. Singh, S.D. Dutta, P.P. Pronko: J. Appl. Phys. **86**, 2281 (1999)
16 D.L. Pappas, K.L. Saenger, J. Bruley, W. Krakow, J.J. Cuomo, T. Gu, R.W. Collins: J. Appl. Phys. **71**, 5675 (1992)
17 H.C. Ong, R.P.H. Chang: Phys. Rev. B **55**, 13213 (1997)
18 A. Borghesi, G. Guizzetti: In: *Handbook of Optical Constants of Solid II* (E.D. Palik, Ed.) (Academic Press 1991) p. 449
19 D.F. Edwards, H.R. Philipp: In: *Handbook of optical constants of solids* (E.D. Palik ed.) (Academic Press 1985) p. 665
20 P.J. Fallon, V.S. Veerasamy, C.A. Davis, J. Robertson, G.A.J. Amaratunga, W.I. Milne, J. Koskinen: Phys. Rev. B **48**, 4777 (1993)
21 P. A VanRompay, M. Nantel, P.P. Pronko: Appl. Surf. Sci. **127–129**, 1023 (1998)
22 A.S. Loir, F. Garrélie, J.L. Subtil, F. Goutaland, M. Belin, R. Le Harzic, C. Donnet, Y. Ouerdane, F. Rogemond, P. Laporte: Appl. Surf. Sci. **208–209**, 553 (2003)
23 J. Perrière, E. Millon, W. Seiler, C. Boulmer-Leborgne, V. Craciun, O. Albert, J.C. Loulergue, J. Etchepare: J. Appl. Phys. **91**, 690 (2002)

Available online at www.sciencedirect.com

SCIENCE DIRECT

Thin Solid Films 482 (2005) 287–292

thin solid films

www.elsevier.com/locate/tsf

Nickel-incorporated amorphous carbon film deposited by femtosecond pulsed laser ablation

N. Benchikh[a], F. Garrelie[a], C. Donnet[a,*], B. Bouchet-Fabre[b], K. Wolski[c], F. Rogemond[a], A.S Loir[a], J.L. Subtil[a]

[a]*Laboratoire Traitement du Signal et Instrumentation, UMR 5516, Université J. Monnet, Bâtiment F-10 rue Barrouin, 42000 Saint-Etienne, France*
[b]*Laboratoire Francis Perrin, SPAM, Bât 522, CEA Saclay, 91191 Gif-sur-Yvette Cedex, France*
[c]*Ecole Nationale Supérieure des Mines de Saint-Etienne, Centre SMS-URA CNRS 5146, 158 cours Fauriel, 42023 Saint-Etienne, Cedex 02, France*

Available online 7 January 2005

Abstract

Metal-containing diamond-like carbon films (Me-DLC), with metallic particles embedded in a DLC matrix, have become good candidates to improve many film properties (including mechanical properties and adhesion) and to enhance the tribological behavior in severe conditions. Previous studies on the properties of Me-DLC coatings have reported lower compressive stresses and higher wear resistance compared to undoped DLC. In many cases, the presence of metal inclusions enhances adhesion on metallic substrates. The present study investigates the composition and nanostructure of DLC coating alloyed with 50 at.% concentration of nickel. The film is deposited by femtosecond pulsed laser ablation (PLD) by ablating sequentially graphite and nickel targets. The chemical composition and the bonding characteristics of this film are determined by X-ray Photoelectron Spectroscopy (XPS), Near Edge X-ray Absorption Spectroscopy (NEXAFS) and Electron Energy Loss Spectroscopy (EELS) imaging. The chemical composition, the carbon hybridization and the morphology of the a-C:Ni film at the microscopic scale are discussed, in relation to the thermodynamic phase diagram of the Ni–C system.

Keywords: Diamond-like carbon; Femtosecond pulsed laser deposition; Doped DLC; Laser ablation

1. Introduction

Diamond-like carbon (DLC) films exhibit excellent mechanical and tribological properties [1–4], intermediate to those of graphite and diamond, and therefore cover a wide range of applications. However, practical applications of DLC are still limited, in particular due to high internal stresses and insufficient adhesion onto various substrates. Therefore, to lower the stress, to enhance the adhesion and to reach a wider range of functional properties, metallic and non-metallic elements have been introduced into the carbonaceous network. These elements include Si, N, F, B, P and various metals. These doped and alloyed DLC films are successfully used in many industrial applications [5–7]. Recent researches suggest several new applications for doped or alloyed DLC films, including metal-containing DLC films (Me-DLC) [4,8–10], e.g. as microelectrodes in micro-electrochemical analysis, emitters in advanced field emission devices, solid lubricant films or magnetic films. Understanding the correlation between the deposition's parameters, the film's composition and nanostructure, and their properties is required.

Pulsed laser deposition (PLD) has proved to be an effective technique for the deposition of a wide variety of thin film materials, extending from DLC to oxides or nanostructured materials [11–13]. Pulsed laser deposition of DLC leads to high purity films with a predominance of sp^3 hybridization (diamond) at low deposition temperature. High mechanical properties, with hardness values ranging between 20 and 70 GPa have been obtained with DLC films deposited by PLD [11,12]. Such depositions have been achieved by ablating graphite target using excimer or YAG

* Corresponding author. Tel.: +33 4 77 91 58 01; fax: +33 4 77 91 57 81.
E-mail addresses: Christophe.Donnet@univ-st-etienne.fr (C. Donnet), nadia.benchikh@univ-st-etienne.fr (N. Benchikh).

0040-6090/$ - see front matter © 2004 Elsevier B.V. All rights reserved.
doi:10.1016/j.tsf.2004.11.162

lasers, with nanosecond pulse durations [12]. Deposition can be also achieved in a reactive atmosphere, such as nitrogen, to deposit a-CN_x films [14].

For a few years, femtosecond lasers have been used in pulsed laser deposition. In this case, the kinetic energy of the ejected particles can be increased up to a few keV [15], which is much higher than in the nanosecond regime, and original properties of the coatings, including lower stress [16], could be related to such a high value of the kinetic energy. Some of us have recently published papers on the behavior of the plasma induced by femtosecond laser ablation of a graphite target [17], the deposition of DLC films by femtosecond PLD [18–20], and on the tribological behavior of those DLC films [21]. Since 1999 with the first results of femtosecond pulsed laser deposited DLC films [15,21,22], various kinds of films have been deposited by femtosecond PLD, including DLC [15,21–23], CN [24], $BaTiO_3$ [25], PTFE [26], ZnO [16,27], BN [28], TiN [29], Al–Mg–B–Ti [30], semiconductors [31] and quasicrystals [32]. Such a deposition process often leads, except for DLC materials, to nanostructured films with grain size in the nanometer scale and properties significantly different from nanosecond pulsed laser deposited films.

Although the nanosecond PLD has been largely investigated on DLC films, there is little in the current literature on the properties of doped and alloyed DLC films deposited by nanosecond PLD. Wei et al. [33,34] have incorporated Ti, Cu and Si in DLC by nanosecond PLD, with a significant reduction of stress, hardness and Young modulus, whatever the nature of the alloying elements. An increase of wear resistance has been observed in the case of Ti incorporation, attributed to a fraction of Ti bonded to carbon. More recently, Lackner et al. [35] have deposited a-$Si_{1-x}C_xH$ (x=0.80–0.97) by ablating a Si target in a reactive Ar/C_2H_2 atmosphere. Some mechanical and optical properties of the films have been studied versus the silicon content. From the study of the optoelectronic properties of a-C:B films deposited by nanosecond PLD, Tian et al. [36] have demonstrated a slight improvement of the energy conversion efficiency of these films.

However, from our knowledge, no work has been yet published on the investigations of the structure and properties of doped or alloyed DLC films deposited by femtosecond PLD. As nanostructures have been evidenced in most of femtosecond pulsed laser deposited films, such as GaAs [31] or oxides [25], one can expect particular structure of Ni incorporated amorphous carbon films. The aim of this work is to present preliminary investigations on the chemical composition of a-C:Ni films deposited by this technique. Ni has been selected due to its well known chemical affinity with carbon, thus favorable to the formation of a nanocomposite structure constituted by metallic nickel inclusion into the carbonaceous matrix. These preliminary film characterizations include the identification of the chemical composition and bonding states by X-ray Photoelectron Spectroscopy (XPS) and Near Edge X-ray Absorption Fine Structure (NEXAFS). The microstructure has been investigated by Electron Energy Loss Spectroscopy (EELS, Imaging mode) in a Transmission Electron Microscope (TEM).

2. Experimental procedure

Nickel-containing DLC film have been deposited by alternatively ablating graphite (purity 99.997%) and nickel (purity 99.9%) targets introduced in a deposition chamber evacuated to a base pressure of 10^{-6} hPa by a turbomolecular pump. The films have been deposited at room temperature onto p-type silicon substrates at a target-to-substrate distance of 36 mm. The femtosecond laser (Concerto, BMI/TCL, λ=800 nm, pulse duration 150 fs, repetition rate 1 kHz, energy per pulse 1.5 mJ) has been focused alternatively, by using a shutter, on each target, rotating at 32 rpm. The laser has been focused with an incident angle of 45° on the targets, with an energy density set to 2.6 J/cm^2 (±20%). 25 sequences of ablation of each target during 4s have been performed, taking into account the similar deposition rate of pure carbon (30 nm/mn) and pure nickel (35 nm/mn) determined in a preliminary set of experiments. Thus the 200 s co-deposition should lead to a film thickness in the range of 100 nm, with a composition near 50 at.% C/50 at.% Ni.

The film have been analyzed by X-ray photoelectron spectroscopy (XPS, Cameca spectrometer) with a MgKα source (1253.6 eV) working in direct acquisition mode at a resolution of 1 eV with a step of 0.25 eV for direct acquisition spectra and 0.10 eV for detailed acquisition spectra. The spectrometer has been calibrated to ensure that the $Cu2p_{3/2}$ and Cu3p peaks were located at 932.6 and 75.1 eV, respectively. The chamber base pressure was approximately 2.10^{-9} hPa. XPS analysis has been performed before and after in situ Ar^+ sputtering of the surface.

Near Edge X-ray Absorption Fine Structure (NEXAFS) measurements have been performed in LURE-SuperAco on the SAGEMOR line. The photon energy was calibrated at the C K-edge using an HOPG sample as reference. NEXAFS spectra are the ratio of the sample signal collected by a chaneltron in a total electron yield (TEY) mode to the signal of the gold grid monitoring the beam intensity. The penetration depth of the incident photon is a few nm and escape depth of electrons is about 10 nm. The experimental resolution has been estimated to 0.1 eV at the C K-edge. The C and O K-edges have been recorded with a step of 0.1 to 0.3 eV.

The films have also been deposited onto a copper grid (diameter 3 mm) previously covered by a holey amorphous carbon film. These films have been examined by EELS in a LEO 912 energy filtered Transmission Electron Microscope (EFTEM) at 120 kV.

3. Results and discussions

Both carbon and oxygen are detected by XPS in the a-C and a-C:Ni films, whereas Ni is detected specifically in the metal-containing film. Since the presence of oxygen may be attributed to the oxidized surface layer, a similar spectrum has been performed after carrying a sputter cleaning of the surface in the UHV chamber of the spectrometer as shown in Fig. 1. No other contaminants are detected. Even if the oxygen signal has been found to decrease after sputter cleaning, it is still present in the film (approximatively 7 at.%), certainly as a contaminant incorporated during deposition. From the calibration procedure of the spectrometer, the precise comparison of the C1s core level signals related to the a-C and a-C:Ni films is ambiguous. In both films, we have observed (not shown) a dissymmetric C1s signal broader than those related to diamond and graphite. The lowest binding energy component of the carbon–carbon bond is generally assigned to the sp^2 hybridization (284.5 eV), whereas the highest one is generally assigned to the sp^3 hybridization (285.3 eV) [37], even if other authors have found that the latter hybridization may be detected in a rather wide binding energy range leading to controversial interpretations [38]. Since the amorphous nature of the DLC films generally induces a broadening of the C1s core level signals and due to the well known small energy difference ($\approx$1 eV) between these two contributions [38] and the resolution of 1 eV of our spectrometer, no deconvolution between the sp^2 and sp^3 contribution will be discussed here. A small shoulder near 288 eV is identified and may be attributed to the presence of CO bonds, in agreement with the persistence of a significant O1s peak detected in both films consecutive to sputter cleaning. The Ni 2p feature is shown in Fig. 2. The Ni $2p_{1/2}$ and $2p_{3/2}$ peaks are located respectively at 870.2 and 852.8 eV, corresponding to an energy shift of 17.4 eV between both contributions.

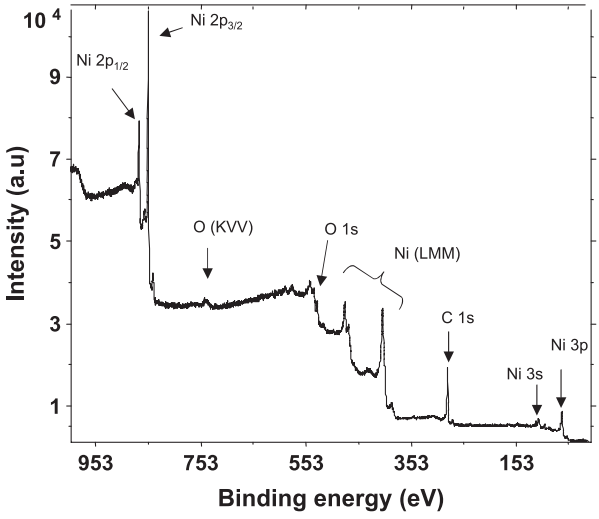

Fig. 1. XPS spectrum of the a-C:Ni film.

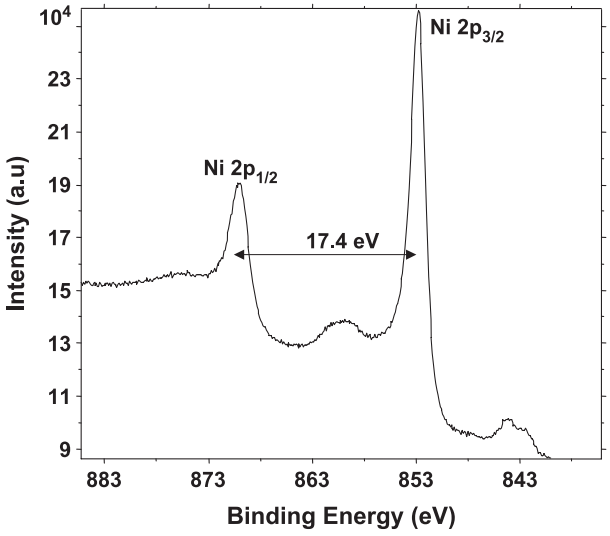

Fig. 2. Photoelectron signal related to the Ni2p level of the a-C:Ni film.

From the literature, the $Ni2p_{3/2}$ peak is located at 852.3 and 853.2 eV, respectively, for metallic nickel and nickel oxide [39]. No reference related to the XPS identification of the Ni–C bond has been found in the literature, even if the related peak should be probably located between the two previous values. Taking into account the energy resolution of our spectrometer and our experimental energy position of the $Ni2p_{3/2}$ peak, it is not possible to conclude unambiguously by XPS on the nature of the chemical state of nickel. Further experiments with a higher energy resolution are in progress.

In order to obtain a more detailed analysis of the C1s contributions in our films, NEXAFS experiments have been performed and the spectra have been compared to those of graphite and diamond. Since NEXAFS has been performed in the total electron yield detection mode, the probed thickness is similar in XPS and NEXAFS. Fig. 3 shows the NEXAFS C(1s) K-edge spectra of the a-C and a-C:Ni films, compared to the spectra of references of

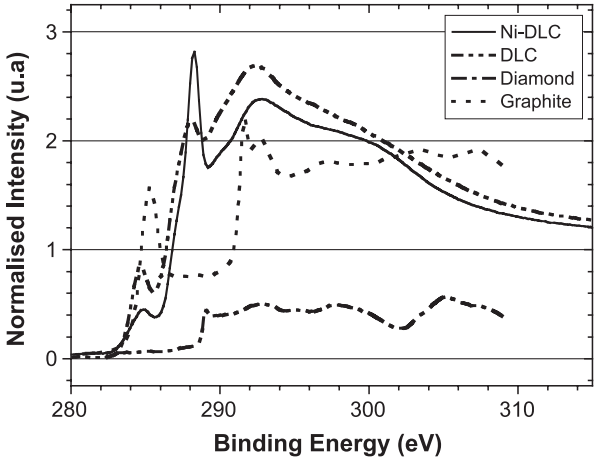

Fig. 3. C1s XANES spectra's from a-C, a-C:Ni, diamond and graphite.

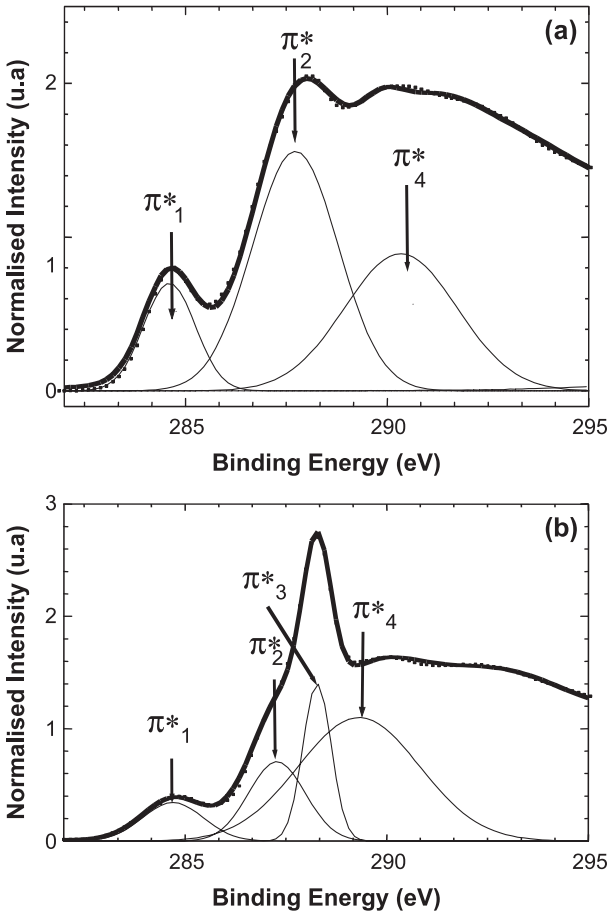

Fig. 4. Detailed curve fit analysis of the XANES spectra of (a) the a-C film and (b) the a-C:Ni film.

highly pure graphite (HOPG) and diamond. In NEXAFS spectroscopy, the photo-electron from each atomic core level probes the antibonding states π* and σ*. The spectra of the absorption edges may be decomposed into two energy regions: the transitions to the π* states, for energies under the ionization potential (IP) which depends on each bonding configuration, and the core-to-continuum excitations with the transitions to the σ* states above IP [40]. One observes a general reorganisation of the carbon local surrounding when nickel is introduced in the presence of oxygen as contaminant, characterized in the

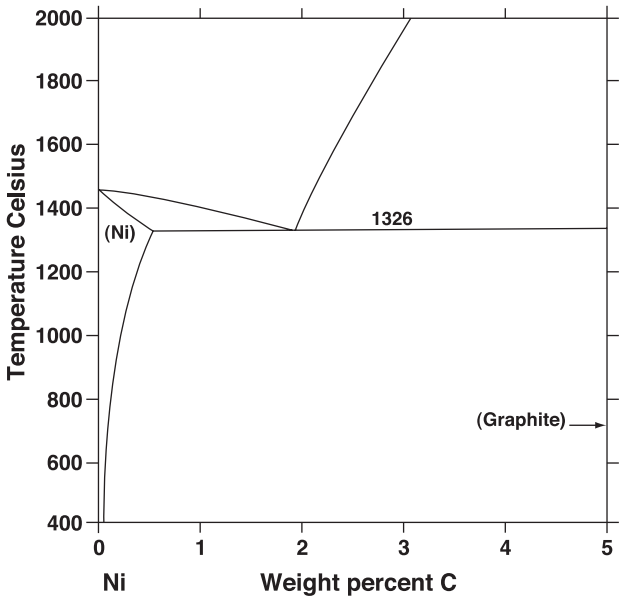

Fig. 6. The Ni–C phase diagram (from Ref. [41]).

a-C:Ni spectrum by a less extended and flatter σ* region as in graphite. In Fig. 4a and b are shown the curve fit analysis of the a-C and a-C:Ni spectra using four independent (Gaussian) π* and σ* states. The first resonance π_1*, attributed to C=C π* state [40], presents a small shift from 284.6 to 284.7 eV, while the energies of the other π* states decrease of about 0.4 eV, as Ni is incorporated into the film. The carbon–oxygen bonding may contribute to the resonances π_2* ($\approx 287.6 \pm 0.3$ eV) and π_4* ($\approx 289.9 \pm 0.5$ eV), with less intensity in the a-C:Ni. Due to the presence of oxygen, the effect of introducing Ni into the oxygen-containing carbon films may keep the carbon matrix rather free of oxygen, which is probably concentrated at the interface between quite pure nickel clusters and quite pure DLC matrix. The interface between carbon and nickel is also characterized by a much localised π_3* state at 288.4 eV, with a width half compared to the other contributions, which may thus be attributed to C–Ni bonding. Since the signal of the contribution's nickel is localised in the energy region of the carbon's transition π* states, the quantification of carbon sp^2 and sp^3 hybridizations has not been performed.

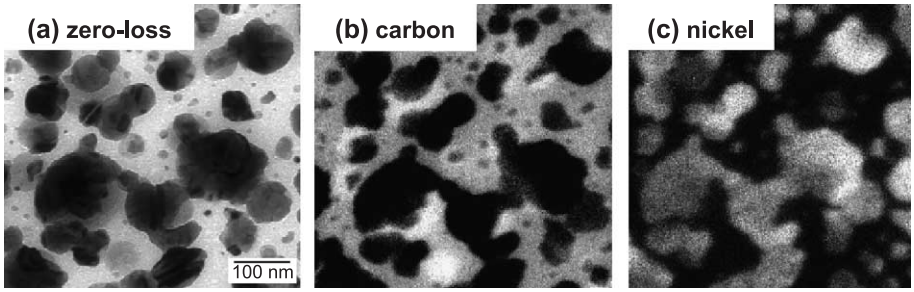

Fig. 5. Energy filtering (EFTEM) images of (a) zero-loss, (b) carbon and (c) nickel related to the a-C:Ni film. Carbon and nickel are identified by the bright areas respectively in (b) and (c).

Specimens were also examined by EELS, giving evidence of the nanostructure of the films. The zero-loss image (Fig. 5a) indicates the morphology of the films, consisting of dark nodules (100 nm or less range) dispersed in a brighter matrix. The C1s and Ni2p images (Fig. 5b and c, respectively) clearly indicate that the a-C:Ni film is constituted by nanometer scale nodules dispersed in the carbonaceous matrix. TEM experiments in the diffraction mode are actually in progress to go further in the identification of the crystallographic phases and DLC/nickel interface in the a-C:Ni film.

In agreement with Ref. [31], nanostructures of metallic materials have been obtained by femtosecond PLD. Investigations allowed us to identify nanocristallites of nickel included in an amorphous matrix of DLC, with an average size of 100 nm. Nickel is known to be a "carbophobic" element, as demonstrated by the Ni–C phase diagram depicted in Fig. 6, showing that even at a temperature of 400 °C, a mixture of Ni and C consists in metallic Ni (with a very small amount of C in solid solution) and graphitic carbon. This phase distribution is probably unchanged at lower temperature. Further works is in progress to confirm or not the presence of Ni–C bonds in the a-C:Ni films deposited by femtosecond PLD, with various concentrations of Ni in the films, in order to extend the explored region of the phase diagram. The comparison with other metallic elements exhibiting different chemical affinities with carbon will be also of great interest. The chemistry and nanostructure of a-C:Me films deposited by femtosecond PLD will thus be more deeply explored.

4. Conclusion

According to our knowledge, we have presented the first attempts to deposited metal-containing DLC films by femtosecond laser deposition. Nickel has been selected since it is known to form a metallic phase without any significant carbon dissolution nor carbide near room temperature. The main conclusions are the following:

(a) In agreement with the literature related to femtosecond PLD, a nanostructured material has been deposited by alternatively ablating graphite and nickel under vacuum. Nodules of nickel in the 100 nm size range are dispersed in the carbonaceous matrix of the a-C:Ni film containing about 50 at.% of Ni.
(b) Oxygen contaminants are affected by the presence of nickel and a fraction of nickel (no quantification available) seems to be bonded to carbon, as deduced from NEXAFS results.
(c) Presumably nickel is predominantly in the metallic form, but further investigations are necessary to characterize the nanostructure and chemistry of the films, by XPS at higher energy resolution, transmission electron microscopy and grazing angle X-ray diffraction.

Acknowledgements

We are grateful to the Laboratoire de Tribologie et Dynamique des Systèmes UMR 5513 of Ecole Centrale de Lyon and particularly B. Vacher for her help and experimental support with TEM/EELS, and Dr. M.I. De Barros for the NEXAFS spectra of the diamond and graphite references.

References

[1] J. Robertson, Mater. Sci. Eng., R 37 (4–6) (2002) 129.
[2] A. Erdemir, C. Donnet, in: B. Bhushan (Ed.), Modern Tribology Handbook, vol. II, CRC Press, 2001, p. 871.
[3] E.W. Plummer, X. Ismail, R. Matzdorf, A.V. Melechko, J.D.R. Zhang, Prog. Surf. Sci. 67 (2001) 17.
[4] C. Donnet, Surf. Coat. Technol. 100–101 (1998) 180.
[5] O. Hurasky-Schönwert, Technical Report, Environmentally Compatible Tribo-Systems in Gearing, Chair of Machine Tools-Gear Research Group, Aachen University of Technology (RWTH).
[6] J. Güttler, J. Reschke, Surf. Coat. Technol. 60 (1993) 531.
[7] M. Murakawa, T. Komori, S. Taeuchi, K. Miyoshi, Surf. Coat. Technol. 120–121 (1999) 646.
[8] G.C. Ficcabrino, X.-M. Tang, Sens. Actuators, B 35–36 (1996) 247.
[9] R. Wachter, A. Cordery, S. Proffitt, Diamond Relat. Mater. 7 (1998) 687.
[10] P.B. Oliete, T.C. Rojas, A. Fernandez, A. Gedanken, Y. Koltypin, F. Palacio, Acta Mater. 52 (2004) 2165.
[11] A.A. Voevodin, M.S. Donley, Surf. Coat. Technol. 82 (1996) 199.
[12] D.B. Chrisey, C.K. Hubler (Eds.), Pulsed Laser Deposition of Thin Films, Naval Research Laboratory, Washington, DC, 1994.
[13] J. Bulír, M. Jelínek, V. Vorlícek, J. Zemek, V. Perina, Thin Solid Films 292 (1997) 318.
[14] T. Szörenyi, C. Fuchs, E. Fogarassy, Surf. Coat. Technol. 125 (2000) 308.
[15] F. Qian, V. Craciun, R.K. Singh, S.D. Dutta, P.P. Pronko, J. Appl. Phys. 86 (1999) 2281.
[16] J. Perrière, E. Million, W. Seiler, C. Boulmer-Leborgne, V. Craciun, O. Albert, J.C. Louloergue, J. Etchepare, J. Appl. Phys. 91 (2) (2002) 690.
[17] A.-S. Loir, F. Garrelie, J.-L. Subtil, F. Goutaland, M. Belin, R. Le Harzic, C. Donnet, Y. Ouerdane, F. Rogemond, P. Laporte, Appl. Surf. Sci. 208–209 (2003) 553.
[18] F. Garrelie, A.-S. Loir, F. Goutaland, C. Donnet, R. Le Harzic, B. Angleraud, Y. Ouerdane, P. Laporte, SPIE Proc. 4760 (2002) 301.
[19] F. Garrelie, A.S. Loir, C. Donnet, F. Rogemond, R. Le Harzic, M. Belin, E. Audouard, P. Laporte, Surf. Coat. Technol. 163–164 (2003) 306.
[20] A.-S. Loir, F. Garrelie, C. Donnet, M. Belin, B. Forest, F. Rogemond, P. Laporte, Thin Solid Films 453–454 (2004) 531.
[21] A.V. Rode, B. Luther-Davies, E.G. Gamaly, J. Appl. Phys. 85 (8) (1999) 4222.
[22] P.S. Bank, L. Dinh, B.C. Stuart, M.D. Feit, A.M. Komashko, A.M. Rubenchikh, M.D. Perry, W. McLean, Appl. Phys., A 69 (1999) S347 (Suppl.).
[23] M. Okoshi, S. Higuchi, M. Hanabusa, Appl. Surf. Sci. 154–155 (2000) 376.
[24] Zs. Geretovszky, Z. Kantor, T. Szörenyi, Appl. Surf. Sci. 208–209 (2003) 547.
[25] E. Millon, J. Perrière, R.M. Défourneau, D. Défourneau, O. Albert, J. Etchepare, Appl. Phys., A 77 (1) (2003) 73.
[26] M. Womack, M. Vendan, P. Molian, Appl. Surf. Sci. 221 (2004) 99.
[27] M. Okoshi, K. Higashikawa, M. Hanabusa, Appl. Surf. Sci. 154–155 (2000) 424.

[28] C.R. Lululescu, H. Miyake, S. Sato, Appl. Surf. Sci. 197–198 (2002) 499.
[29] Z. Zhang, P.A. VanRompay, J.A. Nees, R. Clarke, X. Pan, P.P. Pronko, Appl. Surf. Sci. 154–155 (2000) 165.
[30] Y. Tian, M. Wolmack, P. Molian, C.C.H. Lo, J.W. Anderegg, A.M. Russel, Thin Solid Films 418 (2002) 129.
[31] T.W. Trelenberg, L.N. Dinh, C.K. Saw, B.C. Stuart, M. Balooch, Appl. Surf. Sci. 221 (2004) 364.
[32] R. Teghil, L. D'Alessio, A. Santagata, M. Zaccagnino, D. Ferro, D.J. Sordelet, Appl. Surf. Sci. 210 (2003) 307.
[33] Q. Wei, R.J. Narayan, J. Narayan, J. Sankar, A.K. Sharma, Mater. Sci. Eng., B 53 (1998) 262.
[34] Q. Wei, A.K. Sharma, J. Sankar, J. Narayan, Compos., Part B 30 (1999) 675.
[35] J.M. Lackner, W. Waldhauser, R. Ebner, A. Fian, G. Jakopic, G. Leising, T. Schöberl, Surf. Coat. Technol. 177–178 (2004) 360.
[36] X. Tian, M. Rusop, Y. Hayashi, T. Soga, Jpn. J. Appl. Phys. 41 (2002) L970.
[37] S. Watanabe, M. Shinohara, H. Kodama, T. Tanaka, M. Yoshida, T. Takagi, Thin Solid Films 420–421 (2002) 253.
[38] G. Speranza, N. Laidani, Diamond Relat. Mater. 13 (2004) 451.
[39] C.D. Wagner, W.M. Riggs, L.E. Davis, J.F. Moulder, in: G.E. Meullenberg (Ed.), Handbook of X-Ray Photoelectron Spectroscopy, Perkin-Elmer, 1979.
[40] J. Stöhr, NEXAFS Spectroscopy, Springer Series, ISBN: 3-540-54422-4, 1996.
[41] A. Gabriel, P. Custafson, Calphad 11 (1987) 203.

Available online at www.sciencedirect.com

SCIENCE DIRECT

Thin Solid Films 494 (2006) 98 – 104

www.elsevier.com/locate/tsf

Nanocomposite tantalum–carbon-based films deposited by femtosecond pulsed laser ablation

N. Benchikh [a], F. Garrelie [a], K. Wolski [b], C. Donnet [a,*], R.Y. Fillit [b], F. Rogemond [a], J.L. Subtil [a], J.N. Rouzaud [c], J.Y. Laval [d]

[a] *Laboratoire Traitement du Signal et Instrumentation, UMR 5516, Université J. Monnet, 10 rue Barrouin, 42000 Saint-Etienne, France*
[b] *Ecole Nationale Supérieure des Mines de Saint-Etienne, Centre SMS - URA CNRS 5146, 158 cours Fauriel, 42023 Saint-Etienne, Cedex 02, France*
[c] *Laboratoire de Géologie de l'Ecole Normale Supérieure de Paris 24, rue Lhomond 75231-Paris Cedex 5, France*
[d] *Laboratoire de Physique du Solide, UPR5 CNRS-ESPCI, 10 rue Vauquelin 75231-Paris Cedex 05, France*

Available online 15 August 2005

Abstract

Nanostructured coatings of metal (tantalum) containing diamond-like carbon (a-C:Ta) have been prepared by femtosecond pulsed laser deposition (PLD). The films, containing 15 at.% tantalum, have been deposited by ablating sequentially graphite and metallic tantalum in vacuum conditions with an amplified Ti:sapphire laser. The coatings have been investigated by X-ray photoelectron spectroscopy, grazing angle X-ray diffraction, energy filtered transmission electron microscopy, scanning and high resolution transmission electron microscopies. Evidence of metallic α-Ta and β-Ta particles (diameter in the 100 nm range) and smaller quasi-amorphous tantalum clusters embedded in the carbonaceous matrix have been shown. A thin tantalum carbide interface between the carbon matrix and the top surface of the tantalum nodules has also been identified. The ability of femtosecond pulsed laser deposition to synthetize nanocomposite carbon-based films and to control their nanostructure is discussed.

Keywords: Femtosecond laser; Pulsed loser ablation; Doped diamond-like carbon

1. Introduction

The most recent research activities on diamond-like carbon (DLC) films are devoted to improve some of their most critical properties, including both mechanical properties (adhesion, stress, hardness, Young modulus, friction and wear) and other functional properties towards applications in microelectronics or optics. For this purpose, various elements, including Si, N, F, B, various metals and more recently Ge, P and I, are now introduced in the carbon network, thus leading to doped and alloyed DLC films and labeled a-C:X (see [1] and [2–14] related to published works from 2002). An increasing use of these films is observed in various applications, e.g. as microelectrodes in micro-electrochemical analysis, emitters in advanced field emission devices, solid lubricant films or magnetic films. The introduction of a doping/alloying element in the carbonaceous network of the DLC film leads to a wider range of nanostructures and compositions available, in comparison to "pure" DLC films (a-C and a-C:H well known films). The chemistry (in particular the chemical affinity with carbon) and the concentration of the doped/alloyed element strongly affect the nature and the properties of the film, and this is strongly dependent on the deposition process, due to the high versatility from one deposition technique to the other one.

Pulsed laser deposition (PLD) has proved to be an effective technique for low temperature deposition, at low temperature, of a wide variety of thin film materials, extending from DLC to oxides or nanostructured materials [15–17]. In particular, PLD allows for precise control of the concentration of elements impinging upon the growing films, and this is of particular interest to deposit doped and alloyed DLC films in a controlled and reproducible way, compared to

* Corresponding author. Tel.: +33 4 77 91 58 01; fax: +33 4 77 91 57 81.
E-mail address: Christophe.Donnet@univ-st-etienne.fr (C. Donnet).

0040-6090/$ - see front matter © 2005 Elsevier B.V. All rights reserved.
doi:10.1016/j.tsf.2005.07.161

other deposition techniques. Recent papers have highlighted the interest of nanosecond PLD to deposit doped and alloyed DLC and other carbon-based films. Wei et al. [18] have compared the structure and the mechanical properties of a-C:Cu, a-C:Ti and a-C:Si films deposited by nanosecond PLD. Contrary to adhesion, the stress, hardness, friction and wear depend on the alloying element. Mominuzzaman et al. [19] have shown the influence of P doping (1–7 wt.%) on the optical gap and electrical resistivity of the films. Zhu et al. [20] have shown how Ni and Co catalysts in ablated graphite targets may control the formation of both carbon nanotubes and metal nanocrystals. Trusso et al. [21] have performed reactive (N_2) PLD on a SiC target to study the optical gap and the index of refraction of the deposited SiCN-based film. Suda et al. [22] have investigated a-C:B films deposited by nanosecond PLD, with a required boron concentration making the film suitable for electron emission studies. Morstein et al. [23] and Willmott and Spillmann [24] use the versatility of PLD to deposit MeC_xN_{1-x} (Me=Zr, Zr–Al, Ti, V) films, with highlights on their composition, microstructure, optical and mechanical properties. In particular, the friction coefficient of some of these films was found to be significantly lower than the friction coefficient of most other coatings with similar high hardness values. Orlianges et al. [25] have shown the influence of Ni and Ta doping on the electrical properties of metal-doped carbon films.

Femtosecond lasers challenge excimer lasers for high-quality thin film preparation and high-precision micromachining. The pulse duration makes possible to achieve higher spatial resolution but also higher laser intensity than nanosecond lasers. In this case, the kinetic energy of the ejected species can be increased up to a few keV [26] leading to lower stress values in the film [27]. Femtosecond laser ablation is used from 1999 to deposit various kinds of films, in particular pure DLC films [26,28–33]. These films exhibit sp^3 content in the range 40–75%, with interesting mechanical properties, low friction and high wear resistance.

From our knowledge, the present work belongs to the first attempts to deposit an a-C:X film by femtosecond PLD. Some of us have already deposited a-C:Ni in similar deposition conditions, thus leading to a distribution of metallic Ni clusters embedded in the carbon network [34]. In the present work, tantalum has been selected due to its high chemical affinity with carbon, contrary to nickel. The films have been investigated by coupling X-ray photoelectron spectroscopy (XPS), grazing incident angle X-ray diffraction (GIXRD), high resolution scanning and transmission electron microscopies (SEM, HRTEM) and energy filtered transmission electron microscopy (EFTEM).

2. Experimental details

We have synthetized films containing 85 at.% carbon and 15 at.% tantalum by ablating respectively a target of pure graphite (purity 99.997%) and a target of pure tantalum (purity 99.9%). The principle of this co-deposition consists to focus alternatively, by using a shutter, the femtosecond laser (Concerto, BMI/TCL, λ=800 nm, pulse duration 150 fs, repetition rate 1 kHz, energy per pulse 1.5 mJ) during 9s onto the graphite's target, and thus during 1s onto the tantalum's target. Those irradiation times have been selected to achieve the desired stoichiometry, taking into account the deposition rate of each element determined in a preliminary set of experiments (deposition rate of carbon=22 nm/mm, deposition rate of tantalum=35 nm/mm). This sequence of ablation is repeated during a certain number of runs depending on the thickness required for the coatings. Typically 240 runs of 1s with tantalum crossed with 241 runs of 9s with carbon lead to films in the micrometer range. The last ablated species is systematically carbon. The films were grown at room temperature in a deposition chamber evacuated to a base pressure of 10^{-5} Pa. The laser has been focused with an incident angle of 45° on the targets, with an energy density of 2.6 J/cm^2 (±20%). More details on this deposition procedure have been published in a previous paper [34]. The film deposited onto a p-type silicon substrate has been analyzed by XPS (Riber spectrometer) with a MgKα source (1253.6 eV) working in direct acquisition mode at a resolution of 0.5 eV, with a step of 0.1 eV for detailed acquisition spectra of each element. The spectrometer energies were calibrated using the Au $4f_{1/2}$ peak and Cu $2p_{3/2}$ at 84.0 and 932.6 eV respectively. XPS analysis has been performed before and after in situ Ar^+ sputtering of the surface to remove the adventitious surface layers. The film surface has been observed by using a scanning electron microscope equipped with a field emission gun (FEG–SEM, JEOL 6500F). The size distribution of the particles in the film has been quantified by an analysis soft imaging system (SIS). The surface free energy (or surface tension) of the film has been determined by contact angle measurements in atmospheric conditions using a CAM-PLUS MICRO device from TANTEC Products, Inc. Two test liquids (water and formamide) have been used to estimate the surface energies (polar and dispersive components) of both a-C and a-C:Ta, by measuring the contact angles between the solvents and the surface. GIXRD measurements have been performed at different incident angles in order to adjust the X-ray penetration depth to the particles size and the layer thickness. We have used a D5000 goniometer link together with a XP18 rotating anode and the Dosophatex system. A K_α copper radiation was used. HRTEM has been carried out on a JEOL 2010 microscope equipped with an field emission gun and operating at 200 kV. The resolution in the lattice fringe mode is 0.11 nm. Local elemental analysis has been performed thanks to a PGT energy selective X-ray analyzer allowing in situ analysis on volumes smaller than 100 nm^3, with a precision of 0.1%. For HRTEM observations, coatings have been directly deposited on a classical TEM copper grid (diameter of 3 mm), previously covered by a holey amorphous carbon film. Examination of

the sample was focused on parts of the sample lying across the holes to obtain information free of the contribution of the supporting carbon film. These films have been also examined by EELS in a LEO 912 energy filtered transmission electron microscope (EFTEM) at 120 kV.

3. Results and discussion

Some characteristics and basic properties of the investigated a-C:Ta films containing 15 at.% of tantalum deposited on the silicon or copper grid substrates are summarized in Table 1. The compressive stress, quantified by measuring the surface curvature of the substrate before and after deposition of 1 μm film of a-C:Ta, are in the GPa range, as for undoped DLC obtained in the same deposition conditions [31]. The surface energy of the a-C:Ta film is 34.2 mN/m, with polar and dispersive components, respectively, 0.1 mN/m and 34.1 mN/m. We have deposited a pure a-C film using the same conditions as the a-C:Ta film, but without any Ta incorporation. The surface energy of the a-C film is 32.2 mN/m, with polar and dispersive components respectively 12.0 mN/m and 20.2 mN/m. From the present results, one can observe that the incorporation of 15 at.% of Ta does not induce any significant variation of surface energy, due to a decrease of the polar component together with an increase of the dispersive one when 15 at.% of Ta is introduced in the carbon film. These values of surface energy are in agreement with already published data of surface energies related to a-C:Me films, showing a systematic decrease of the polar component with metal incorporation, and a significant difference of the polar component from one metal to another [35]. The dispersion of surface energy values observed in the literature is frequently explained by the adsorption of oxygen on the surface, which may be responsible for a lower polar component [35]. SEM observations (Fig. 1a) show evidence of the nanostructure of the film surface. These features, analyzed by the imaging system, allow quantification of the size distribution of clusters present in the film (Fig. 1b). A wide size distribution is observed between 15 nm and 175 nm. The average size is 82 nm with a standard deviation of 49 nm. Specimens have been also examined by EELS, confirming, through a transmission view, the nanostructure of the film. The zero-loss image (Fig. 2a) of a 100 nm thick coating highlights the morphology of the films, consisting of dark nodules (100 nm or less on this picture) dispersed in a brighter matrix. The tantalum image hasn't been recorded due to its high electron core level energy unachievable with the equipment at hand. The C1s and O1s images (Fig. 2b and c, respectively) clearly indicate that the a-C:Ta film is constituted by nanometer-scale nodules dispersed in the carbonaceous matrix. These nodules do not contain carbon. However a thin carbon layer containing oxygen (less than 10 nm) can be observed around the dark nodules. Some traces of oxygen (not quantified) have been identified also in the carbonaceous matrix. The presence of carbon around the nodules localized on the top surface of the film (see Fig. 2c) is consistent with a last deposition sequence performed with the carbon target (as indicated in the Experimental section).

A more detailed investigation of the a-C:Ta film has been achieved by HRTEM. In order to observe the a-C:Ta by transmission in the high resolution mode, one sequence of 9s for carbon ablation followed by one sequence of 1s for

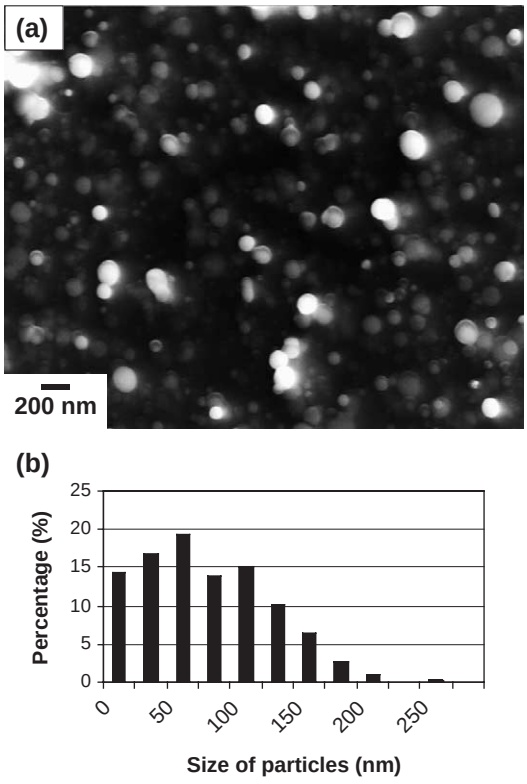

Fig. 1. (a) FEG–SEM image of C:Ta film, (b) size distribution of the clusters embedded in the film.

Table 1
Deposition of the a-C:Ta films by femtosecond pulsed laser ablation of tantalum and graphite

Substrate	Laser fluence (J/cm^2)	Ablation sequences	Film composition	Film thickness
Silicium	2.6	C ablation: 24 sequences of 9 s Ta ablation: 23 sequences of 1 s C ablation: 241 sequences of 9 s Ta ablation: 240 sequences of 1 s	Ta 15 at.% C 85 at.%	100 nm 1 μm
Copper grid		C ablation: 1 sequences of 10 s Ta ablation: 1 sequences of 1 s		Not measured

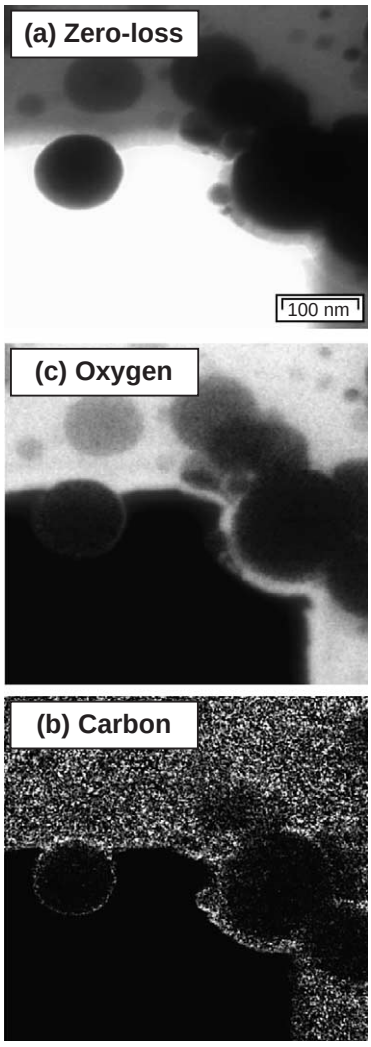

Fig. 2. Energy filtered (EFTEM) images of (a) zero-loss, (b) carbon and (c) oxygen related to the a-C:Ta film. Carbon and oxygen are identified by the bright areas, respectively, in (b) and (c).

tantalum ablation have been carried out to limit the thickness of the film (Table 1). The combination of both sequences correspond to a theoretical film thickness of 4 nm, taking into account the ablation rates of C and Ta (see Experimental section). Since the distribution of Ta in the deposited film is not homogeneous due to the formation of nodules, the size of the nodules is significantly higher than the theoretical thickness of 4 nm. A characteristic 0.3×0.3 μm portion of the sample is imaged on the Fig. 3a. The particle size varies from about 10 nm (small grey particles) up about 100 nm (large black particles). All these particles are spheroidal as proved by their constant circular shape in the image, when the sample is tilted of ±20° according to the incident electron beam. From their contrast point of view, three types of particles can be recognized: large black particles which represent the major component of the sample, large dark grey ones and light grey small ones (which are only a minor phase). In situ punctual elemental analyses by Electron Dispersive Spectroscopy (EDS) mode and high resolution TEM imaging have been performed on the particles lying across the hole of the TEM holey grid, in order to avoid the contribution of the amorphous carbon supporting film. The three types of particles are essentially constituted by tantalum. Only the external part contains higher amount of carbon, due to the smaller thickness and consequently of higher relative contribution of the carbon deposit due to the first carbon ablation. A crystalline structure is clearly visible in the dark particles (Fig. 3b), whereas the light grey small ones appear completely amorphous. The dark grey particles show an intermediate organisation where only a short range order can be imaged (Fig. 3c).

In order to go further in the investigation of the crystalline structure, the a-C:Ta film (100 nm thick) has been analyzed by GIXRD. The spectrum (Fig. 4) has been obtained with an incident X-ray beam angle of 0.7°. We

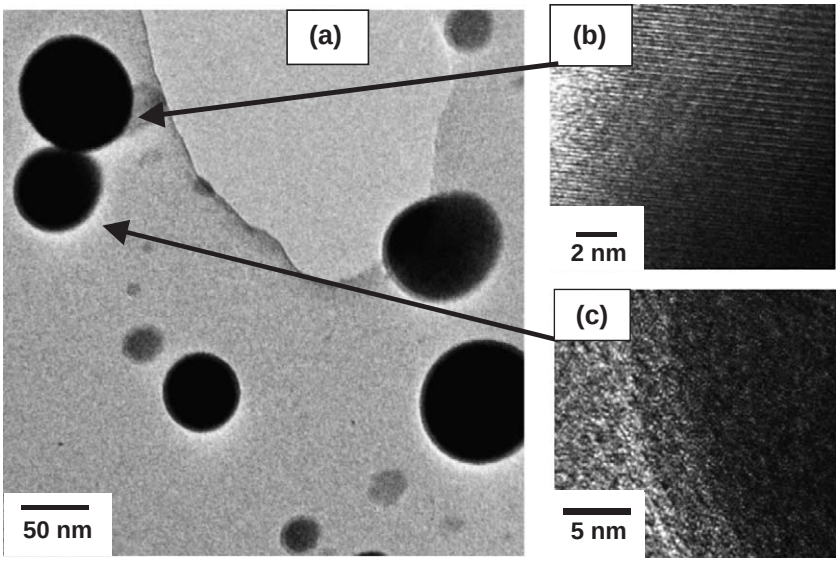

Fig. 3. Transmission electron microscopy image of (a) the a-C:Ta film. High resolution images of (b) black nodules and (c) light black nodules.

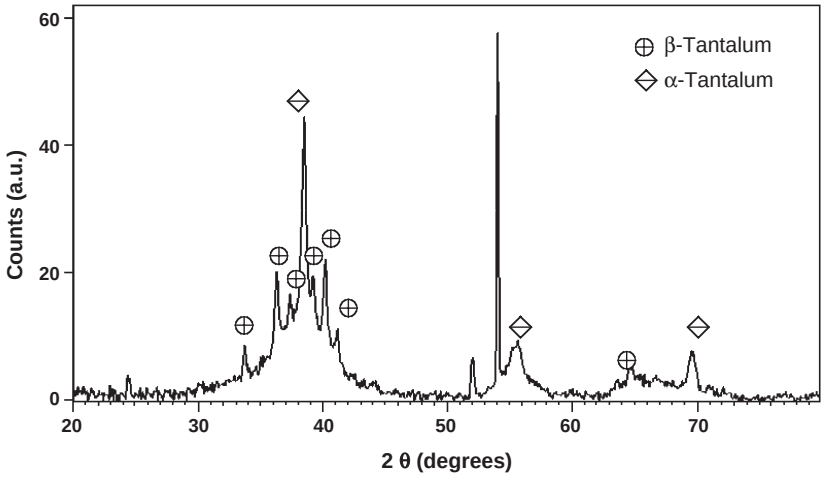

Fig. 4. Grazing angle X-ray diffraction spectra of the a-C:Ta film, observed with an incident X-ray beam angle of 0.7°. The un-indexed peaks correspond to the doped-Si substrate.

identify three main contributions corresponding to the different phases present in the film:

- a centered cubic tantalum phase (α-Ta) which is the stable phase in normal pressure and temperature conditions. The tantalum target used for deposition is α-Ta.
- a metastable phase, corresponding to metallic tetragonal tantalum (β-Ta), which has been already observed at high temperatures (>800 °C) [36].
- probably an amorphous phase whose signal corresponds to the bump centered on the most intense peak of the stable phase ($2\theta = 38°$).

The full width at half maximum (FWHM) of the two first crystalline phases identified above are consistent with nodule sizes in the range of 100 nm. The wide signal related to the third phase is consistent with nodule sizes less than 10 nm. These last nodules are probably the light grey small ones which appear also amorphous by HRTEM. From the combination of the previous investigations, we have observed that the present a-C:Ta film (15 at.% Ta) consists in three kinds of metallic nodules with diameters in the 10–100 nm range. Indeed, for films other than pure DLC (including metallic films), femtosecond PLD leads to nanostructured films with grain size in the nanometer scale and properties significantly different from nanosecond PLD films [27,40]. The nanostructure seems to originate from the drastic effects of femtosecond laser–matter interaction, as phase explosion [37] or explosive melting [38]. Moreover, mass spectrometry analyses of the plasma plume [39] shows the presence of clusters in the plume, which can be correlated to the nanostructure of the films. As the deposition technique is a non-equilibrium one, we have obtained in the present work two crystalline phases (α-Ta and the metastable β-Ta), compared to the only one present in the target (α-Ta). The metastable phase is present at high temperatures (higher than 800 °C), leading to the conclusion that species in the plasma plume induced by femtosecond ablation reached temperatures higher than 800 °C. The carbonaceous structure in the tantalum alloyed DLC appears to be quite similar to the carbonaceous structure related to pure DLC films deposited by the same femtosecond PLD process [41]. Further investigations are in progress to correlate the nature of the species in the plasma plume during the femtosecond laser ablation of the metal target and the nature of the metallic phases observed in the film.

By HRTEM, we have observed that the external part of most nodules contains higher amount of carbon. This may be attributed to the well known chemical affinity between tantalum and carbon through the formation of carbides. Since GIXRD investigations do not identify any tantalum carbide phase, probably such a carbide, if it exists, is so thin and/or so imperfectly crystallized, that the diffraction technique is unable to identify it. One way to go further is to perform XPS in order to investigate the top surface of the film, which is consisted of a thin carbon layer (in agreement with the deposition procedure) covering the tantalum nodules.

Carbon, tantalum and a low quantity of oxygen (less than 2%) are detected by XPS in the C:Ta film. The presence of oxygen may be attributed to the adventitious surface layers, since its signal decreases after carrying a sputter cleaning of the surface in the UHV chamber analysis of the spectrometer. The spectrum of the film shows an asymmetric C1s signal broader (FWHM ≈ 2 eV) than those related to diamond and graphite (FWHM = 1 eV). Fig. 5a shows the curve fit analysis of this C1s signal in four Gaussian contributions, using the Sherwood model. The highest binding energy component (1), located at 285.3 eV, is generally assigned to the carbon sp^3 hybridization whereas the second component (2), located at 284.2 eV, is generally assigned to the carbon sp^2 hybridization with the well-known 1 eV energy difference between these two contribu-

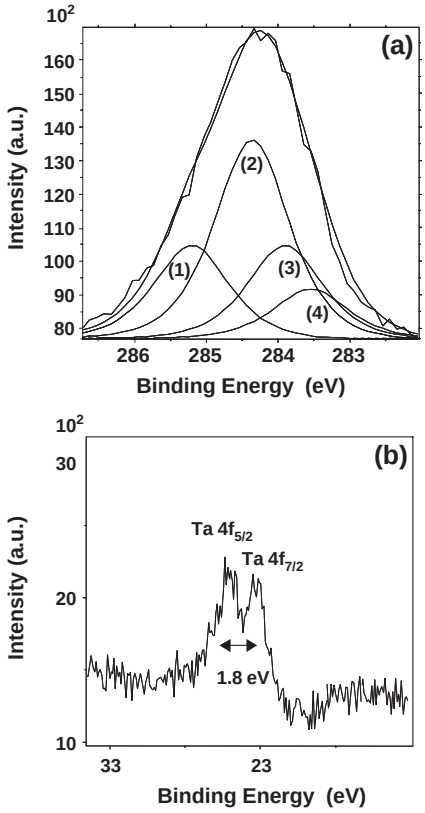

Fig. 5. Photoelectron spectra of the a-C:Ta film related to (a) C1s core level with detailed curve fit analysis (four contributions) and (b) the Ta4f core level corresponding to a tantalum carbide chemical bond.

tions [42]. However such an interpretation is known to be controversial in DLC films. Moreover, a peak located at 285.1 eV has been also attributed to graphene layers on TaC [43], which could be consistent with our contribution located at 285.3 eV. The two lowest binding energy components (3) and (4), respectively, at 283.9 eV and 283.5 eV, may be attributed to the tantalum–carbon bond in TaC carbides [43]. The affinity of tantalum with carbon is confirmed with the Ta 4f feature shown in Fig. 5b where the Ta $4f_{7/2}$ and $4f_{5/2}$ peaks are located respectively at 23.1 eV and 24.9 eV. From the literature the peak $4f_{7/2}$ is located at 21.5 eV, 22.9 eV and 26.6 eV, respectively, for metallic tantalum [44], tantalum carbide [43] and tantalum oxide [45]. Taking into account the energy resolution of our spectrometer and the experimental position of the $Ta4f_{7/2}$ peak in the present work, we can conclude that the thin top surface layer probed by XPS is mainly constituted by tantalum carbide. No attempt to quantify the stoichiometry of the carbide has been performed, since such an approach requires a specific deep XPS investigations, as proposed in [46]. In conclusion, due to the chemical affinity of tantalum with carbon, and also to the high energy of the species impinging on the growing film in femtosecond PLD [41], the interface of tantalum nodules and the carbonaceous matrix seems to be constituted by a very thin tantalum carbide phase.

4. Conclusion

The deposition of nanostructured coatings of tantalum-doped diamond-like carbon (a-C:Ta) by femtosecond PLD has been investigated. Tantalum has been selected due to the well-known chemical affinity between tantalum and carbon through the formation of carbides. The main conclusions of this study are the following

(a) Tantalum is synthetized as clusters with a size distribution in the range of 15 to 175 nm.
(b) These tantalum clusters appear under three distinct phases: the first crystalline phase (α-Ta) is the stable phase and correspond to that of the target, the second crystalline phase is a metastable phase (β-Ta) and has been already observed at high temperatures, and a third component, corresponding to the smallest clusters, which is an amorphous phase.
(c) The DLC matrix is Csp^3-rich, as already observed in previous published works.
(d) As expected, due to the chemical affinity between tantalum and carbide, and to the high energy of the impinging species in femtosecond PLD, the interface between the tantalum clusters and the carbonaceous matrix is a tantalum carbide phase.

Acknowledgments

The authors acknowledge Béatrice VACHER (Ecole Centrale de Lyon, Laboratoire de Tribologie et Dynamique des Systèmes UMR 5513) for EFTEM investigations. The authors also acknowledge Mr Paul JOUFFREY for the use of the SEM–FEG apparatus (EMSE: Ecole des Mines de Saint-Etienne), Mr Gilles BLANC (EMSE) for his help for SEM–FEG imaging and Mr Pierre PASSET (EMSE) for XPS analysis.

References

[1] A. Erdemir, C. Donnet, in: B. Bhushan (Ed.), Modern Tribology Handbook, vol. II, CRC Press, 2001, p. 871.
[2] Y.Y. Chang, D.Y. Wang, W. Wu, Thin Solid Films 420–421 (2002) 241.
[3] K. Baba, R. Hatada, Surf. Coat. Technol. 158–159 (2002) 272.
[4] R. Wang, C. Mercer, A.G. Evans, C.V. Cooper, H.K. Yoon, Diamond Relat. Mater. 11 (2002) 1797.
[5] W. Wu, J. Ting, Thin Solid Films 420 (2002) 166.
[6] I. Gerhards, C. Ronnong, U. Vetter, H. Hofsäss, H. Gibhardt, G. Eckoled, Q. Li, S.T. Lee, Y.L. Huang, M. Seibt, Surf. Coat. Technol. 158–159 (2002) 114.
[7] D. Nilsson, F. Svahn, U. Wiklund, S. Hogmark, Wear 252 (2003) 1084.
[8] T.I.T. Okpalugo, P.D. Maguire, A.A. Ogwu, J.A.D. McLaughlin, Diamond Relat. Mater. 13 (2004) 1549.
[9] P. Zhang, B.K. Tay, G.Q. Yu, S.P. Lau, Y.Q. Fu, Diamond Relat. Mater. 13 (2004) 459.
[10] T. Thiery, Y. Pauleau, J.J. Grob, D. Babonneau, Thin Solid Films 466 (2004) 10.

[11] C.P. Lungu, I. Mustata, G. Musa, V. Zaroschi, A.M. Lungu, K. Iwasaki, Vacuum 76 (2004) 127.
[12] C.Q. Hu, W.T. Zheng, B. Zheng, J.J. Li, X.M. Bai, H.W. Tian, Q. Jiang, X.Y. Wang, J.Q. Zhu, S.H. Meng, X.D. He, J.C. Han, Vacuum 77 (2004) 63.
[13] L. Kumari, S.V. Subramanyam, A. Gayen, V. Jayaram, Thin Solid Films 471 (2005) 252.
[14] M. Ikeyama, S. Nakao, Y. Miyagawa, S. Miyagawa, Surf. Coat. Technol. 191 (2005) 38.
[15] A.A. Voevodin, M.S. Donley, Surf. Coat. Technol. 82 (1996) 199.
[16] D.B. Chrisey, C.K. Hubler (Eds.), Pulsed Laser Deposition of Thin Films, Naval Research Laboratory, Washington, DC, 1994.
[17] J. Bulír, M. Jelínek, V. Vorlícek, J. Zemek, V. Perina, Thin Solid Films 292 (1997) 318.
[18] Q. Wei, R.J. Narayan, J. Narayan, J. Sankar, A.K. Sharma, Mater. Sci. Eng., B 53 (1998) 262.
[19] S.M. Mominuzzaman, T. Soga, T. Jimbo, M. Umeno, Diamond Relat. Mater. 10 (2001) 1839.
[20] S. Zhu, C.H. Su, J.C. Cochrane, S. Lehoczky, I. Muntele, D. Ila, Diamond Relat. Mater. 10 (2001) 1190.
[21] S. Trusso, F. Barreca, F. Neri, J. Appl. Phys. 92 (5) (2002) 2485.
[22] Y. Suda, Y. Suganuma, Y. Sakai, K. Suzuki, J. Tsujino, N. Homma, Appl. Surf. Sci. 197–198 (2002) 603.
[23] M. Morstein, P.R. Willmott, H. Spillmann, M. Döbeli, Appl. Phys., A 75 (2002) 647.
[24] P.R. Willmott, H. Spillmann, Appl. Surf. Sci. 197–198 (2002) 432.
[25] J.C. Orlianges, C. Champeaux, A. Catherinot, A. Pothier, P. Blondy, P. Abelard, B. Angleraud, Thin Solid Films 453–454 (2004) 291.
[26] F. Qian, V. Craciun, R.K. Singh, S.D. Dutta, P.P. Pronko, J. Appl. Phys. 86 (4) (1999) 2281.
[27] J. Perrière, E. Millon, W. Seiler, C. Boulmer-Leborgne, V. Craciun, O. Albert, J.C. Loulergue, J. Etchepare, J. Appl. Phys. 91 (2) (2002) 690.
[28] P.S. Banks, L. Dinh, B.C. Stuart, M.D. Feit, A.M. Komashko, A.M. Rubenchik, M.D. Perry, W. McLean, Appl. Phys., A 69 (1999) S347 (Suppl.).
[29] D.-S. Yao, J.-R. Liu, L.-G. Wang, C.-X. Yu, R.-J. Zhan, Chin. Phys. Lett. 17 (7) (2000) 540.
[30] M. Okoshi, S. Higuchi, M. Hanabusa, J. Appl. Phys. 86 (3) (1999) 1768.
[31] F. Garrelie, A.S. Loir, C. Donnet, F. Rogemond, R. Le Harzic, M. Belin, E. Audouard, P. Laporte, Surf. Coat. Technol. 163–164 (2003) 306.
[32] A.-S. Loir, F. Garrelie, C. Donnet, M. Belin, B. Forest, F. Rogemond, P. Laporte, Thin Solid Films 453–454 (2004) 531.
[33] A.S. Loir, F. Garrelie, C. Donnet, F. Rogemond, J.L. Subtil, B. Forest, M. Belin, P. Laporte, Surf. Coat. Technol. 188–189 (2004) 728.
[34] N. Benchikh, F. Garrelie, C. Donnet, B. Bouchet-Fabre, K. Wolski, F. Rogemond, A.S. Loir, J.L. Subtil, Thin Solid Films 482 (2005) 287.
[35] P. Zhang, B.K. Tay, G.Q. Yu, S.P. Lau, Y.Q. Fu, Diamond Relat. Mater. 13 (2004) 459.
[36] P.T. Moseley, C.J. Seabrook, Acta Crystallogr., B 29 (1973) 1170.
[37] A. Miotello, R. Kelly, Appl. Phys., A 69 (1999) 67.
[38] V.N. Tokarev, A.F.H. Kaplan, Lasers Eng. 7 (1998) 295.
[39] R. Teghil, L. D'Alessio, A. Santagata, M. Zaccagnino, D. Ferro, D.J. Sordelet, Appl. Surf. Sci. 210 (2003) 307.
[40] T.W. Trelenberg, L.N. Dinh, B.C. Stuart, M. Balooch, Appl. Surf. Sci. 229 (2004) 268.
[41] A.S. Loir, F. Garrelie, J.L. Subtil, F. Goutaland, M. Belin, R. LeHarzic, C. Donnet, Y. Ouerdane, F. Rogemond, P. Laporte, Appl. Surf. Sci. 208–209 (2003) 553.
[42] S.T. Jackson, R.G. Nuzzo, Appl. Surf. Sci. 90 (1995) 195.
[43] J. Walter, W. Boonchuduang, S. Hara, J. Alloys Compd. 305 (2000) 259.
[44] C.D. Wagner, W.M. Riggs, L.E. Davis, J.F. Moulder in Handbook of X-ray Photoelectron Spectroscopy, Perking Elmer Corporation, Physical Electronics Division.
[45] Y. Okazaki, T. Tateishi, Y. Ito, Mater. Trans., JIM 38 (1) (1997) 78.
[46] O.Y. Khyzhun, J. Alloys Compd. 259 (1997) 47.

Available online at www.sciencedirect.com
ScienceDirect
Talanta 72 (2007) 310–314
Talanta
www.elsevier.com/locate/talanta

Short communication

Characterization of different diamond-like carbon electrodes for biosensor design

R. Maalouf [a,b,c], H. Chebib [b], Y. Saikali [b], O. Vittori [c], M. Sigaud [c], F. Garrelie [d], C. Donnet [d], N. Jaffrezic-Renault [a,*]

[a] *Center of Electrical Engineering of Lyon, CEGELY, UMR/CNRS 5005, Ecole Centrale Lyon, 69134 Ecully Cedex, France*
[b] *Laboratory of Chemistry, Lebanese University, Fanar, Beirut, Lebanon*
[c] *Laboratory of Analytical Electrochemistry, Claude Bernard University, Lyon I, 43 Boulevard du 11 Novembre 1918, Villeurbanne Cedex, France*
[d] *Laboratory of Signal Processing and Instrumentation, UMR/CNRS 5516, Jean Monnet University, Saint Etienne, France*

Received 6 April 2006; received in revised form 18 October 2006; accepted 19 October 2006
Available online 4 December 2006

Abstract

Diamond-like carbon (DLC) films are gaining big interest in electrochemistry research area. DLC electrodes made with different ratio of sp^3/sp^2 carbon hybridization or doped with different percentages of nickel were characterized electrochemically by cyclic voltammetry and by amperometric measurements towards hydrogen peroxide. SiCAr1 and SiCNi5% were chosen as sensitive transducers for the elaboration of amperometric glucose biosensors. Immobilization of glucose oxidase was carried out by cross-linking with glutaraldehyde. Measurements were made at a fixed potential + 1.0 V in 40 mM phosphate buffer pH 7.4. SiCAr1 seems to be more sensitive for glucose, 0.6875 μA/mM, than SiCNi5%, 0.3654 μA/mM. Detections limits were 20 μM and 30 μM, respectively. Apparent Michaelis-Menten constants were found around 3 mM. Forty-eight percent and 79% of the original response for 0.5 mM glucose remained after 10 days for both biosensors, respectively.

Keywords: Diamond-like carbon; Biosensors; Glucose oxidase; Amperometric measurements

1. Introduction

Biosensors, combining a selective biological recognition element and a sensitive transducer, are of increasing importance in many areas such as medicine, food quality and safety control, and environmental pollution monitoring. Amperometric enzyme electrodes hold a leading position among biosensor systems presently available and have already found a large commercial market. The most common enzymes used in monoenzymatic systems are oxidases; especially glucose oxidase due to its low price and high stability. Such devices combine the specificity of the enzyme for recognizing a given target analyte, whilst their sensitivity is greatly influenced by the transducer [1–3]. The most employed electrochemical transducers are platinum, gold and carbonaceous materials [4,5]. Carbon electrodes exist in different allotropes and they are widely used in the field of biosensors. Glassy carbon (GC) electrodes are often used as transducers [6–8] by employing a modified GC electrode or by changing the methods of enzyme immobilisation in the aim to get sensitive, stable and reproducible biosensor. Graphite, porous carbon [9] and carbon films [10,11] electrodes are also used as transducers in the field of biosensors.

Diamond-like carbon films are gaining now big interest. These films are chemically stable, optically transparent and achieve good mechanical properties, low coefficient of friction, and strong wear resistance. Due to these properties, DLC films found application in variety of areas such as electronic, optical, mechanical and biomedical applications. Pulsed laser deposition of diamond-like carbon leads to high purity films with a predominance of sp^3 hybridization (diamond) at low deposition temperature. Since the last ten years, femtosecond lasers have been used in pulsed laser deposition. In this case, the kinetic energy of the ejected particles can be increased up to a few keV, which is much higher than in nanosecond regime. Original properties of these coatings, including lower stress and good adherence, may be related to such a

* Corresponding author. Tel.: +33 4 72 18 62 43; fax: +33 4 78 43 37 17.
E-mail address: Nicole.Jaffrezic@ec-lyon.fr (N. Jaffrezic-Renault).

0039-9140/$ – see front matter © 2006 Elsevier B.V. All rights reserved.
doi:10.1016/j.talanta.2006.10.025

high value of the kinetic energy. These advantages allow the development of DLC coatings without any adhesion underlayer [12].

Diamond-like-carbon films constitute a new research area in electrochemistry. They have been used as electrodes in electrochemical microgravimetry on quartz crystal electrodes [13], as nitrogenated DLC films (N:DLC) for metal tracing analysis [14] and as coatings for polycarbonate membranes used as permselective barriers in glucose oxidase biosensors [15,16]. We have tested amorphous DLC electrodes in a preliminary work for the development of a glucose amperometric biosensor. It can be seen that DLC films can be used as transducers in the field of biosensors nevertheless they are less sensitive then glucose oxidase/glassy carbon electrodes [17]. Properties of DLC films can be adjusted depending on their application. Thus, the sp^3/sp^2 carbon hybridization ratio may be adjusted and controlled according to the deposition process and conditions. Their conductivity also can be controlled by doping elements such as metals, Si and N.

The present study deals with characterization and the comparison of different diamond-like carbon films as matrices for biosensor design. Some of these films are elaborated with different ratio of sp^3/sp^2 carbon hybridization and others are doped with Ni. Cyclic voltammetry and amperometric measurements aim to see whether properties of DLC films affect their sensitivities towards hydrogen peroxide. The behavior of the most sensitive electrodes for H_2O_2 will be studied for biosensor elaboration by using a conventional glucose oxidase assay system.

2. Experimental

2.1. Materials

Glucose Oxidase (GOD, EC 1.1.3.4, 130 U/mg) was kindly given by the Laboratory of Biomolecular Electronics, IMBG, Kiev, Ukraine. Bovine Serum Albumin (BSA, Fraction V) and α-D(+)-glucose were obtained from Sigma. Glutaraldehyde, 24-wt.% solution in water, was purchased from Acros Organics. Hydrogen peroxide 30% and chemicals used for preparing buffer solution, sodium hydroxide and potassium dihydrogen phosphate were obtained, respectively, from Fluka, Sigma and Prolabo. Glucose standard solutions were elaborated by diluting a 1 M α-D(+)-glucose stock solution prepared 24 h before use to establish the anomeric equilibrium between α and β forms of D-glucose. Ultra-pure water (resistivity > 18.2 MΩ cm, Elga System) was used for the preparation of all solutions.

2.2. Measurements and apparatus

Voltammetric and amperometric experiments were carried out using a Voltalab 10 (PGZ100 & VoltaMaster 4). The electrochemical cell consisted of a three-electrode system with a platinum plate (0.54 cm^2) and a saturated calomel electrode (SCE) as counter and reference electrode, respectively. Diamond-like carbon electrodes with an effective surface of 0.15 cm^2 were used as working electrodes. A magnetic stirred and a stirring bar provide the convective transport. All potentials were reported versus SCE. The background current was allowed to decay to a steady value before aliquots of substrate solution were added. The biosensor response was measured as the difference between total and residual current.

2.3. Diamond-like carbon films deposition

These films were prepared by the Laboratory of Signal Processing and Instrumentation, Jean Monnet-University, France. Nickel containing DLC films have been deposited by femtosecond pulsed laser deposition by ablating alternatively graphite (purity 99.997%) and nickel (purity 99.9%) targets under vacuum conditions at room temperature onto p-silicon substrates at a target to substrate distance of 36 mm. The femtosecond laser (Concerto, BMI/TCL, Ti-Saphir, $\lambda = 800$ nm, pulse duration 300–350 fs, repetition rate 1 kHz, energy per pulse 1 mJ, energy density 2.6 J/m^2) has been alternatively focused on the targets with an incident angle of 45°, by using a shutter rotating at 32 rpm.

Two percentages of nickel have been introduced in diamond-like carbon films according to the conditions mentioned below. For the first sample, six sequences of ablation on each target have been performed alternatively during 89 s for graphite and 1 s for nickel. A similar procedure has been carried out for the second sample, with 16 sequences of ablation on each target during 32 s for graphite and 1 s for the nickel. Taking into account the deposition rate of pure carbon (22 nm/min) and pure nickel (35 nm/min), nickel incorporated DLC film thickness is estimated in the range of 200 nm for both samples. Percentages of nickel in diamond-like carbon films have been determined by X-ray photoelectron spectroscopy (XPS) and Rutherford backscattering spectroscopy (RBS). They showed 2 at.% for the first sample (SiCNi2%) and 5 at.% for the second one (SiCNi5%) [14].

Three other types of DLC films have been elaborated by femtosecond pulsed laser ablation onto p-silicon substrates under argon pressure at room temperature. Normally DLC films made under vacuum show a predominance of sp^3 hybridized carbon [15]. Thus, working under argon pressure and modifying this pressure leads to DLC films with different ratio of sp^3/sp^2 carbon hybridization. $P_{Ar} = 2 \times 10^{-2}$ mbar (SiCAr1), $P_{Ar} = 5 \times 10^{-1}$ mbar (SiCAr2) and $P_{Ar} = 5 \times 10^{-3}$ mbar (SiCAr3) were used, respectively, for the deposition of DLC films by ablation graphite target during 10 min.

All diamond-like-carbon electrodes cited below were cleaned with ultra-pure water and with optical paper before use.

2.4. Enzyme immobilization

Immobilization was carried out by cross-linking with glutaraldehyde. Thus, a mixture of 5% glucose oxidase, 5% BSA and 10% glycerol in phosphate buffer 20 mM pH 7.4 was prepared. The glycerol was used as a plasticizer in order to avoid cracks appearing in the biolayer. DLC electrodes were coated with a thin layer of this mixture and kept 20 min in

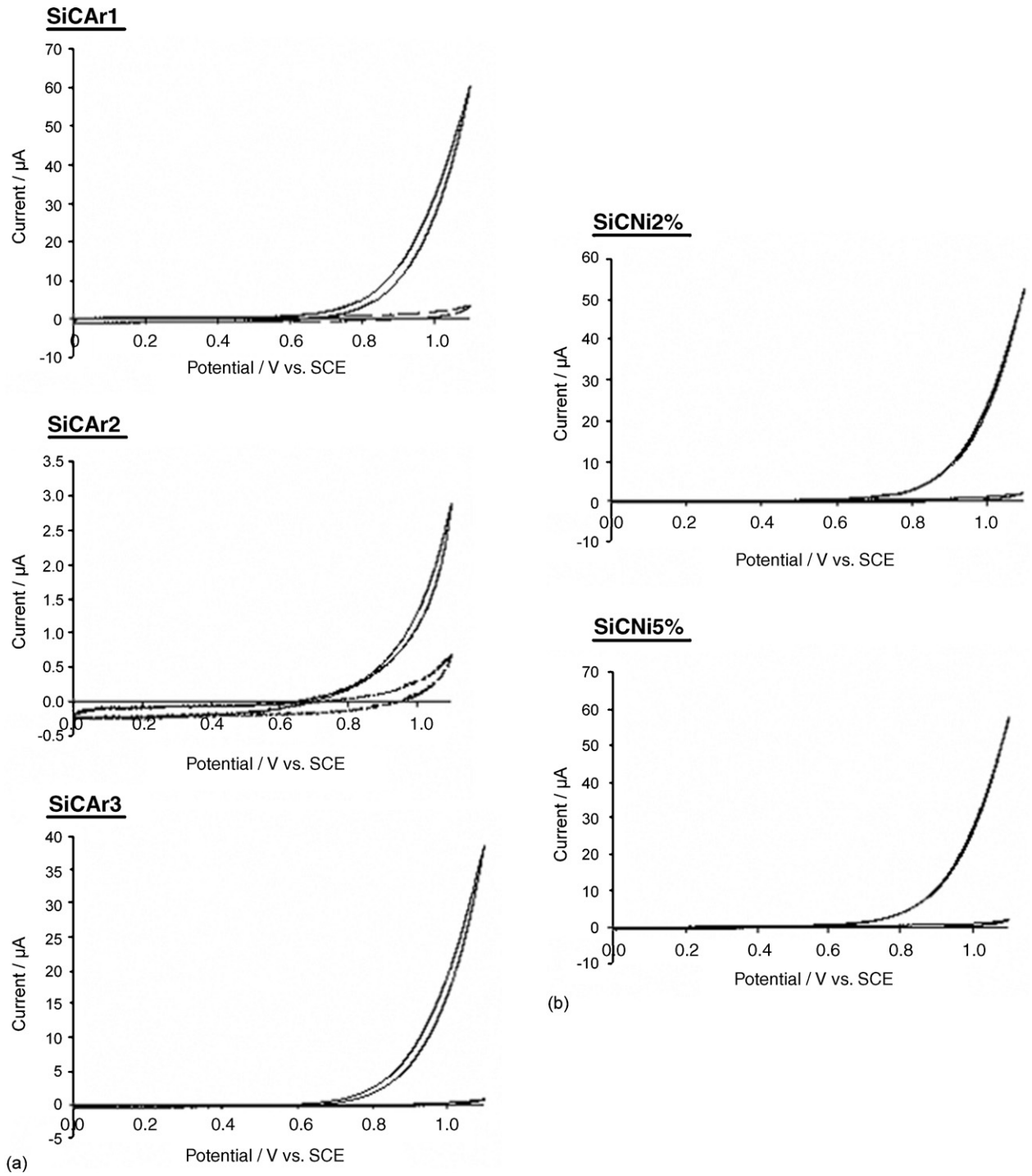

Fig. 1. (a) Cyclic Voltammograms of DLCs films with different ratio of sp^3/sp^2 carbon hybridization in 40 mM PB solution, pH 7.4 with and without 5 mM H_2O_2. (b) Cyclic Voltammograms of Ni-containing DLCs films in 40 mM PB solution, pH 7.4 with and without 5 mM H_2O_2.

glutaraldehyde vapor at room temperature. This bifunctional compound (OHC–$(CH_2)_3$–CHO) links covalently from each side to the amine groups of GOD and BSA, respectively, creating a stable biopolymer. The resulting enzyme electrodes were allowed to dry in air and were thoroughly washed and stored in 40 mM phosphate buffer (PB) solution, pH 7.4, at 4 °C when not in use.

3. Results and discussions

3.1. Hydrogen peroxide detection

Glucose biosensors are based on the fact that glucose oxidase, a flavoenzyme, catalyses the oxidation of glucose to gluconic acid in the presence of oxygen. Since hydrogen peroxide is the

Table 1
Hydrogen peroxide sensitivity of different diamond-like carbon electrodes in 40 mM PB solution, pH 7.4

Electrodes	SiCArl	SiCAr2	SiCAr3	SiCNi2%	SiCNi5%
Sensitivity (μA/mM)	4.4463	1.1872	2.0397	3.4659	4.6401

co-product of this reaction; its electroactivity can be used to obtain a measurable current signal.

$$\beta\text{-d-Glucose} + O_2 \leftrightarrow \text{GluconicAcid} + H_2O_2$$

$$H_2O_2 \leftrightarrow O_2 + 2H^+ + 2e^-$$

DLC electrodes were initially characterized electrochemically by recording their cyclic voltammograms between 0.0 V and 1.1 V in 40 mM phosphate buffer solution, pH 7.4 with and without 5 mM H_2O_2. The catalytic voltammograms obtained in the presence of hydrogen peroxide exhibit a greater sensitivity for SiCAr1 and SiCNi5% electrodes; no observable plateau was distinguished (Fig. 1a and b). After analysis of these responses, a potential of +1.0 V was chosen for H_2O_2 amperometric detection.

Amperometric measurements were carried out in PB solution at +1.0 V by injecting H_2O_2 aliquots; each addition result in a 0.02 mM increment in concentration. The comparison of DLCs electrodes according to H_2O_2 sensitivity is shown in Fig. 2. Their corresponding sensitivities are presented in Table 1. Since SiCAr1 and SiCNi5% electrodes enable a more satisfactory determination of hydrogen peroxide, 4.4463 μA/mM and 4.6401 μA/mM, respectively, their behavior will be studied for biosensor elaboration by using a glucose amperometric assay system.

3.2. Enzyme measurements

To evaluate the possible application and the behavior of the above-mentioned DLCs electrodes in biosensor construction, glucose biosensors were fabricated following the procedure previously described. Kinetics studies of the immobilized enzyme

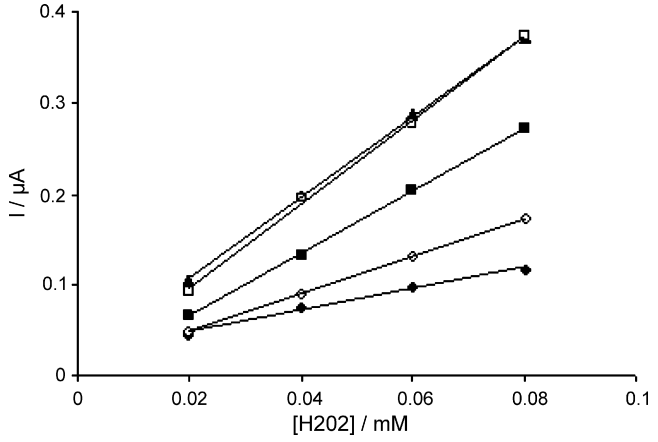

Fig. 2. Hydrogen peroxide calibrations curves for SiCAr1 (Δ), SiCAr2 (♦), SiCAr3 (◊), SiCNi2% (■) and SiCNi5% (□) electrodes for successive additions of 0.02 mM H_2O_2 in 40 mM PB, pH 7.4.

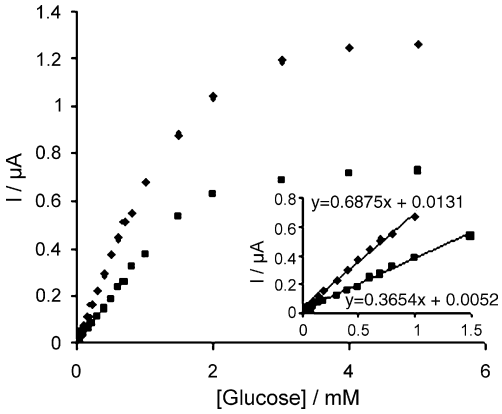

Fig. 3. Glucose Calibration curves for SiCAr 1 (♦) and SiCNi 5% (■) biosensors for successive additions of glucose in 40 mM PB, pH 7.4.

were carried out by plotting the electrochemical response to increasing concentrations of glucose. Fig. 3 shows the curves of DLCs electrodes, SiCAr1 and SiCNi5%, in 40 mM PB, pH 7.4 at a measurement potential of +1.0 V for successive additions of glucose.

The SiCAr1 glucose biosensor displays a linearity range up to 1 mM and until 1.5 mM for SiCNi5%. Corresponding detections limits were 20 μM and 30 μM, respectively. Even if these two electrodes have exhibited the same sensitivity for hydrogen peroxide, SiCAr1 biosensor shows higher sensitivity for glucose, 0.6875 μA/mM with $R = 0.9984$, than SiCNi5% biosensor, 0.3654 μA/mM with $R = 0.9982$. This fact can be explained by the use of two different topographical and constitutional structure electrodes leading to different and various interaction phenomenons between the immobilized biopolymer and the electrode surface. From the Lineweaver-Burk plots, apparent Michaelis-Menten constants of 3.38 mM and 3.09 mM were obtained, respectively, for SiCAr1 and SiCNi5% biosensors. The apparent K_m which depends on enzyme and not on the substrate is almost the same for both electrodes.

3.3. Operational and storage stability

The stability of enzyme sensors was usually limited by the deactivation and loss of enzyme. The deactivation of enzyme was mainly caused by unsuitable temperature. So, enzyme electrode needs to be kept at 4 °C. The loss of enzyme is highly related to the way the enzyme is fixed to the electrode (adsorption to the electrode, entrapment into a polymer, cross-linking with a bifunctional compound . . .).

The operational stability during 10 h for SiCAr1 and SiCNi5% glucose biosensors and their storage stability were tested in 40 mM phosphate buffer pH 7.4 containing 0.5 mM glucose.

The operational stability of both biosensors during ten working hours is presented in Fig. 4. The current response for 0.5 mM glucose seems to be very stable for SiCAr1 while it increases very slowly for SiCNi5%. It may be explained by the swollen of the biolayer with time allowing easily access of glucose to the electrode surface leading therefore to increasing quantity of

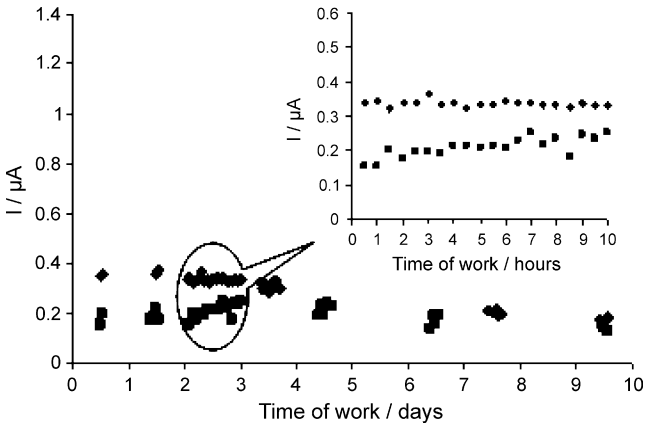

Fig. 4. Operational and storage stability of SiCAr1 (♦) and SiCNi5% (■) biosensors for 0.5 mM glucose concentration.

H_2O_2. It is illustrated in Fig. 4 by the slow increasing of the slope after 10 h of work.

The storage stability of SiCAr1 and SiCNi5% has been examined by checking periodically their activities. The current response of these two biosensors for 0.5 mM glucose remained almost unchanged during the three first days, and ∼48% and ∼79% of the original response remained after 10 days, respectively (Fig. 4). In fact, it can be deduced from X-ray photoelectron spectroscopy (XPS), near edge X-ray absorption fine structure (NEXAFS) and transmission electron microscope (TEM) that nickel is predominantly present in the metallic form in DLC films. They have the shape of nodules which are dispersed in the carbonaceous matrix [18]. In addition, AFM measurements provide an average roughness (Ra) of 2 nm for non-doped diamond-like carbon electrodes and 32 nm for nickel doped DLC electrodes. Thus, the higher roughness of SiCNi5% electrodes explains the better biolayer immobilization leading therefore to a more stable biosensor.

4. Conclusion

This work has been concerned with the characterization and the comparison of different diamond-like carbon electrodes for biosensor construction. DLC films appear to be very interesting in the electrochemical biosensor field. Evaluation of these electrodes was carried out by comparing their sensitivities towards hydrogen peroxide. The most sensitive electrodes were explored and studied for the development of a conventional glucose biosensor. SiCAr1 glucose oxidase based biosensor seems to be more sensitive than SiCNi5% but its main drawback is the stability that may be increased by fixing the enzyme differently on the electrode surface.

Acknowledgements

This work was done in the framework of Beyrouth-Rhone-Alpes MIRA program of a Rhone-Alpes Prioritary Thematic Action and of the Japan-France IRCP Project.

References

[1] J. Castillo, S. Gaspar, S. Leth, M. Niculescu, A. Mortari, I. Bontidean, V. Soukharev, S.A. Dorneanu, A.D. Ryabov, E. Csöregi, Sens. Actuators, B 102 (2004) 179.
[2] J. Wang, J. Pharm. Biomed. Anal. 19 (1999) 47.
[3] D.G. Georganopoulou, R. Carley, D.A. Jones, M.G. Boutelle, Faraday Discuss. 116 (2000) 291.
[4] J.-J. Xu, H.-Y. Chen, Anal. Chim. Acta 423 (2000) 101.
[5] S. Zhang, N. Wang, H. Yu, Y. Niu, C. Sun, Bioelectrochemistry 67 (2005) 15.
[6] H. Liu, H. Li, T. Ying, K. Sun, Y. Qin, D. Qi, Anal. Chim. Acta 358 (1998) 137.
[7] S. Yabuki, F. Mizutani, Sens. Actuator, B 108 (2005) 651.
[8] Han Nim Choi, Min Ah Kim, Won-Yong Lee, Anal. Chim. Acta 537 (2005) 179.
[9] V.G. Gavalas, N.A. Chaniotakis, T.D. Gibson, Biosens. Bioelectron. 13 (1998) 1205.
[10] M.E. Ghica, C.M.A. Brett, Anal. Chim. Acta 532 (2005) 145.
[11] M. Florescu, C.M.A. Brett, Talanta 65 (2005) 306.
[12] A.S. Loir, PhD thesis, University Jean Monnet, Saint Etienne (2004).
[13] J.M. Moon, S. Park, Y.K. Lee, G.S. Bang, Y.K. Hong, C. Park, J.C. Jeon, J. Electroanal. Chem. 464 (1999) 230.
[14] L.X. Liu, E. Liu, Surf. Coat. Technol. 198 (2005) 189.
[15] S.P.J. Higson, P.M. Vadgma, Anal. Chim. Acta 300 (1995) 85.
[16] S.P.J. Higson, P.M. Vadgma, Anal. Chim. Acta 300 (1995) 77.
[17] R. Maalouf, O. Vittori, Y. Saikali, H. Chebib, A.S. Loir, F. Garrelie, C. Donnet, N. Jaffrezic-Renault, Mater. Sci. Eng. C 26 (2006) 564.
[18] N. Benchikh, F. Garrelie, C. Donnet, B. Bouchet-Fabre, K. Wolski, F. Rogemond, A.S. Loir, J.L. Subtil, Thin Solid Films 482 (2005) 287.

Solid State Sciences xxx (2008) 1–4

Contents lists available at ScienceDirect

Solid State Sciences

journal homepage: www.elsevier.com/locate/ssscie

Structural and electrical characterization of boron-containing diamond-like carbon films deposited by femtosecond pulsed laser ablation

A. Sikora [a], A. Berkesse [b], O. Bourgeois [b], J.-L. Garden [b], C. Guerret-Piécourt [c], J.-N. Rouzaud [d], A.-S. Loir [a,*], F. Garrelie [a], C. Donnet [a]

[a] Laboratoire Hubert Curien, UMR CNRS 5516, Université Jean Monnet, 18 Rue Pr. B. Lauras, 42000 Saint-Etienne, France
[b] Institut Néel, UPR 2940 CNRS, 25 Avenue des Martyrs, 38042 GRENOBLE Cedex 9, France
[c] Laboratoire de Tribologie et Dynamique des Systèmes, UMR 5513 CNRS, Ecole Centrale de Lyon, 36 Avenue Guy de Collongue, 69134 ECULLY Cedex, France
[d] Laboratoire de Géologie, UMR 8538 CNRS, Ecole Normale Supérieure, 45 Rue d'Ulm, 75230 Paris Cedex 05, France

ARTICLE INFO

Article history:
Received 1 May 2008
Received in revised form 26 June 2008
Accepted 17 July 2008
Available online xxx

Keywords:
Boron-doped DLC
Femtosecond
Pulsed laser deposition
Resistivity

ABSTRACT

The present study investigates the influence of the incorporation of boron in Diamond-Like Carbon (DLC) films deposited by femtosecond laser ablation, on the structure and electrical properties of the coatings within the temperature range 70–300 K. Doping with boron has been performed by ablating alternatively graphite and boron targets. The film structure and composition have been highlighted by coupling Atomic Force Microscopy (AFM), Scanning Electron Microscopy equipped with a field emission gun (SEM-FEG) and High Resolution Transmission Electron Microscopy (HRTEM). Boron dilution ranges between 2 and 8% and appears as nanometer size clusters embedded in the DLC matrix. Typical resistivity values are 100 W cm for pure a-C films, down to few W cm for a-C:B films at room temperature. The resistance decreases exponentially when the temperature increases in the range 70–300 K. The results are discussed considering the classical model of hopping conduction in thin films. Some coatings show temperature coefficients of resistance (TCR) as high as 3.85%. TCRs decrease when the doping increases. Such high values of TCR may have interests in the use of these films as thermometer elements in micro and nanodevices.

1. Introduction

Diamond-like carbon (DLC) films are very attractive and valuable because of their exclusive capacity to present a combination of unique properties which can be tailored over a wide range, depending on the deposition process: tribological, electrical or functionalization properties [1]. Introduction of foreign elements, including metals allows an accurate control of electrical conduction properties and may give to DLC coatings a semiconducting behavior. It has been demonstrated that the electrical properties of DLC are strongly dependent on the physical structure of the thin film [2] and on the deposition procedure: sputtering, pulsed laser deposition, etc.

The present study investigates the influence of the incorporation of boron in Diamond-Like Carbon (DLC) films deposited by using femtosecond pulsed laser deposition (PLD) on the structure and electrical properties of the coatings within a temperature range of 77–300 K. The final objective is to identify the potentialities of a-C:B coatings in thin film thermometry within this temperature range. It is commonly accepted that for doped amorphous carbon materials the conduction mechanism for electrons is dominated by hopping transport either in hydrogen doped [3] or boron doped [4] DLC due to metal to insulator transition as the temperature is lowered. Materials exhibiting metal to insulator transition have been already widely used as resistive thermometer at low temperature [5–7] and over larger temperature ranges [8,9]. Due to a significant increase of resistance as the temperature is lowered, niobium nitride (NbN) as well as amorphous Nb–Si films are used to design sensitive thin film resistive thermometers. There is nowadays an increasing demand for more highly sensitive thermometers for temperature measurements closer to room temperature, especially in nanocalorimetry for applications in nanomagnetism, biophysics or infrared bolometry.

In the past years, various techniques, including vacuum arc [10], magnetron sputtering [11], arc discharge plasma CVD [12], thermal CVD [4] and pulsed laser deposition (PLD) [13–17] have been chosen to deposit boron-doped DLC films. PLD is widely used for the deposition of various thin films, in particular, near room temperature, pure DLC films with a predominance of sp^3 hybridization [18], and doped/alloyed DLC films, thanks to an accurate control of the concentration of the incorporated foreign elements. For a few years, pulsed laser ablation is performed using femtosecond pulse duration, with an increase of the kinetic energy of the

* Corresponding author. Tel.: +33 (0)4 77 91 58 01; fax: +33 (0)4 77 91 57 81.
E-mail address: anne.sophie.loir@univ-st-etienne.fr (A.-S. Loir).

1293-2558/$ – see front matter © 2008 Elsevier Masson SAS. All rights reserved.
doi:10.1016/j.solidstatesciences.2008.07.013

ejected particles up to a few kiloelectronvolts [19]. In such conditions, original film properties may be achieved, including lower stress and higher adhesion [18,20]. In the femtosecond regime, clusters of a few tens nanometers of diameter [21,22] are generally formed during the ablation of most materials. These particles may be incorporated into the carbonaceous network by co-ablation of carbon and an other material [23–25]. The objective of the present work is to deposit, by femtosecond PLD, a-C:B films containing boron nano-sized clusters embedded in the carbonaceous matrix, and to characterize their electrical resistivity in the temperature range of 77–300 K, depending on the boron concentration.

2. Experimental

Boron-containing DLC films have been deposited by alternatively ablating graphite (purity 99.997%) and boron (purity 99.97%) targets in a deposition chamber evacuated to a base pressure of 10^{-4} Pa. The films have been deposited at room temperature onto sapphire and *n*-type silicon substrates. The femtosecond laser (Concerto, BMI/TCL, $\lambda = 800$ nm, pulse duration 150 fs, repetition rate 1 kHz, energy per pulse 1.2 mJ) has been used with the same parameters detailed elsewhere [23]. The energy density has been set to 5 J cm^{-2} ($\pm$20%). The irradiation times on the boron and carbon targets have been selected to achieve the desired stoichiometry, taking into account the deposition rate of each element (deposition rate of carbon = 34 nm min^{-1}, deposition rate of boron = 21 nm min^{-1}). Typically 23 runs of 1 s with boron crossed with 24 runs of 14 s with carbon lead to a 4% boron-doped DLC film with a thickness of about 200 nm. The last ablated species is systematically carbon. Boron concentrations of 2, 4 and 8 at% have been studied. Pure a-C and boron films with similar thicknesses have been also deposited for an experimental comparison. Atomic Force Microscopy (AFM) observations have been carried out in the contact mode in air by using a VEECO© CP-II atomic force microscope. The film surfaces have been observed by using a scanning electron microscope equipped with a field emission gun (FEG-SEM, JEOL 6500F). High Resolution Transmission Electron Microscopy (HRTEM) has been carried out on a JEOL 2010 microscope equipped with a field emission gun and operating at 200 kV. Pure boron coatings have been directly deposited on a classical TEM copper grid (diameter of 3 mm), previously covered by a holey amorphous carbon film. Examination of the sample was focused on parts of the sample lying across the holes to obtain information free of the contribution of the supporting carbon film.

A standard four-probe technique has been used to measure the electrical resistance of the films. The measurements have been performed on sapphire substrates by using four platinum electrical leads: two for the current application and two for the voltage. A specific measurement chain has been used based on a very low dc current source down to nanoampere and a dc voltmeter in the ohmic regime. The electrical experiment has been carried out in a 4He cryostat in order to sweep the temperature from 4 to 300 K. Due to very high resistance of the DLC, most of the samples have been characterized over a reduced temperature range from 50 K or higher temperature up to 300 K. The sample area relevant for the calculation of the resistance is the surface between the voltage leads: 0.5 mm long and 2 mm large for a thickness of thin films of 200 nm.

3. Results and discussion

Pure boron film has been observed by FEG-SEM and AFM (Fig. 1(a) and (b)). These pictures show evidences of the nanostructure of the film surface. A wide size distribution of spherical boron particles (from few tens to few hundreds nanometers) is observed. The use of other elements in many femtosecond PLD thin coatings has also exhibited this kind of particles [21,22,24]. Typical clusters observed by HRTEM have been depicted in Fig. 1(c) and (d). The smallest and the biggest ones exhibit a diameter of about 30 nm (as shown in Fig. 1(c)) and 150 nm, respectively. The first observations give evidences of amorphous state for the smallest nodules whereas the biggest ones are entirely crystallized, as already observed for Ta clusters deposition by femtosecond PLD [26]. Other studies are under progress in order to elucidate and

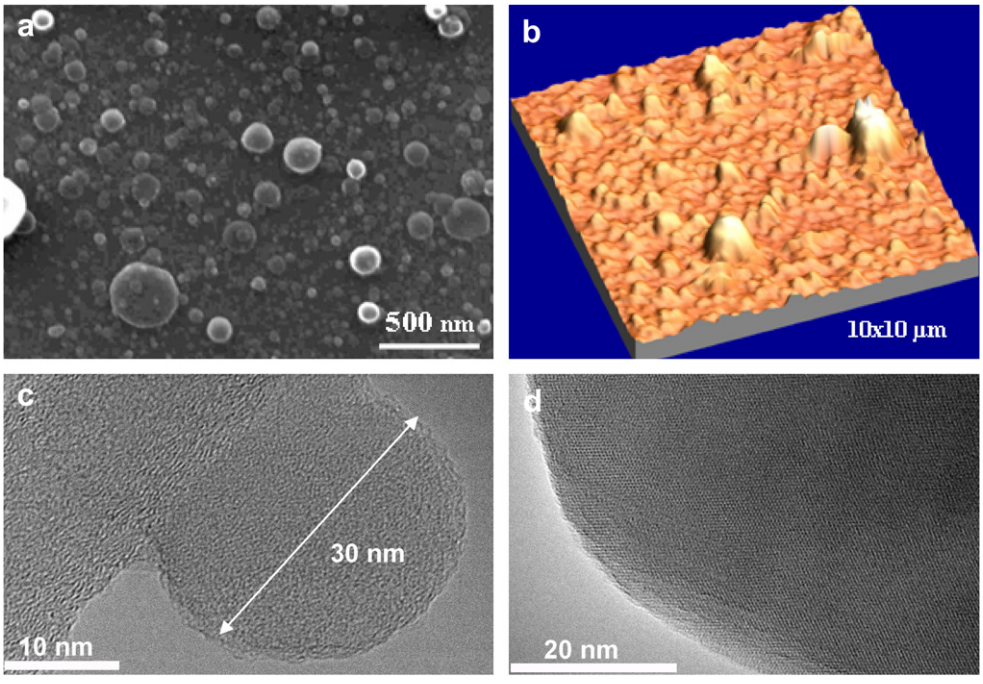

Fig. 1. FEG-SEM (a), 3D AFM (b) topography images, HRTEM ((c) and (d)) structure images of a 100% boron film. Typical smallest and a part of the biggest boron clusters are represented ((c) and (d), respectively).

Please cite this article in press as: A. Sikora et al., Structural and electrical characterization of boron-containing diamond-like carbon films deposited by femtosecond pulsed laser ablation, Solid State Sci. (2008), doi:10.1016/j.solidstatesciences.2008.07.013

confirm the crystallographic structure of boron particles. For the B-doped films, the same type of nodules has been also evidenced and these clusters seem obviously to be less numerous compared to the pure boron films. The DLC matrix between the nodules appears to be quite smooth, with an average roughness previously measured of about 1 nm for pure DLC films deposited in similar conditions [26].

The resistance vs. temperature of pure and 8% boron-doped DLC films have been measured. A strong increase of resistance is observed as the temperature is lowered as expected in the case of a metal to insulator transition; the measured electrical characteristics are assembled in Table 1.

In the case of regular variable range hopping (VRH) conduction processes the following law is expected for the variation of the resistance of amorphous disordered electronic systems.

$$R(T) = R_0 \exp\,(T_0/T)^x \tag{1}$$

where R_0 and T_0 are parameters related to the density of state at the Fermi energy and to the localisation length (see Refs. [3,27]) and $x = 0.25$ for 3D systems.

In order to better understand the mechanisms underlying the electrical conduction the logarithm of the resistance vs. $T^{-0.25}$ has been drawn in Fig. 2. Pure DLC and boron-doped DLC seem to follow correctly the Mott VRH law. The x exponent (depending on the samples) ranges between 0.25 and 0.35 which is in agreement with previous measurements confirming a conduction mechanism based on hopping between localized state near the Fermi level [4].

In Fig. 3, a log–log scale has been used to represent all the different dopings studied. The a-C, as previously mentioned, is in a stronger localized phase as compared to a-C:B whatever the doping level.

A decrease of the resistivity is observed with the introduction of boron in the carbon network, which seems to be quite independent on the amount of boron in the range of 2–8%. This behavior has been confirmed yet by Kleinsorge et al. for a-C:B films deposited with a filtered cathodic vacuum arc system [28] but is completely opposite to the observations reported by Tian et al. [16] where the resistivity of the boron-doped DLC film shows a small decrease for a small amount of boron (1%) and finally increases with boron content for larger amount. However, the resistivity of the undoped DLC films is significantly different in those studies, which both lead to comparable values of resistivity of a-C:B films, in the 10^1–10^2 Ohm cm range. This is significantly higher than the resistivity values obtained in our films, in the 1–5 Ohm cm range. Films of Ref. [16] have been deposited by nanosecond PLD and may probably exhibit an atomic doping whereas our films obtained by femtosecond PLD exhibit a distribution of boron nanoparticles in an amorphous matrix of DLC. Such a difference in the architecture of the film may explain why we do not obtain similar resistivity values for similar boron concentrations. Moreover, as reported in an earlier study related to a-C:Ni and a-C:Ta films deposited by femtosecond PLD [29], the introduction of metallic nanoparticles in a DLC film leads to a decrease of the sp^3 content, due to the graphitization by impingement of the clusters of the doping materials. This nanoparticle bombardment during the film growth, combined with the incorporation of boron is sufficient to modify the resistivity value of the doped films, compared to pure DLC, without any spectacular dependence with the boron content in the range of 2–8%.

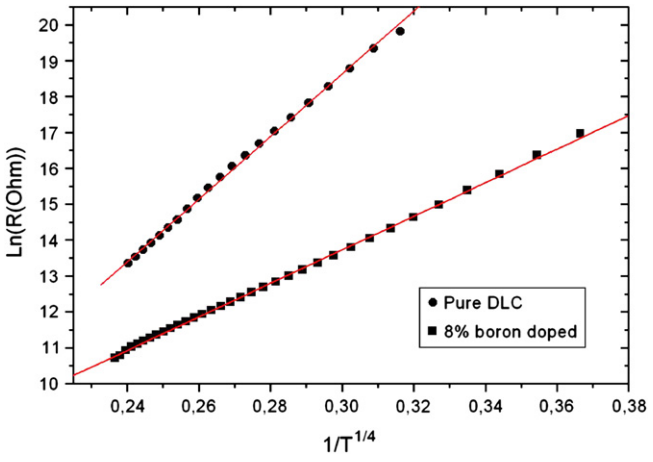

Fig. 2. Logarithm of the resistance vs. $T^{-0.25}$ for pure DLC and 8% boron-doped DLC. The straight lines are simple linear fits following the Mott law of variable range hopping conduction.

Considering the large increase of resistance at low temperature, it is quite natural to apply that kind of new materials to sensitive measurement of temperature. We have then calculated the temperature coefficient of resistance α, which evaluates the thermometer sensibility, for the different DLC films as it is presented in Fig. 4; α is defined by

$$\alpha = -\frac{1}{R(T)}\frac{\mathrm{d}R(T)}{\mathrm{d}T} \tag{2}$$

Indeed, for a small difference of temperature, the higher the α is, the larger the variation of the relative resistance is. The coefficient can be then compared to other materials used for highly sensitive thermometry. Coefficients at 300 K as high as 0.02 (see Table 1) have been obtained which is significantly higher than the typical 0.01 value related to regular NbN thin films, a common thermometer used for sensitive thermal measurements [7,9]. Moreover, in the 77–300 K range, α values of the present a-C:B (8%) film are

Table 1
Summary of the electrical characteristics of pure and boron-doped DLC thin films as compared to regular room temperature NbN thermometer [9]

Sample	Doping	R_{77K} (MΩ)	R_{300K} (kΩ)	ρ_{300K} (Ω cm)	R^{300K}_{square} (kΩ m^{-1})	α_{300K}(K^{-1}))
AS16	0%	X	1250	100	5100	0.02
AS36	2%	6.64	26.67	2.13	106.67	0.01
AS39	4%	6.79	12.93	1.3	51.72	0.004
AS49	8%	5.32	57.74	4.61	230.96	0.012
NbN	X	0.009	0.308	0.025	1.23	0.01

R^{square}_{300K} is the resistance per square and α_{300K} (K^{-1}) is the temperature coefficient as defined in the text, both calculated at 300 K.

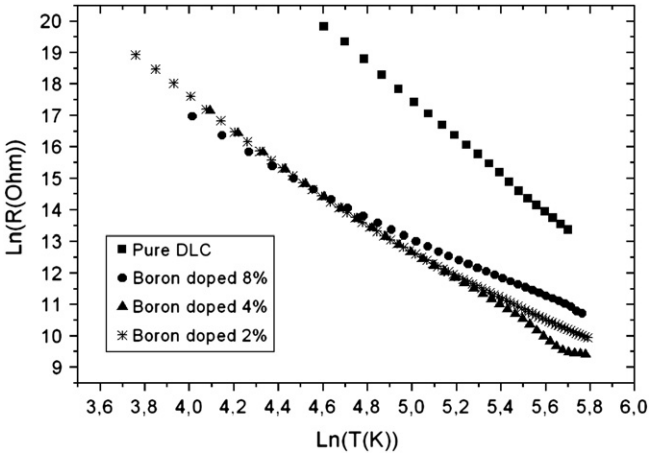

Fig. 3. Logarithm of the resistance vs. ln(T). A clear difference between pure and doped DLCs is illustrated.

Please cite this article in press as: A. Sikora et al., Structural and electrical characterization of boron-containing diamond-like carbon films deposited by femtosecond pulsed laser ablation, Solid State Sci. (2008), doi:10.1016/j.solidstatesciences.2008.07.013

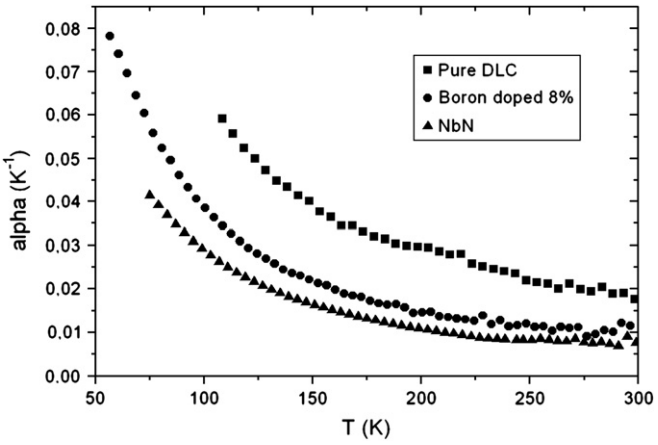

Fig. 4. Temperature coefficient of the resistance for pure DLC and 8% doped DLC as compared to highly nitrogen doped niobium (NbN).

systematically higher than α values related to NbN, and this difference is more significant as the temperature decreases (see Fig. 4).

The use of different deposition parameters (fluence and pressure) for pure DLC leads to α coefficients up to 4%. These values become competitives as compared to YBaCuO or VO_x thin film thermometers [30]. Hence this opens up quite interesting thermometric applications for highly sensitive thermal measurement at room temperature in calorimetry or bolometry.

4. Conclusion

Femtosecond pulsed laser ablation is used to deposit pure boron, a-C and a-C:B (2–8%) films. Boron-doped DLC films are constituted by boron nanoparticles embedded in the carbonaceous matrix. According to the diameter of these boron clusters, their nanostructure is either amorphous or crystallized. Electrical measurements have allowed to characterize the resistance and temperature coefficient evolution of the films within the range 77–300 K. The boron doped and pure DLC films follow correctly the Mott VRH law with a power coefficient in the 0.25–0.35 range. This confirms a conduction mechanism based on hopping between localized state near the Fermi level. Further investigations are in progress to try to determine more precisely the film nanostructure. The goal is to go deeper in the relationships between the deposition process, the nature of the film and the promising electrical properties reported in this article.

Acknowledgements

The authors acknowledge E. André, P. Lachkar, P. Brosse-Maron and the electronic shop for significant technical helps, the Région Rhône-Alpes and the Agence Nationale de la Recherche (ANR Programme Blanc 2007) for financial support.

References

[1] J. Robertson, Mater. Sci. Eng. 37 (2002) 129.
[2] E. Staryga, G.W. Bak, Diamond Relat. Mater. 14 (2005) 23.
[3] C. Godet, J.-P. Kleider, J. Mater. Sci. Mater. Electron. 14 (2006) 413.
[4] P.N. Vishwakarma, S.V. Subramanyam, J. Appl. Phys. 100 (2006) 113702.
[5] R. Cabanel, J. Chaussy, J. Geneste, J. Mazuer, J.C. Villegier, Thin Solid Films 185 (1990) 145.
[6] F. Fominaya, T. Fournier, P. Gandit, J. Chaussy, Rev. Sci. Instrum. 68 (1997) 4191.
[7] O. Bourgeois, S. Skipetrov, F. Ong, J. Chaussy, Phys. Rev. Lett. 94 (2005) 057007.
[8] D.W. Denlinger, A.N. Abarra, K. Allen, P.W. Rooney, M.T. Messer, S.K. Watson, F. Hellman, Rev. Sci. Instrum. 65 (1994) 946.
[9] O. Bourgeois, E. Andre, C. Macovei, J. Chaussy, Rev. Sci. Instrum. 77 (2006) 126108.
[10] M. Chhowalla, Y. Yin, G.A. Amaratunga, D.R. McKenzie, T. Frauenheim, Appl. Phys. Lett. 69 (1996) 2344.
[11] S. Nekkanty, M.E. Walter, Surf. Coat. Technol. 183 (2004) 1.
[12] Z.Q. Ma, B.X. Liu, Sol. Energy Mater. Sol. Cells 69 (2001) 339.
[13] W. Kautek, S. Pentzien, A. Conradi, J. Krüger, K.W. Brzezinka, Appl. Surf. Sci. 106 (1996) 158.
[14] H.F. Cheng, F.Y. Chuang, C.H. Tsai, W.C. Wang, C.M. Huang, I.N. Lin, Appl. Surf. Sci. 142 (1999) 504.
[15] Y. Suda, Y. Suganuma, Y. Sakai, K. Suzuki, J. Tsujino, N. Homma, Appl. Surf. Sci. 197–198 (2002) 603.
[16] X. Tian, M. Rusop, Y. Hayashi, T. Soga, T. Jimbo, M. Umeno, Jpn. J. Appl. Phys. 41 (2002) L970.
[17] X.M. Tian, M. Rusop, Y. Hayashi, T. Soga, T. Jimbo, M. Umeno, Sol. Energy Mater. Sol. Cells 77 (2003) 105.
[18] F. Garrelie, A.S. Loir, C. Donnet, F. Rogemond, R. Le Harzic, M. Belin, E. Audouard, P. Laporte, Surf. Coat. Technol. 163–164 (2003) 306.
[19] F. Qian, V. Craciun, R.K. Singh, S.D. Dutta, P.P. Pronko, J. Appl. Phys. 86 (1999) 2281.
[20] A.S. Loir, F. Garrelie, C. Donnet, M. Belin, B. Forest, F. Rogemond, P. Laporte, Thin Solid Films 453–454 (2004) 531.
[21] S. Eliezer, N. Eliaz, E. Grossman, D. Fisher, I. Gouzman, Z. Henis, S. Pecker, Y. Horovitz, M. Fraenkel, S. Maman, Y. Lereah, Phys. Rev. B 69 (2004) 144119.
[22] S. Amoruso, G. Ausanio, R. Bruzzese, M. Vitiello, X. Wang, Phys. Rev. B 71 (2005) 33406.
[23] N. Benchikh, F. Garrelie, C. Donnet, B. Bouchet-Fabre, K. Wolski, F. Rogemond, A.S. Loir, J.L. Subtil, Thin Solid Films 482 (2005) 287.
[24] N. Benchikh, F. Garrelie, K. Wolski, C. Donnet, R.Y. Fillit, F. Rogemond, J.L. Subtil, J.N. Rouzaud, J.Y. Laval, Thin Solid Films 494 (2006) 98.
[25] N. Benchikh, F. Garrelie, C. Donnet, K. Wolski, R.Y. Fillit, F. Rogemond, J.L. Subtil, J.N. Rouzaud, J.Y. Laval, Surf. Coat. Technol. 200 (2006) 6272.
[26] F. Garrelie, A.S. Loir, F. Goutaland, R. Le Harzic, B. Angleraud, Y. Ouerdane, P. Laporte, SPIE Proc. 4760 (2002) 301.
[27] P.A. Lee, T.V. Ramakrishnan, Rev. Mod. Phys. 52 (1985) 287.
[28] B. Kleinsorge, A. Ilie, M. Chhowalla, W. Fukarek, W.I. Milne, J. Robertson, Diamond Relat. Mater. 7 (1998) 472.
[29] N. Sbai-Benchikh, Thesis, University Saint-Etienne, 2004.
[30] P.C. Shan, Z. Celik-Butler, D.P. Butler, A. Jahanzeb, C.M. Travers, W. Kula, R. Sobolewski, J. Appl. Phys. 80 (1996) 7118.

Please cite this article in press as: A. Sikora et al., Structural and electrical characterization of boron-containing diamond-like carbon films deposited by femtosecond pulsed laser ablation, Solid State Sci. (2008), doi:10.1016/j.solidstatesciences.2008.07.013

Available online at www.sciencedirect.com
SCIENCE DIRECT®
ELSEVIER
Applied Surface Science 208–209 (2003) 553–560
applied surface science
www.elsevier.com/locate/apsusc

Study of plasma expansion induced by femtosecond pulsed laser ablation and deposition of diamond-like carbon films

A.-S. Loir[a,*], F. Garrelie[a], J.-L. Subtil[a], F. Goutaland[a], M. Belin[b], R. Le Harzic[a], C. Donnet[a], Y. Ouerdane[a], F. Rogemond[a], P. Laporte[a]

[a]*Laboratoire Traitement du Signal et Instrumentation, CNRS UMR 5516, Université Jean Monnet, 23 Rue du Docteur Paul Michelon, 42023 Saint-Etienne Cedex 02, France*
[b]*Laboratoire de Tribologie et Dynamique des Systèmes, CNRS UMR 5513, Ecole Centrale de Lyon, BP 163, 69134 Ecully Cedex, France*

Abstract

Diamond-like carbon (DLC) films were deposited in high vacuum conditions at room temperature, by ablating graphite targets with femtosecond laser pulses. The structure of the films deposited onto silicon substrates were characterized by Raman spectroscopy and X-ray absorption near edge spectroscopy (XANES). Films exhibit unusual structure, Raman spectra showing the presence of nanocrystalline diamond in amorphous matrix. Plasma plume was imaged by a gated ICCD camera in the UV-Visible range. The behavior of the plume shape as well as the kinetic energy of the particles are investigated. The behavior of the expansion dynamics of the plume and the properties of thin films are studied in order to determine the optimal growth conditions for femtosecond pulsed laser deposition of DLC films.

PACS: 81.15.Fg; 52.25.-b; 52.50.Jm; 61.10.Ht

Keywords: DLC; Pulsed laser deposition; Plasma

1. Introduction

For about 10 years, parallel to the numerous physical (PVD) and chemical (CVD) conventional vapor deposition techniques of thin films, pulsed laser deposition (PLD) has proven its efficiency as an alternative technique allowing the production of high quality films. A wide variety of materials is concerned, such as oxides, nanostructured materials or hard and wear resistant diamond-like carbon (DLC) coatings, for example. DLC films have widespread applications such as optical windows, storage disks, biomedical coatings or micro-electromechanical devices (MEMs). Such depositions were first achieved by ablating the bulk material using excimer or YAG lasers, with nanosecond pulse duration [1]. For a few years, higher intensity values have been reached on the ablated surface with femtosecond lasers. In this case, the kinetic energy of the ejected particles is increased up to a few keV, which is much higher than in the nanosecond regime, and original properties of the coatings could be related to such a high value. Some of us have recently published a paper on the tribological behavior of DLC films which we elaborate by ablating graphite targets

* Corresponding author. Tel.: +33-4-77-48-51-78; fax: +33-4-77-48-51-20.
E-mail address: anne.sophie.loir@univ-st-etienne.fr (A.-S. Loir).

0169-4332/02/$ – see front matter © 2002 Elsevier Science B.V. All rights reserved.
doi:10.1016/S0169-4332(02)01380-6

with femtosecond laser [2,3]. Although the nanosecond PLD has been largely investigated, there is little in the current literature on the properties of the femtosecond PLD films or plasma [4–10]. In the present work, attention is first paid to the plasma expansion, the dynamics of which are analyzed following the luminescence of the ionized or excited particles, then to the microstructure of the films in terms of sp^2 to sp^3 carbon hybridization ratio by X-ray absorption near edge spectroscopy (XANES), as much as in terms of their nanocrystalline or amorphous constitution using Raman spectroscopy.

2. Experimental set-up

Diamond-like carbon thin films were deposited onto silicon, at room temperature, by ablating high purity graphite target (99.997%). The femtosecond laser (Concerto, TCL) working at 800 nm, with an output energy per pulse of 1.5 mJ and a pulse duration of 150 fs at a repetition rate of 1 kHz, is focused with an incidence angle of 45° onto the target. Fluences studied in this paper are obtained by keeping constant the energy on the target surface and by changing the illuminated area size. Details of the experimental arrangement have been presented previously [2]. The dynamics of the expansion of the plasma plume induced by the laser irradiation of the target were studied. The velocities of the species reaching the surface of the substrate were determined through the images of the plume taken with an intensified charged-coupled device (ICCD) gated camera HAMAMATSU. The luminescence of the plume in the visible range (400–800 nm) and in the UV-Visible range (200–800 nm) was collected at various time delays after a single shot laser pulse. Several techniques were used to characterize the films as described in [2].

In order to access the structure of our films, we present here Raman characterizations and XANES spectra. The carbon hybridizations of the films were investigated by XANES performed at the Canadian Synchrotron Radiation Facility on the SGM beamline. The data were collected in the total electron yield mode by directly monitoring the sample current, and were normalized to the simultaneously recorded signal from a nickel mesh. The resolution is better than 0.2 eV at the carbon K-edge. Raman spectra were acquired in the visible region using the 488 or 514 nm line of an argon laser. A laser output power of 60 mW was used resulting in an incident power on the sample of about 5 mW. The spectra have been collected through a Jobin-Yvon U1000 spectrometer and a cooled photomultiplier. A retrodiffusion configuration was used to get the highest signal to noise ratio.

3. Results and discussion

3.1. Plasma plume investigations

In order to measure the kinetic energies of the ablated species, and to access the spatial distribution of these species, we studied the expansion of the femtosecond laser-induced plasma plume. The light emitted from the excited and ionized species was detected by an ICCD camera. This kind of experiment has been widely used in nanosecond laser ablation [11], whereas, only Garrelie et al. [3,12] and Perrière et al. [7] done the same for femtosecond laser ablation. Time of flight (TOF) measurements of ions have already been used to point out the two components of the ionic species of the plume created by femtosecond laser pulses [4–6].

Plume images were recorded for a single shot exposure at different laser fluences and at different delays after the beginning of the laser pulse. Moreover, the CCD camera integrates the emission over the whole spectra range of the objective lens. Due to the preferential emission of ionic species in the UV range [13], two different objective lenses were used, one transmitting only in the visible range (400–800 nm), and the second one transmitting also in the UV range (200–800 nm), but with lower transmission values.

Fig. 1 shows the plume images recorded at a delay of 400 ns after the laser pulse. Two laser fluences (2.82 and 5.16 J/cm^2) were investigated on the two different spectral ranges. One can note the different behavior of the plasma plume expansion with laser fluence. At this delay, and for these two fluence values, the emitted intensities differ strongly for the two investigated (UV or UV-Visible) ranges. For the higher fluence value, the emission occurs principally in the UV range (by comparison of Fig. 1c and d). As expected, due to the lack of excited species lines in the UV range, one can

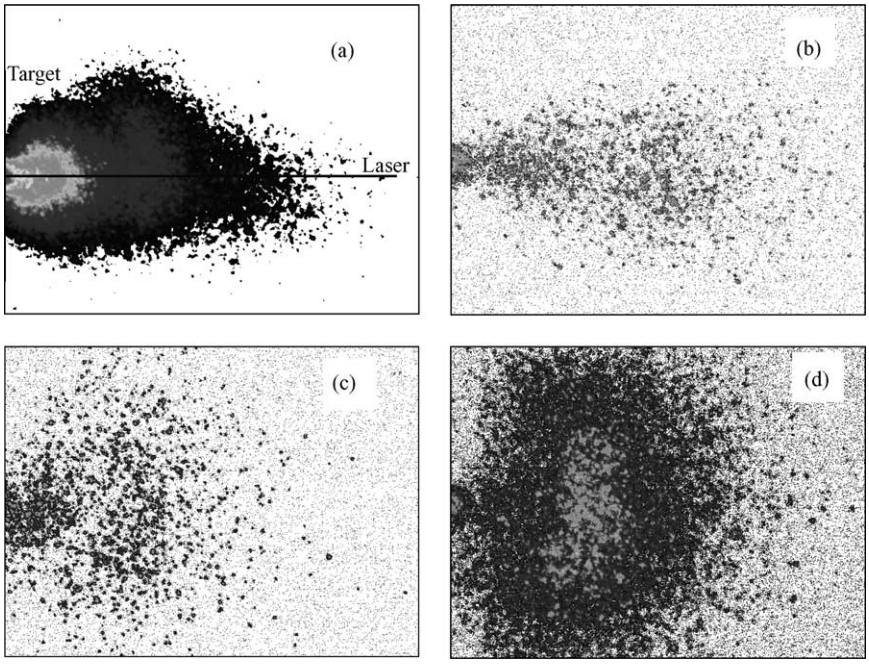

Fig. 1. Images of the plasma plume induced by femtosecond laser ablation of a graphite target, at a delay of 400 ns after the laser pulse (exposure time of 35 ns) for a laser fluence of 2.82 J/cm^2 (a and b) and 5.16 J/cm^2 (c and d) and from the emission in the visible range (a and c) and UV-Visible range (b and d). Size of each image: 5.6 cm × 4.2 cm.

conclude that the higher the fluence, the higher the ionization rate in the plume. When looking at shorter delays (not shown here) the emission occurs in the UV range for both fluences. Whatever the laser fluence value, the higher energy component of the plume seems to be related to ions. Quantitative detection of ions and neutrals in the plasma using spectrally resolved imaging will be the main interest.

In order to access quantitative informations on the plume dynamics, we report in Fig. 2, the velocities deduced from intensity measurements at different levels from the full scale intensity on the images. First, for large delays, practically constant velocities have been derived whatever the intensity threshold or the fluence. This behavior, already observed in nanosecond laser ablation looks like a ''collision-free'' expansion [14]. The half-width intensity front expands with a velocity which is 1.5 times as great as the maximum intensity emission, with no variation between the two fluences, leading to the conclusion that the structure of the plasma plume is similar in both cases. When looking at values obtained at the different fluences, one can observe that the velocities deduced for the lower fluence are greater than those deduced for the higher fluence. However, let us recall the poor transmission values of the objective and the possible influence of the laser spot size variation [10]. Then, some species of the plume may be undetected, leading to these surprising results. In the same way, Perrière et al. [7] do not observe the two components of the energetic distribution in their images, whereas, Qian et al. [4] pointed out a few years ago these two components for the ionic species. The kinetic energy distribution of emitting species was recorded at a delay of 400 ns after the laser pulse from intensity measurements at different distances from the target surface. These profiles are reported in Fig. 3 for the two laser fluences. One can clearly note the two peaks in the distribution obtained for the visible emission range at the lower fluence value. The energies of these two peaks are a few tens and a few hundreds of eV, respectively. A third energy component is ejected at large delays after the laser pulse [3]. The higher energy peak (∼150 eV) at this fluence may be correlated with the peak observed in the distribution at higher fluence. The investigation of these curves for

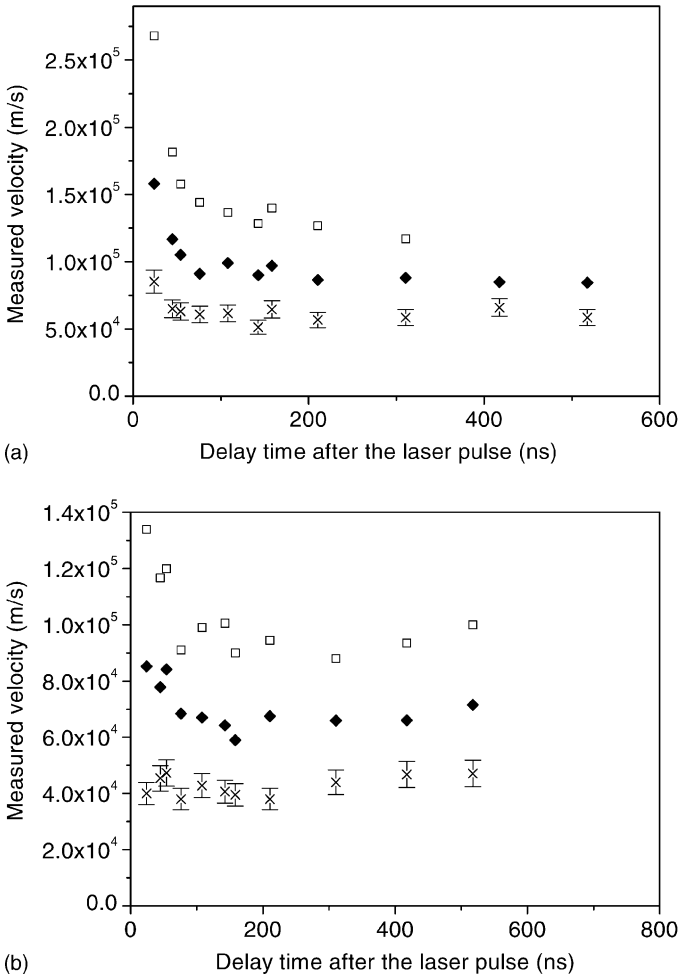

Fig. 2. Velocities of the emitted species (UV-Visible range) vs. expansion time for a laser fluence of 2.82 J/cm^2 (a) and 5.16 J/cm^2 (b) and for different intensity threshold: (×) maximum intensity; (◆) front with half-width intensity; (□) front at 10% of maximum intensity.

the two spectral ranges is the main interest and is in progress.

3.2. Thin film characterizations by Raman spectroscopy and XANES

The surface morphology of the DLC films deposited at different fluences, as well as, internal stress, mechanical properties and tribological behavior have been presented previously [2] and are recalled in Table 1. Raman and XANES spectroscopies are two complementary techniques for the investigation of the film structure and composition. Raman is widely used to obtain the detailed bonding structure of DLCs [15] whereas XANES allows to determine the carbon hybridization distribution with higher spectral energy resolution and less film degradation compared to electron energy loss spectroscopy (EELS) [16]. Figs. 4 and 5 show, respectively, the Raman and XANES spectra related to a selection of deposited films. In Fig. 4, related to the film deposited at a laser fluence of 2.82 J/cm^2(sample B), two broad bands are observed around 1340 and 1500 cm^{-1} along with a sharper peak located at 1140 cm^{-1}. The somewhat noisy structure of the whole spectrum is due to the low power density used in these experiments to avoid changes in the structure of the samples. The "D" and "G" bands, lying around 1340 and 1500 cm^{-1},

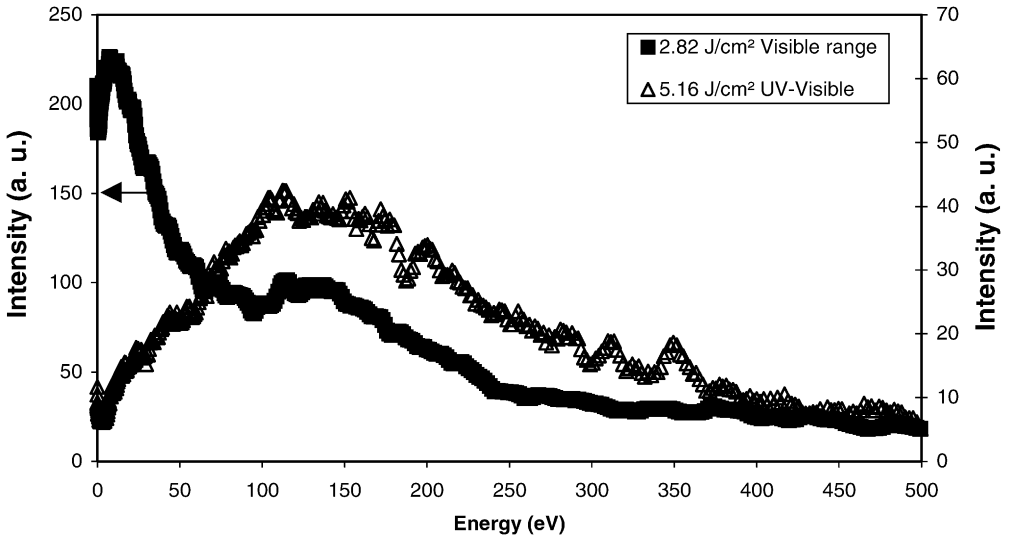

Fig. 3. Energy distributions of the emitted species at a delay of 400 ns after the laser pulse and for the two fluences (2.82 J/cm^2 in the visible range and 5.16 J/cm^2 in the UV-Visible range).

respectively, arise from graphitic sp^2 bonding in disordered carbon, as obtained in numerous works on DLC films deposited by nanosecond PLD [17]. The 1140 cm^{-1} Raman peak has been previously reported in carbon films deposited by various techniques, but its attribution is still controversial. Several authors have attributed this Raman vibration mode either to nanocrystalline diamond [18,19] or to hexagonal diamond crystallite within an amorphous matrix [20]. However, the shapes, widths and spectral positions of the Raman bands lying near 1140 cm^{-1} are different between the studies mentioned previously, rendering difficult direct comparison. Moreover, it has been recently suggested that this attribution may not be exact since the Raman shift does not remain constant when changing the laser excitation wavelength [21]. The authors argue that this peak is due rather to a transpolyacetylene segments fluorescence. However, the films described here are hydrogen-free and the 1150 cm^{-1} bandwidth reported is much larger than in the present case, which is more characteristic of a fluorescence band than of a Raman mode. To further rule out the possibility of a fluorescence process, a second Raman experiment was carried out with an excitation wavelength of 514.5 nm. The Raman spectrum obtained in this case revealed exactly the same structure as the spectrum obtained with an excitation at 488 nm, giving the evidence that the 1140 cm^{-1} band is due to a Raman scattering process. This Raman peak should thus be assigned in the present case to a nanocrystalline phase of diamond vibration mode. The Raman spectra related to the lower fluence (1.35 J/cm^2, sample A) and to the higher fluence (5.18 J/cm^2, sample C) both exhibit similar features. The XANES spectra corresponding to the transitions at the carbon K-edge are depicted in Fig. 5, as a function of the laser fluence. The spectra of graphite and synthetic diamond recorded in the same experimental conditions are also

Table 1
Characteristics and properties of the selected films

Sample	Fluence (J/cm^2)	Spot area ($\times 10^{-4}$ cm^2)	Thickness (nm)	sp^{3}content (%)	Hardness (GPa)	Young's modulus (GPa)	Residual stress (GPa)	Friction coefficient
A	1.35	2.51	250–300	71	20 ± 2.3	240 ± 29	−0.81	0.1–0.2
B	2.82	4.61	120–150	73	25 ± 2.5	260 ± 10	−1.85	0.1–0.2
C	5.18	9.63	85–95	70	18 ± 1.3	210 ± 13	−2.83	0.1–0.2

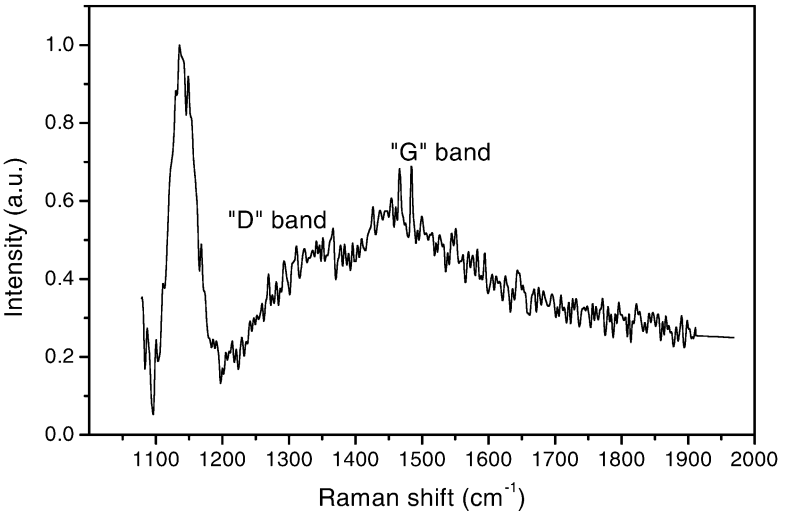

Fig. 4. Raman spectrum of the DLC film deposited at a laser fluence of 2.82 J/cm^2, showing the well-known "D" and "G" bands and a sharper peak located at 1140 cm^{-1}.

plotted in the same figure. The fine structure of the carbon K-edge, which appears to be a mixture of different features, was carefully investigated. The spectra exhibit five distinct contributions at 284.7, 286.4, 287.3, 288.4 and 289.4 eV, respectively, whatever the laser fluence. The peak at 284.7 eV can be attributed to the 1s $\rightarrow \pi^*$ transition, even if it appears slightly below the peak corresponding to this transition in graphite. Such a shift compared to the graphitic reference has already been observed by others [22]. The two consecutive peaks at higher photon energies can be also attributed to 1s $\rightarrow \pi^*$ transitions, described as excitonic

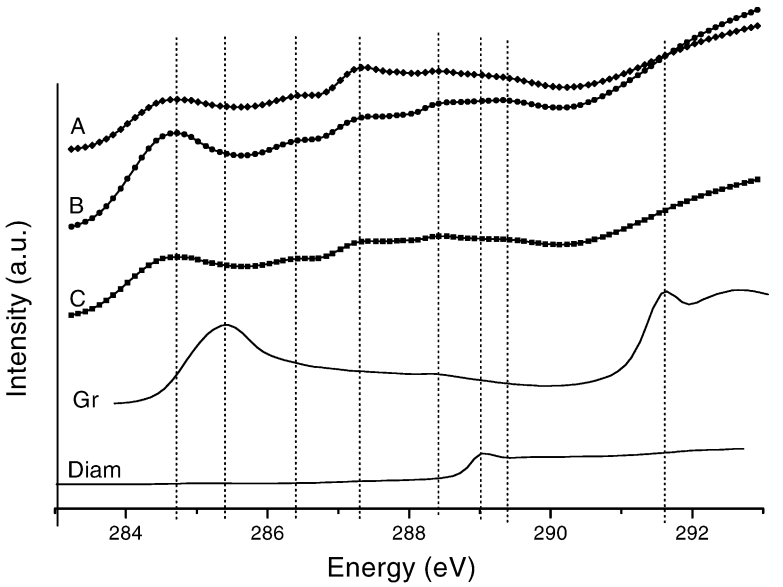

Fig. 5. C 1s K-edge XANES spectra of the DLC films deposited with a laser fluence of: (A) 1.35 J/cm^2; (B) 2.82 J/cm^2; (C) 5.18 J/cm^2. Reference spectra for graphite (Gr) and diamond (Diam).

resonances for films containing hydrogen [23] or other elements such as B or N [24,25]. However, these elements should not be present in our films and this point remains unclear. The somewhat complex feature which was observed may thus be attributed to a mixture of different forms of molecular structure in the femtosecond PLD films, without further accurate interpretation currently available. The two last peaks are very close to each other (less than 0.4 eV) of the $1s \rightarrow \sigma^*$ peak of synthetic diamond, whose absorption edge appears at 289.0 eV. A precise comparison between the three DLC samples indicates that the respective contribution of each peak depends very little on the laser fluence. An estimation of the $sp^3/(sp^2 + sp^3)$ ratio may be deduced from the spectra, according to the method proposed by Pappas et al. [26]. Results are depicted in Table 1. The films have a predominant sp^3 hybridization (70–73%) and the slight differences in the hybridization from one film to the other are not significant from our point of view. The rather high sp^3 content deduced from XANES experiments is consistent with the presence of a nanocrystallized diamond phase deduced from Raman investigations. Garrelie et al. [2] showed that these DLC films obtained by femtosecond PLD exhibit a promising tribological behavior, with friction coefficient in the 0.1–0.2 range over long sliding periods in ambient air, under high mechanical contact pressure (in the GPa range). A wear coefficient of 1.6×10^{-8} mm^3/(N m) of the DLC film deposited at 2.82 J/cm^2, when sliding against an uncoated steel ball, demonstrates a high wear resistance.

4. Conclusion

The plasma plume and some structural properties of DLC thin films deposited by a femtosecond PLD process have been investigated. The analysis of the dynamics of the emitted species of the plasma plume in UV and visible ranges shows the existence of three components with different behavior. Raman spectroscopy reveals a diamond nanocrystalline phase in an amorphous matrix, in agreement with a 70% sp^3 hybridization ratio deduced from XANES spectroscopy. Detailed investigations of the plasma plume are needed to determine the neutral and ion behavior in order to optimize the properties of DLC films for tribological applications in other words to control the deposition process. From the preliminary tribological tests, femtosecond PLD appears to be a promising technique to achieve high tribological performances on ta-C films.

Acknowledgements

The present study was supported by the Région Rhône-Alpes, the Conseil Général de la Loire (France) and the European Union (1997–1999 FEDER program). The authors acknowledge M. Kasrai (CSRF, Wisconsin-Madison) for XANES experiments.

References

[1] D.B. Chrisey, C.K. Hubler (Eds.), Pulsed Laser Deposition of Thin Films, Naval Research Laboratory, Washington, DC, 1994.
[2] F. Garrelie, A.-S. Loir, C. Donnet, F. Rogemond, R. Le Harzic, M. Belin, E. Audouard, P. Laporte, Surf. Coat. Technol. 163–164 (2003) 306.
[3] F. Garrelie, A.-S. Loir, F. Goutaland, C. Donnet, R. Le Harzic, B. Angleraud, Y. Ouerdane, P. Laporte, Diamond-like carbon deposited by femtosecond pulsed laser ablation: evidence of nanocrystalline diamond, SPIE Proc. 4760 (2002) 301.
[4] F. Qian, V. Craciun, R.K. Singh, S.D. Dutta, P.P. Pronko, J. Appl. Phys. 86 (1999) 2281.
[5] P.S. Banks, L. Dinh, B.C. Stuart, M.D. Feit, A.M. Komashko, A.M. Rubenchick, M.D. Perry, W. McLean, Appl. Phys. A 69 (1999) S347.
[6] S. Amoruso, X. Wang, C. Altucci, C. de Lisio, M. Armenante, R. Bruzzese, N. Spinelli, R. Velotta, Appl. Surf. Sci. 186 (2002) 358–363.
[7] J. Perrière, E. Millon, W. Seiler, C. Boulmer-Leborgne, V. Craciun, O. Albert, J.C. Loulergue, J. Etchepare, J. Appl. Phys. 91 (2) (2002) 690.
[8] M. Ye, C.P. Grigoropoulos, J. Appl. Phys. 89 (9) (2001) 5183.
[9] Z. Zhang, P. VanRompay, J.A. Nees, R. Clarke, X. Pan, P.P. Pronko, Appl. Surf. Sci. 154–155 (2000) 165.
[10] H. Köster, K. Mann, Appl. Surf. Sci. 109–110 (1997) 428.
[11] D.B. Geohegan, Appl. Phys. Lett. 62 (13) (1992) 1463.
[12] F. Garrelie, C. Jonin, E. Baubeau, E. Audouard, P. Laporte, A. Catherinot, C. Champeaux, Femtosecond Laser Ablation of Graphite: Study of the Plasma Plume and Thin Films Deposition, CLEO CFK5, 7–12 May 2000, 615.
[13] A.R. Striganov, N.S. Sventitskii, in: Tables of Spectral Lines of Neutral and Ionized Atoms, IFI/Plenum Press, New York, 1968.
[14] J.C.S. Kools, T.S. Baller, S.T. de Zwart, J. Dieleman, J Appl. Phys. 71 (9) (1992) 4547.
[15] A.C. Ferrari, Diamond Relat. Mater. 11 (2002) 1053.
[16] T.W. Capehart, T.A. Perry, C.B. Beetz, D.N. Belton, G.B. Fisher, C.E. Beall, B.N. Yates, J.W. Taylor, Appl. Phys. Lett. 55 (1989) 957.

[17] Q. Wei, J. Sankar, J. Narayan, Surf. Coat. Technol. 146–147 (2001) 250.
[18] J. Schwan, S. Ulrich, H. Roth, H. Ehrhardt, S.R.P. Silva, J. Robertson, R. Samlenski, R. Brenn, J. Appl. Phys. 79 (3) (1996) 1416.
[19] T. Sharda, T. Soga, T. Jimbo, M. Umeno, Diamond Relat. Mater. 10 (2001) 1592.
[20] S.R.P. Silva, G.A.J. Amaratunga, E.K.H. Salje, K.M. Knowles, J. Mater. Sci. 29 (1994) 4962.
[21] A.C. Ferrari, J. Robertson, Phys. Rev. B 63 (2001) 121405.
[22] S. Bhattacharyya, M. Lübbe, P.R. Bressler, D.R.T. Zahn, F. Richter, Diamond Relat. Mater. 11 (2002) 8.
[23] F.L. Coffman, R. Cao, P.A. Pianetta, S. Kapoor, M. Kelly, L.J. Terminello, Appl. Phys. Lett. 69 (4) (1996) 568.
[24] R. Gago, I. Jimenez, T. Sajavaara, E. Rauhala, J.M. Albella, Diamond Relat. Mater. 10 (2001) 1165.
[25] J.C. Sanchez-Lopez, C. Donnet, F. Lefèbvre, C. Fernandez-Ramos, A. Fernandez, J. Appl. Phys. 90 (2) (2001) 675.
[26] D.L. Pappas, K.L. Saenger, J. Bruley, W. Krakow, J.J. Cuomo, J. Appl. Phys. 71 (11) (1992) 5675.

Appl. Phys. A 90, 211–217 (2008)
DOI: 10.1007/s00339-007-4325-x

Applied Physics A
Materials Science & Processing

F. GARRELIE[1,✉]
N. BENCHIKH[1]
C. DONNET[1]
R.Y. FILLIT[2]
J.N. ROUZAUD[3]
J.Y. LAVAL[4]
A. PAILLERET[5]

One-step deposition of diamond-like carbon films containing self-assembled metallic nanoparticles, by femtosecond pulsed laser ablation

[1] Laboratoire Hubert Curien (ex-LTSI), UMR 5516, Université Jean Monnet, 18 rue Professeur Benoît Lauras, 42000 Saint-Etienne, France
[2] Ecole Nationale Supérieure des Mines de Saint-Etienne, Centre SMS – URA CNRS 5146, 158 cours Fauriel, 42023 Saint-Etienne Cedex 02, France
[3] Ecole Normale Supérieure de Paris, Laboratoire de Géologie, 24 rue Lhomond, 75231 Paris Cedex 05, France
[4] Laboratoire de Physique du Solide, UPR5 CNRS-ESPCI, 10 rue Vauquelin, 75231 Paris Cedex 05, France
[5] Université Pierre et Marie Curie Paris VI, Laboratoire Interfaces et Systèmes Electrochimiques, CNRS-UPR 15, Boite courrier 133, 4 place Jussieu, 75252 Paris Cedex 05, France

Received: 20 September 2007/Accepted: 1 October 2007
Published online: 13 November 2007 •

ABSTRACT Femtosecond pulsed laser ablation has been used for the deposition of various thin films by co-ablating pure graphite and pure metallic targets (nickel or tantalum) under vacuum conditions with an amplified Ti:sapphire laser working at 800 nm, with about 1.5 mJ per pulse at a repetition rate of 1 kHz. The plasma plume created during the femtosecond pulsed laser deposition process has been investigated, by fast imaging and spectroscopic characterizations, depending on the ablated target and deposition conditions. Particular attention has been paid to the correlation between the film nanostructure and the plasma plume properties, in terms of ejected species and energies of impinging species on the substrate. The tantalum clusters in the tantalum-doped carbon films appear under two crystalline phases: a stable phase (α-Ta) corresponding to that of the target, and a metastable phase (β-Ta), already observed at high temperatures. The presence of this metastable phase (β-Ta) is correlated to the temperature of the clusters measured from the plasma plume investigation.

PACS 81.15.Fg; 81.07.Bc; 68.55.-a

1 Introduction

Diamond-like carbon (DLC) films are widely used in many applications, mainly in mechanical devices in high-loaded contacts, due to their excellent tribological behavior [1]. However, the extended use of DLC in various other applications, including sensors, electrodes, field-emission devices, magnetic films or optical components, require us to tailor the physical properties of the films to meet the design requirements. The incorporation of heteroatoms (labeled 'X') in the carbonaceous network may significantly extend most of the physical properties of DLC films, by forming new architectures of a-C:X films, including nanocomposite or multilayered structures [2]. Moreover, in the future, some applications will need a combination of dedicated physical properties with high wear resistance and/or low friction, such as in electrical contacts. Consequently, the use of a-C:X films is expected to further increase in coming years. Among the different processes used to deposit a-C:X films, pulsed laser deposition (PLD) offers paramount advantages, including the possibility to deposit at room temperature hydrogen-free DLC films (a-C) with a high Csp^3 hybridization [3, 4], and the ability to control accurately the elemental composition of the a-C:X films over wide concentration ranges of various heteroatoms [5–13]. Most of these works have been performed by using nanosecond excimer lasers. Femtosecond lasers challenge excimer lasers for high quality thin film preparation and high-precision micromachining. The ultrashort pulse duration (in the 10^2 fs range) makes it possible to achieve higher laser power density (up to 10^{15} W cm^{-2}) without any interaction between the laser pulse and the plasma plume, in comparison to nanosecond lasers. The nature and energy distribution of the species in the femtosecond plasma plume are thus significantly different than in a nanosecond plasma plume, with consequences on the properties of the deposited films. Ultra-short laser pulses can significantly reduce the extent of heat diffusion into the target, leading to extreme conditions of temperature and pressure in the irradiated areas [14, 15]. The kinetic energy of the fastest ejected species can be increased up to a few keV [16], which is responsible for an adhesion increase of the film on various substrates [17]. The subsequent relaxation of the heated zone results in the ablation of the target surface through various mechanisms, including phase explosion [18] or explosive melting [19], with the formation of clusters and nanoparticles identified by mass spectrometry analyses and fast imaging of the plasma plume [20, 21]. This leads to the formation of self-assembled nanostructured films with grain sizes in the nanometer scale and properties significantly different from nanosecond PLD films [22–28]. Moreover, femtosecond lasers allow deposition of films which exhibit fewer droplets, compared to nanosecond PLD, as already investigated for DLC [29–34]. These results considerably widen the potentialities of PLD

✉ Fax: +33-4-77-91-57-81, E-mail: garrelie@univ-st-etienne.fr

to deposit nanocomposite or nanolayered coatings with complex compositions. As far as DLC films are concerned, by combining carbon and metal co-ablation, specific a-C:X compositions with metallic nano-inclusions in the carbonaceous network may be achieved in a controlled and reproducible way, over wide ranges of X concentrations. The present contribution highlights the nanostructure of such films, combined with plasma plume investigations in terms of temperature and kinetic energy of the ablated species. Two metals have been selected, nickel (Ni) and tantalum (Ta), taking into account respectively their low and high chemical affinity with respect to carbon. A designed one-step deposition procedure allowing alternative co-ablation of both elements has been carried out. Metallic concentrations ranging from less than 1% (doping) up to 15% (alloying) have been explored. The nanocomposite films have been investigated by surface analysis including Rutherford backscattering spectroscopy (RBS), field emission gun secondary electron microscopy (FEG-SEM), atomic force microscopy (AFM), grazing incidence angle X-ray diffraction (GIXRD) and high-resolution transmission electron microscopy (HRTEM). The nature of the emitting species and the kinetic energy of the particles in the plasma plumes have been investigated by temporally resolved emission spectroscopy and fast imaging. The objective is to correlate the composite film nanostructure with the femtosecond laser deposition process. We present in this paper a synthesis of our investigations, based on preliminary results partially published in previous papers [35–37].

2 Experimental

a-C:X films (X = Ni or Ta) have been deposited by ablating alternatively a target of graphite (purity 99.997%) and a target of the selected metal (purity 99.9%). The principle of this co-deposition consists in focusing alternatively, by using a computer-assisted mechanical shutter, the femtosecond laser beam in high-vacuum conditions (10^{-5} Pa) onto the targets. The coated substrate is located in front of the target surface at a distance of about 4 cm. The femtosecond laser is a Concerto (BMI/TCL), with a wavelength of 800 nm, a pulse duration of 150 fs, a repetition rate of 1 kHz and an energy per pulse of 1.5 mJ. Deposition has been performed at room temperature. The laser has been focused with an incident angle of 45° on the targets, with an energy density of 2.6 J cm^{-2} (±20%). This value of energy density is in the medium range experimentally available with the equipment at hand (1–5 J cm^{-2}). Previous pure DLC films have been optimized in these conditions [17, 33, 34]. The deposition rate of each pure element is 22 and 35 nm mn^{-1}, respectively, for carbon and metal (no measurable difference between Ni and Ta). Table 1 summarizes the deposition parameters, which may be adjusted to achieve a design thickness Z nm and a design composition [Ni] at.% or [Ta] at.% in the a-C:Ni or a-C:Ta films. These film specifications depend on both the numbers N_C and N_{Me} of alternative ablation sequences on each target, with the ablation times respectively τ_C and τ_{Me}. The duration of ablation of the metal target has been systematically fixed at $\tau_{Me} = 1$ s per ablation sequence, so that the stoichiometry of the doped/alloyed film has been achieved by adjusting τ_C. Note that there is no interaction between the carbon and metal plasma plumes, which expand alternatively towards the substrate. The first and last deposited element is systematically carbon. Such a high number of alternative short sequences is favorable to the formation of a nanocomposite structure. But, this setup may also be performed with a lower number of alternative longer sequences, to achieve a multilayered structure.

The spatio-temporal behavior of the plasma plume created by the ablation of the graphite or metallic targets has been investigated by using a fast shuttered intensified CCD camera (5 ns exposure time). The electronic device of the acquisition setup has been synchronized with the laser pulse with the use of an independent electronic device tailoring both the femtosecond laser and the acquisition setup. This spatially and temporally resolved imaging of the laser-induced plasma plume has been completed by temporally resolved emission spectroscopy. These measurements allow us to access the nature of the emitting species and the kinetic energy of the particles, which is correlated to the quality of the films.

The film surface has been observed by using a scanning electron microscope equipped with a field-emission gun (FEG-SEM, Jeol 6500F). The size distribution of the particles in the film has been quantified by an analysis soft imaging system (ANALYSIS 833, ENSMSE). AFM imaging experiments were carried out in the contact mode in air by using AFM equipment from Molecular Imaging. For this imaging purpose, silicon nitride triangular cantilevers bearing pyramidal silicon nitride tips have been used. Their spring constant was 0.38 N m^{-1}. The scan rate used for all experiments was 0.4 Hz (or 8000 nm s^{-1}). All three-dimensional AFM images shown hereafter are topography images that underwent a plane correction process. For GIXRD measurements, different incident angles have been used in order to adjust the X-ray penetration depth to the particle size and the layer thickness. We have used a D5000 goniometer link together with a XP18 rotating anode and the Dosophatex system. Cu K_α copper radiation was used. HRTEM has been carried out on a Jeol 2010 microscope equipped with a field-emission gun and operating at 200 kV. The resolution in the lattice fringe mode is 0.11 nm. Local elemental analysis has been performed thanks to a PGT energy-selective X-ray analyzer allowing in situ analysis on volumes smaller than 100 nm^3, with a precision of 0.1%. For HRTEM observations, coatings have been directly deposited on a classical TEM copper grid (diameter 3 mm), previously covered by a holey amorphous carbon film. Examination of

	a-C:Me (2 at. %)	a-C:Me (15 at. %)
Number of carbon ablation sequences, N_C	31	241
Number of metal ablation sequences, N_{Me}	30	240
Duration of each carbon ablation sequence, τ_C (s)	89	9
Duration of each metal ablation sequence, τ_{Me} (s)	1	1

TABLE 1 Ablation sequences for the deposition of doped/alloyed DLC films (thickness of 1 μm) with two typical concentrations of incorporated metal (Ni or Ta), at a laser energy density of 2.6 J cm^{-2}

the sample was focused on parts of the sample lying across the holes to obtain information free of the contribution of the supporting carbon film. These films have also been examined by electron energy loss spectroscopy (EELS) in a LEO 912 energy-filtered transmission electron microscope (EFTEM) at 120 kV.

3 Results and discussion

The femtosecond laser ablation of pure Ni and Ta films has been first investigated. FEG-SEM observations (Fig. 1) clearly show the surface morphology of the films constituted by a stacking of clusters, whatever the nature of the metal. The average size of the clusters is in the 50–150 nm range, with a distribution size ranging roughly from 20 to about 250 nm. The behavior of the plasma plume created above the nickel or tantalum targets by femtosecond laser ablation has been examined by fast imaging of the plume recorded at different delays after the laser pulse (Fig. 2). The atomic mass of the metal target has a strong influence on the expansion behavior, as expected due to kinetic energy conservation with respect to atomic mass. As observed in many papers [23, 26, 38], two plume components characterized by different expansion velocities are observed (not shown here). The nature of the species present in the plasma plume during the femtosecond laser ablation of the metal target has been investigated by spectroscopic emission measurements. The spectrum recorded at a delay of 1 μs after the ablation of the pure tantalum target is reported in Fig. 3. The emission is characterized by a continuum spectrum which is attributed to the slower component of the plume, i.e. hot nanoparticles [21, 38]. This continuum spectrum can be compared to a black-body emission spectrum. The nanoparticle temperature is deduced from the wavelength of the maximum emission using the formula

$$T \approx \frac{1}{1.2}\frac{\beta}{\lambda_{\max}}, \tag{1}$$

where β is a constant [38].

The morphology of the films deduced from FEG-SEM observations can thus be correlated to the investigation of the plasma plume, as the morphology of the films reveals an average size in the nanometer range. A temperature of the nanoparticles of about 4000 K is deduced from these measurements. These results give strong evidence that the nanoparticles identified by FEG-SEM in the film are pre-existing in the femtosecond laser plasma plume.

When looking at the influence of the laser intensity on the characteristic size of the nanoparticles, very similar sizes and size distributions are observed (Fig. 4). As deduced from the plasma plume expansion behavior, no major difference in the expansion velocities is observed. The shape of the plume appears to be modified by an increase of the laser fluence (Fig. 2). This has already been observed for many materials [33, 39], as well as, in our case, a higher laser fluence being obtained by focusing the laser beam with a constant energy per pulse, thus leading to a modification of the gradients in the initial stages of the plume expansion. However, when looking at the influence of the laser intensity on the characteristic size of the films, no noticeable influence is noted in the available range. Generally, a slight increase in the nanoparticle size is expected with increasing laser fluence [26].

A study of pure DLC films in the same experimental configuration has been published elsewhere [33, 34, 39]. These films are amorphous, as investigated by HRTEM. The Csp^3 content is about 70%, as deduced from X-ray absorption near

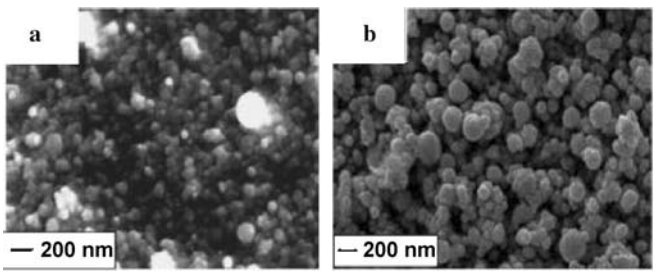

FIGURE 1 FEG-SEM images of pure Ni (**a**) and Ta (**b**) films deposited by femtosecond laser ablation at a laser fluence of 2.6 J cm^{-2}

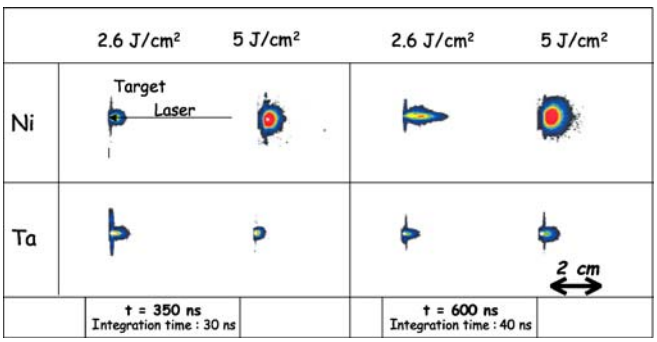

FIGURE 2 Plasma images recorded at different delays after femtosecond laser ablation of pure nickel and tantalum targets at laser fluences of 2.6 J cm^{-2} and 5 J cm^{-2}

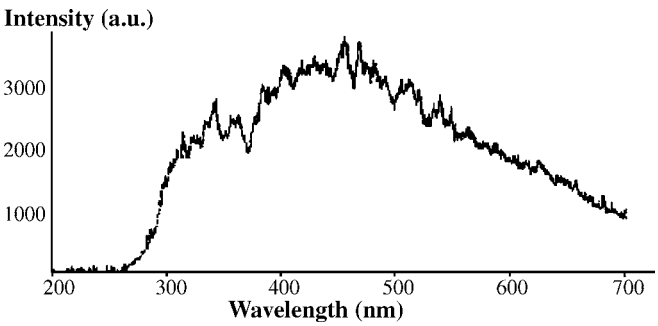

FIGURE 3 Emission spectroscopy spectrum of the tantalum plasma created under femtosecond ablation of a pure tantalum target, recorded at a delay of 1 μs after the laser pulse

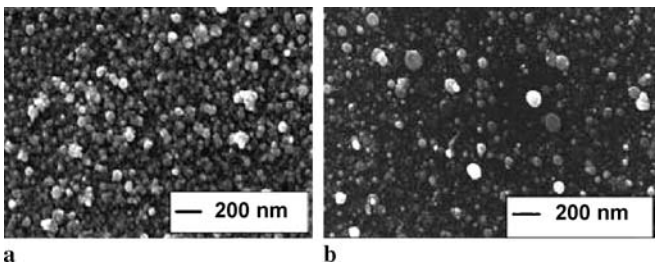

FIGURE 4 FEG-SEM images of pure tantalum films deposited by femtosecond laser ablation at fluences of 1.5 J cm^{-2} (**a**) and 3.7 J cm^{-2} (**b**)

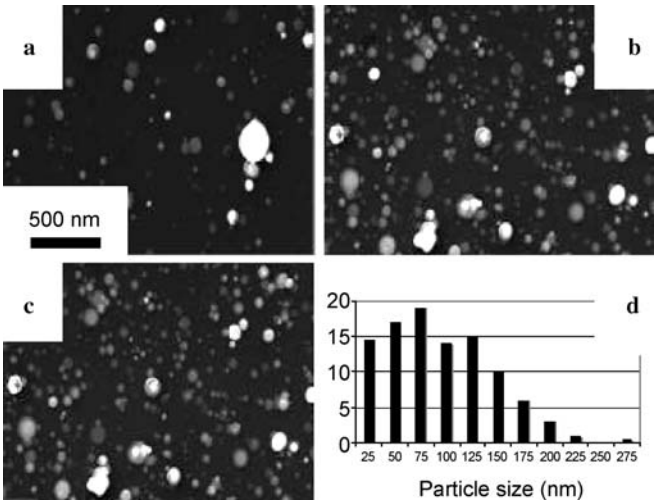

FIGURE 5 FEG-SEM surface images of the a-C:Ta films deposited by femtosecond laser ablation (2.6 J cm^{-2}) with atomic metal concentrations of (**a**) 2%, (**b**) 5% and (**c**) 15%. (**d**) Size distribution of the surface nanoparticles related to (**c**)

edge spectroscopy (XANES), without any significant effect of the laser fluence within the range 1.5–5.2 J cm^{-2}. High-density bulk materials have been obtained, as revealed by spectroscopic ellipsometry [28], with a few-nm-thick sp^2-rich top layer which is denser and thicker in femtosecond PLD than in nanosecond PLD. The plume expansion, in terms of kinetic energies of the emitting species, can be correlated to the structure of the films deposited in both pulse-duration regimes. The high kinetic energy of the fastest carbon species leads to a material densification [25, 39] and sp^3 to sp^2 configuration relaxation, as predicted by the subplantation model [40].

By performing co-ablation of C and Ni (or Ta) as described in Sect. 2, nanocomposite a-C:Me films have been deposited at a fluence of 2.6 J cm^{-2}. FEG-SEM observations (Fig. 5, related to a-C:Ta) show evidence of the nanostructure of the film surface. A quantification of the size distribution of the nanoparticles present in the film is deduced from image analysis. A wide size distribution is observed between 20 nm and 250 nm whatever the metal incorporated. The average size of the nanoparticles contained in the tantalum-doped film is about 80 nm, with a standard deviation of 50 nm, as deduced from Fig. 5d related to the a-C:Ta film containing 15 at. % of tantalum. The average size of the nanoparticles contained in the nickel-doped film is about 60 nm, with a standard deviation of 40 nm. Due to the morphology obtained respectively for pure metallic films and pure diamond-like-carbon films, nanoparticles contained in the nanocomposite a-C:Me films seem to be composed of metallic elements, as we will demonstrate later by EFTEM and HRTEM experiments. From the results obtained in the case of pure metallic films, the size of the nanoparticles shows no clear dependence on the concentration of metal, suggesting no noticeable coalescence between the nanoparticles on the surface.

Atomic force microscopy analyses performed in the contact mode in air on those films (Fig. 6) allowed us to observe first a roughness in a-C:Me films that is more important than in pure DLC films. Indeed, the RMS was about 2 nm only for these latter films (images not shown) while it is higher

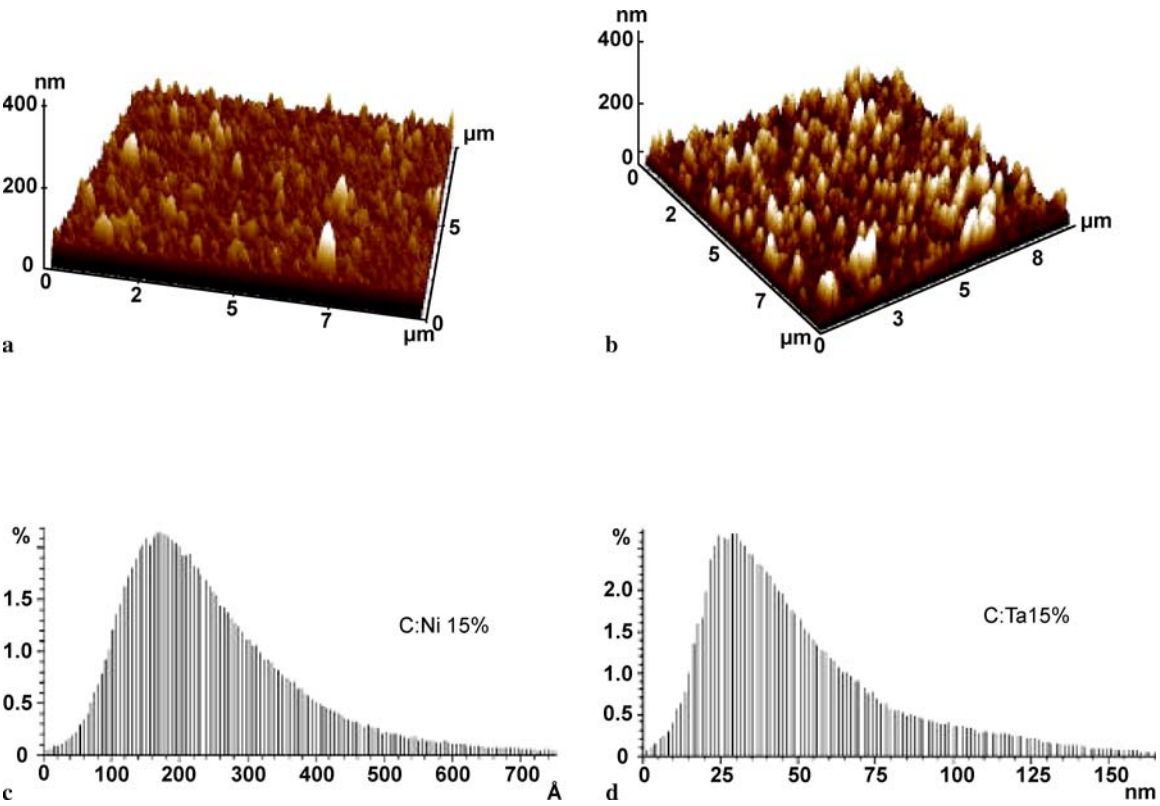

FIGURE 6 Three-dimensional AFM topography images obtained in the contact mode in air for films doped with (**a**) nickel 15 at. %, (**b**) tantalum 15 at. %. The corresponding height histograms are shown respectively in (**c**) and (**d**)

than 16 nm for the a-C:Ni or a-C:Ta films. It thus appears that the presence of the metallic clusters strongly influences the roughness of the a-C:Me films. In the case of a-C:Ni films, AFM studies also showed that the RMS was weakly influenced by the nickel content (RMS for C:Ni 2% = 28.7 nm, figure not shown, RMS for C:Ni 15% = 30.2 nm, see the corresponding image and histogram in Fig. 6a and c, respectively), whereas in the case of a-C:Ta films the roughness strongly increases with the tantalum content (RMS for C:Ta 2% = 16.7 nm, figure not shown, RMS for C:Ta 15% = 60.9 nm, see the corresponding image and histogram in Fig. 6b and d, respectively). From the comparison of these RMS data, one can also deduce that, at 15 at. % of metals, a-C:Ta films are rougher than C:Ni films. The AFM topography images can also give information about the height of the metallic clusters only on the condition that vertical profiles taken from these pictures are considered. Thus, by choosing the vertical profiles crossing the highest metallic nodules observed in our AFM images, one can define the height range described by all these nodules for each of the samples investigated. In all cases, the smallest nodules were found to have a height that makes them hardly visible by comparison with the initial roughness of the carbonaceous matrix. The maximum height of the metallic clusters characterized in our AFM images is about 186 nm for a-C:Ni 2 at. %, 181 nm for a-C:Ni 15 at. %, 121 nm for a-C:Ta 2 at. % and 210 nm for a-C:Ta 15 at. %. It thus appears that those height measurements using AFM are coherent with the morphological observations and the width measurements using SEM/FEG and reported above if we admit that the particles are approximately spherical. This assumption appears justified for particle sizes in the range of a hundred nanometers (or more), whereas a shape anisotropy has been observed by Ausanio et al. [41] for significantly smaller nickel nanoparticles. Indeed, as evidenced using SEM/FEG, a-C:Ni films present a smaller width distribution of clusters (62 nm) than a-C:Ta films (average size of tantalum clusters = 80 nm) leading to a different surface quality, smoother when nickel is incorporated.

From the deposition of the pure metal films and pure carbon films described previously, the a-C:Me films deposited by the sequential co-ablation process are undoubtedly constituted by metallic inclusions dispersed in the carbonaceous matrix. This assumption has been confirmed by EFTEM and HRTEM experiments. Figure 7 shows a cross-sectional view of an a-C:Ni film (15 at. % Ni), confirming, through a transmission view, the nanostructure of the film. The zero-loss

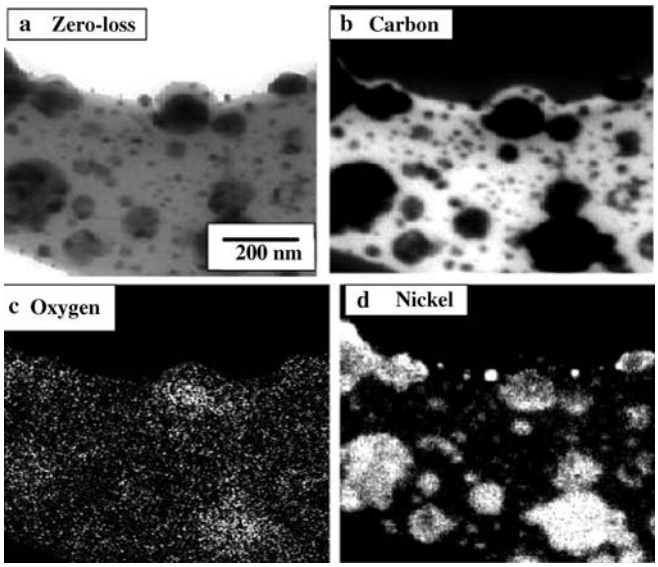

FIGURE 7 Energy-filtered TEM images of (**a**) zero-loss, (**b**) carbon, (**c**) oxygen and (**d**) nickel related to the a-C:Ni film. Carbon, oxygen and nickel are identified by the *bright areas* respectively in (**b**)–(**d**)

image (Fig. 7a) of a 100-nm-thick coating highlights the morphology of the films, consisting of dark nodules dispersed in a brighter matrix. The C 1*s* and O 1*s* images (Fig. 7b and c, respectively) clearly indicate that the a-C:Ni film is constituted by nanometer-scale nickel nodules (Fig. 7d) dispersed in the carbonaceous matrix. These nodules do not contain detectable carbon. Some traces of oxygen (not quantified) have been identified also in the carbonaceous matrix, probably due to water-vapor contamination during the deposition process. The same feature has been observed in the a-C:Ta films [36], but with tantalum nodules surrounded by a thin carbonaceous layer (less than 10-nm thick), as depicted from the observation of nodules located on the edge of a hole of the film (Fig. 8). This carbon layer, depicted in Fig. 8b, may result from the strong chemical affinity of tantalum with respect to carbon. The tantalum image has not been recorded due to its high electron core level energy unachievable with the equipment at hand.

In order to go further in the investigation of the crystalline structure, the a-C:Ta and a-C:Ni films with a metal concentration of 15 at. % (100-nm thick) were analyzed by GIXRD. In the case of the a-C:Ni film (spectrum not shown), only the contribution corresponding to the metallic fcc nickel phase,

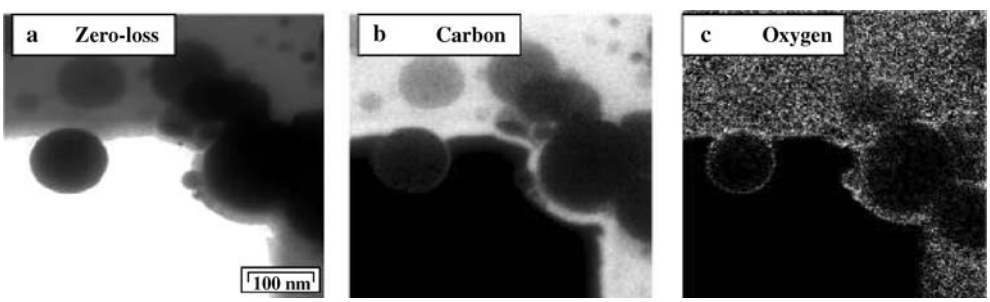

FIGURE 8 Energy-filtered TEM images of (**a**) zero-loss, (**b**) carbon and (**c**) oxygen related to the a-C:Ta film. Carbon and oxygen are identified by the *bright areas* respectively in (**b**) and (**c**). The tantalum image has not been recorded due to its high electron core level energy unachievable with the equipment at hand

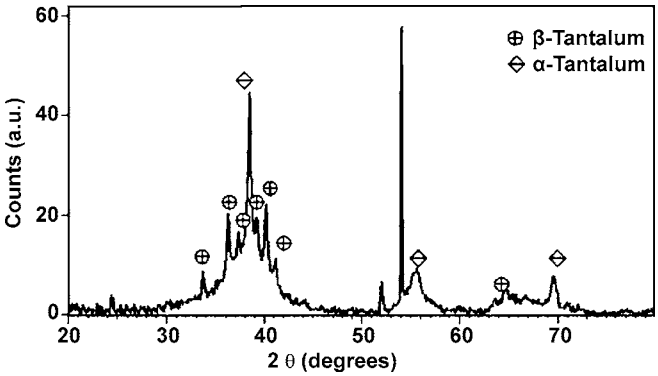

FIGURE 9 GIXRD spectrum related to the a-C:Ta (15 at. %) film deposited by femtosecond laser ablation, at a fluence of 2.6 J cm^{-2}

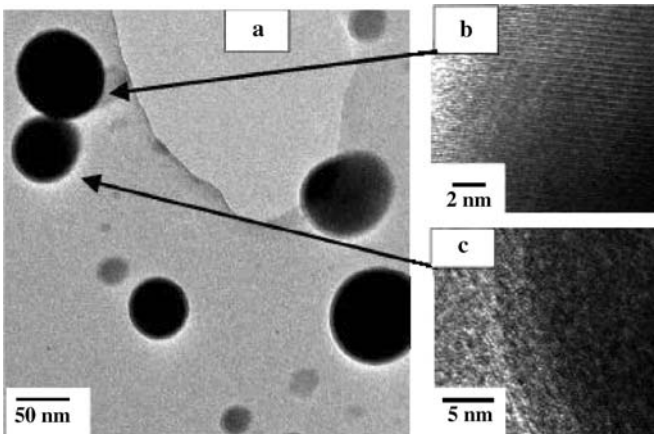

FIGURE 10 (**a**) Transmission electron microscopy image of the a-C:Ta film (15 at. %). High-resolution images of (**b**) black nodules and (**c**) dark grey nodules

which is the stable phase of nickel in normal pressure and temperature conditions, is considered. In the case of the a-C:Ta film (Fig. 9), we identify three main contributions corresponding to the different phases present in the film:

- a centered cubic tantalum phase (α-Ta), which is the stable phase in normal pressure and temperature conditions. The tantalum target used for deposition is α-Ta;
- a metastable phase, corresponding to metallic tetragonal tantalum (β-Ta), which has been observed at high temperatures ($> 800\,^{\circ}$C) [42];
- probably an amorphous phase whose signal corresponds to the bump centered on the most intense peak of the stable phase ($2\theta = 38^{\circ}$).

The full width at half maximum (FWHM) of the first two crystalline phases identified above are consistent with nodule sizes in the range of 100 nm. The wide signal related to the third phase is consistent with nodule sizes of less than 10 nm. From the analysis of the continuum spectrum of the tantalum plasma (Fig. 3), a nanoparticle temperature of about 4000 K has been estimated. This temperature is much higher than the required temperature for the formation of metallic tetragonal tantalum (β-Ta), 800 °C. We can then conclude that tantalum nanoparticles may have suffered an allotropic transformation during their trip in the plasma plume towards the substrate.

Due to the various phases observed by GIXRD, a more detailed investigation of the a-C:Ta film has been achieved by HRTEM. In order to observe the a-C:Ta film by transmission in the high-resolution mode, one sequence of 9 s for carbon ablation followed by one sequence of 1 s for tantalum ablation have been carried out to limit the thickness of the film. The combination of both sequences corresponds to a theoretical film thickness of 4 nm, taking into account the ablation rates of C and Ta (see Sect. 2). Since the distribution of Ta in the deposited film is not homogeneous due to the formation of nodules, the size of the nodules is significantly higher than the theoretical thickness of 4 nm. A characteristic $0.3 \times 0.3\ \mu m^2$ portion of the sample is imaged in Fig. 10a. The particle size varies from about 10 nm (small grey particles) up about 100 nm (large black particles). All these particles are spheroidal as proved by their constant circular shape in the image, when the sample is tilted by $\pm 20^{\circ}$ according to the incident electron beam. From their contrast point of view, three types of particles can be recognized: large black particles which represent the major component of the sample, large dark grey ones and small light grey ones (which are only a minor phase). In situ punctual elemental analyses by electron-dispersive spectroscopy (EDS) mode and high-resolution TEM imaging have been performed on the particles lying across the holes of the TEM holey grid, in order to avoid the contribution of the amorphous carbon supporting film. The three types of particles are essentially constituted by tantalum. Only the external part contains a higher amount of carbon, due to the smaller thickness and consequently the higher relative contribution of the carbon deposit due to the first carbon ablation. A crystalline structure is clearly visible in the dark particles (Fig. 10b), whereas the small light grey ones appear completely amorphous. The dark grey particles show an intermediate organization where only a short-range order can be imaged (Fig. 10c). In the case of aluminium nanoparticle synthesis by femtosecond PLD, Eliezer et al. [24] also observed, at least in some nanoparticles, both amorphous and nanocrystalline structures of Al.

From the combination of the previous investigations, we have observed that the present a-C:Me films (15 at. % of Ta or Ni) consist in a distribution of metallic nodules with diameters in the 10–250 nm range. Indeed, for most films, including metallic films, other than pure DLC, femtosecond PLD leads to nanostructured films with grain size in the nanometer scale and properties significantly different from nanosecond PLD films [22]. The nanostructure seems to originate from the drastic effects of the femtosecond laser–matter interaction, as phase explosion [18] or explosive melting [19]. Moreover, mass spectrometry analyses of the plasma plume [20] and plasma plume spectroscopic investigations [26] show the presence of clusters in the plume, which can be correlated to the nanostructure of the films. As the deposition technique is a non-equilibrium one, we have obtained, in the case of Ta incorporation, two crystalline phases (α-Ta and the metastable β-Ta), compared to only one present in the target (α-Ta). The metastable phase is only reported at high temperature (higher than 800 °C), leading to the conclusion that species in the plasma plume induced by femtosecond ablation reach temperatures higher than 800 °C. No metastable phase is observed in the case of nickel incorporation. In

both cases, the carbonaceous matrix of the film appears to be quite similar to the one obtained in pure a-C films deposited by the same procedure [39]. Further investigations are in progress to correlate the nature of the species in the plasma plume during the femtosecond laser ablation of the metal target and the nature of the metallic phases observed in the film.

4 Conclusion

This paper presents the effect of the incorporation of various metals (nickel and tantalum) in DLC films, as deposited by femtosecond pulsed laser ablation. As we have reported in our previous articles, femtosecond PLD is a versatile deposition process allowing us to synthesize metallic clusters from the ablation of metallic targets. These clusters are incorporated in an amorphous carbon-based matrix by sequential ablation of both the carbon and metal targets. Fast imaging of the plasma plume and emission spectroscopy measurements have been achieved in order to correlate the properties of the films with the main features of the plasma plume, such as the nature and the energy of the deposited species. The size distribution of the tantalum nanoparticles has been examined by FEG-SEM. The crystallinity of these nanoparticles has been investigated by grazing incidence X-ray diffraction. These tantalum clusters appear under three distinct phases: the first crystalline phase (α-Ta) is the stable phase and corresponds to that of the target, the second crystalline phase is a metastable phase (β-Ta) and has been observed at high temperatures, and a third component, corresponding to the smallest clusters, is an amorphous phase. The presence of this metastable phase (β-Ta) has been correlated to the temperature of the clusters measured from the plasma plume investigation. In conclusion, sequential femtosecond pulsed laser ablation of carbon and metal leads to specific carbon/metal nanocomposite films, with potentially interesting functional properties. A possible way to achieve higher quality of the films would be to control and design the laser pulse, such as by a temporal shaping, in order to produce the required species or kinetic energy of the species necessary to a particular phase growth. In the future, the integration of such films may be considered in various systems, such as amperometric or calorimetric sensors, for example.

REFERENCES

1 A. Erdemir, C. Donnet, in *Wear: Materials, Mechanisms and Practices*, ed. by G. Stachowiak (Wiley, New York, 2006), pp. 191–222
2 J. Robertson, Mater. Sci. Eng. R **37**, 129 (2002)
3 D.B. Chrisey, C.K. Hubler (eds.), *Pulsed Laser Deposition of Thin Films* (Naval Research Laboratory, Washington, DC, 1994)
4 A.A. Voevodin, M.S. Donley, Surf. Coat. Technol. **82**, 199 (1996)
5 Q. Wei, R.J. Narayan, J. Narayan, J. Sankar, A.K. Sharma, Mater. Sci. Eng. B **53**, 262 (1998)
6 S.M. Mominuzzaman, T. Soga, T. Jimbo, M. Umeno, Diam. Relat. Mater. **10**, 1839 (2001)
7 S. Zhu, C.H. Su, J.C. Cochrane, S. Lehoczky, I. Muntele, D. Ila, Diam. Relat. Mater. **10**, 1190 (2001)
8 S. Trusso, F. Barreca, F. Neri, J. Appl. Phys. **92**, 2485 (2002)
9 Y. Suda, Y. Suganuma, Y. Sakai, K. Suzuki, J. Tsujino, N. Homma, Appl. Surf. Sci. **197–198**, 603 (2002)
10 M. Morstein, P.R. Willmott, H. Spillmann, M. Döbeli, Appl. Phys. A **75**, 647 (2002)
11 P.R. Willmott, H. Spillmann, Appl. Surf. Sci. **197–198**, 432 (2002)
12 J.C. Orlianges, C. Champeaux, A. Catherinot, A. Pothier, P. Blondy, P. Abelard, B. Angleraud, Thin Solid Films **453–454**, 291 (2004)
13 R.J. Narayan, Diam. Relat. Mater. **14**, 1319 (2005)
14 B. Rethfeld, K. Sokolowski-Tinten, D. von der Linde, S.I. Anisimov, Appl. Phys. A **79**, 767 (2004)
15 L.V. Zhigilei, Appl. Phys. A **76**, 339 (2003)
16 P.A. VanRompay, M. Nantel, P.P. Pronko, Appl. Surf. Sci. **127–129**, 1023 (1998)
17 A.-S. Loir, F. Garrelie, C. Donnet, M. Belin, B. Forest, F. Rogemond, P. Laporte, Thin Solid Films **453–454**, 531 (2004)
18 A. Miotello, R. Kelly, Appl. Phys. A **69**, 67 (1999)
19 V.N. Tokarev, A.F.H. Kaplan, Lasers Eng. **7**, 295 (1998)
20 R. Teghil, L. D'Alessio, A. Santagata, M. Zaccagnino, D. Ferro, D.J. Sordelet, Appl. Surf. Sci. **210**, 307 (2003)
21 S. Amoruso, G. Ausanio, R. Bruzzese, L. Gragnaniello, L. Lanotte, M. Vitiello, X. Wang, Appl. Surf. Sci. **252**, 4863 (2006)
22 J. Perriere, E. Millon, W. Seiler, C. Boulmer-Leborgne, V. Craciun, O. Albert, J.C. Loulergue, J. Etchepare, J. Appl. Phys. **91**, 690 (2002)
23 O. Albert, S. Roger, Y. Glinec, J.C. Loulergue, J. Etchepare, C. Boulmer-Leborgne, J. Perriere, E. Millon, Appl. Phys. A **76**, 319 (2003)
24 S. Eliezer, N. Eliaz, E. Grossman, D. Fisher, I. Gouzman, Z. Henis, S. Pecker, Y. Horovitz, M. Fraenkel, S. Maman, Y. Lereah, Phys. Rev. B **69**, 144 119 (2004)
25 S. Amoruso, R. Bruzzese, N. Spinelli, R. Velotta, M. Vitiello, X. Wang, G. Ausanio, V. Iannotti, L. Lanotte, Appl. Phys. Lett. **84**, 4502 (2004)
26 S. Amoruso, G. Ausanio, R. Bruzzese, M. Vitiello, X. Wang, Phys. Rev. B **71**, 33 406 (2005)
27 S. Amoruso, G. Ausanio, C. de Lisio, V. Iannotti, M. Vitiello, X. Wang, L. Lanotte, Appl. Surf. Sci. **247**, 71 (2005)
28 T. Katsuno, C. Godet, J.C. Orlianges, A.S. Loir, F. Garrelie, A. Catherinot, Appl. Phys. A **81**, 471 (2005)
29 F. Qian, V. Craciun, R.K. Singh, S.D. Dutta, P.P. Pronko, J. Appl. Phys. **86**, 2281 (1999)
30 P.S. Banks, L. Dinh, B.C. Stuart, M.D. Feit, A.M. Komashko, A.M. Rubenchik, M.D. Perry, W. McLean, Appl. Phys. A **69**, S347 (1999)
31 M. Okoshi, S. Higuchi, M. Hanabusa, J. Appl. Phys. **86**, 1768 (1999)
32 D.-S. Yao, J.-R. Liu, L.-G. Wang, C.-X. Yu, R.-J. Zhan, Chin. Phys. Lett. **17**, 540 (2000)
33 F. Garrelie, A.S. Loir, C. Donnet, F. Rogemond, R. Le Harzic, M. Belin, E. Audouard, P. Laporte, Surf. Coat. Technol. **163–164**, 306 (2003)
34 A.S. Loir, F. Garrelie, C. Donnet, F. Rogemond, J.L. Subtil, B. Forest, M. Belin, P. Laporte, Surf. Coat. Technol. **188–189**, 728 (2004)
35 N. Benchikh, F. Garrelie, C. Donnet, B. Bouchet-Fabre, K. Wolski, F. Rogemond, A.S. Loir, J.L. Subtil, Thin Solid Films **482**, 287 (2005)
36 N. Benchikh, F. Garrelie, K. Wolski, C. Donnet, R.Y. Fillit, F. Rogemond, J.L. Subtil, J.N. Rouzaud, J.Y. Laval, Thin Solid Films **494**, 98 (2006)
37 N. Benchikh, F. Garrelie, C. Donnet, K. Wolski, R.Y. Fillit, F. Rogemond, J.L. Subtil, J.N. Rouzaud, J.Y. Laval, Surf. Coat. Technol. **200**, 6272 (2006)
38 D. Grojo, J. Hermann, A. Perrone, J. Appl. Phys. **97**, 063 306 (2005)
39 A.S. Loir, F. Garrelie, J.L. Subtil, F. Goutaland, M. Belin, R. Le Harzic, C. Donnet, Y. Ouerdane, F. Rogemond, P. Laporte, Appl. Surf. Sci. **208–209**, 553 (2003)
40 J. Robertson, Mater. Sci. Eng. R **37**, 129 (2002)
41 G. Ausanio, S. Amoruso, A.C. Barone, R. Bruzzese, V. Ianotti, L. Lanotte, M. Vitiello, Appl. Surf. Sci. **252**, 4678 (2006)
42 P.T. Moseley, C.J. Seabrook, Acta Cryst. B **29**, 1170 (1973)

Applied Surface Science xxx (2008) xxx–xxx

Contents lists available at ScienceDirect

Applied Surface Science

journal homepage: www.elsevier.com/locate/apsusc

Adaptive control of femtosecond laser ablation plasma emission

M. Guillermin, C. Liebig, F. Garrelie *, R. Stoian, A.-S. Loir, E. Audouard

Laboratoire Hubert Curien (UMR 5516 CNRS), Université Jean Monnet, 42000 Saint Etienne, France

ARTICLE INFO

Article history:
Received 7 June 2008
Received in revised form 21 July 2008
Accepted 28 July 2008
Available online xxx

Keywords:
Femtosecond laser
Plasma
Pulse Shaping
Thin film deposition

ABSTRACT

The influence of temporal pulse shaping on plasma plume generated by ultrafast laser irradiation of aluminum is investigated. Time resolved plasma emission spectroscopy is coupled with a temporal shaping procedure in a closed loop. The ionic emission is enhanced relative to the neutral one via an adaptive optimization strategy. The plasma emission efficiency in case of optimized and ultrashort temporal shapes of the laser pulses are compared, evidencing an enhancement of the ionization degree of the plasma plume. Simplified temporal shapes of the femtosecond laser pulses are extracted from the optimized shape and their corresponding effect on laser induced plasma emission is discussed.

1. Introduction

Femtosecond lasers have achieved great practical interest in recent years for several applications such as precise machining, laser induced spectroscopy or biological characterization [1]. Femtosecond laser can also be used for thin film deposition of a wide variety of materials, such as diamond-like carbon [2–4], oxides [5,6], nitrides [7–9], or quasicrystals [10]. Short pulse laser irradiation has the ability to bring materials into highly non-equilibrium states and to induce rapid transformations, leading to the formation of metastable phases. Femtosecond laser ablation can drive particular thermodynamical pathways of the ablated matter close to the critical point [11,12], with influence in nanoparticles formation [13–16]. The plasma plume induced by femtosecond laser irradiation was analysed by several techniques, including time of flight analysis [2,17] or temporally resolved emission spectroscopy [18–20] and differs significantly in its kinetic properties from the plume generated by conventional ns pulses. Plasma kinetic and excitation control is a key parameter in thin films or nanoparticles synthesis, since it can improve the reactivity or the growth kinetics. A possible way to achieve higher film quality and better control of the ablation development is to regulate the interaction via spatio-temporal modification of the laser beam. Few studies were reported on the use of temporal shaped femtosecond pulses for the elaboration of thin films, mainly with double pulses for diamond-like carbon [21] or silicon carbide [22]. Further progress was made in plasma regulation for spectroscopic application [23,24] suggesting control potential by complex pulse forms. Especially for complex interaction phenomena, pulse tailoring can be connected with feedback loops. Largely applied in femtochemistry [25], adaptive optimization techniques based on real-time pulse tailoring can open large possibilities for controling the overall course of laser–matter interaction. Since prior knowledge of the interaction between laser and matter is not available, the relation between a particular temporally shaped pulse and the induced effects is not easily predictable. In that case, adaptive optimization procedures may deliver the most effective way to drive the systems in a defined state [11,26]. In the context of laser ablation, the use of adaptive pulse shaping has been recently reported for ion ejection efficiency [11,26,27] and for the generation of nanoparticles with tailored size [28]. Applications in spectroscopy and pulse characterization were suggested as well [29,30]. We report here on the possibility of tailoring the plasma plume by adaptive temporal shaping. The outcome has potential interest for thin films elaboration or nanoparticles synthesis.

We present preliminary results on the use of an adaptive feedback optimization procedure that adjust the laser temporal form for modulating plasma optical properties. This work is focused on the enhancement of the ionic emission with respect to the neutral emission lines of the plasma induced by laser irradiation of an aluminum sample.

2. Experimental setup and methods

The experimental setup is depicted in Fig. 1. A Ti:saphirre laser beam (centered at 800 nm) with 150 fs pulse duration is focused

* Corresponding author.
E-mail address: florence.garrelie@univ-st-etienne.fr (F. Garrelie).

0169-4332/$ – see front matter © 2008 Elsevier B.V. All rights reserved.
doi:10.1016/j.apsusc.2008.07.207

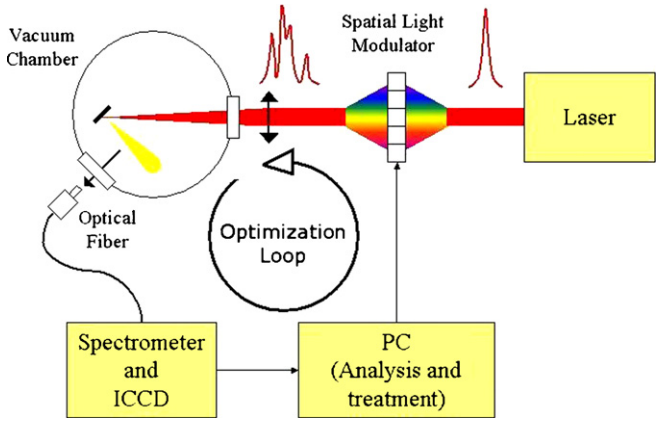

Fig. 1. Schematic description of the experimental setup.

into a vacuum chamber ($\sim 10^{-5}$ Pa) on pure aluminum target (99.9%), generating the ablation plasma. The fluence is controlled by precise positioning of the focusing lens and set at a value of 5.8 J/cm^2, well above the ablation threshold for Al. Prior amplification, the pulses from the femtosecond oscillator are spectrally dispersed in a zero-dispersion unit and the spatially-separated frequency components pass through a pixellated liquid crystal array acting as a Spatial Light Modulator (SLM). The device allows relative retardation of spectral components, tailoring in turn the temporal shape of the pulse [31]. The programmable nature of the SLM permits its insertion in closed loops involving rapid quantification of laser interaction, allowing thus to exercise control on the experimental results of irradiation. In this respect, plasma optical emission provides the necessary feedback by evaluating the result of the laser action.

Optical emission of the plasma plume is collected through a focusing lens with an optical fiber and injected onto the entrance slit of a spectrometer/monochromator (Chromex 500 IS/SM) equipped with two different diffraction gratings, both blazed at 400 nm (300 grooves/mm and 1200 grooves/mm). An ultrafast Intensified Charge-Coupled Device (ICCD Hamamatsu Orca 12 ER) is coupled at the output of the spectrometer, allowing a minimum temporal resolution of 3 ns. In the monochromator mode, the spectrometer is connected with a photomultiplier (Hamamatsu R-928P) and a 1 mm slit is placed before the collection lens to increase the spatial resolution. This setup permits temporal measurements of a limited spatial and spectral domain of the plasma plume. A synchronization device driven by computer is used to timely control the injection and ejection of seed pulses in and out of the amplification stages of the laser system and to trigger a delay generator (Stanford Research DG 535) which controls the camera acquisition with a temporal resolution better than 0.2 ns. All spectra reported in this article are recorded at a delay of 100 ns after the laser impact and with a time-width of 300 ns. These parameters have been chosen to maximize the acquired intensity.

This study aims to realize adaptive temporal tailoring of femtosecond pulses based on optical emission of the plasma in order to enhance the ionic population of the plasma plume with respect to the neutral one. Visible spectral lines, including the ones used to monitor ionic and neutral components of the ablated matter, are summarized in Table 1 [32,33]. We limit this study at the most intense lines. Atomic lines between 358.65 and 358.74 nm (Table 1, d) are representative of Al II population while lines at 394.40 and 396.15 nm (Table 1, e and f) give information on neutral population. The comparison of the relative intensity of these two groups of lines provides indication on the state of ionization of the ablated matter. We choose the difference between ionic and neutral lines intensity as relevant parameter (named fitness) to characterize the efficiency of a particular temporal shape to enhance the ionic population with respect to the neutral component of the plasma plume. We make the difference of ionic versus neutral lines in a given spectral range and this constitutes the quantification of the laser interaction process in a given spectral range. In order to lock up temporal shapes that maximize the fitness, we used a numerical optimization loop based on an adaptive evolutionary strategy. An initial group of arbitrary temporal shapes are chosen and tested in the experiment, while recording the irradiation results through the acquisition device. The group of corresponding spectral phase masks is ranked according to the fitness defined above. The best masks are selected, allowing to create by genetic propagators a new population that will be tested in the same way. The procedure is iteratively repeated until the convergence of the optimization loop is realized. A high number of acquisitions is needed and each acquisition is made with 15 laser shots. To ensure the stability of the experiment, the target was rotated and a new site of irradiation was sputtered before any acquisition. In all this study, temporal shapes of laser pulses are measured with a cross-correlation device. The pulse shape is determined by second order nonlinear intensity cross-

Table 1
Evolution of studied lines with femtosecond and temporally optimized pulses (the multiplication factor is given with respect to lines intensity obtained with the short pulse)

Species	Wavelength (nm)	Multiplication factor		
		Optimized	DP 10 ps	S 6 ps
Al II (a)	281.701	2.94	1.9	2.22
Al I (b)	308.215	0.54	0.44	0.56
Al I (c)	309.271 and 309.284	0.56	0.44	0.54
Al II (d)	From 358.656 to 358.745	3.24	2.79	3.17
Al I (e)	394.401	0.54	0.4	0.5
Al I (f)	396.152	0.59	0.43	0.52
Al II (g)	466.306	3.64	3.44	3.96
Al II (h)	559.330	1.99	1.76	2.07
Al II (i)	618.157 and 618.168	0.6	0.55	0.66
Al II (j)	623.334 and 623.347	2.55	2.82	2.65
Al II (k)	624.480, 624.493 and 624.510	2.93	2.97	3.67
Al II (l)	704.206	1.87	1.85	1.48
Al II (m)	705.660	2.55	1.69	1.38
All visible lines		0.65	0.51	0.61
Neutral lines		0.56	0.43	0.52
Ionic lines		2.15	1.87	2.1
Total intensity (integrated between 200 and 800 nm)		0.76	0.67	0.76

Please cite this article in press as: M. Guillermin, et al., Adaptive control of femtosecond laser ablation plasma emission, Appl. Surf. Sci. (2008), doi:10.1016/j.apsusc.2008.07.207

correlation between a Fourier limited reference femtosecond pulse and the experimentally generated shaped pulse, allowing us to determine the envelope of the tailored pulse. Ex situ characterizations of ablation craters are realized with an optical profilometer and an Atomic Force Microscope (for irradiation respectively with 6 and 3 pulses).

3. Results and discussion

The above-described setup was used to enhance the ionic population of the plasma plume with respect to neutral species. The optimization loop leads to a shaped pulse that enhances the ionic versus neutral emission ratio in the plasma plume at a given time moment. The difference between ionic and neutrals emission intensities is used as the fitness parameter in order to reduce the noise effect on the optimization. However, in presenting the results, we have attempted to describe the pulse shaping effect on the emission spectrum using the ratio of line intensities generated by temporally shaped, respectively direct short pulse laser irradiation. The comparison between the intensity of atomic and ionic lines chosen for optimization under the femtosecond pulse (short pulse SP) and the optimized pulse (OP) is given in Fig. 2. Integrated intensity corresponding to Al II is augmented by a factor 3.24 while intensity of Al I is reduced by 1.76. The temporal shape of the optimized pulse is depicted in Fig. 3 with the behavior of the fitness during the optimization run given on the inset. The result of the optimization represents an improved shape that the adaptive loop is able to provide with respect to the demanded request on augmentation of ionic spectral emission. It consists of a series of femtosecond pulses separated by 1–2 ps distributed on an envelop of 6 ps. The ps elongation suggests a change in the heating conditions. We also evaluate the amount of ablated matter in each case by measuring the volume of ablation craters and no significant differences are observed between SP and OP. Additionally, we perform measurements of the temporal dynamics of the concerned lines using a photomultiplier device. No temporal shift of the maximum plasma emission lines or additional retardation is observed. This indicates that the observed changes in the plasma emission spectrum are directly related to the behavior of electron occupation number for each atomic level. Effects observed on chosen lines for optimization are also visible for other lines. A summary of changes is given in Table 1. The observed neutral lines are all reduced by a factor close to 2 when the optimized pulse is applied. Ionic lines intensities are all augmented except the Al II line corresponding to the highest level accessible by our measurements device (Table 1, i). The intensity of this line is reduced by a factor 1.66. Finally, we observe that the integrated intensity of the whole spectrum between 200 nm and 800 nm corresponding to the acquisition at a delay of 100 ns after the laser impact and with a width of 300 ns is reduced by a factor 1.32.

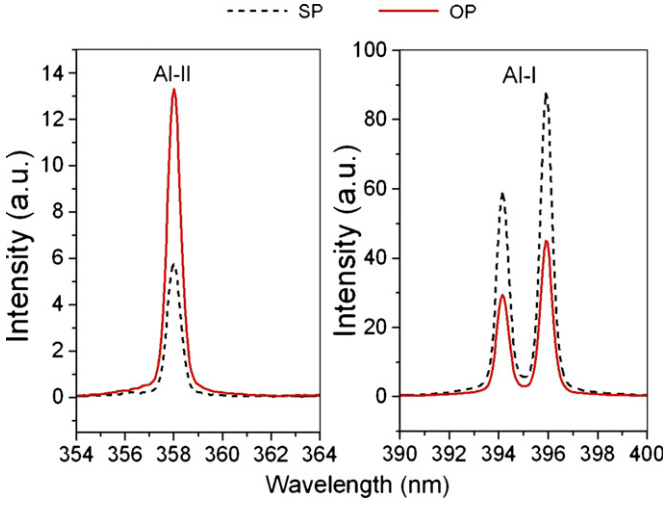

Fig. 2. Evolution of lines chosen for optimization with short pulse (SP) and optimized pulse (OP).

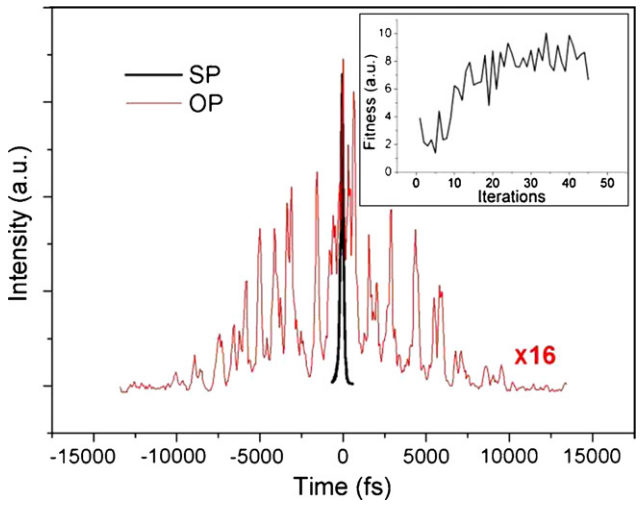

Fig. 3. Temporal shapes of short and optimized pulses (cross-correlation traces). Inset: Fitness behavior during the optimization.

To provide a better understanding of the optimization results, we have attempted to simplify the form of irradiation pulse according to features observed in the optimized pulse. The analysis of the optimized shape allows extracting two particular shapes: a double pulse (DP) with delay of 10 ps and a long pulse (LP) with a temporal width of 6 ps (Fig. 4a and b). The corresponding effects on plasma emission are summarized in Table 1. The double pulse is the most efficient to reduce the intensity of the neutral lines chosen for the optimization, while the long pulse is the best shape to enhance the used ionic lines. This can be speculatively explained by a shielding effect [34] because the delay between the two pulses is longer than electron phonon coupling time for aluminum (few ps [35]). Total emission of the plasma in the 200–800 nm spectral range is the same when optimized or long pulses are applied, while it is reduced with the double pulse irradiation. To analyse the effect of pulse separation, we observe plasma emission with double pulses with delay of 5.5 and 14 ps and with long pulses of 5.4 and 6.3 ps durations. The intensity of 358.73 nm ionic lines is maximum for the double pulses with delay of 10 ps and long pulse of 6 ps and the intensity of 394.4 nm neutral line present a minimum for the stretched pulse of 6 ps duration.

The double pulse shape improves the fitness of the optimization through a reduction of the neutral species in the plasma while the long pulse leads to an augmentation of the ionic species emission and allows producing a higher total emission of the plasma. This could evidence a competition process in the yield of optical plasma emission between re-heating of the plasma with double pulses separated by a delay longer than the electron-phonon coupling time and enhancement of the amount of ablated matter determined by the irradiation with the long pulse. Further experiments are planed to elucidate mechanisms involved in plasma optical response in solid matter ablated by temporally shaped femtosecond pulses.

Please cite this article in press as: M. Guillermin, et al., Adaptive control of femtosecond laser ablation plasma emission, Appl. Surf. Sci. (2008), doi:10.1016/j.apsusc.2008.07.207

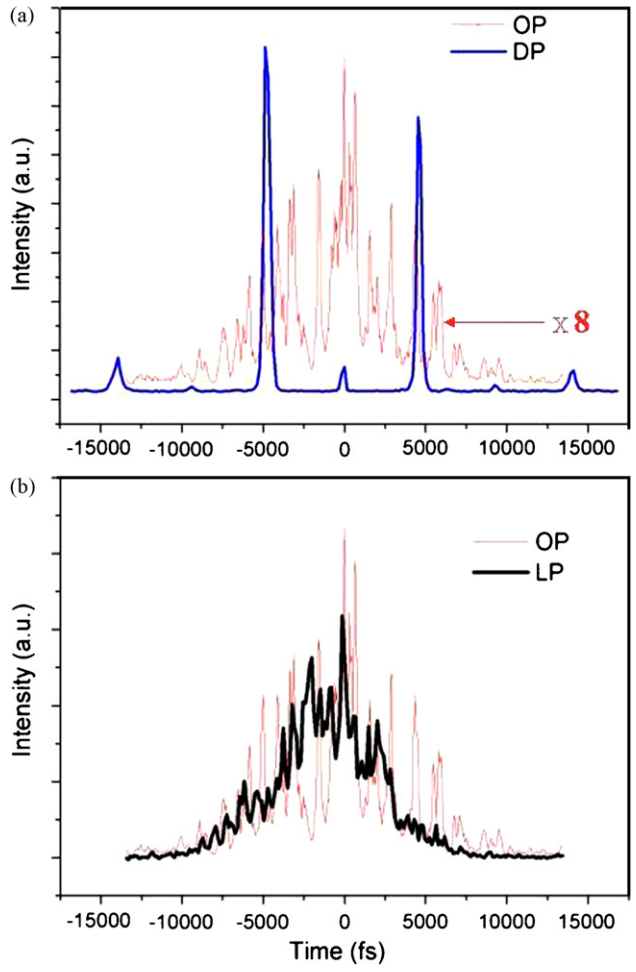

Fig. 4. Simplified temporal shapes derived from the optimized pulse (a) double pulse (DP) with a delay of 10 ps and (b) long pulse (LP) of 6 ps duration.

4. Conclusion

In this study, we show the possibility to achieve control on the plasma optical response by material irradiation with temporally shaped femtosecond pulses. We applied an adaptive optimization loop to lock up temporal shapes fulfilling user-designed constraints on plasma optical emission. The pulses that improved the ionic versus neutral emission show a structured temporal form extending on several ps. Laser energy deposition with series of femtosecond pulses leads to a reduction of the neutral species emission while energy deposition in the picosecond timescale augments the ionic emission and allows an enhancement of the global emission of the plasma plume.

Acknowledgment

The financial support of ANR is gratefully acknowledged.

References

[1] F. Dausinger, F. Lichtner, H. Lubatschowski, Femtosecond Technology for Technical and Medical Applications, Topics in Applied Physics, Vol. 96, Springer, 2004.
[2] F. Qian, V. Craciun, R.K. Singh, S.D. Dutta, P.P. Pronko, J. Appl. Phys. 86 (4) (1999) 2281.
[3] P.S. Banks, L. Dinh, B.C. Stuart, M.D. Feit, A.M. Komashko, A.M. Rubenchik, M.D. Perry, W. McLean, Appl. Phys. A 69 (Suppl.) (1999) S347.
[4] F. Garrelie, A.S. Loir, C. Donnet, F. Rogemond, R. Le Harzic, M. Belin, E. Audouard, P. Laporte, Surf. Coat. Technol. 163–164 (2003) 306.
[5] M. Okoshi, K. Higashikawa, M. Hanabusa, Appl. Surf. Sci. 154–155 (2000) 424.
[6] J. Perrière, E. Millon, W. Seiler, C. Boulmer-Leborgne, V. Craciun, O. Albert, J.C. Loulergue, J. Etchepare, J. Appl. Phys. 91 (2) (2002) 690.
[7] Z. Zhang, P.A. VanRompay, J.A. Nees, R. Clarke, X. Pan, P.P. Pronko, Appl. Surf. Sci. 154–155 (2000) 165.
[8] C.R. Luculescu, H. Miyake, S. Sato, Appl. Surf. Sci. 197–198 (2002) 499.
[9] S. Geretovszky, Z. Kantor, T. Szörényi, Appl. Surf. Sci. 208–209 (2003) 547.
[10] R. Teghil, L. D'Alessio, A. Santagata, M. Zaccagnino, D. Ferro, D.J. Sordelet, Appl. Surf. Sci. 210 (2003) 307.
[11] J.P. Colombier, P. Combis, A. Rosenfeld, I.V. Hertel, E. Audouard, R. Stoian, Phys. Rev. B 74 (2006) 224106.
[12] M.E. Povarnitsyn, T.E. Itina, M. Sentis, K.V. Khishchenko, P.R. Levashov, Phys. Rev. B 75 (2007) 235414.
[13] S. Eliezer, N. Eliaz, E. Grossman, D. Fisher, I. Gouzman, Z. Henis, S. Pecker, Y. Horovitz, M. Fraenkel, S. Maman, Y. Lereah, Phys. Rev. B 69 (2004) 144119.
[14] S. Amoruso, G. Ausanio, R. Bruzzese, M. Vitiello, X. Wang, Phys. Rev. B 71 (2005) 033406.
[15] S. Barcikowski, A. Hahn, A.V. Kabashin, B.N. Chichkov, Appl. Phys. A 87 (2007) 47.
[16] S. Amoruso, R. Bruzzese, X. Wang, N.N. Nedialkov, P.A. Atanasov, Nanotechnology 18 (2007) 145612.
[17] P.P. Pronko, Z. Zhang, P.A. Van, Rompay, Appl. Surf. Sci. 208–209 (2003) 492.
[18] F. Claeyssens, M.N.R. Ashfold, E. Sofoulakis, C.G. Ristoscu, D. Anglos, C. Fotakis, J. Appl. Phys. 91 (9) (2002) 6162.
[19] D. Grojo, J. Hermann, A. Perrone, J. Appl. Phys. 97 (2005) 063306.
[20] S. Amoruso, R. Bruzzese, M. Vitiello, N.N. Nedialkov, P.A. Atanasov, J. Appl. Phys. 98 (2005) 044907.
[21] N. Jegenyes, Z. Toth, B. Hopp, J. Klebniczki, Z. Bor, C. Fotakis, Appl. Surf. Sci. 252 (2006) 4667.
[22] C. Ristoscu, G. Socol, C. Ghica, I.N. Mihailescu, D. Gray, A. Klini, A. Manousaki, D. Anglos, C. Fotakis, Appl. Surf. Sci. 252 (2006) 4857.
[23] A. Assion, M. Wollenhaupt, L. Haag, F. Mayorov, C. Sarpe-Tudoran, M. Winter, U. Kutschera, T. Baumert, Appl. Phys. B 77 (2003) 391.
[24] T. Gunaratne, M. Kangas, S. Singh, A. Gross, M. Dantus, Chem. Phys. Lett. 423 (2006) 197.
[25] R.S. Judson, H. Rabitz, Phys. Rev. Lett. 68 (10) (1992) 1500.
[26] R. Stoian, A. Mermillod-Blondin, N.M. Bulgakova, A. Rosenfeld, I.V. Hertel, M. Spyridaki, E. Koudoumas, P. Tzanetakis, C. Fotakis, Appl. Phys. Lett. 87 (2005) 124105.
[27] H. Dachraoui, W. Husinsky, Phys. Rev. Lett. 97 (2006) 107601.
[28] R. Hergenröder, M. Miclea, V. Hommes, Nanotechnology 17 (2006) 4065.
[29] R. Ackermann, E. Salmon, N. Lascoux, J. Kasparian, P. Rohwetter, K. Stelmaszczyk, S. Li, A. Lindinger, L. Wöste, P. Béjot, L. Bonacina, J.-P. Wolf, Appl. Phys. Lett. 89 (2006) 171117.
[30] V.V. Lozovoy, B. Xu, Y. Coello, M. Dantus, Optics Express 16 (2) (2008) 592.
[31] A.M. Weiner, Rev. Sci. Instrum. 71 (5) (2000) 1929.
[32] A.R. Striganov, N.S. Sventitskii, Table of Spectral Lines of Neutral and Ionized Atoms, Ifi/Plenum, New York, Washington, 1968.
[33] N.I.S.T. internet database.
[34] A. Semerok, C. Dutouquet, Thin Solid Films 453–454 (2004) 501.
[35] N.N. Nedialkov, P.A. Atanasov, S. Amoruso, R. Bruzzese, X. Wang, Appl. Surf. Sci. 253 (2007) 7761.

Please cite this article in press as: M. Guillermin, et al., Adaptive control of femtosecond laser ablation plasma emission, Appl. Surf. Sci. (2008), doi:10.1016/j.apsusc.2008.07.207

Conclusion générale

Ce manuscrit présente une partie significative de mon travail de recherche depuis ma nomination à l'Université Jean Monnet de Saint Etienne. Mes recherches portent principalement sur l'élaboration de matériaux par ablation laser femtoseconde, la caractérisation du procédé de dépôt via le plasma généré, ou encore l'interaction laser-matière.

Cette communauté scientifique est très active et j'ose espèrer que nos études auront pu contribuer même très modestement à la connaissance globale dans ce domaine. Les collaborations mises en place dans le cadre de ces études m'ont en tout cas apporté énormément, tant d'un point de vue scientifique que relationnel ou encore humain.

En guise de conclusion, plûtot que de dresser un bilan ou un résumé de ces travaux, je voudrais mettre en avant, à la fois tout l'intérêt et même la passion que m'a inspirée mon activité professionnelle, mais également la difficulté de combiner une recherche de qualité suffisante pour travailler sur des projets nationaux ou internationaux, apporter l'encadrement nécessaire aux étudiants que j'ai eu la chance de suivre, présenter ses résultats en conférence ou avoir un taux de publication suffisant, tout en ayant une activité d'enseignement riche en implications, couteuse en temps et de qualité suffisante pour répondre aux attentes légitimes des étudiants.

J'ose espèrer que le dynamisme et l'implication dont je peux avoir fait preuve auront réussi à combler le manque de temps nécessaire à une recherche et un enseignement de qualité.

Enfin, ce manuscrit n'aurait pu exister sans la participation des étudiants et collègues avec qui j'ai eu plaisir à travailler au cours de ces années, et je tiens à les en remercier chaleureusement.

Enfin, je souhaiterai remercier ma famille et mes proches, en commençant bien entendu par Manu et nos rayons de soleil quotidien, Louisa et Margaux, qui finalement ont participé à ce que mon travail d'enseignante-chercheur m'apporte tant de satisfactions.